ACTION AND MECHANISM OF HERBAL GLYCANS

EDITED BY: SP Li, Manuel A. Coimbra and Jing Zhao
PUBLISHED IN: Frontiers in Pharmacology

frontiers Research Topics

frontiers

ISSN 1664-8714
ISBN 978-2-88974-933-1
DOI 10.3389/978-2-88974-933-1

About Frontiers

Frontiers is more than just an open-access publisher of scholarly articles: it is a pioneering approach to the world of academia, radically improving the way scholarly research is managed. The grand vision of Frontiers is a world where all people have an equal opportunity to seek, share and generate knowledge. Frontiers provides immediate and permanent online open access to all its publications, but this alone is not enough to realize our grand goals.

Frontiers Journal Series

The Frontiers Journal Series is a multi-tier and interdisciplinary set of open-access, online journals, promising a paradigm shift from the current review, selection and dissemination processes in academic publishing. All Frontiers journals are driven by researchers for researchers; therefore, they constitute a service to the scholarly community. At the same time, the Frontiers Journal Series operates on a revolutionary invention, the tiered publishing system, initially addressing specific communities of scholars, and gradually climbing up to broader public understanding, thus serving the interests of the lay society, too.

Dedication to Quality

Each Frontiers article is a landmark of the highest quality, thanks to genuinely collaborative interactions between authors and review editors, who include some of the world's best academicians. Research must be certified by peers before entering a stream of knowledge that may eventually reach the public - and shape society; therefore, Frontiers only applies the most rigorous and unbiased reviews.
Frontiers revolutionizes research publishing by freely delivering the most outstanding research, evaluated with no bias from both the academic and social point of view. By applying the most advanced information technologies, Frontiers is catapulting scholarly publishing into a new generation.

What are Frontiers Research Topics?

Frontiers Research Topics are very popular trademarks of the Frontiers Journals Series: they are collections of at least ten articles, all centered on a particular subject. With their unique mix of varied contributions from Original Research to Review Articles, Frontiers Research Topics unify the most influential researchers, the latest key findings and historical advances in a hot research area! Find out more on how to host your own Frontiers Research Topic or contribute to one as an author by contacting the Frontiers Editorial Office: frontiersin.org/about/contact

ACTION AND MECHANISM OF HERBAL GLYCANS

Topic Editors:
SP Li, University of Macau, China
Manuel A. Coimbra, University of Aveiro, Portugal
Jing Zhao, University of Macau, China

Citation: Li, S., Coimbra, M. A., Zhao, J., eds. (2022). Action and Mechanism of Herbal Glycans. Lausanne: Frontiers Media SA. doi: 10.3389/978-2-88974-933-1

Table of Contents

frontiers in Pharmacology

EDITORIAL
published: 24 March 2022
doi: 10.3389/fphar.2022.883055

Editorial: Action and Mechanism of Herbal Glycans

Shaoping Li[1,2]*, *Manuel A. Coimbra*[3] *and Jing Zhao*[1,2]

[1]State Key Laboratory of Quality Research in Chinese Medicine, University of Macau, Macao, Macao SAR, China, [2]Joint Laboratory of Herbal Glycoengineering and Testing, University of Macau, Macao, Macao SAR, China, [3]Department of Chemistry, University of Aveiro, Aveiro, Portugal

Keywords: action, mechanism, herb, glycan, intestinal microbial flora

Editorial on the Research Topic

Action and Mechanism of Herbal Glycans

Extensive evidence shows that natural glycans from medicinal plants, fungi and marine organisms have a variety of biological activities with beneficial effects to human body. Discovering target molecules, such as glycan receptors, growth or angiogenesis factors and enzymes, is a key step to track the signaling pathway involved in the succession of glycan effects and understand the pathological mechanisms. Actually, glycans are still the "sleeping giant" of research in herbal medicine, and how they contribute to phytotherapeutic effects are still not clear. Generally, the therapeutic efficacy of a drug mainly depends on its concentration at the site of action. Therefore, how polysaccharides are absorbed and distributed to the site of action is always questionable, as well as their mechanisms of action. Technological advances in glycobiology and glycochemistry are paving the way for a new era in developing sweet solutions to sticky situations.

In this Research Topic of *Action and Mechanism of Herbal Glycans*, a perspective article by Xie et al. proposes polysaccharides as potential therapeutic agents of epilepsy. Besides regulation of inflammatory factors, neurotransmitters, ion channels, and antioxidant reactions, the beneficial effects of polysaccharides treating epilepsy may mainly derive from their targeting on intestinal microbial flora, considered as "intestinal brain organ" or "adult's second brain", through "brain gut axis". Indeed, *Astragalus* (*Astragalus membranaceus* (Fisch.) Ege. var. *mongholicus* (Ege.) Hsiao) polysaccharides (APS) could ameliorate diet-induced cholesterol gallstone formation in mice, and the protective effect of APS, at least partially, results from modulation of gut microbiota (Zhuang et al.). APS seems to improve the diversity of the gut microbiota and increase the relative abundance of the Bacteroidetes phylum, suggesting that APS might be a potential strategy for the prevention of cholesterol gallstone disease. An inulin (CPPF) from Codonopsis Radix (*Codonopsis pilosula* (Franch.) Nannf.) (Zou et al.) was shown to have restorative effects on intestinal mucosal immunity, anti-inflammatory activity and gut microbiota of immunosuppressed mice. As a potential prebiotic substance, a gut microbiota restorative effect was presented by mainly modulating the relative abundance of *Eubacteriales*, including *Oscillibacter*, unidentified *Ruminococcus* and Lachnospiraceae. All results indicated that CPPF was a medicinal prebiotic with enhancing mucosal immune, anti-inflammatory and microbiota modulatory activities.

Cardiovascular protective effects of plant polysaccharides (Dong et al.) were reviewed. These effects derive from anti-oxidative stress, restoring the metabolism of biological macromolecules, regulating the apoptosis cascade to reduce cell death, and inhibiting inflammatory signal pathways, which is beneficial for developing more effective drugs with low side effects for management of cardiovascular diseases. Burdock (*Arctium lappa* L.) fructooligosaccharide (Ding et al.), a water-soluble inulin-type oligosaccharide, was shown potential to protect rat renal tubular epithelial cells (NRK-52E cells) against the reduced cell viability and significantly increased apoptosis rate induced

OPEN ACCESS

Edited and reviewed by:
Michael Heinrich,
University College London,
United Kingdom

***Correspondence:**
Shaoping Li
spli@um.edu.mo

Specialty section:
This article was submitted to Ethnopharmacology, a section of the journal Frontiers in Pharmacology

Received: *24 February 2022*
Accepted: *10 March 2022*
Published: *24 March 2022*

Citation:
Li S, Coimbra MA and Zhao J (2022) Editorial: Action and Mechanism of Herbal Glycans. Front. Pharmacol. 13:883055. doi: 10.3389/fphar.2022.883055

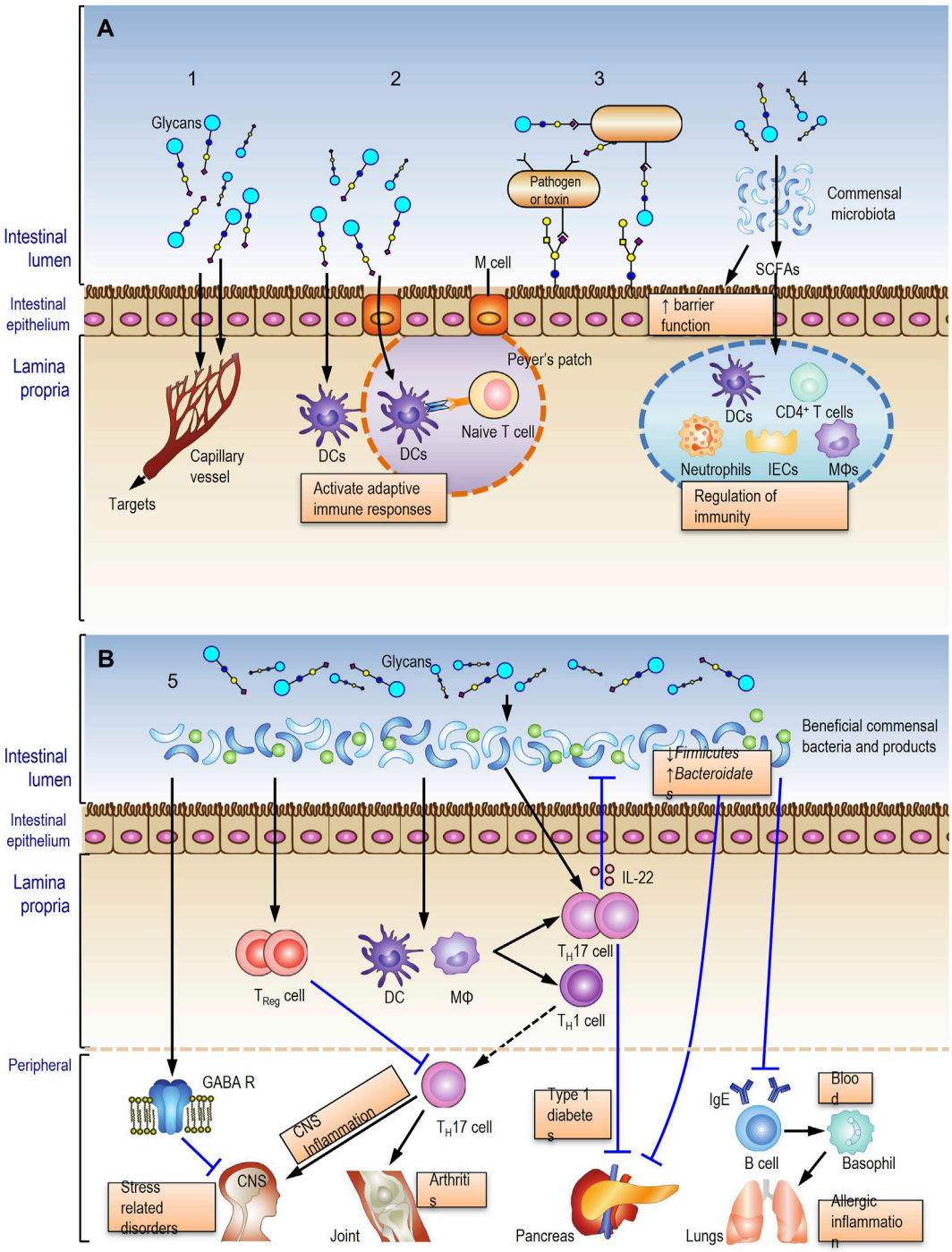

FIGURE 1 | Five potential action modes of oral herbal glycans. Modes 1-4 **(A)** and mode 5 **(B)** described in fulltext.

by high glucose, through inhibiting apoptosis and oxidative stress through the Nrf2/HO-1 signaling pathway. Pomegranate peel (*Punica granatum* L.) polysaccharides (Chen et al.) was shown to have potential to ameliorate the symptoms of psoriasis through inhibition of the inflammatory cytokines by suppressing NF-κB and STAT3 signaling pathways and improving skin barrier protection via enhancing aquaporin-3 and filaggrin. Theoretical and experimental evidence has been provided for clinical application of pomegranate peel polysaccharides against psoriasis.

One of the major pharmacological activities of polysaccharides is immunomodulation. Structural characterization and immunomodulatory activity of a novel polysaccharide (LHPW) from Lycopi Herba (*Lycopus lucidus* Turcz. var. *hirtus* Regel) (Zhang et al.) were determined. LHPW was mainly composed of

galactose, glucose, fructose and arabinose. It was shown to be able to activate macrophage RAW264.7 and promote splenocyte proliferation. Ginseng (*Panax ginseng* C. A. Mey.) polysaccharides (WGP) showed to significantly increase mRNA and protein levels of complement component 4, one of the core components of the complement system in human hepatocytes (Liu et al.). E-box1 and Sp1 regions play key roles in WGP-induced component 4 transcription. The results provide a new explanation for the intrinsic mechanism by which ginseng boosts human immune capacity. Glycoproteins from *Isodon japonicus* var. *glaucocalyx* (Maxim.) H.W.Li. (Ren et al.) also seems to regulate macrophage polarization and alleviate lipopolysaccharide-induced acute lung injury in mice via TLR4/NF-κB pathway, providing evidence that supports the traditional application of *Isodon japonicus* var. *glaucocalyx* (Maxim.) H.W.Li. in inflammation-linked diseases. A bee pollen polysaccharide from *Rosa rugosa* Thunb (Yang et al.) was reported to promote pancreatic β-Cell proliferation and insulin secretion. In alloxan-induced diabetic mice, oral administration of the acidic fraction of bee pollen polysaccharide effectively decreased the blood glucose, drink intake and urine. It directly stimulated phosphorylation of p38, ERK and AKT to maintain the islet function and mass. In addition, Mori Fructus (*Marus alba* L.) polysaccharides (Bian et al.) was shown to attenuate alcohol-induced liver damage by regulating fatty acid synthesis, degradation and glycerophospholipid metabolism in mice, and effects of different molecular weight polysaccharides from *Dendrobium officinale* Kimura & Migo (Tao et al.) on human colorectal cancer and transcriptome were also reported.

In summary, the complex relationship between glycans, the gut microbiota and host health are currently considered to comprehensively underpin the multiple activities of herbal glycans. We hypothesized five action modes for oral herbal polysaccharides (**Figure 1**) based on current evidence, which will be helpful to comprehensively understand the action and mechanism of herbal glycans.

1. Few polysaccharides or their digested oligosaccharide fragments may be absorbed into bloodstream to act on the targets (**Figure 1A**, mode 1).
2. Polysaccharides or their digested fragments initiate intestinal adaptive immune responses in Peyer's patches or in mesenteric lymph nodes (**Figure 1A**, mode 2).
3. Glycans in glycosylated molecules recognize and bind to the pathogen resulting in limited adhesion and a reduced risk of infection (**Figure 1A**, mode 3).
4. Glycans are metabolized by the gut microbiota into short-chain fatty acids (SCFAs) to modulate immune response (**Figure 1A**, mode 4).
5. Glycans interact with the gut microbiota and induce beneficial commensal bacteria growth to improve the host health (**Figure 1B**).

Last but not least, we appreciate all authors, reviewers and guest editors for their contribution. We also would like to take the opportunity of this Research Topic publication to celebrate 70th birthday of Professor Hui Ji, Chinese Pharmaceutical University, China.

AUTHOR CONTRIBUTIONS

All authors listed have made a substantial, direct, and intellectual contribution to the work and approved it for publication.

Conflict of Interest: The authors declare that the research was conducted in the absence of any commercial or financial relationships that could be construed as a potential conflict of interest.

frontiers in Pharmacology

ORIGINAL RESEARCH
published: 25 June 2021
doi: 10.3389/fphar.2021.691995

Structural Characterization and Immunomodulatory Activity of a Novel Polysaccharide From Lycopi Herba

Wuxia Zhang, Yihua Hu, Jiaqi He, Dongdong Guo, Jinzhong Zhao and Peng Li**

Department of Basic Science, Shanxi Agricultural University, Jinzhong, China

Lycopi Herba has been broadly used as a traditional medicinal herb in Asia due to its ability to strengthen immunity. However, it is still obscure for its material basis and underlying mechanisms. Polysaccharide, as one of the most important components of most natural herbs, usually contributes to the immunomodulatory ability of herbs. Here, we aimed to detect polysaccharides from Lycopi Herba and examine their potential immunomodulatory activity. A novel polysaccharide (LHPW) was extracted from Lycopi Herba and purified by DEAE-52 cellulose chromatography and G-100 sephadex. According to physicochemical methods and monosaccharide composition analysis, LHPW was mainly composed of galactose, glucose, fructose, and arabinose. NMR and methylation analyses indicated that LHPW was a neutral polysaccharide with a backbone containing →3,6)-β-D-Galp-(1→, →4)-β-D-Galp-(1→ and →4)-α-D-Glcp-(1→, with the branches of →1)-β-D-Fruf-(2→ and →6)-α-D-Galp-(1→. Immunological tests indicated that LHPW could activate macrophage RAW264.7 and promote splenocyte proliferation. This study discovered a novel polysaccharide from Lycopi Herba and showed it was a potential immunomodulator.

Keywords: Lycopi Herba, polysaccharide, structure, immunological activity, NF-κB pathway

OPEN ACCESS

Edited by:
Jing Zhao,
University of Macau, China

Reviewed by:
Kit Leong Cheong,
Shantou University, China
Kambiz Jahanbin,
Shahrood University of Technology, Iran

****Correspondence:***
Wuxia Zhang
wuxia200758@163.com
Peng Li
lipengcuc@163.com

Specialty section:
This article was submitted to Inflammation Pharmacology, a section of the journal Frontiers in Pharmacology

Received: *07 April 2021*
Accepted: *07 June 2021*
Published: *25 June 2021*

Citation:
Zhang W, Hu Y, He J, Guo D, Zhao J and Li P (2021) Structural Characterization and Immunomodulatory Activity of a Novel Polysaccharide From Lycopi Herba. Front. Pharmacol. 12:691995. doi: 10.3389/fphar.2021.691995

INTRODUCTION

By virtue of the efficacy and safety, traditional Chinese medicine (TCM) is getting back up to a crucial status in the health area (Zhang et al., 2020). Among them, Lycopi Herba from the dry overground part of the Labiaceae plant *Lyscopus lucidus* Turcz. var. hirtus Regel is a traditional Chinese medicine that is mainly used for promoting blood circulation, removing blood stasis, and strengthening immunity (Lee et al., 2010). Modern pharmacological research displayed that Lycopi Herba possesses a series of activities such as cardiotonic, anti-allergic, anti-inflammatory, anticancer, and antithrombotic activities (Shin et al., 2005; Lee et al., 2008; Kim and Oh, 2018), while it is still unclear which components are mainly responsible for its biological activities. In recent years, some components have been identified for Lycopi Herba, such as luteolin-7-O-β-D-glucuronide methyl ester, phenolic compounds, and oligosaccharides (Lee et al., 2010; Yang et al., 2010; Lu et al., 2018). Among the kinds of components, polysaccharides have received a lot of attention in recent years for their variety of bioactivities, such as immunomodulatory, antitumor, antioxidative, and hypoglycemic activities with lower toxicity and side effects (Kardošová and Machová, 2006; Schepetkin and Quinn, 2006). However, little is known about the polysaccharides of Lycopi Herba for their structures and biological activities.

Here, we aimed to detect polysaccharides from Lycopi Herba and examine their biological activities. As the unique structural features, polysaccharides usually interact with the immune system in the human body and demonstrate immunoregulatory activities. Some polysaccharides such as

lentinan have been developed as immunomodulators (Deng et al., 2020). Therefore, we also mainly focused on the immunoregulatory abilities of polysaccharides from Lycopi Herba.

Generally, polysaccharides were extracted from Lycopi Herba and purified by DEAE-52 cellulose chromatography and G-100 sephadex. The monosaccharide composition was analyzed by high-performance liquid chromatography. The polysaccharide backbone was characterized by NMR and methylation analyses. The immunomodulatory ability of polysaccharides was determined by using the phagocytic capacity and lymphocyte proliferation assay. As a result, a neutral polysaccharide LHPW was obtained from Lycopi Herba. The structure of LHPW, including molecular weight, monosaccharide composition, and glycosyl linkages, was systematically characterized. The immunological examination showed that LHPW could activate macrophage RAW264.7 and promote splenocyte proliferation, indicating LHPW might be a potential immunomodulatory agent.

MATERIALS AND METHODS

Herbs and Chemicals

Dried Lycopi Herba was purchased from Bozhou of Anhui Province in China, and identified by the Laboratory of Chinese Medicine, College of Life Sciences, Shanxi Agricultural University. A voucher specimen (No. 20200832) has been deposited at the Laboratory of Functional Polysaccharides, Shanxi Agricultural University. Bovine serum albumin and standard monosaccharides were purchased from Solarbio Science & Technology Co., Ltd. (Beijing, China). Lipopolysaccharide (LPS), 3-(4,5-dimethyl-2-triazolyl)-2,5-diphenyltetrazolium bromide (MTT), trifluoroacetic acid (TFA), and concanavalin A (ConA) were purchased from Sigma-Aldrich. (E)-3-[(4-methylphenylsulfonyl]-2-propenenitrile (BAY 11-7082) was purchased from Beyotime Biotech. All other chemicals were of analytical grade as available.

Animals and Cells

Kunming mice were purchased from Shanxi Medical University, China. The mice were maintained on a standard pellet diet and water *ad libitum* at 21°C. All experiments were performed under the Regulations of Experimental Animal Administration issued by the State Committee of Science and Technology of the People's Republic of China. The RAW264.7 cell line was previously preserved in our laboratory. Spleen lymphocytes were obtained by cell strainers and red blood cell lysis buffer.

Extraction and Purification of Crude Polysaccharide

The dried Lycopi Herba powder was defatted and extracted three times with distilled water at 80°C for 2 h at the ratio of 1:10 (W/V). The supernatants were concentrated and collected with three times alcohol sedimentation. The precipitate was dissolved, dialyzed, and lyophilized to obtain Lycopi Herba crude polysaccharide (LHP). After being purified by DEAE-cellulose column (OH^- form) and sephadex G-100 which was eluted with distilled water, polysaccharide LHPW was obtained. Endotoxin contamination was routinely monitored in the laboratory using a chromogenic Limulus Amebocyte Lysate Assay Kit (Xiamen Limulus Reagent Factory, China). LPS existed at a concentration of <0.1 ng/ml in the preparation of LHPW.

Characterization of Polysaccharide

Molecular Weight Determination

As described previously (Zhang et al., 2013), the molecular weight of LHPW was determined by high-performance gel permeation chromatography (HPGPC) on three columns (Waters Ultrahydrogel 250, 1,000, and 2,000; 30 cm × 7.8 mm; 6 μm particles) in series. The columns were calibrated with T-series Dextrans (5.2, 11.6, 23.8, 48.6, 148, 273, and 410 kDa). Sodium acetate (3 mM) was used as eluant, and the flow rate was kept at 0.5 ml/min. 100 μl sample was injected for each run. The calibration curve of log (Mw) vs. elution time (T) is as follows: log (Mw) = −0.1719 T + 11.58.

Infrared Spectra Analysis

2 mg purified LHPW was ground with dried KBr and pressed into a pellet for Fourier transform infrared spectrophotometer (BRUKER TENSOR 27, BRUCK, Germany) measurement between 400 and 4,000 cm^{-1} (Zhao et al., 2014).

Chemical Composition Analysis

The contents of neutral carbohydrates, proteins, and uronic acids in LHPW were determined by the phenol–sulfuric acid method, Bradford's method, and *m*-hydroxydiphenyl–sulfuric acid method, respectively. Monosaccharide compositions were analyzed by high-performance anion exchange chromatography (HPAEC) after being hydrolyzed by the 3 M trifluoroacetic acid (TFA) for 2 h (Hu et al., 2020). The hydrolysates were dried by adding 200 μl methanol under nitrogen flow twice, diluted with deionized water, and filtered before injections. A Dionex ICS-5000 (Thermo Scientific Co., Waltham, MA, United States) equipped with a CarboPac™ PA-20 analytical column (3 mm × 150 mm) and an electrochemical detector was employed. Gradient elution with mobile phase NaOH (15 mM) and sodium acetate (100 mM) containing a fixed 15 mM NaOH was employed, and the flow rate was 0.3 ml/min. The column temperature was set at 30°C. Sixteen monosaccharides such as fucose (Fuc), galactosamine (GalN), rhamnose (Rha), arabinose (Ara), glucosamine (GlcN), galactose (Gal), glucose (Glc), N-acetyl-D-glucosamine (GlcNAc), xylose (Xyl), mannose (Man), fructose (Fru), ribose (Rib), galacturonic acid (GalA), guluronic acid (GulA), glucuronic acid (GlcA), and mannuronic acid (ManA), were used as standards. The monosaccharides were identified and quantified by the retention times and corresponding calibration curves of the pure standards. The content of each monosaccharide was expressed as mol% of the total content of monosaccharides.

Methylation Analysis

The glycosidic linkages of LHPW were analyzed by methylation analysis based on our previous method with some changes (Zhang et al., 2016). 3 mg dried LHPW was dissolved in 1 ml dried dimethyl sulfoxide (DMSO). After the addition of NaOH, the mixture was sonicated. Methyl iodide (3.6 ml) was added as the methylation reagent, and the mixture was stirred for 60 min at 30°C. The per-methylated product was hydrolyzed, reduced, and acetylated. The partially methylated alditol acetates were analyzed using a gas chromatography–mass spectrometry (GC–MS) system (Shimadzu GCMS-QP 2010) equipped with an RXI-5 SIL MS column (30 m × 0.25 mm × 0.25 μm). The temperature program was started at 120°C, followed by a 3°C/min gradient up to 250°C, isothermal for 5 min. The inlet temperature was 250°C, the detector temperature was 250°C/min, the carrier gas was helium, and the flow rate was 1 ml/min.

Nuclear Magnetic Resonance Analysis

50 mg dried LHPW was dissolved in 2 ml of D_2O and lyophilized. This procedure was repeated three times to completely replace H with D, and the sample was finally dissolved in 0.5 ml D_2O for NMR analysis. Deuterated acetone was used as the internal reference. The ^1H NMR, ^{13}C NMR, ^1H-^1H COSY, HSQC, and HMBC spectra of LHPW were recorded with a Bruker AM 500 spectrometer with a dual probe in the FT mode at room temperature.

Determination of Immunomodulatory Effects of Polysaccharide

Determination of the Phagocytic Capacity and TNF-α Production

RAW 264.7 cells were cultured in 96-well plates (1×10^5 cells/well) and incubated for 24 h. Then cells were treated with various concentrations of LHPW (50, 100, and 200 μg/ml) or LPS (2 mg/ml) for 24 h. The cell supernatants were collected and stored at −80°C. TNF-α proteins were measured using the enzyme-linked immunosorbent assay (ELISA) kits (R&D) according to the instructions. Then 0.5 mg/ml MTT was added to the plates and further incubated for 4 h at 37°C. The optical density was measured at 570 nm. Also, RAW 264.7 cells were pretreated with PBS or BAY 11-7082 (3 μM) for 1 h before incubation with 200 μg/ml or 2 μg/ml LPS for 24 h. Then the TNF-α proteins were measured.

The phagocytic ability of macrophages was measured using neutral red uptake. Cells (1×10^5 cells/well) were pipetted into 96-well plates and treated with various concentrations of LHPW (50, 100, and 200 μg/ml) for 12 h. Then 0.07% neutral red solution was added and incubated for 2 h. The medium was discarded, and cells were washed twice with PBS. Lysis buffer (1% glacial acetic acid: ethanol = 1:1, 100 μl/well) was added, and the optical density of each well was measured at 540 nm. The RMPI1640 medium and LPS (2 μg/ml) were used as the blank and positive control, respectively. The phagocytosis index was calculated by the following equation:

$$\text{Phagocytosis index} = \frac{\text{Abs}_{\text{sample}}}{\text{Abs}_{\text{blank control}}}. \quad (1)$$

NF-κB Activation and Nuclear Translocation Assay

The RAW 264.7 cells were immunofluorescence-labeled according to the manufacturer's instruction using a Cellular NF-κB Translocation Kit (Beyotime Biotech) (Xu et al., 2008). Briefly, after washing and fixing, cells were incubated with a blocking buffer for 1 h to block nonspecific binding. Next, cells were incubated with the primary NF-κB p65 antibody for 1 h, followed by incubation with a FITC-labeled Goat Anti-Rabbit IgG (H+L) secondary antibody for 1 h, and then with 4′,6-diamidino-2-phenylindole (DAPI) for 5 min before observation. Finally, p65 protein (green) and nuclei fluoresce (blue) were viewed by laser confocal microscopy.

Lymphocyte Proliferation Assay

Lymphocyte proliferation assays were evaluated *in vitro* by the MTT method. The cells (1×10^7/ml) were incubated with different concentrations of LHPW (50, 100, and 200 μg/ml) with or without Con A (5 μg/ml) and LPS (2 μg/ml) for 48 h. MTT was added, and the samples were further incubated for 4 h at 37°C. The optical density was measured at 570 nm.

Statistical Analysis

Results were expressed as mean ± SD. Statistical analyses were performed with one-way or two-way ANOVA by using the GraphPad Prism 5.0 software. One-way ANOVA analysis was used for the statistical analysis among three or more groups of an experiment with one factor. Two-way ANOVA was used for the statistical analysis of the experiment with two factors.

RESULTS

Extraction, Isolation, and Purification of Polysaccharide

The extraction and purification scheme of polysaccharide LHPW is shown in **Figure 1**. Crude polysaccharide LHP was isolated from Lycopi Herba with a yield of 2.70 ± 0.15%, through hot water extraction, followed by ethanol precipitation and lyophilization. DEAE-52 cellulose column (OH^- form) and G-100 sephadex were applied for further purification of the LHP. Finally, a novel heteropolysaccharide designated LHPW was obtained, with the yield of 2.53 ± 0.17% from LHP.

Molecular Weight Determination

The molecular weight of the polysaccharides is closely related to their physicochemical properties and biological activities (Duan and Kasper, 2011). The molecular weight of LHPW was calculated to be 5,255 Da (T: 45.750 min) in reference to standard dextrans (**Supplementary Figure S1A**). The symmetrical narrow peak on HPGPC indicated the molecular weight homogeneity and the high purity of LHPW.

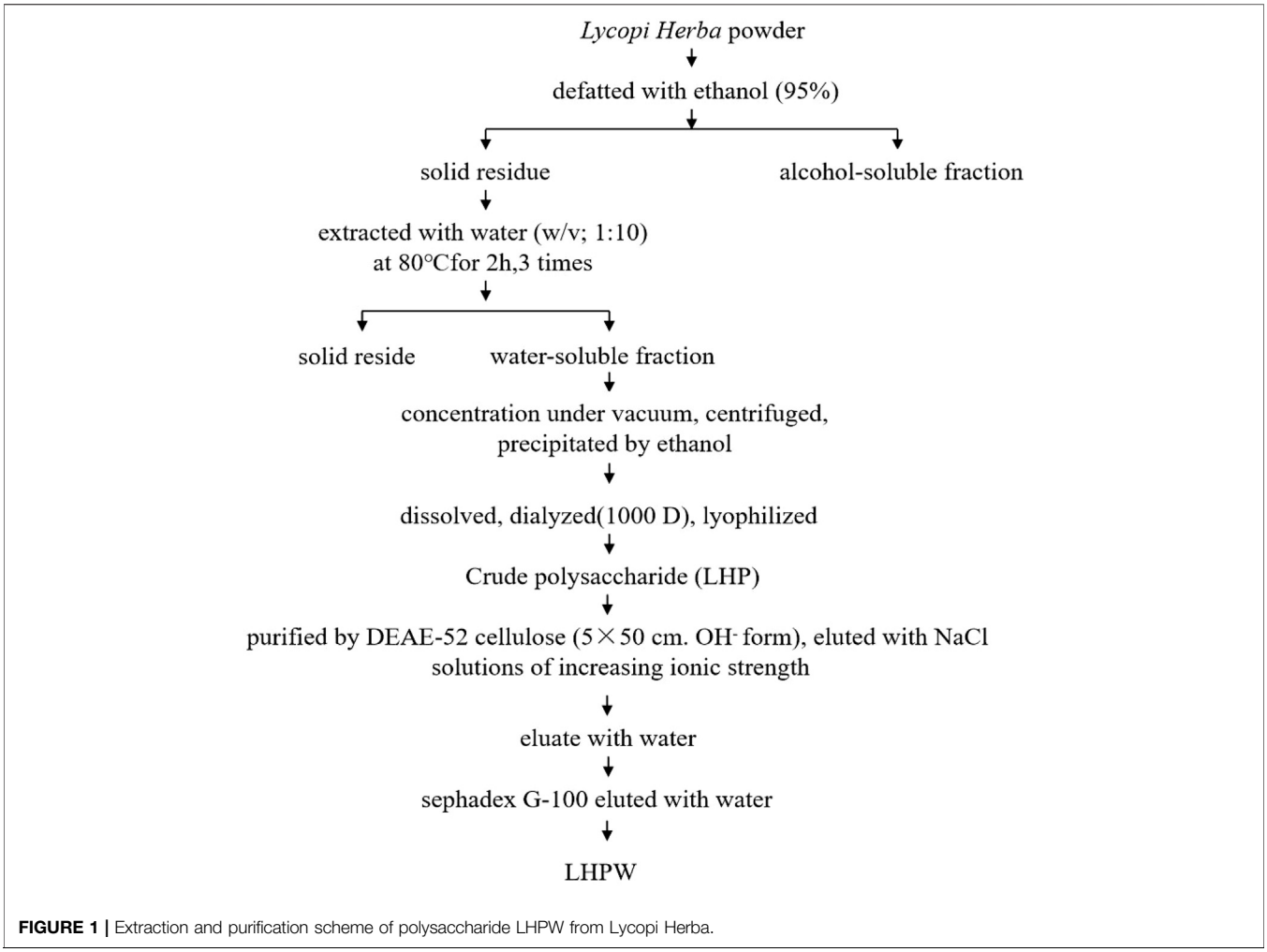

FIGURE 1 | Extraction and purification scheme of polysaccharide LHPW from Lycopi Herba.

Infrared Spectra Analysis

FTIR spectra of LHPW are shown in **Supplementary Figure S1B**. A typical absorbance band at 3391.81 cm^{-1} was due to the hydroxyl groups stretching vibration in the constituent sugar residues. The bands in the region of 2932.34 cm^{-1} were the characteristic absorption of C-H stretching vibration in the sugar ring. The absorbance peaks near 1640.32 cm^{-1} suggested that uronic acid content was low in LHPW. The peaks nearby 1,350–1,450 cm^{-1} may be caused by the variable angular vibration of C–H. The peaks at 950–1,200 cm^{-1} suggested the presence of C–O–C and C–O chemical bonds (Kačuráková et al., 2000). The peaks nearby 937 and 818 cm^{-1} were the characteristic absorption peaks of furanose.

Chemical Compositions and Neutral Monosaccharide Composition Analysis

The preliminary chemical composition results showed that the neutral carbohydrate, protein, and uronic acid contents of LHPW were 96.20 ± 2.85%, 4.18 ± 0.34%, and 3.51 ± 0.32%, respectively. These results showed that LHPW was mainly composed of neutral carbohydrates.

To determine the monosaccharide composition, LHPW was hydrolyzed by trifluoroacetic acid, and the hydrolysates were analyzed by high-performance anion exchange chromatography (HPAEC). As shown in **Figure 2**, the monosaccharide composition analysis indicated that LHPW was mainly composed of galactose, glucose, fructose, arabinose, and mannose at a molar ratio of 48.7:24.2:15.4:10.5:1.2. Galacturonic acid (GalA), glucuronic acid (GlcA), guluronic acid (GulA), and mannuronic acid (ManA) were used as four uronic acid standards. The absence of peaks in the corresponding positions of the samples indicated that there was no uronic acid in the polysaccharide LHPW.

Methylation Analysis

After two times methylation, the infrared spectra results show that the methylation is complete (**Supplementary Figure S2**). Methylated LHPW was analyzed by GC-MS in this experiment to elucidate the types of glycosyl linkages (**Table 1**). The GC-MS chromatogram was included as Supporting Material (**Supplementary Figure S3**). In the methylation process, 1,2-Fruf were reduced to 1,2-Manp and 1,2-Glcp, so we can obtain the methylated sugar 3,4,6-Me3-Manp and 3,4,6-Me3-Glcp. The

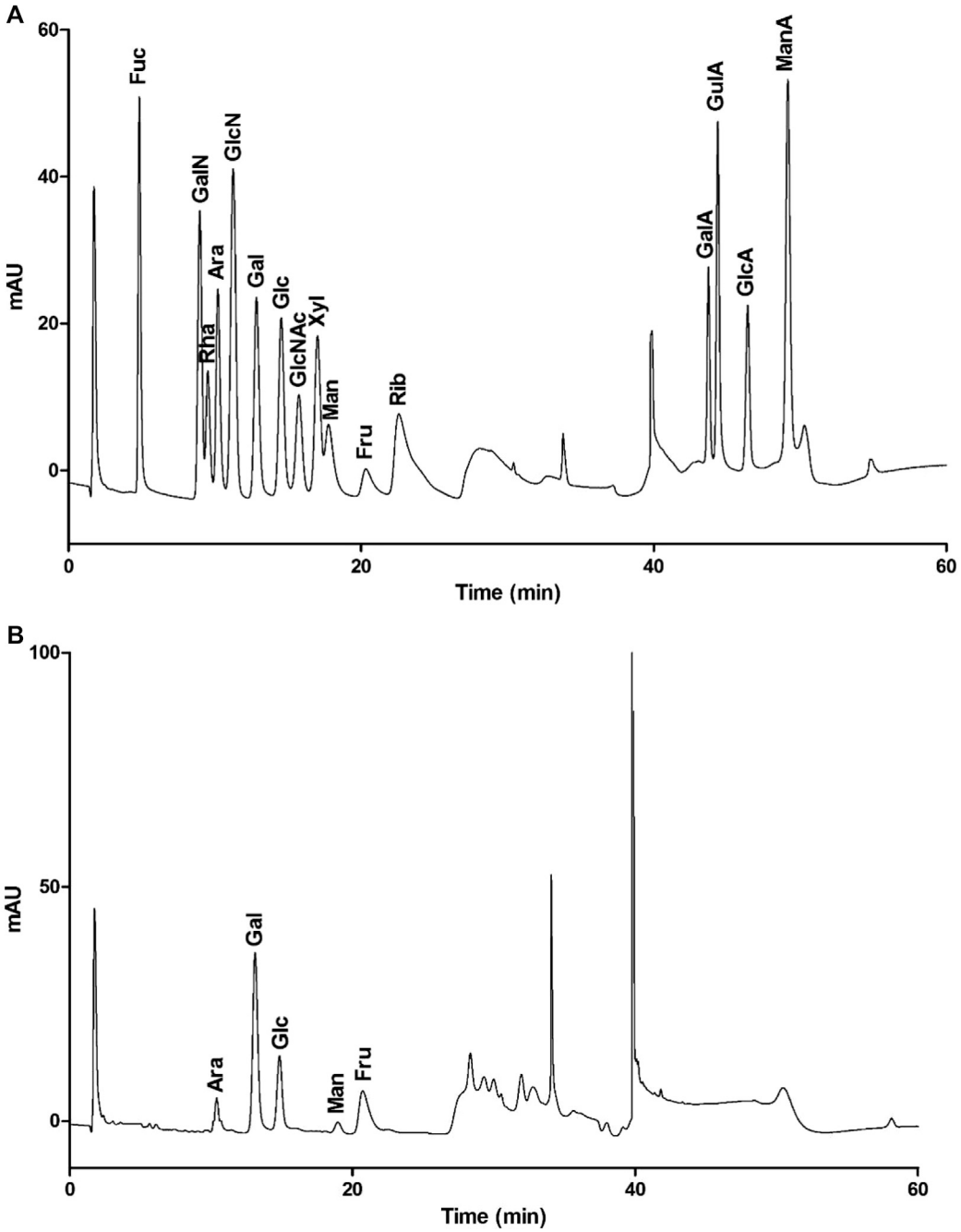

FIGURE 2 | Monosaccharide composition of mixed monosaccharide standards **(A)** and LHPW **(B)**.

total amount of nonreducing terminals was consistent with that of branching residues, suggesting that LHPW was a branched polysaccharide (Chen et al., 2019).

Nuclear Magnetic Resonance Analysis

Nuclear magnetic resonance (NMR) spectroscopy was used to reveal the precise structural information of LHPW. The C/H chemical shifts of all monosaccharide residues were assigned as completely as possible and listed in **Table 2** based on the above results, 2D NMR spectra, and data available in the literature (Han et al., 2018; Chen et al., 2019). In the ^{1}H NMR spectrum of LHPW (**Figure 3A**), signals at δ 4.88, 5.29, 5.32, 4.41, 4.88, and 5.14 ppm corresponded to H-1 of **A**, **B**, **E**, **F**, **G**, and **H**, respectively. The resonances in the region of 90–109 ppm in ^{13}C NMR were attributed to the anomeric carbon atoms of LHPW. As shown in **Figure 3B**, the main signals at δ 99.10, 104.69, 93.76, 104.47 99.10, and 105.17 ppm were assigned to the C-1 of **A**, **C**, **E**, **F**, **G**, and C-2 of **D**, respectively. In the DEPT-135 spectra, the inverted

TABLE 1 | Methylation analysis of LHPW.

No.	Rt	Methylated sugar	Mass fragments (m/z)	Molar ratios	Type of linkage
1	9.375	2,3,5-Me_3-Araf	43,71,87,101,117,129,161	2.28	Araf-(1→
2	13.033	3,4-Me2-Arap	43,71,87,99,101,113,117,129,161,189	1.53	→2)-Arap-(1→
3	14.538	2,3-Me2-Arap	43,71,87,101,117,129,161,189	1.83	→4)-Arap-(1→
4	16.228	2,3,4,6-Me_4-Glcp	43,71,87,101,117,129,145,161,205	5.89	Glcp-(1→
5	17.451	2,3,4,6-Me_4-Galp	43,71,87,101,117,129,145,161,205	4.67	Galp-(1→
6	20.488	3,4,6-Me3-Manp	43,71,87,99,101,129,161,189	4.44	→1)- Fruf--(2→
7	20.828	3,4,6-Me3-Glcp	43,71,87,99,101,129,161,189	7.55	→1)- Fruf--(2→
8	21.07	2,3,6-Me3-Galp	43,87,99,101,113,117,129,131,173,233	6.14	→4)-Galp-(1→
9	21.388	2,3,6-Me3-Glcp	43,87,99,101,113,117,129,131,173,233	9.47	→4)-Glcp-(1→
10	22.213	2,4,6-Me3-Galp	43,87,99,101,117,129,161	1.23	→3)-Galp-(1→
11	22.404	2,3,4-Me3-Glpc	43,87,99,101,117,129,161,189	3.01	→6)-Glcp-(1→
12	22.67	2,3,4-Me3-Manp	43,87,99,101,117,129,161,189	1.38	→6)-Manp-(1→
13	24.407	2,3,4-Me3-Galp	43,87,99,101,117,129,161,189	39.56	→6)-Galp-(1→
14	29.558	2,4-Me2-Galp	43,87,101,117,129,159,189,233	10.02	→3,6)-Galp-(1→

TABLE 2 | ^{1}H NMR and ^{13}C NMR spectral assignments for LHPW.

Residues	Glycosyl residues	H1a,b	H2	H3	H4	H5	H6a.b	
		C1	C2	C3	C4	C5	C6	
A	→6)-α-D-Galp-(1→	4.88	3.76	3.84	4.07	3.98	3.79	3.57
		99.10	69.71	70.73	70.08	70.66	67.78	
B	→4)-α-D-Glcp-(1→	5.29	3.53	3.86	3.54	3.75	3.78	ns
		101.14	72.88	74.58	78.35	72.53	61.95	
C	→3,6)-β-D-Galp-(1→	4.44	3.54	3.65	4.07	3.84	3.93	3.83
		104.69	71.31	81.5	69.82	74.81	70.76	
D	→1)-β-D-Fruf-(2→	3.80,3.60	ns	4.15	3.99	3.75	3.65	3.73
		62.13	105.17	78.3	75.63	82.41	63.47	
E	α-D-Glcp-(1→	5.32	3.44	3.65	3.36	3.75	3.71	3.61
		93.76	72.59	73.98	70.59	75.74	61.67	
F	→4)-β-D-Galp-(1→	4.41	3.45	3.57	3.96	3.44	3.56	
		104.47	73.21	73.97	79.03	74.36	62.74	
G	α-D-Galp-(1→	4.88	3.74	3.84	3.96	4.07	3.79	3.57
		99.1	69.7	70.7	72.52	70.08	62.78	
H	α-L-Araf-(1→	5.14	4.1	3.84	4.03	3.73	3.61	
		110.62	82.62	77.97	85.22	62.64		

*Note: **A**-**H** represent the Glycosyl residues in the corresponding rows.*

signal at δ 67.78, 63.47, 62.78, and 62.64 ppm were attributed to C-6 of **A**, **D**, **G**, and C-5 of **H** residues, respectively (**Figure 3C**). In agreement with the results of monosaccharide composition, there was no absorption peak near 170–180 ppm in ^{13}C NMR, which confirms that there was no uronic acid in LHPW (**Supplementary Figure S4**).

The COSY (**Supplementary Figure S5A**) and HSQC spectrum (**Supplementary Figure S5B**) were employed to analyze the assignation of other signals in ^{1}H NMR and ^{13}C NMR. The corresponding heterocephalic hydrogen signal and heterocephalic carbon signal of residue **A** were 99.10 and 4.88 ppm in the HSQC. The cross peaks at δ H/H 4.88/3.76, 3.76/3.84, 3.84/4.07, and 4.07/3.98 ppm were detected in ^{1}H–^{1}H COSY, which suggested that the signals at δ 4.88, 3.76, 3.84, 4.07, and 3.98 ppm corresponded to H-1, H-2, H-3, H-4, and H-5 of the residue →6)-α-D-Galp-(1→ (residue **A**), respectively. According to HSQC, C-1, C-2, C-3, C-4, and C-5 of the residue A were δ 99.10, 69.71, 70.73, 70.08, and 70.66 ppm, respectively. The chemical shift of C-6 was 67.78 ppm.

The corresponding heterocephalic hydrogen signal of heterocephalic carbon signal δ104.47 is δ4.41 in the HSQC. The cross peaks at δH/H 4.41/3.45, 3.45/3.57, 3.57/3.96, and 3.96/3.44 ppm were detected in ^{1}H–^{1}H COSY, which suggested that the signals at δ4.41, 3.45, 3.57, 3.96, and 3.44 ppm corresponded to H-1, H-2, H-3, H-4, and H-5 of the residue →4)-β-D-Galp-(1→ (residue **F**), respectively. Corresponding C-1, C-2, C-3, C-4, C-5, and C-6 were δ104.47, 73.21, 73.97, 79.03, 74.36, and 62.74, respectively. Similarly, the other proton and carbon signals of the rest of the residues were analyzed by the same method.

For fructose residues, the signal at δ105.17 ppm was the typical peak of →1)-β-D-Fruf-(2→, which was assigned to C-2 of fructose. Other carbon signals at 62.13, 78.3, 75.63, 82.41, and 63.47 ppm were correspondingly assigned to C-1, C-3, C-4, C-5, and C-6 of →1)-β-D-Fruf-(2→.

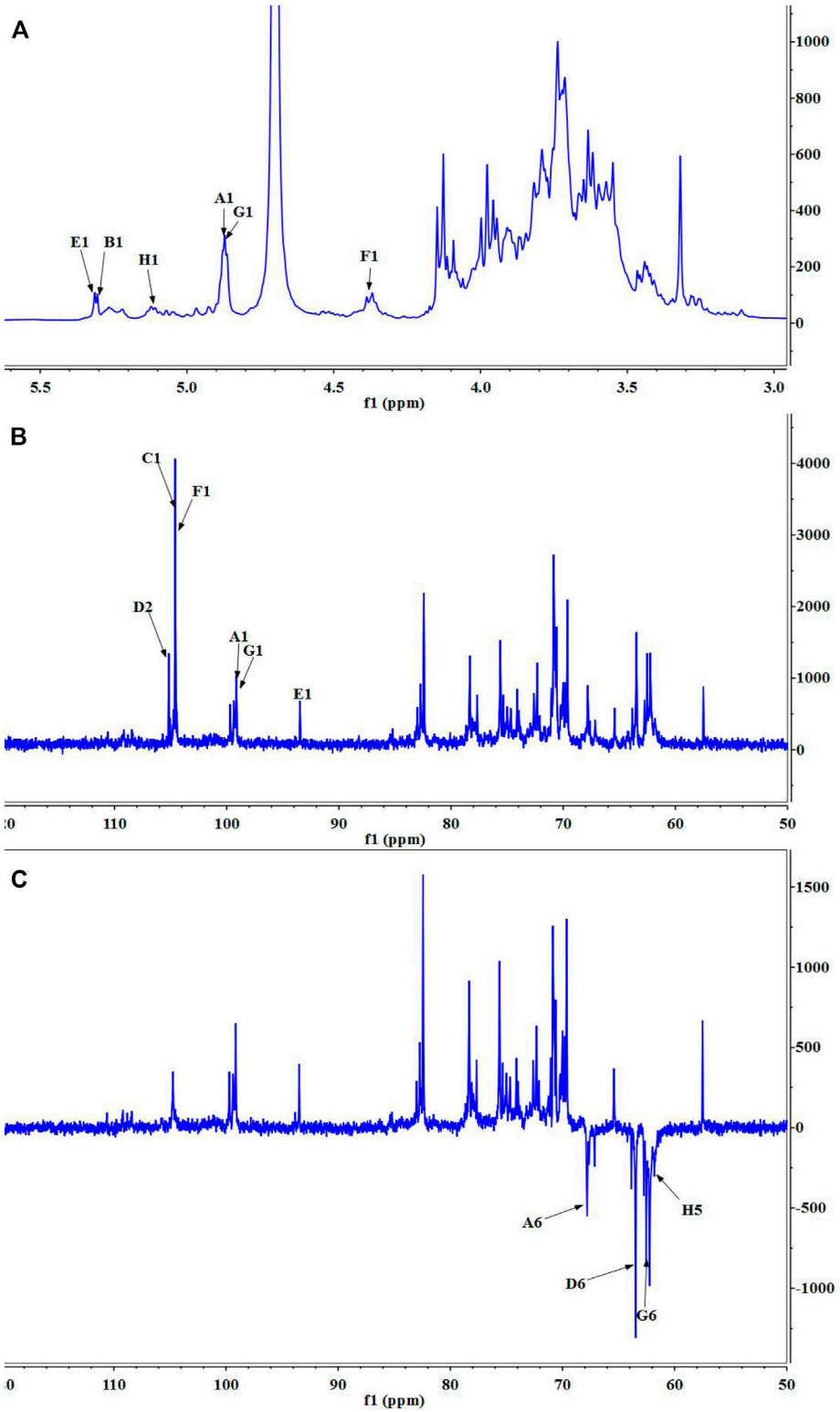

FIGURE 3 | 1D NMR spectra of LHPW: **(A)** ^{1}H NMR, **(B)** ^{13}C HMR, and **(C)** DEPT 135. Same as **Table 2**, A–H represent the Glycosyl residues →6)-α-D-Galp-(1→, →4)-α-D-Glcp-(1→, →3,6)-β-D-Galp-(1→, →1)-β-D-Fruf-(2→, α-D-Glcp-(1→, →4)-β-D-Galp-(1→, α-D-Galp-(1→, α-L-Araf-(1→. The number 1–6 represent the location of hydrogen or carbon in the Glycosyl residues.

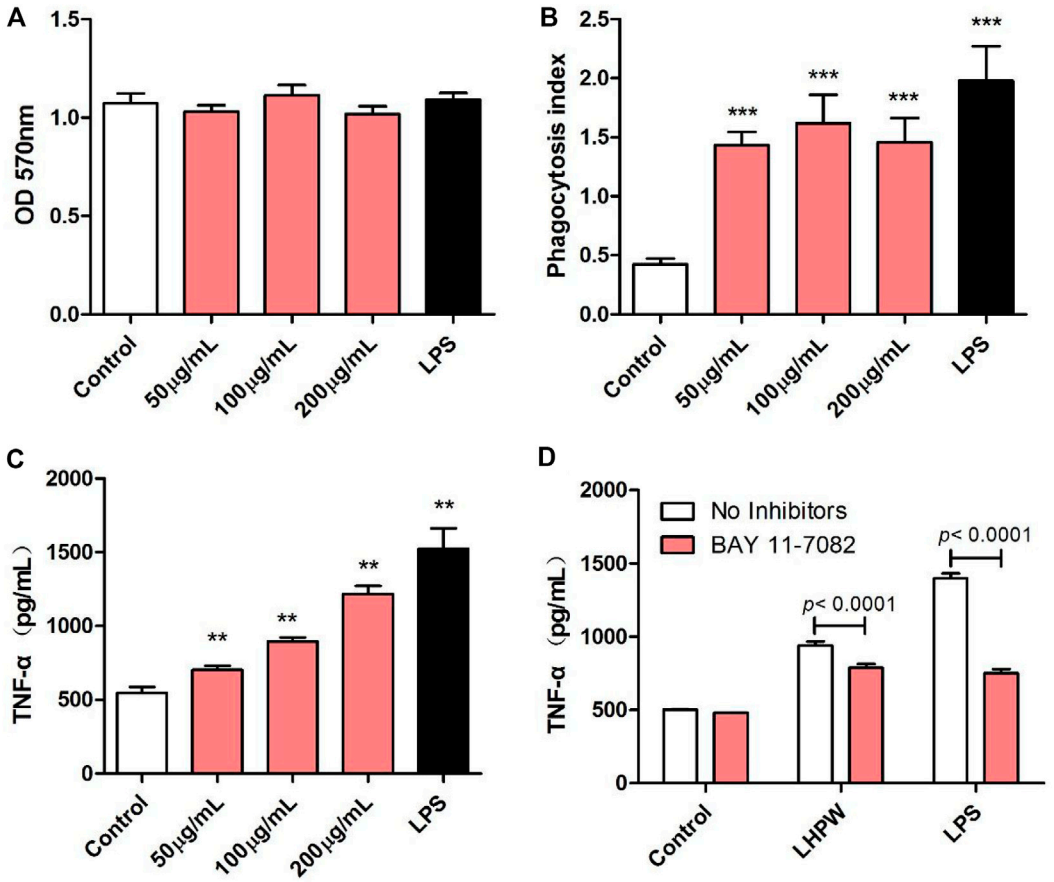

FIGURE 4 | Effects of LHPW on the phagocytosis index, TNF-α production of RAW 264.7 cells. After RAW 264.7 cells were treated with various concentrations of LHPW (50, 100, and 200 μg/ml), the cell cytotoxicity **(A)**, neutral red phagocytosis index **(B),** and TNF-α production **(C)** were tested. Data shown were mean ± SD of three independent experiments. (***) $p < 0.001$, (**) $p < 0.01$, and (*) $p < 0.05$ compared with the control. **(D)** RAW 264.7 cells were pretreated with PBS (No inhibitors) or BAY 11-7082 (3 μM) for 1 h before incubation with 200 μg/ml LHPW or 2 μg/ml LPS for 24 h.

The HMBC spectra (**Supplementary Figure S5C**) were applied to confirm the glycosyl residues, backbone, and substitution sites of polysaccharides. In the HMBC spectrum, cross peak at δ 104.69/3.96 and δ 104.47/3.96 ppm represented the correlation between C-1 of residue **C** and H-4 of residue **F**, C-1 of residue **F** and H-4 of residue **B**, respectively. Based on the above results, the backbone of LHPW was confirmed by the linkages of →3,6)-β-D-Galp-(1→4)-β-D-Galp-(1→4)-α-D-Glcp-(1→. To further confirm the branches of LHPW, the HMBC spectrum for other residues was analyzed. Cross peaks C-2 and H-1a, b of residue **D** were detected in the HMBC, suggesting the presence of →1)-β-D-Fruf-(2→1)-β-D-Fruf-(2→. In addition, these cross peaks showed the correlation between C-2 of residue **D** and H-6a, b of residue **A**, C-1 and H-6a, b of residue **A**, C-1 of residue **A** and H-6 of residue **C**. The content of other glycoside bonds is relatively small, and no more connection information can be observed in HMBC. Therefore, the glycoside bonds of the main components are analyzed. Based on the above information, the possible structure of polysaccharide LHPW is proposed as **Supplementary Figure S6**.

Immunological Activities of Polysaccharide

Effects of LHPW on the Phagocytic Capacity and TNF-α Production of RAW 264.7 Cells

The immunologic action of polysaccharides usually begins with activating major immune cells such as macrophages, natural killer (NK) cells, and lymphocytes (Chen et al., 2012). Macrophages play a very important role in the immune system and perform various complex biological functions such as phagocytosis, surveillance, chemotaxis, and destruction of extraneous materials (Sica et al., 2008). Thus, the effects of LHPW on macrophages were first evaluated. MTT assay showed that LHPW had no cell cytotoxicity to RAW 264.7 cells at different concentrations (**Figure 4A**). As shown in **Figure 4B**, LHPW could remarkably enhance the phagocytosis of macrophages. Also, LHPW could significantly promote the TNF-a production of RAW 264.7 cells in a dose-dependent manner (**Figure 4C**).

Owing to the critical role of NF-κB in the progression of immunity, we detected the effect of LHPW on the activation of NF-κB. To determine whether this NF-κB activation was involved in LHPW-induced cytokine production, we treated RAW 264.7

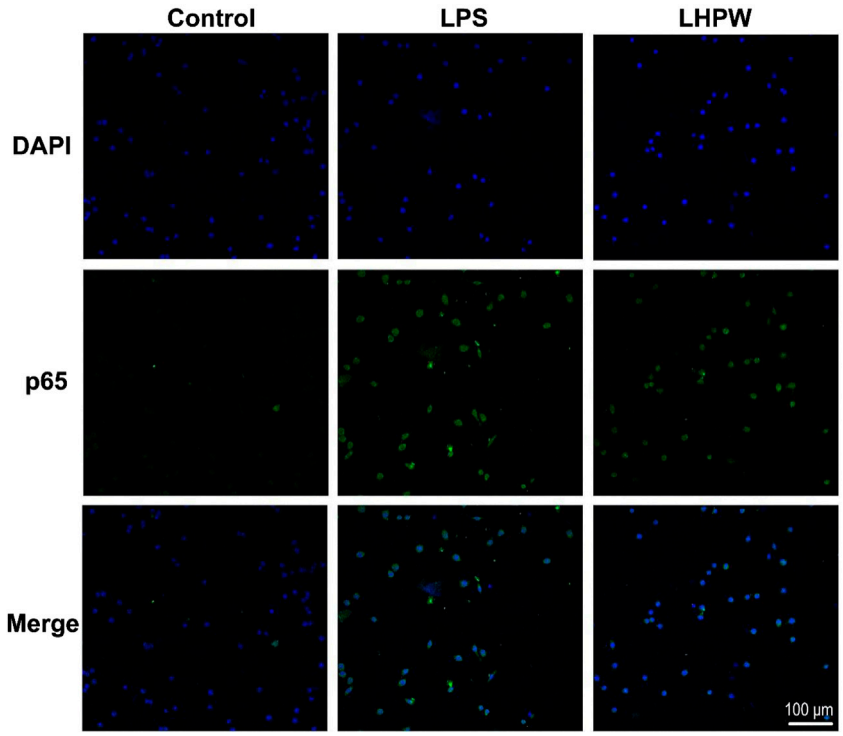

FIGURE 5 | LHPW activates the NF-κB p65 protein in RAW 264.7 cells. After being treated with 200 μg/ml LHPW or 2 μg/ml LPS for 3 h, NF-κB p65 protein translocated into nuclei (DAPI) was obtained by laser confocal microscopy. The scale bar was placed at the bottom right, and all images have the same scales.

cells with LHPW and LPS in the presence or absence of BAY 11-7082, a well-described inhibitor of NF-κB. Results showed that treatment with BAY 11-7082 at 3 μM partly suppressed TNF-α secretion induced by LHPW in RAW 264.7 cells (**Figure 4D**)

By the use of a Cellular NF-κB Translocation Kit, p65 protein translocation into nuclei was visualized in RAW 264.7 cells after exposure to LHPW and LPS. As shown in **Figure 5**, all stimuli resulted in the localization of the NF-κB transcription factor p65 protein in nuclei, indicating that LHPW could activate the key NF-κB protein p65 in the RAW 264.7 cells.

Effect of LHPW on Splenocyte Proliferation

The proliferation of spleen cells is one of the most important steps in the activation pathway of cell-mediated or humoral immunity (Zhao et al., 2006). The effects of the polysaccharide on lymphocyte proliferation were tested to examine the strength of immune-enhancing activity of LHPW. Concanavalin A (ConA) and lipopolysaccharide (LPS) were used to stimulate T-lymphocyte and B-lymphocyte proliferation, respectively (Cerqueira et al., 2004). As shown in **Figure 6A**, LHPW had the potential in promoting the proliferation of spleen lymphocytes. LHPW also could improve ConA-stimulated T-cell proliferation in a concentration-dependent fashion (**Figure 6B**). In addition, LHPW could not promote LPS-induced splenocyte proliferation (**Figure 6C**). Our results indicated that the novel heteropolysaccharide LHPW from Lycopi Herba mainly promoted T-cell–associated lymphocyte proliferation.

DISCUSSION

In recent years, only some oligosaccharides have been identified from Lycopi Herba. For example, stachyose is a tetrasaccharide composed of "Galactose–Galactose–Glucose–Fructose" and has been reported to have the ability to balance the intestinal micro-ecosystem by selective proliferation of the bifidobacteria. A mixture of α-galactooligosaccharides (GOS) from the roots of Lycopi Herba could elicit a significant increase in humoral immunity, and enhancing in splenocyte proliferation (Yang et al., 2010). However, there are still no bioactive polysaccharides extracted from Lycopi Herba. Here, we aimed to detect potential polysaccharides from Lycopi Herba and explore their structural and biological features.

As a result, a novel water-soluble polysaccharide LHPW with a molecular weight of 5,255 Da was first isolated from Lycopi Herba. The preliminary chemical component analysis indicated that LHPW was mainly composed of neutral carbohydrates (96.20 ± 2.85%). Monosaccharide composition analysis showed that LHPW was mainly composed of galactose, glucose, fructose, and arabinose, and contained no uronic acids. Moreover, ^{13}C NMR displayed that there were no peaks near 170–180 ppm, confirming no uronic acids in LHPW. All these results demonstrated that LHPW was a neutral polysaccharide with a backbone containing →3,6)-β-D-Galp-(1→, →4)-β-D-Galp-(1→ and →4)-α-D-Glcp-(1→, with the branches of →1)-β-D-Fruf-(2→ and →6)-α-D-Galp-(1→. The structural characteristics of polysaccharides, such as

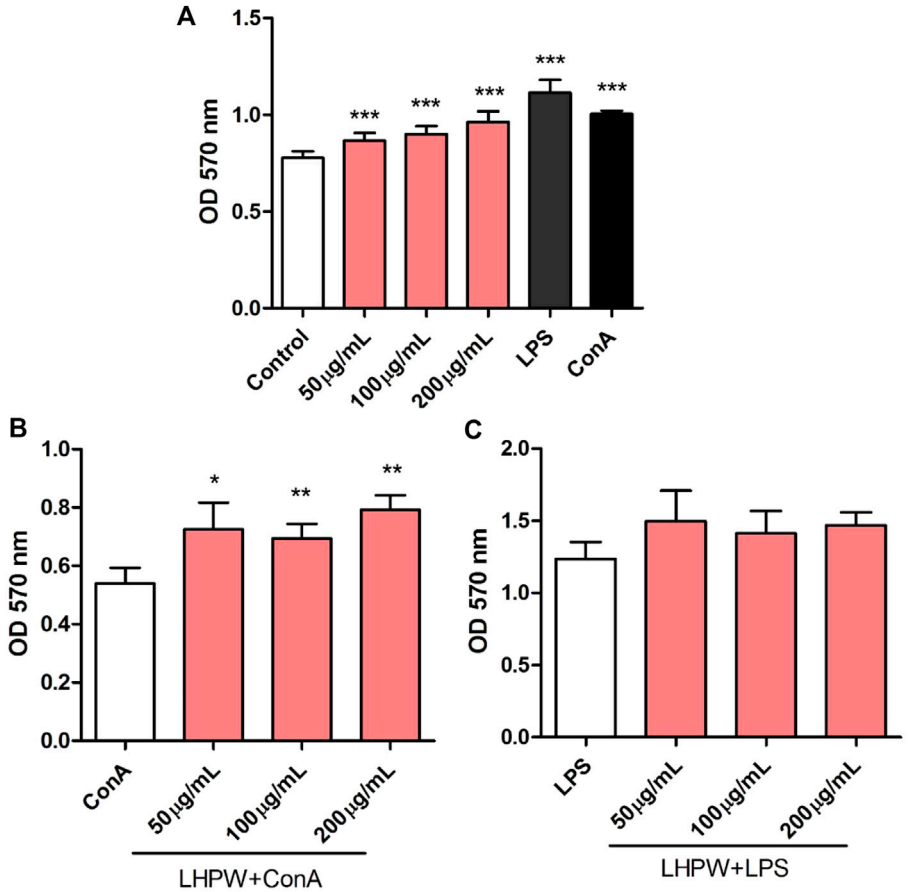

FIGURE 6 | Effects of LHPW on splenocyte proliferation. The mice spleen cells were incubated with LHPW at different concentrations (50, 100, and 200 μg/ml) alone **(A)**, in the presence of mitogens Con A (5 μg/ml) **(B)** or LPS (2 μg/ml) **(C)** for 48 h. MTT was added and incubated. The optical density was then measured at 570 nm. Data were shown as mean ± SD of three independent experiments. (***) $p < 0.001$, (**) $p < 0.01$, and (*) $p < 0.05$ compared with the control group **(A)**, ConA group **(B),** or LPS group **(C)**.

molecular weight, chemical composition, glycosidic linkage, conformation, and degree of branching, determine their immunomodulating actions (Methacanon et al., 2005). Previously, many studies have reported that neutral polysaccharides have potential as an immunomodulator or supplement in functional food to enhance immunity. For example, a neutral polysaccharide SMP-0b extracted from *Solanum muricatum* could significantly stimulate proliferation and NO production of RAW 264.7 macrophage cells (Yue et al., 2020); a neutral polysaccharide SPW-2, purified from the leaves of *Sambucus adnata* Wall, exerted an immunomodulatory effect by activating macrophages and enhancing the host immune system function (Yuan et al., 2020); a neutral polysaccharide WSRP-1b from *Kushui rose* waste possessed immunomodulatory activity by enhancing phagocytosis of macrophages, increasing the production of ROS, NO, cytokines (IL-6 and TNF-α), and activating the NF-κB signaling pathway (Wu et al., 2020). Inspired by these studies of the immunomodulatory activity of neutral polysaccharides, we also examined the immunomodulatory ability of LHPW through a series of experiments.

The immune response plays an important role in disease development because severe inflammation and suppressed immunization can increase the risk of infections, multiple organ failure, or death (Sharma et al., 2015). It has been reported that many traditional Chinese herbs with the effect of promoting blood circulation and removing blood stasis could also enhance the body's immune function, which was beneficial to balance immune responses to infection (Fan et al., 2020). To confirm the effect of LHPW on immune response and exposit the molecular mechanism, we used the macrophage RAW 264.7 as induced model cells. Our data indicated that LHPW can enhance the phagocytosis of macrophages, significantly promote the TNF-α production of RAW 264.7 cells, and activate the NF-κB p65 protein translocation into nuclei. Macrophages are immune effector cells that orchestrate a diverse array of functions, including inflammatory response, tissue repair, immune responses, and so on (Jang and Nair, 2013). Thus, our results suggested that LHPW could exert an immune effect by activating macrophages. TNF-α is a potent pro-inflammatory mediator secreted by activated M1 macrophages, which plays a variety of biological effects, such as cell differentiation, proliferation, and

multiple pro-inflammatory effects (Wu et al., 2015). Many studies have found that autoimmune-related disorders are correlated with downregulated TNF-α expression (Elenkov and Chrousos, 2002; Russo and Polosa, 2005). Therefore, LHPW which could promote the TNF-α production may have a therapeutic and preventive effect on these diseases. Splenocyte proliferation assay showed it can promote the proliferation of spleen lymphocytes and ConA-stimulated T cells. It should be noted that the immunological study for LHPW here is still preliminary, and more in-depth studies are needed in the following work. Nevertheless, these data implied the novel polysaccharide LHPW from Lycopi Herba had the potential to be a natural immunoregulatory supplement for preparing functional foods and nutraceuticals.

DATA AVAILABILITY STATEMENT

The original contributions presented in the study are included in the article/**Supplementary Material**; further inquiries can be directed to the corresponding authors.

AUTHOR CONTRIBUTIONS

WZ designed the research, performed the experiments, analyzed the data, and wrote the manuscript. YH and JH performed the experiments and analyzed the data. and DG analyzed the NMR data. JZ and PL supervised the work and wrote and reviewed the manuscript.

FUNDING

This work was supported by the National Natural Science Foundation of China (Nos. 31800678 and 81703945), Science and Technology Innovation Fund of Shanxi Agricultural University (Nos. 2017YJ40 and 2016YJ17), and Science and Technology Innovation Project of Colleges and Universities in Shanxi Province (Nos. 2019L0365 and 2019L0360).

ACKNOWLEDGMENTS

The authors gratefully acknowledge the assistance of Yangzhou BoRui Saccharide Biotech Co. Ltd. (www.polyscilife.com) in data analysis.

SUPPLEMENTARY MATERIAL

The Supplementary Material for this article can be found online at: https://www.frontiersin.org/articles/10.3389/fphar.2021.691995/full#supplementary-material

REFERENCES

Cerqueira, F., Cordeiro-Da-Silva, A., Gaspar-Marques, C., Simões, F., Pinto, M. M. M., and Nascimento, M. S. J. (2004). Effect of Abietane Diterpenes from Plectranthus Grandidentatus on T- and B-Lymphocyte Proliferation. *Bioorg. Med. Chem.* 12 (1), 217–223. doi:10.1016/j.bmc.2003.10.006

Chen, X., Nie, W., Fan, S., Zhang, J., Wang, Y., Lu, J., et al. (2012). A Polysaccharide from Sargassum Fusiforme Protects against Immunosuppression in Cyclophosphamide-Treated Mice. *Carbohydr. Polym.* 90 (2), 1114–1119. doi:10.1016/j.carbpol.2012.06.052

Chen, W., Zhu, X., Ma, J., Zhang, M., and Wu, H. (2019). Structural Elucidation of a Novel Pectin-Polysaccharide from the Petal of Saussurea Laniceps and the Mechanism of its Anti-HBV Activity. *Carbohydr. Polym.* 223, 115077. doi:10.1016/j.carbpol.2019.115077

Deng, L. J., Qi, M., Li, N., Lei, Y. H., Zhang, D. M., and Chen, J. X. (2020). Natural Products and Their Derivatives: Promising Modulators of Tumor Immunotherapy. *J. Leukoc. Biol.* 108 (2), 493–508. doi:10.1002/JLb.3mr0320-444r

Duan, J., and Kasper, D. L. (2011). Oxidative Depolymerization of Polysaccharides by Reactive Oxygen/nitrogen Species. *Glycobiology* 21 (4), 401–409. doi:10.1093/glycob/cwq171

Elenkov, I. J., and Chrousos, G. P. (2002). Stress Hormones, Proinflammatory and Antiinflammatory Cytokines, and Autoimmunity. *Ann. N. Y Acad. Sci.* 966, 290–303. doi:10.1111/j.1749-6632.2002.tb04229.x

Fan, T.-T., Cheng, B.-L., Fang, X.-M., Chen, Y.-C., and Su, F. (2020). Application of Chinese Medicine in the Management of Critical Conditions: A Review on Sepsis. *Am. J. Chin. Med.* 48, 1315–1330. doi:10.1142/s0192415x20500640

Han, K., Jin, C., Chen, H., Wang, P., Yu, M., and Ding, K. (2018). Structural Characterization and Anti-a549 Lung Cancer Cells Bioactivity of a Polysaccharide from Houttuynia Cordata. *Int. J. Biol. Macromolecules* 120 (Pt A), 288–296. doi:10.1016/j.ijbiomac.2018.08.061

Hu, W., Ye, X., Chantapakul, T., Chen, S., and Zheng, J. (2020). Manosonication Extraction of RG-I Pectic Polysaccharides from Citrus Waste: Optimization and Kinetics Analysis. *Carbohydr. Polym.* 235, 115982. doi:10.1016/j.carbpol.2020.115982

Jang, J. C., and Nair, M. G. (2013). Alternatively Activated Macrophages Revisited: New Insights into the Regulation of Immunity, Inflammation and Metabolic Function Following Parasite Infection. *Curr. Immunol. Rev.* 9 (3), 147–156. doi:10.2174/15733955096613210232548

Kačuráková, M., Capek, P., Sasinková, V., Wellner, N., and Ebringerová, A. (2000). FT-IR Study of Plant Cell wall Model Compounds: Pectic Polysaccharides and Hemicelluloses. *Carbohydr. Polym.* 43(2), 195–203. doi:10.1016/S0144-8617(00)00151-X

Kardošová, A., and Machová, E. (2006). Antioxidant Activity of Medicinal Plant Polysaccharides. *Fitoterapia* 77 (5), 367–373. doi:10.1016/j.fitote.2006.05.001

Kim, K.-Y., Oh, T. W., Ma, J.-Y., and Park, K.-I. (2018). Ethanol Extract ofLycopus lucidusTurcz. Ex Benth Inhibits Metastasis by Downregulation of Runx-2 in Mouse Colon Cancer Cells. *Evidence-Based Complement. Altern. Med.* 2018, 1–8. doi:10.1155/2018/9513290

Lee, Y. J., Kang, D. G., Kim, J. S., and Lee, H. S. (2008). Lycopus Lucidus Inhibits High Glucose-Induced Vascular Inflammation in Human Umbilical Vein Endothelial Cells. *Vasc. Pharmacol.* 48 (1), 38–46. doi:10.1016/j.vph.2007.11.004

Lee, M.-J., Lee, H.-S., Park, S.-D., Moon, H.-I., and Park, W.-H. (2010). Protective Effects of Luteolin-7-O-β-D-Glucuronide Methyl Ester from the Ethyl Acetate Fraction of Lycopi Herba against Pro-oxidant Reactive Species and Low-Density Lipoprotein Peroxidation. *J. Enzyme Inhib. Med. Chem.* 25 (5), 702–707. doi:10.3109/14756360903524312

Lu, Y.-H., Tian, C.-R., Gao, C.-Y., Wang, W.-J., Yang, W.-Y., Kong, X., et al. (2018). Protective Effect of Free Phenolics from Lycopus Lucidus Turcz. Root on Carbon Tetrachloride-Induced Liver Injury *In Vivo* and *In Vitro*. *Food Nutr. Res.* 62, 1398. doi:10.29219/fnr.v62.1398

Methacanon, P., Madla, S., Kirtikara, K., and Prasitsil, M. (2005). Structural Elucidation of Bioactive Fungi-Derived Polymers. *Carbohydr. Polym.* 60 (2), 199–203. doi:10.1016/j.carbpol.2004.12.006

Russo, C., and Polosa, R. (2005). TNF-α as a Promising Therapeutic Target in Chronic Asthma: a Lesson from Rheumatoid Arthritis. *Clin. Sci. (Lond)* 109 (2), 135–142. doi:10.1042/cs20050038

Schepetkin, I. A., and Quinn, M. T. (2006). Botanical Polysaccharides: Macrophage Immunomodulation and Therapeutic Potential. *Int. Immunopharmacol.* 6 (3), 317–333. doi:10.1016/j.intimp.2005.10.005

Sharma, A., Yang, W.-L., Matsuo, S., and Wang, P. (2015). Differential Alterations of Tissue T-Cell Subsets after Sepsis. *Immunol. Lett.* 168 (1), 41–50. doi:10.1016/j.imlet.2015.09.005

Shin, T., Kim, S., Suk, K., Ha, J., Kim, I., Lee, M., et al. (2005). Anti-allergic Effects of on Mast Cell-Mediated Allergy Model. *Toxicol. Appl. Pharmacol.* 209 (3), 255–262. doi:10.1016/j.taap.2005.04.011

Sica, A., Allavena, P., and Mantovani, A. (2008). Cancer Related Inflammation: the Macrophage Connection. *Cancer Lett.* 267 (2), 204–215. doi:10.1016/j.canlet.2008.03.028

Wu, X., Xu, W., Feng, X., He, Y., Liu, X., Gao, Y., et al. (2015). TNF-a Mediated Inflammatory Macrophage Polarization Contributes to the Pathogenesis of Steroid-Induced Osteonecrosis in Mice. *Int. J. Immunopathol Pharmacol.* 28 (3), 351–361. doi:10.1177/0394632015593228

Wu, M., Feng, H., Song, J., Chen, L., Xu, Z., Xia, W., et al. (2020). Structural Elucidation and Immunomodulatory Activity of a Neutral Polysaccharide from the Kushui Rose (Rosa Setate X Rosa Rugosa) Waste. *Carbohydr. Polym.* 232**,** 115804. doi:10.1016/j.carbpol.2019.115804

Xu, Z., Lin, S., Wu, W., Tan, H., Wang, Z., Cheng, C., et al. (2008). Ghrelin Prevents Doxorubicin-Induced Cardiotoxicity through TNF-alpha/NF-Kb Pathways and Mitochondrial Protective Mechanisms. *Toxicology* 247 (2-3), 133–138. doi:10.1016/j.tox.2008.02.018

Yang, X., Zhao, Y., He, N., and Croft, K. D. (2010). Isolation, Characterization, and Immunological Effects of α-Galacto-oligosaccharides from a New Source, the Herb Lycopus Lucidus Turcz. *J. Agric. Food Chem.* 58 (14), 8253–8258. doi:10.1021/jf101217f

Yuan, L., Zhong, Z.-C., and Liu, Y. (2020). Structural Characterisation and Immunomodulatory Activity of a Neutral Polysaccharide from Sambucus Adnata Wall. *Int. J. Biol. Macromol.* 154, 1400–1407. doi:10.1016/j.ijbiomac.2019.11.021

Yue, H., Xu, Q., Bian, G., Guo, Q., Fang, Z., and Wu, W. (2020). Structure Characterization and Immunomodulatory Activity of a New Neutral Polysaccharide SMP-0b from Solanum Muricatum. *Int. J. Biol. Macromol.* 155, 853–860. doi:10.1016/j.ijbiomac.2019.11.071

Zhang, W., Mu, H., Zhang, A., Cui, G., Chen, H., Duan, J., et al. (2013). A Decrease in Moisture Absorption-Retention Capacity of N-Deacetylation of Hyaluronic Acid. *Glycoconj J.* 30 (6), 577–583. doi:10.1007/s10719-012-9457-3

Zhang, W., Li, P., Song, D., Niu, H., Shi, S., Wang, S., et al. (2016). Structural Characterization and Biological Activities of Two α-glucans from Radix Paeoniae Alba. *Glycoconj J.* 33 (2), 147–157. doi:10.1007/s10719-015-9647-x

Zhang, L., Yu, J., Zhou, Y., Shen, M., and Sun, L. (2020). Becoming a Faithful Defender: Traditional Chinese Medicine against Coronavirus Disease 2019 (COVID-19). *Am. J. Chin. Med.* 48 (4), 763–777. doi:10.1142/s0192415x2050038x

Zhao, C., Li, M., Luo, Y., and Wu, W. (2006). Isolation and Structural Characterization of an Immunostimulating Polysaccharide from Fuzi, Aconitum Carmichaeli. *Carbohydr. Res.* 341 (4), 485–491. doi:10.1016/j.carres.2005.11.032

Zhao, T., Mao, G., Feng, W., Mao, R., Gu, X., Li, T., et al. (2014). Isolation, Characterization and Antioxidant Activity of Polysaccharide from Schisandra Sphenanthera. *Carbohydr. Polym.* 105, 26–33. doi:10.1016/j.carbpol.2014.01.059

Conflict of Interest: The authors declare that the research was conducted in the absence of any commercial or financial relationships that could be construed as a potential conflict of interest.

frontiers in Pharmacology

ORIGINAL RESEARCH
published: 28 June 2021
doi: 10.3389/fphar.2021.688073

Bee Pollen Polysaccharide From *Rosa rugosa* Thunb. (Rosaceae) Promotes Pancreatic β-Cell Proliferation and Insulin Secretion

*Siwen Yang, Yunhe Qu, Jiyu Chen, Si Chen, Lin Sun, Yifa Zhou and Yuying Fan**

Engineering Research Center of Glycoconjugates Ministry of Education, Jilin Provincial Key Laboratory of Chemistry and Biology of Changbai Mountain Natural Drugs, School of Life Sciences, Northeast Normal University, Changchun, China

Insufficient pancreatic β-cell or insulin-producing β-cell are implicated in all types of diabetes mellitus. Our previous studies showed bee pollen polysaccharide RBPP-P improves insulin resistance in type 2 diabetic mice by inhibiting liver fat deposition. However, its potential of regulating β-cell function and integrity is not fully known. Herein, we observed that β-cell proliferation (n = 10), insulin synthesis (n = 5, p = 0.01684) and insulin incretion (n = 5, p = 0.02115) were intensely activated in MIN6 cells when treatment with RBPP-P. In alloxan-induced diabetic mice, oral administration of RBPP-P (n = 10) effectively decreased the blood glucose (p = 0.0326), drink intake (p < 0.001) and urine (p < 0.001). It directly stimulated phosphorylation of p38 (p = 0.00439), ERK (p = 0.02951) and AKT (p = 0.0072) to maintain the islet function and mass. Thus, our data suggest that RBPP-P is a natural compound to regulate β-cell proliferation and function, indicating it might have therapeutic potential against type 1 diabetes.

Keywords: bee pollen polysaccharides, insulin secretion, β-cell proliferation, T1DM, antidiabetic activity

OPEN ACCESS

Edited by:
Jing Zhao,
University of Macau, China

Reviewed by:
Marcia Barbosa Aguila,
Rio de Janeiro State University, Brazil
Yuhui Wang,
University of California, Berkeley, United States

****Correspondence:***
Yuying Fan
fanyy033@nenu.edu.cn

Specialty section:
This article was submitted to Ethnopharmacology, a section of the journal Frontiers in Pharmacology

Received: *30 March 2021*
Accepted: *18 June 2021*
Published: *28 June 2021*

Citation:
Yang S, Qu Y, Chen J, Chen S, Sun L, Zhou Y and Fan Y (2021) Bee Pollen Polysaccharide From Rosa rugosa *Thunb. (Rosaceae) Promotes Pancreatic β-Cell Proliferation and Insulin Secretion. Front. Pharmacol. 12:688073. doi: 10.3389/fphar.2021.688073*

INTRODUCTION

Type 1 diabetes (T1DM) is an autoimmune disorder characterized by the destruction of insulin-producing pancreatic β-cell and resultant hyperglycemia (Wilcox et al., 2016; Katsarou et al., 2017). The treatment of diabetes is mainly based on administration of insulin, the replacement or regeneration of insulin-producing cells, pancreas transplantation (Atkinson et al., 2014). Near perfect control of blood glucose levels can be restored by pancreas or islet transplantation, without the risk of serious hypoglycemic episodes that are associated with intensive insulin therapy. However, current protocols are inadequate to prevent islet rejection long-term, caused harmful side effects and some of them are expensive (Hirshberg et al., 2003). Around 80% of the world's population uses natural plants and their bioactive compositions for effective, less expensive and low-toxicity treatment (World Health Organization, 2017). These compounds have relative ability to reduce blood glucose while maintaining their growth and secreting properties targeting the endogenous β-cell. Thus, increasing the number of pancreatic β-cell or enhancing the function of islets is an effective way to treat T1DM (Mustafa et al., 2012; Vetere et al., 2014; Alejandro et al., 2015).

The proliferation of β-cell is exquisitely regulated to meet metabolic demand through complex mechanisms that involve the integration and interaction of multiple factors (Bernal-Mizrachi et al., 2014), but the mechanisms are still unclear. Insulin is synthesized by pancreatic β-cell and plays a predominant role in glucose homeostasis. Insulin or insulin-like growth factor (IGF) knockout

non-diabetic mice exhibited the decrease of β-cell mass, suggesting that their important roles in regulation of β-cell proliferation (Sabir et al., 2018). Mice have two genes encoding insulin, Ins1 and Ins2. The absence of Ins1 hinders the progress of T1DM, but the absence of Ins2 accelerates the development of T1DM (Babaya et al., 2006). Besides that, the transcription of the insulin gene is regulated by many factors, including MafA, Pdx1 and Neuro D1 (Zhang et al., 2020). Several signaling pathways also participated in β-cell proliferation. Recent studies have suggested crosstalk between AKT and islet-enriched transcription factors (Humphrey et al., 2010; Weng et al., 2020). MAPKs, including ERKs, JNKs and p38-MAPKs, have been found to be associated with cell survival, proliferation and stress response (Trempolec et al., 2013).

Bee pollen is the most popular natural health food in the world, and polysaccharide is the main bioactive components. Studies have shown that bee pollen polysaccharides have different functions, such as immunomodulation (Li et al., 2009), hypoglycemic (Gong et al., 2017), hypolipidemic (Denisow et al., 2016), anti-aging (Graikou et al., 2008) and anti-tumor (Wang et al., 2013). In our previous work, bee pollen polysaccharide from *Rosa rugosa* Thunb. (Rosaceae) were isolated and fractionated into three fractions (RBPP, RBPP-N, RBPP-P), RBPP-P could reduce the levels of blood glucose and lipid in type 2 diabetes (T2DM) mice by alleviating liver steatosis and insulin resistance (Gong et al., 2017). However, the mechanism of RBPP-P in the treatment of protecting the pancreas functions and promoting insulin secretion in T1DM is not fully elucidated. Thus, in this study we evaluated the effects of RBPP-P on β-cell proliferation and pancreas function *in vitro* and *in vivo*.

MATERIALS AND METHODS

Bee Pollen Polysaccharides Preparation and Fractionation

Bee pollen obtained from *Rosa rugosa* Thunb. (Rosaceae) was isolated and fractionated based on our previous report (Gong et al., 2017). Briefly, bee pollen powder was extracted with hot water and polysaccharides (RBPP) were precipitated by ethanol. RBPP was further fractionated by DEAE-cellulose chromatography into the acidic fraction (RBPP-P).

Bee Pollen Polysaccharides Characterization

The total carbohydrate content was determined using the phenol sulfuric acid method with glucose as the standard. The sugar compositions were analyzed by HPLC, and the structural feature of RBPP-P was analyzed by FT-IR and ^{13}C-NMR as described in previous publications (Gong et al., 2017).

Cell Culture

MIN6 cells (mice pancreatic β-cell line) were obtained from the American Type Culture Collection. MIN6 cells were maintained in DMEM supplemented with 15% fetal calf serum, 2 mM L-glutamine (Gibco, 35050-061), 1 mM pyruvate (Aladdin, S104174) and 285 μM β-mercaptoethanol (Gen-view, GM195) at 37°C in a 5% CO_2 incubator.

Cell Viability Assay

For MTT assay, MIN6 cells were seeded at the density of 1.5×10^4 cells on 96-well plate for 24 h. They were grown in pretreatment medium without (as control) or with 0.01, 0.1, and 1.0 mg/ml of polysaccharides for 24 h. The media were removed and 100 μl MTT (0.5 mg/ml) was added and incubated for additional 4 h. For dissolving formazon, 50 μl of 20% SDS/0.04% HCl solution was added to each well, and incubated in 37°C overnight. The absorbance at 570 nm was measured using a microplate reader (Biotek, United States). Cell proliferation under all the conditions was expressed as a percentage of the control, which was set at 100%.

Ki-67 Immunostaining

MIN6 cells were seeded on 24-well tissue culture plate at 1.5×10^5 cells and incubated for 24 h. The cells were grown for 24 h in pretreatment medium without (as control) or with 0.1 mg/ml of polysaccharides. After that, cells were gently washed with PBS and then fixed for 20 min at room temperature in 4% paraformaldehyde. Fixed cells were permeabilized in 0.1% Triton X-100/PBS for 15 min and then blocked with 2% BSA/5% bovine serum in PBS at room temperature for 20 min. Afterward, cells were incubated with a rabbit monoclonal antibody against Ki-67 (CST, 9129S, 1:500) for 1 h. After washing with PBS, cells were incubated with Alexa Flur™ 594-conjugated goat anti rabbit antibody (Invitrogen, A11072, 1:100) and DAPI (1:500) for 40 min. The images were taken using epi-fluorescence microscope (Olympus BX51) with ×40objective.

Insulin Secretion Assay

MIN6 cells were seeded in 48-well plate at 5×10^4 cells for 24 h, followed by 0.1 mg/ml polysaccharides or 30 mM KCl for 24 h. Then cells were incubated in KRB balanced buffer (115 mM NaCl, 4.8 mM KCl, 2.5 mM $CaCl_2$, 1.2 mM $MgSO_4$, 1.2 mM KH_2PO_4, 20 mM $NaHCO_3$, and 16 mM HEPES; pH 7.4) containing 0.2% BSA for 2 h. Medium was then replaced with KRB containing 5.5 mM glucose, 5.5 mM glucose plus 30 mM KCl or 5.5 mM glucose plus 1.0 mg/ml of different polysaccharides for 1 h, respectively. Supernatant was collected and insulin content was measured by ELISA (Innovation Beyond Limits, Germany). The cells were lyzed with lysis buffer (Boster, AR0102) for measurement of total protein content. The insulin secretion was defined as insulin content/protein content.

qRT-PCR Assay

qRT-PCR was established as described previously (Yang et al., 2020). MIN6 cells were isolated using TRIZOL (Invitrogen) and cDNA was generated from 1 μg of RNA using M-MLV reverse transcriptase (Promega, Fitchburg, WI, United States). The 20 μl of PCR mixture contained 1 μl of cDNA. Real-time PCR assays were conducted with a LC480 Light Cycler (Roche, Germany) using the applied primer sequences listed **Table 1**. PCR amplification was conducted as following: denaturation at 95°C

TABLE 1 | Primers used in the quantitative real-time PCR experiment.

Gene name	Forward (5′-3′)	Reverse (5′-3′)
Insulin1	CACTTCCTACCCCTGCTGG	ACCACAAAGATGCTGTTTGACA
Insulin2	GCTTCTTCTACACACCCATGTC	AGCACTGATCTACAATGCCAC
MafA	AGGAGGAGGTCATCCGACTG	CTTCTCGCTCTCCAGAATGTG
Pdx1	CCCCAGTTTACAAGCTCGCT	CTCGGTTCCATTCGGGAAAGG
Gapdh	AGGTCGGTGTGAACGGATTTG	TGTAGACCATGTAGTTGAGGTCA

for 30 s, annealing at 56°C for 30 s, and extension at 72°C for 45 s. GAPDH were used as internal standards for mRNAs. Relative expression of genes was determined using a comparative method ($2^{-\triangle CT}$).

Western Blot

Pancreas were lyzed in lysis buffer, containing 50 mM Tris-Cl (pH 7.5), 150 mM NaCl, 1 mM EGTA, 1% TritonX-100, 100 mM NaF, 10 mM $Na_4P_2O_7$ and 1 mM PMSF. The supernatants were collected after centrifugation, and the protein concentration was determined using the Coomassie Brilliant Blue (BBi, A610037-0025) assay. 30 μg tissue lysate was detected by western blot and probed for antibodies against phospho-p38 (Thr180/Tyr182) antibody (CST, 9215), p38 antibody (CST, 9212), phospho-ERK1/2 (Thr202/Tyr204) antibody (CST, 9101), ERK1/2 antibody (CST, 9107), phospho-Akt (Ser473) antibody (CST, 9271), Akt antibody (CST, 9272), actin (BD Biosciences, 612,657). Quantification was performed using the ImageJ software (Rockville, MD, United States).

Animal Treatment

Male C57BL/6J mice were obtained from GemPharmatech Co., Ltd. (Nanjing, China). All experiments were approved by the Animal Care and Use Committee of Northeast Normal University (SYXK 2018-0015). The mice were housed in a temperature-controlled facility (21°C, 12 h light/12 h dark cycle, 60–70% humidity), provided standard laboratory chow and water, and were subjected to treatment at 5 weeks of age.

Induction T1DM

To induce T1DM, the animals in the experimental group were fasted for 24 h, able to freely asscess water. Mice were injected intraperitoneally with fresh prepared alloxan (ALX, 150 mg/kg; sigma, A7413) saline solution for consecutive five days. Fasting blood glucose of the animals were measured and only the mice with blood glucose levels above 200 mg/dl were used for the experiments.

Experimental Design

Thirty mice were randomly divided into three groups (n = 10) and treated oral daily for 28 days. Group I: normal control; Group II: ALX control; Group III: ALX mice treated with RBPP-P (100 mg/kg). Fasting blood glucose (FBG), body weight and food intake were measured each week of the experiment. Urine volume and water consumption of animals were evaluated on the 28th days of the experiment. At the end of study, blood and organ samples were collected for the determination of biochemical parameters.

Serum Biochemical Analyses

Mice were analysis for insulin after overnight fasting when the animal assays finished. Serum were abtained and insulin level was measured using competitive enzyme-linked immunosorbent assay kits (Innovation Beyond Limits, Germany) according to the manufacturer's instructions. Ketone bodies was measured using competitive enzyme-linked immunosorbent assay kits (Zhenke biology, China) according to the manufacturer's instructions.

Immunohistochemistry

Based on our previous report (Fan et al., 2017), the pancreas was fixed in 4% paraformaldehyde and then a small part of the complete pancreas was cut. The pancreas tissues were soaked in 15% sucrose and 30% sucrose dehydrated overnight, respectively. The dehydrated tissues were embedded in OCT Compound (SAKURA, 4583) and frozen in −80°C. The tissues were subsequently sliced into 8 μm sections using freezing microtome (LEICA CM1850UN).

Sections were fixed with 4% paraformaldehyde for 20 min. Then permeabilized with 0.5% Triton X-100/SDS/PBS for 20 min, and blocked with 5%FBS/PBS/1% BSA for 3 h at room temperature. The slides were then stained with insulin (CST, 3014) and glucagon (Boster Biological Technology, BM1621) antibody overnight at 4°C. After washed, slides were dark incubated with FITC-conjugated goat anti-rabbit IgG (ABclonal, AS011) and Cy3-conjugated goat anti-rabbit IgG (ABclonal, AS008) for 2 h at room temperature. Sections were then washed with PBST and PBS for 5 min, followed incubated with Hoechest 33342 for 10 min at room temperature. After three washes with PBS, the slides were covered with fluorescence decay resistant medium (Boster, AR1109). Pancreatic sections were imaged using a light microscopy (Olympus BX51). The insulin-positive area and pancreatic area were measured using ImageJ software (Rockville, MD, United States).

Statistical Analysis

The results were expressed as the means ± s.d. Statistical analysis of the data was performed using Student's t-test and two-way repeated-measures ANOVA with Dunnett's post-hoc test (IBM SPSS Statistics 17.0, Armonk, NY, United States). All experiments were repeated at least three times. The level of significance was set at $^{*}p < 0.05$, $^{**}p < 0.01$, $^{***}p < 0.001$.

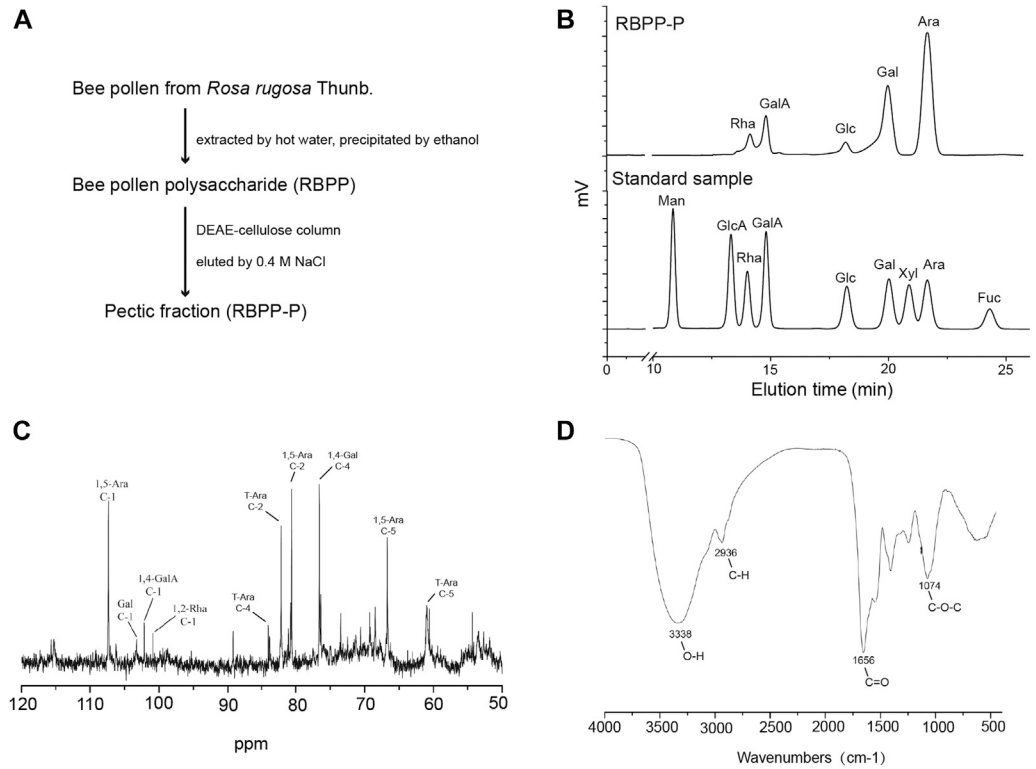

FIGURE 1 | Preparation and characterization of bee pollen polysaccharide. **(A)** The procedure used to prepare RBPP-P from *Rosa rugosa* Thunb. (Rosaceae). **(B)** Analysis of the monosaccharide composition of RBPP-P using high performance liquid chromatography (HPLC). **(C)** Analysis of chemical structure of RBPP-P using ^{13}C-nuclear magnetic resonance (^{13}C-NMR). **(D)** Analysis of the chemical structure of RBPP-P using fourier transform-infrared spectroscopy (FT-IR).

RESULTS

Preparation and Characterization of RBPP-P

Bee pollen polysaccharide (RBPP) was obtained from *Rosa rugosa* Thunb. (Rosaceae) by hot water extraction and ethanol precipitation. It was then separated by DEAE-Cellulose column and eluted with 0.4 M NaCl into an acidic fraction (RBPP-P), contains 93.6% of total carbohydrate (**Figure 1A**). Monosaccharide composition analysis by HPLC showed that RBPP-P is mainly composed of Ara (arabinose, 50.6%), Gal (galactose, 22.6%), GalA (galacturonic acid, 12.8%) and Rha (rhamnose, 5.6%), Glc (glucose, 4.4%), indicating that the polysaccharides we extracted are consistent with before (**Figure 1B**). Structural features of RBPP-P were characterized by analyzing ^{13}C-NMR and FT-IR spectrum (**Figures 1C,D**), indicated that RBPP-P contained more proportion of arabinogalactan (AG) fragments and small amounts of rhamnogalacturonan I (RG-I) and homogalacturonan (HG) domains.

RBPP-P Activated β-Cell Proliferation and Insulin Synthesis *in vitro*

To investigate the polysaccharide caused proliferative effect, MIN6 cells were treated with increasing concentration of bee pollen polysaccharides for 24 h. Cell viabilities were assessed by MTT assay. Concentration-effect relationship indicated that the enhancement of cell proliferation by RBPP-P was 20.8, 45 and 30.3% at the concentration of 0.01, 0.1 and 1.0 mg/ml (**Figure 2A**). Followed, carried out Ki-67 immunostaining which cells stained with Ki-67 (in red) and DAPI (in blue) under epi-fluorescence microscope. Ki-67 only stained the proliferating cells in the active cell cycle, but not the resting cells. When compared with control cells, RBPP-P appeared more cells in active cell cycle (**Figure 2B**). The results were consistent with that of MTT assay that RBPP-P might play a role on stimulation cell proliferation.

We further investigated the potential role of RBPP-P in regulation of insulin expression. When compared with control cells, 0.1 mg/ml of RBPP-P activated the Ins2 mRNA in Min6 cells, but not Ins1 (**Figure 2C**). Because MafA is a master regulator of the insulin gene, we determined the effect of RBPP-P on its expression and found that MafA was strongly increased in potassium chloride (KCl) and RBPP-P cells (**Figure 2D**). Pdx1 (pancreas-duodenum homeobox1) is a key transcription factor which activated insulin synthesis and stimulated pancreatic beta cell proliferation. As expected, the expression of Pdx1 was stimulated with RBPP-P treatment (**Figure 2D**).

Next, we performed glucose stimulated insulin secretion. KCl treated at 30 mM induced strong insulin secretion in cells. Compared to control cells, RBPP-P also exhibited insulin release at basal glucose. (**Figure 2E**). Collectively, these data

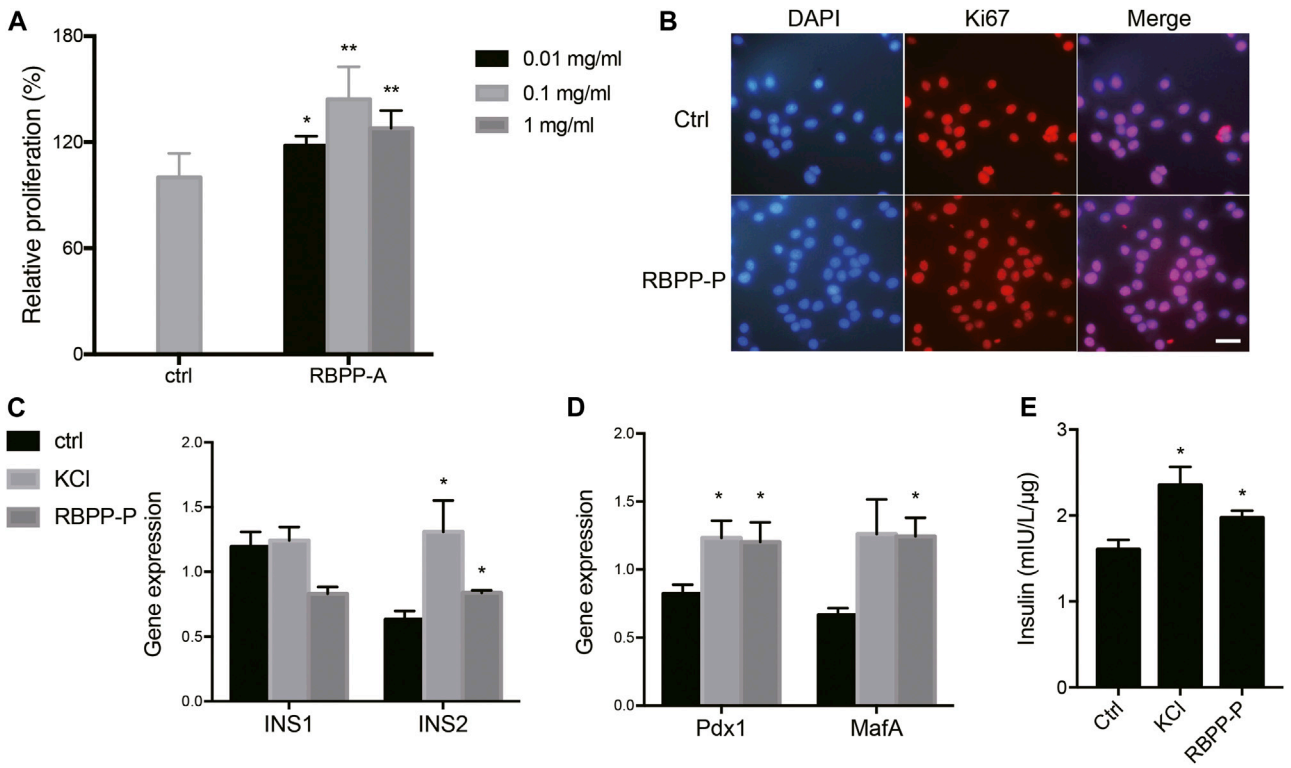

FIGURE 2 | Effects of RBPP-P on cell viability, insulin gene expression and insulin secretion. **(A)** RBPP-P promoted cell proliferation by MTT assay (n = 5). **(B)** RBPP-P promoted cell proliferation by Ki-67 immunostaining (n = 10). Scale bar, 100 μm. **(C)** qRT-PCR was used to evaluate the Ins1 and Ins2 levels in Min6 cells (n = 5). **(D)** qRT-PCR was used to evaluate the Pdx1 and MafA levels in Min6 cells (n = 5). mRNA levels were normalized to Gapdh mRNA. **(E)** Insulin secretion levels in Min6 cells (n = 5). All data are expressed as mean ± s. d. *p < 0.05, **p < 0.01, vs. control.

supported that RBPP-P modulates MafA and Pdx1 protein and activates Ins2 gene expression, showed its ability to activate β-cell proliferation and insulin synthesis.

RBPP-P Reduced Blood Glucose and Alleviated the Symptoms of Diabetes in ALX-Induced Diabetic Mice

We additionally investigated whether RBPP-P activation in β-cells reverses the hyperglycemia induced by alloxan (ALX). Intraperitoneal injection of alloxan monohydrate (150 mg/kg) caused over 2-fold elevation of blood glucose level, which was maintained over a period of 4 weeks. Daily oral treatment with 100 mg/kg of RBPP-P for 4 weeks, led to a significant decrease in fasting blood glucose (FBG) levels (**Figures 3A,B**). The results were in accordance with the previous results that RBPP-P had an anti-diabetes potential in HFD-mice.

Weight loss, polyphagia, polyuria and polydipsia are the main features of T1DM. Although administration of RBPP-P had the potential to block the ALX effect on body weight (**Figure 3C**), RBPP-P failed to reverse the increase in food intake after ALX damaged (**Figure 3D**). However, after treatment for 4 weeks, RBPP-P mice showed significantly decrease in water consumption (**Figure 3E**), urinary volume (**Figure 3F**) and ketone bodies level (**Figure 3G**) compared with ALX mice. This suggested that RBPP-P has shown a significant antidiabetic effect in alloxan-induced diabetic mice.

RBPP-P Restored Islet Function of ALX-Mice

Islet β-cell dysfunction leads to insulin insufficiency, a contributor to the onset of hyperglycemia in T1DM. We performed immunofluorescent staining of pancreatic sections using specific antibodies against insulin and glucagon. The C57BL/6J group showed islets of normal size, however, the ALX group observed reduction in the size of the insulin-expressing β-cells, enlarged the area of glucagon-expressing α-cells, and the disappearance of islet borders. This damage was considerably reduced after the administration of the RBPP-P, which was highly expressed of β-cells, and decreased α-cells located in the outer rim of the pancreatic islets (**Figure 4A**). It was demonstrated that RBPP-P displayed significantly increased the β-cell area/pancreatic area ratio with ALX group (**Figure 4B**). In addition, the insulin level was significantly increased of the RBPP-P treatment compared to the ALX mice (**Figure 4C**). These results showed RBPP-P

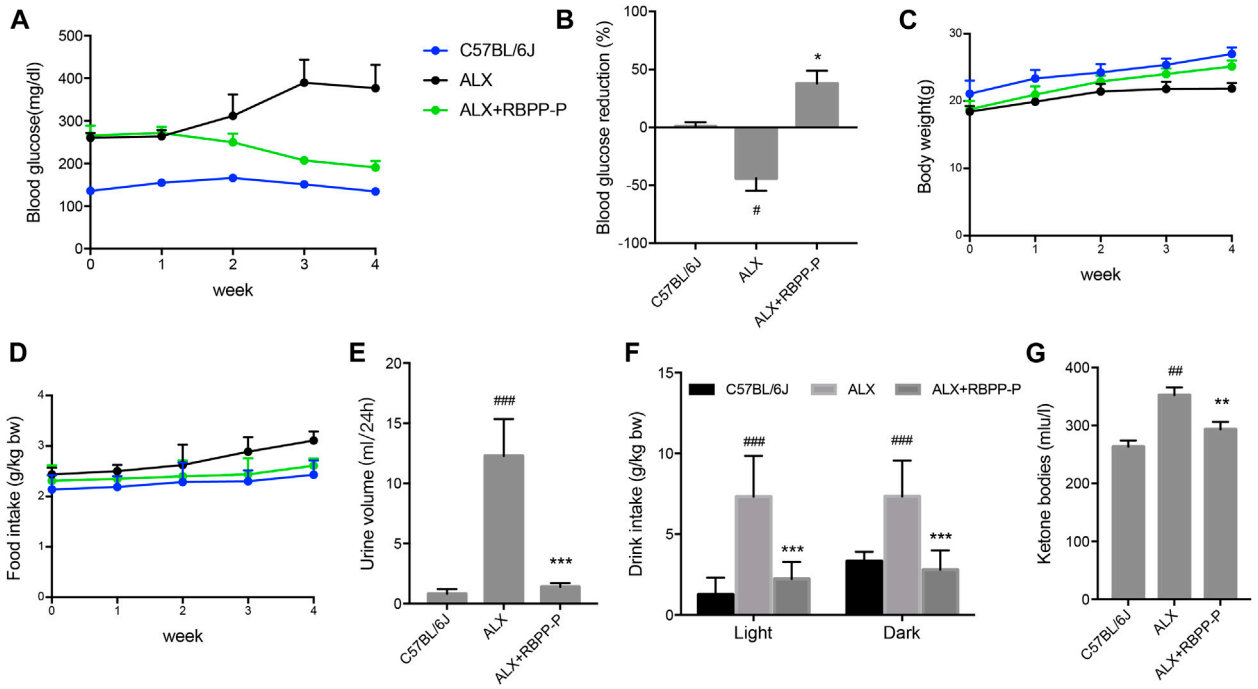

FIGURE 3 | Treatment with RBPP-P for 4 weeks improved hyperglycaemia and daily indicates in ALX mice (n = 10). Fasting blood glucose **(A)** and blood glucose reduction **(B)** were measured. **(C)** Body weight **(D)** Food intake. **(E)** Urine volume **(F)** Water intake **(G)** Serum ketone bodies. All data are expressed as mean ± s. d. $^{\#}p$ < 0.05, $^{\#\#}p$ < 0.01, vs. C57BL/6J mice; $^{*}p$ < 0.05, $^{**}p$ < 0.01, vs. ALX mice.

preserved structural integrity of pancreatic and restored islet function.

RBPP-P Stimulates MAPK and AKT Signaling Pathways

MAPK and AKT pathways have been shown to play key roles in regulation of the cell proliferation in mammalian cells. To elucidate if these classic pathways involved in RBPP-P reversed hyperglycemia in ALX-induced mice, we tested the expression levels focusing on pancreatic islet. Results showed that RBPP-P treated mice exhibited increased the phosphorylated levels of p38, ERK1/2 and Akt (S473) compared to C57BL/6J mice (**Figures 5A,B**). Taken together with other results in mice, suggested that AKT and MAPK signaling induction by RBPP-P plays a critical role in regulation of hypoglycemia.

DISCUSSION

The relevance between diabetes and β-cell dysfunction is a fundamental research topic for the development of new therapies increasing insulin secretion and optimizing metabolism of T1DM. Here, we prepared the active bee pollen polysaccharide RBPP-P from *Rosa rugose*, attempted to examine the effect of anti-T1DM and possible molecular mechanism of RBPP-P improving β-cell function.

Deregulation of a subset of transcriptional regulators in pancreatic β-cell is underlined a fundamental cause of β-cell dysfunction leading to T1DM (Harmon et al., 2005). The results that RBPP-P activated Ins2 gene expression by modulating MafA1 and Pdx1, which are critical transcription factors for insulin gene expression and secretion. Thus, RBPP-P promotes insulin production and induces expression of transcription regulators maintaining β-cell maturity.

T1DM is a metabolic disease characterized by impaired insulin secretion and resultant hyperglycemia (Lebovita, 2010). Weight loss, polyphagia, polyuria and polydipsia are the main features of T1DM (Bibak et al., 2014). Numerous studies have shown that alloxan destroys insulin-producing β-cells, a chemical commonly used in laboratories to make diabetic models (Katahira et al., 2020). Administration of RBPP-P (100 mg/kg) for 4 weeks showed marked hypoglycemic effect in ALX-induced diabetic mice. RBPP-P significantly reduced the signs of polydipsia and polyuria seen in diabetic mice, which could be the result of better control of hyperglycemia in T1DM. However, body weight and food intake were not significantly different between RBPP-P and ALX animals. Studies have reported that polysaccharides could restore damaged islets (Yang et al., 2019), histological examination in our studies showed RBPP-P significantly reversed the damage in islet induced by alloxan, increased the β-cell area/pancreatic area ratio. These results are

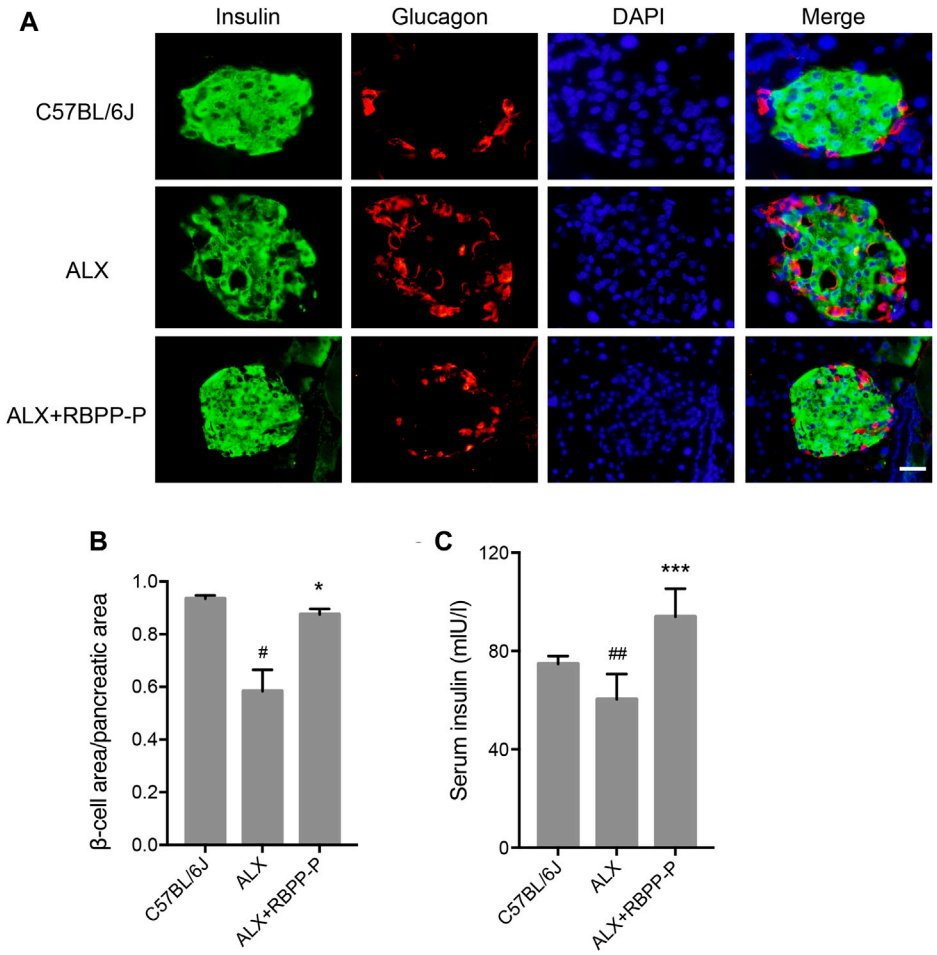

FIGURE 4 | Effects of the RBPP-P on islet histology. **(A)** Immunofluorescence (IF) staining for insulin (green) and glucagon (red). Scale bar, 100 μm. **(B)** β-cell area/pancreatic area ratio, measured by immunofluorescence staining ($n = 5$). **(C)** Insulin levels in serum ($n = 10$). All data are expressed as mean ± s. d. $^{\#}p < 0.05$, vs. C57BL/6J mice; $^{*}p < 0.05$, vs. ALX mice.

consistent with our previous work of RBPP-P carried out on the model of diabetes induced by HFD (Gong et al., 2017).

Cell proliferation, growth and survival are mediated by complex intracellular signaling network including several major pathways: PI3K/Akt and MAPK (p38, Erk and JNK) (Zhang and Liu, 2002; Song et al., 2019; Xie et al., 2021). We have observed that RBPP-P treatment increases the phosphorylation of p38, Erk1/2 and AKT in pancreas. Increasing evidence showed polysaccharides regulated cell proliferation via one of these signaling pathways or even several pathways synchronously. *Lycium barbarum* polysaccharide induced IGF-1-stimulated proliferation of MCF-7 cell through the ERK pathway (Huang et al., 2012). *Capsosiphon fulvescens* polysaccharides regulated effector β-catenin and Erk1/2 activation induced rat small intestinal epithelial cell proliferation (Go et al., 2011). IGF stimulated INS-1 cell proliferation via its downstream MAPK, which could phosphorylate ERK1/2 and p38 (Trumper et al., 2001). Thus, we speculated RBPP-P could stimulate growth factor to indirectly act on pancreatic beta cell, perhaps it may active multiple growth factors synchronously.

Based on these findings, we have explained how RBPP-P modulates β-cell production and β-cell function. RBPP-P activated key transcription factor MafA and Pdx1 in β-cells, increasing insulin expression and insulin secretion. RBPP-P also upregulates the phosphorylation levels of p38, ERK and AKT, promotes β-cell proliferation. Oral administration of RBPP-P showed potential hypoglycemic activities, improving the symptoms of diabetes, protecting the pancreas in T1DM mice, which maintains β-cell function and glucose homeostasis. Thus, RBPP-P could be used as a potentially natural functional food for the prevention and treatment of T1DM. Further pharmacological and biochemical studies are underway to elucidate the specific mechanism of RBPP-P for β-cell insulin secretion.

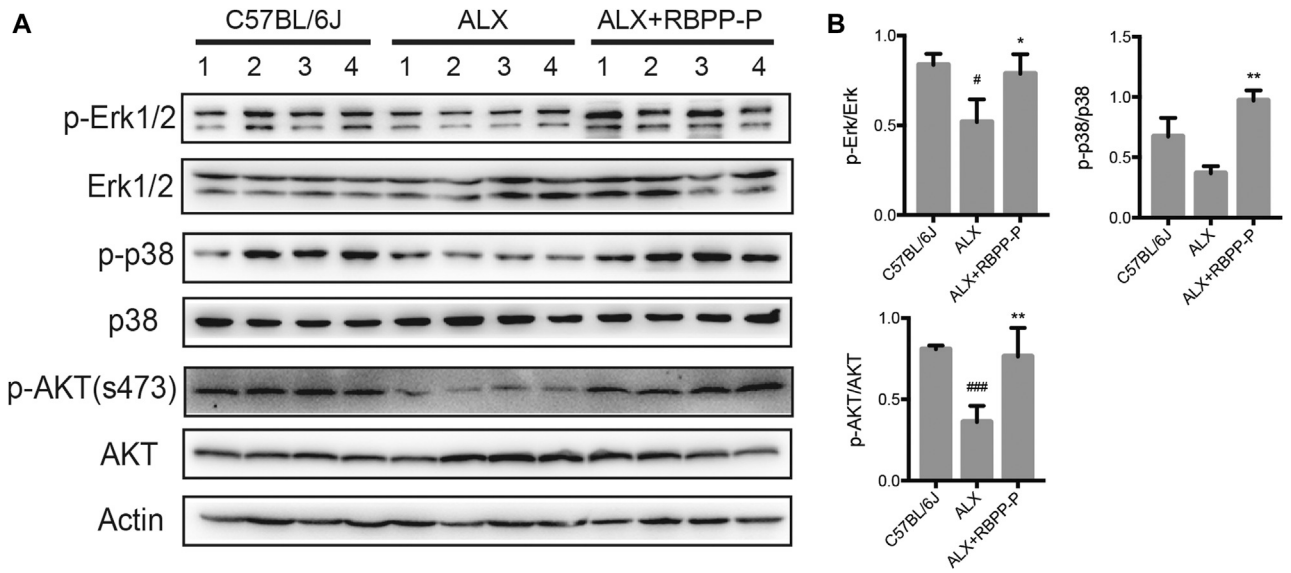

FIGURE 5 | The expression of AKT and MAPK signaling pathways in RBPP-P mice pancreas. **(A)** The MAPK and AKT signaling pathways were analyzed using western blotting **(B)** Band density was measured using the ImageJ. All data are expressed as mean ± s. d. $^{\#}p < 0.05$, $^{\#\#\#}p < 0.001$, vs. C57BL/6J mice; $^{*}p < 0.05$, $^{**}p < 0.01$, vs. ALX mice.

DATA AVAILABILITY STATEMENT

The raw data supporting the conclusion of this article will be made available by the authors, without undue reservation, to any qualified researcher.

ETHICS STATEMENT

The animal study was reviewed and approved by the Animal Care and Use Committee of Northeast Normal University (SYXK 2018-0015).

AUTHOR CONTRIBUTIONS

All authors participated in the design of the study. SY were responsible for most experiments *in vivo* and *in vitro*. YQ prepared the polysaccharide fraction. JC detected mice pancreatic islets morphologies. SC examined insulin secretion of RBPP-P. LS revised the manuscript. YZ contributed to suggest in revised manuscript. YF contributed to data interpretation and the manuscript.

FUNDING

This work was supported by the National Natural Science Foundation of China (No. 31872674) and the Jilin Talent Development Foundation Grant (No. 20200301018RQ), and Fundamental Research Funds for the Central Universities (No. 2412019ZD009).

REFERENCES

Alejandro, E. U., Gregg, B., Blandino-Rosano, M., Cras-Méneur, C., and Bernal-Mizrachi, E. (2015). Natural History of β-cell Adaptation and Failure in Type 2 Diabetes. *Mol. Aspects Med.* 42, 19–41. doi:10.1016/j.mam.2014.12.002

Atkinson, M. A., Eisenbarth, G. S., and Michels, A. W. (2014). Type 1 Diabetes. *The Lancet* 383, 69–82. doi:10.1016/S0140-6736(13)60591-7

Babaya, N., Nakayama, M., Moriyama, H., Gianani, R., Still, T., Miao, D., et al. (2006). A New Model of Insulin-Deficient Diabetes: Male NOD Mice with a Single Copy of Ins1 and No Ins2. *Diabetologia* 49, 1222–1228. doi:10.1007/s00125-006-0241-4

Bernal-Mizrachi, E., Kulkarni, R. N., Scott, D. K., Mauvais-Jarvis, F., Stewart, A. F., and Garcia-Ocana, A. (2014). Human -Cell Proliferation and Intracellular Signaling Part 2: Still Driving in the Dark without a Road Map. *Diabetes* 63, 819–831. doi:10.2337/db13-1146

Bibak, B., Khalili, M., Rajaei, Z., Soukhtanloo, M., Hadjzadeh, M. A., and Hayatdavoudi, P. (2014). Effects of Melatonin on Biochemical Factors and Food and Water Consumption in Diabetic Rats. *Adv. Biomed. Res.* 3, 173. doi:10.4103/2277-9175.139191

Denisow, B., and Denisow-Pietrzyk, M. (2016). Biological and Therapeutic Properties of Bee Pollen: A Review. *J. Sci. Food Agric.* 96, 4303–4309. doi:10.1002/jsfa.7729

Fan, Y., Wang, N., Rocchi, A., Zhang, W., Vassar, R., Zhou, Y., et al. (2017). Identification of Natural Products with Neuronal and Metabolic Benefits through Autophagy Induction. *Autophagy* 13, 41–56. doi:10.1080/15548627.2016.1240855

Go, H., Hwang, H.-J., and Nam, T.-J. (2011). Polysaccharides from Capsosiphon Fulvescens Stimulate the Growth of IEC-6 Cells by Activating the MAPK Signaling Pathway. *Mar. Biotechnol.* 13, 433–440. doi:10.1007/s10126-010-9314-y

Gong, H. Q., Li, X. Z., Yang, S. W., Yang, L. L., Fan, Y. Y., and Zhou, Y. F. (2017). Pectic Bee Pollenpolysaccharide from *Rosa Rugosa* Alleviates Diet-Induced

Hepatic Steatosis and Insulin Resistance via Induction of AMPK/mTOR-mediated Autophagy. *Molecules* 22, 699. doi:10.3390/molecules22050699

Graikou, K., Aligiannis, N., Chondrogianni, N., Kapeta, S., Gonos, E., and Chinou, I. (2008). Chemical Analysis and Anti-aging Properties of Greek Pollen. *Planta Med.* 74, 33. doi:10.1055/s-0028-1084582

Harmon, J. S., Stein, R., and Robertson, R. P. (2005). Oxidative Stress-Mediated, post-translational Loss of MafA Protein as a Contributing Mechanism to Loss of Insulin Gene Expression in Glucotoxic Beta Cells. *J. Biol. Chem.* 280, 11107–11113. doi:10.1074/jbc.M410345200

Hirshberg, B., Rother, K. I., Digon, B. J., III, Lee, J., Gaglia, J. L., Hines, K., et al. (2003). Benefits and Risks of Solitary Islet Transplantation for Type 1 Diabetes Using Steroid-Sparing Immunosuppression: the National Institutes of Health Experience. *Diabetes Care* 26, 3288–3295. doi:10.2337/diacare.26.12.3288

Huang, X., Zhang, Q.-Y., Jiang, Q.-Y., Kang, X.-M., and Zhao, L. (2012). Polysaccharides Derived from Lycium Barbarum Suppress IGF-1-Induced Angiogenesis via PI3K/HIF-1α/VEGF Signalling Pathways in MCF-7 Cells. *Food Chem.* 131, 1479–1484. doi:10.1016/j.foodchem.2011.10.039

Humphrey, R. K., Yu, S.-M., Flores, L. E., and Jhala, U. S. (2010). Glucose Regulates Steady-State Levels of PDX1 via the Reciprocal Actions of GSK3 and AKT Kinases. *J. Biol. Chem.* 285, 3406–3416. doi:10.1074/jbc.M109.006734

Katahira, T., Miyatsuka, T., Miura, M., Suzuki, L., Himuro, M., Nishida, Y., et al. (2020). Conversion of Pancreatic α Cells into Insulin-Producing Cells Modulated by β-cell Insufficiency and Supplemental Insulin Administration. *Biochem. Biophys. Res. Commun.* 521, 178–183. doi:10.1016/j.bbrc.2019.10.100

Katsarou, A., Gudbjörnsdottir, S., Rawshani, A., Dabelea, D., Bonifacio, E., Anderson, B. J., et al. (2017). Type 1 Diabetes Mellitus. *Nat. Rev. Dis. Primers.* 3, 17016. doi:10.1038/nrdp.2017.16

Lebovita, E. H. (2010). Adjunct Therapy for Type 1 Diabetes Mellitus. *Nat. Rev. Endocrinol.* 6, 326–334. doi:10.1038/nrendo.2010.49

Li, F., Yuan, Q., and Rashid, F. (2009). Isolation, Purification and Immunobiological Activity of a New Water-Soluble Bee Pollen Polysaccharide from Crataegus Pinnatifida Bge. *Carbohydr. Polym.* 78, 80–88. doi:10.1016/j.carbpol.2009.04.005

Mustafa, K. G., Ganai, B. A., Akbar, S., Dar, M. Y., and Masood, A. (2012). β-Cell Protective Efficacy, Hypoglycemic and Hypolipidemic Effects of Extracts of Achillea Millifolium in Diabetic Rats. *Chin. J. Nat. Medicines.* 12, 185–189. doi:10.3724/sp.j.1009.2012.00185

Sabir, S., Saleem, A., Akhtar, M., Saleem, M., and Raza, M. (2018). Increasing Beta Cell Mass to Treat Diabetes Mellitus. *Adv. Clin. Exp. Med.* 27, 1309–1315. doi:10.17219/acem/74452

Song, M., Bode, A. M., Dong, Z., and Lee, M.-H. (2019). AKT as a Therapeutic Target for Cancer. *Cancer Res.* 79, 1019–1031. doi:10.1158/0008-5472.CAN-18-2738

Trempolec, N., Dave-Coll, N., and Nebreda, A. R. (2013). SnapShot: P38 MAPK Signaling. *Cell* 152, 656. doi:10.1016/j.cell.2013.01.029

Trumper, A., Trumper, K., Trusheim, H., Arnold, R., and Horsch, D. (2001). Glucose-Dependent Insulinotropic Polypeptide Is a Growth Factor for (INS-1) Cells by Pleiotropic Signaling. *Mol. Endocrinol.* 15, 1559–1570. doi:10.1210/mend.15.9.0688

Vetere, A., Choudhary, A., Burns, S. M., and Wagner, B. K. (2014). Targeting the Pancreatic β-cell to Treat Diabetes. *Nat. Rev. Drug Discov.* 13, 278–289. doi:10.1038/nrd4231

Wang, B., Diao, Q., Zhang, Z., Liu, Y., Gao, Q., Zhou, Y., et al. (2013). Antitumor Activity of Bee Pollen Polysaccharides from *Rosa Rugosa*. *Mol. Med. Rep.* 7, 1555–1558. doi:10.3892/mmr.2013.1382

Weng, Q., Zhao, M., Zheng, J., Yang, L., Xu, Z., Zhang, Z., et al. (2020). STAT3 Dictates β-cell Apoptosis by Modulating PTEN in Streptozocin-Induced Hyperglycemia. *Cell Death Differ* 27, 130–145. doi:10.1038/s41418-019-0344-3

Wilcox, N. S., Rui, J., Hebrok, M., and Herold, K. C. (2016). Life and Death of β Cells in Type 1 Diabetes: A Comprehensive Review. *J. Autoimmun.* 71, 51–58. doi:10.1016/j.jaut.2016.02.001

World Health Organization. (2017). Traditional Medicine, Fact Sheet, No. 134. Available at: http://www.who.int/mediacentre/factsheets/2003/fs134/en/ (Accessed March 11, 2017).

Xie, X., Zu, X., Laster, K., Dong, Z., and Kim, D. J. (2021). 2,6-DMBQ Suppresses Cell Proliferation and Migration via Inhibiting mTOR/AKT and P38 MAPK Signaling Pathways in NSCLC Cells. *J. Pharmacol. Sci.* 145, 279–288. doi:10.1016/j.jphs.2021.01.003

Yang, S., Qu, Y., Zhang, H., Xue, Z., Liu, T., Yang, L., et al. (2020). Hypoglycemic Effects of Polysaccharides from *Gomphidiaceae rutilus* Fruiting Bodies and Their Mechanisms. *Food Funct.* 11, 424–434. doi:10.1039/C9FO02283J

Yang, S., Yan, J., Yang, L., Meng, Y., Wang, N., He, C., et al. (2019). Alkali-soluble Polysaccharides from Mushroom Fruiting Bodies Improve Insulin Resistance. *Int. J. Biol. Macromol.* 126, 466–474. doi:10.1016/j.ijbiomac.2018.12.251

Zhang, F., Ma, D., Zhao, W., Wang, D., Liu, T., Liu, Y., et al. (2020). Obesity-induced Overexpression of miR-802 Impairs Insulin Transcription and Secretion. *Nat. Commun.* 11, 1822. doi:10.1038/s41467-020-15529-w

Zhang, W., and Liu, H. T. (2002). MAPK Signal Pathways in the Regulation of Cell Proliferation in Mammalian Cells. *Cell res* 12, 9–18. doi:10.1038/sj.cr.7290105

Conflict of Interest: The authors declare that the research was conducted in the absence of any commercial or financial relationships that could be construed as a potential conflict of interest.

frontiers in Pharmacology

ORIGINAL RESEARCH
published: 01 July 2021
doi: 10.3389/fphar.2021.701003

Astragalus Polysaccharides Ameliorate Diet-Induced Gallstone Formation by Modulating Synthesis of Bile Acids and the Gut Microbiota

Qian Zhuang†, Xin Ye†, Shuang Shen, Jinnian Cheng, Yan Shi, Shan Wu, Jie Xia, Min Ning, Zhixia Dong and Xinjian Wan**

Digestive Endoscopic Center, Shanghai Jiao Tong University Affiliated Sixth People's Hospital, Shanghai, China

Cholesterol gallstone (CG) disease has relationships with several metabolic abnormalities. *Astragalus* polysaccharides (APS) have been shown to have multiple benefits against metabolic disorders. We attempted to uncover the effect and mechanism of action of APS on diet-induced CG formation in mice. Animals were fed a chow diet or lithogenic diet (LD) with or without APS supplementation. The effect of APS on CG formation was evaluated. The level of individual bile acids (BAs) in gallbladder bile and ileum were measured by liquid chromatography-tandem mass spectrometry. Real-time reverse transcription-quantitative polymerase chain reaction and western blotting were used to assess expression of the genes involved in BA metabolism and the enterohepatic circulation. Cecal contents were collected to characterize microbiota profiles. APS ameliorated LD-induced CG formation in mice. APS reduced the level of total cholesterol, bile acid hydrophobicity index and cholesterol saturation index in gallbladder bile. The protective effect of APS might result from reduced absorption of cholic acid in the intestine and increased hepatic BA synthesis. APS relieved the LD-induced activation of the intestinal farnesoid X receptor and decreased ileal expression of fibroblast growth factor 15. In the liver, expression of cytochrome P450 (*Cyp*) enzyme *Cyp7a1* and *Cyp7b1* was increased, whereas expression of adenosine triphosphate-binding cassette (*Abc*) transporters *Abcg5* and *Abcg8* was decreased by APS. APS improved the diversity of the gut microbiota and increased the relative abundance of the Bacteroidetes phylum. APS had demonstratable benefits against CG disease, which might be associated with enhanced BA synthesis and improved gut microbiota. Our results suggest that APS may be a potential strategy for the prevention of CG disease.

Keywords: gallstones, astragalus polysaccharides, cholesterol, bile acids, enterohepatic circulation, gut microbiota

OPEN ACCESS

Edited by:
Jing Zhao,
University of Macau, China

Reviewed by:
Ivo Pieter Van De Peppel,
University Medical Center Groningen, Netherlands
Rene Cardenas,
National Autonomous University of Mexico, Mexico

****Correspondence:***
Zhixia Dong
dzhixia2013@163.com
Xinjian Wan
slwanxinjian2020@126.com

†These authors have contributed equally to this work

Specialty section:
This article was submitted to Ethnopharmacology, a section of the journal Frontiers in Pharmacology

Received: *27 April 2021*
Accepted: *21 June 2021*
Published: *01 July 2021*

Citation:
Zhuang Q, Ye X, Shen S, Cheng J, Shi Y, Wu S, Xia J, Ning M, Dong Z and Wan X (2021) Astragalus *Polysaccharides Ameliorate Diet-Induced Gallstone Formation by Modulating Synthesis of Bile Acids and the Gut Microbiota. Front. Pharmacol. 12:701003. doi: 10.3389/fphar.2021.701003*

INTRODUCTION

Cholelithiasis is relatively common worldwide. Cholesterol gallstone (CG) disease is the most common type of cholelithiasis (Lammert et al., 2016). Cholecystectomy is the most efficacious treatment in management of symptomatic CG disease, but results in high socioeconomic costs (Everhart and Ruhl, 2009; Lammert et al., 2016). Cholesterol, bile acids (BAs), and phospholipids are the main lipids in bile. Cholesterol hypersaturation in bile is an important prerequisite for CG

formation (Lammert et al., 2016; Di Ciaula et al., 2018). In the normal physiologic state, BAs and phospholipids form mixed micelles in which hydrophobic cholesterol can be solubilized. However, under certain pathophysiologic conditions (e.g., hepatic hypersecretion of cholesterol and deficiency of BAs or phospholipids), the homeostasis of biliary cholesterol can be disturbed. Supersaturated bile of cholesterol leads to the precipitation of cholesterol crystals that accumulate and grow in the gallbladder (Di Ciaula et al., 2018).

Cholesterol, BAs, and phospholipids are secreted into the biliary tract by an elaborate network of transporters. Cholesterol is secreted by the adenosine triphosphate-binding cassette (*Abc*) transporters *Abcg5* and *Abcg8* (Lammert et al., 2016). BA secretion is mediated by bile acid export pump (*Bsep*) and multidrug resistance protein (*Mrp*) 2 (Kunst et al., 2020). *Abcb4* (also known as multidrug resistance protein 3) is a major transporter of phospholipids (Poupon et al., 2013).

BA formation is another crucial catabolic pathway for cholesterol (Jia et al., 2021). BA synthesis can be accomplished *via* two routes. The classical pathway is initiated by cytochrome P450 (*Cyp*) enzyme *Cyp7a1*. The alternative pathway is initiated by *Cyp27a1* (Wahlstrom et al., 2016). *Cyp8b1* and *Cyp7b1* are also crucial enzymes involved in BA synthesis (Wahlstrom et al., 2016). Gallbladder BAs are secreted into the small intestine following food intake. Most BAs are reabsorbed in the ileum and return to the liver *via* the portal circulation (Wahlstrom et al., 2016) in a process known as the "enterohepatic circulation of BAs".

BA synthesis is regulated mainly by the nuclear farnesoid X receptor (*Fxr*), which shows high expression in the liver and small intestine (Kong et al., 2012). *Fxr*-mediated induction of hepatic small heterodimer partner (*Shp*) and intestinal fibroblast growth factor 15 (*Fgf15*; *FGF19* in humans) reduce expression of the genes encoding BA synthetic enzymes (Kong et al., 2012). *Fxr* has varying affinities for different BA species. Cholic acid (CA) and deoxycholic acid (DCA) are agonists of the *Fxr* (de Aguiar Vallim et al., 2013), whereas muricholic acids (MCAs) are *Fxr* antagonists (Sayin et al., 2013).

CG disease has relationships with several metabolic abnormalities (Di Ciaula et al., 2019) and is associated with alteration of the gut microbiota (Wang et al., 2017; Grigor'eva and Romanova, 2020; Wang et al., 2020b). Several types of herbal polysaccharides can improve metabolic disorders (Wu et al., 2019; Sun et al., 2020). *Astragalus* polysaccharides (APS) are natural macromolecules extracted from *Astragalus mongholicus* Bunge, which is a commonly used traditional Chinese medicine. Several studies have reported that APS can ameliorate obesity, insulin resistance, hepatic steatosis, and hypercholesteremia in mice and cell lines (Huang et al., 2017; Ke et al., 2017; Hong et al., 2020). A recent study reported that APS had beneficial effects on high-fat diet-induced metabolic disorders in mice because it could regulate intestinal metabolism as well as gut microbial structure and function (Hong et al., 2020). However, whether APS has a beneficial effect on diet-induced CG formation is not known. Here, we aimed to uncover the effect and mechanism of action of APS on lithogenic diet (LD)-induced CG formation.

MATERIALS AND METHODS

Ethical Approval of the Study Protocol

The study protocol was approved by the Animal Care and Use Committee of Affiliated Sixth People's Hospital within Shanghai Jiao Tong University (Shanghai, China).

Animals and Treatment

After 1 week of acclimatization, 40 male C57BL/6J mice (aged 6 weeks) were divided randomly into four groups (10 mice in each group and five mice in each cage): Chow; LD; LD with low-dose APS (2%; AL group); LD with high-dose APS (8%; AH group).

The chow diet was LAD 0011, and the LD was TP 28900, both of which were from Trophic Diet (Nantong, China). The LD contained 15% fat, 1.25% cholesterol, and 0.5% CA with and without APS supplementation. Mice were fed these diets for 6 weeks. APS was purchased from Ci Yuan Biotechnology (Shanxi, China) and the purity of polysaccharides from *A. mongholicus* was 98%. Mice were housed in standard cages at 20–24°C with 12-h light–dark cycles and *ad libitum* access to food and water. At the end of experimentation, mice were killed after a 12-h fast.

Serum and Bile Analyses and Cholesterol Saturation Index Calculation

Levels of metabolites in serum and bile were measured by enzymatic assays using a microplate reader (BioTek, Winooski, VT, United States). Levels of total cholesterol (TC) and triglycerides (TG) in serum and levels of TC and BAs in gallbladder bile were measured using kits according to manufacturer (Jiancheng Bioengineering Institute, Nanjing, China) instructions. Phospholipid levels in gallbladder bile were measured according to kit instructions (Wako Pure Chemicals, Osaka, Japan). The CSI of gallbladder bile was calculated using the following equation: actual molar percentage of TC in bile/highest concentration of soluble TC at a given bile molarity in the Carey table (Carey, 1978).

Analyses of Bile Acids Species in Bile and the Ileum

Individual BA levels in gallbladder bile and the ileum were measured by negative electrospray liquid chromatography-tandem mass spectrometry (LC-MS/MS) in multiple-reaction-monitoring mode on an Acquity ultra-high-pressure liquid chromatography (UPLC) system (Waters, Milford, MA, United States). Thirty-eight BA standards were weighed accurately and prepared as standard solutions through serial dilution using methanol. UPLC separations were undertaken on an Acquity UPLC BEH C18 column (internal dimensions: 2.1 mm × 100 mm, 1.7 μm; Waters). The temperature of the column was set at 40°C. The injection volume of the sample was 5 μL. Eluents consisted of 0.01% formic acid in water (eluent A) and acetonitrile (eluent B). The flow rate was set at 0.25 ml/min.

TABLE 1 | Primer sequences for quantitative real-time PCR analysis.

Gene	Forward primer	Reverse primer
Cyp7b1	GGAGCCACGACCCTAGATG	TGCCAAGATAAGGAAGCCAAC
Cyp7a1	AGCAGCCTCTGAAGAAGTGAATGG	AGAGCCGCAGAGCCTCCTTG
Cyp8b1	ACACCAAGGACAAGCAGCAAGAC	TGGCTCACTTCCACCCACTCC
Cyp27a1	ACACGGATGCCTTAAACGAGG	GCAGCCAATCCTTTTCTCAAAC
β-klotho	TGTTCTGCTGCGAGCTGTTAC	CCGGACTCACGTACTGTTTTT
Mrp2	GTGTGGATTCCCTTGGGCTTT	CACAACGAACACCTGCTTGG
Mrp3	CTGGGTCCCCTGCATCTAC	GCCGTCTTGAGCCTGGATAAC
Mrp4	GGCACTCCGGTTAAGTAACTC	TGTCACTTGGTCGAATTTGTTCA
Oatp1a1	GTGCATACCTAGCCAAATCACT	CCAGGCCCATAACCACACATC
Oatp1a4	GCTTTTCCAAGATCAAGGCATTT	CGTGGGGATACCGAATTGTCT
Oatp1b2	AGATCAGAGAAGACAAGGCACT	CTTTGGTCGGTGTAGCTTGG
Bsep	TCTGACTCAGTGATTCTTCGCA	CCCATAAACATCAGCCAGTTGT
Asbt	GTCTGTCCCCCAAATGCAACT	CACCCCATAGAAAACATCACCA
Ntcp	CAAACCTCAGAAGGACCAAACA	GTAGGAGGATTATTCCCGTTGTG
Ostα	AGGCAGGACTCATATCAAACTTG	TGAGGGCTATGTCCACTGGG
Ostβ	AGATGCGGCTCCTTGGAATTA	TGGCTGCTTCTTTCGATTTCTG
Fgf15	ATGGCGAGAAAGTGGAACGG	CTGACACAGACTGGGATTGCT
Fgfr4	GCTCGGAGGTAGAGGTCTTGT	CCACGCTGACTGGTAGGAA
Abcb4	CAGCGAGAAACGGAACAGCA	TCAGAGTATCGGAACAGTGTCA
Fxr	GCTTGATGTGCTACAAAAGCTG	CGTGGTGATGGTTGAATGTCC
Shp	TGGGTCCCAAGGAGTATGC	GCTCCAAGACTTCACACAGTG
Abcg5	AGGGCCTCACATCAACAGAG	GCTGACGCTGTAGGACACAT
Abcg8	CTGTGGAATGGGACTGTACTTC	GTTGGACTGACCACTGTAGGT
Gapdh	AGGTCGGTGTGAACGGATTTG	TGTAGACCATGTAGTTGAGGTCA

Cyp7b1, *cytochrome P450 7b1;* Cyp7a1,*cytochrome P450 7a1;* Cyp8b1, *cytochrome P450 8b1;* Cyp27a1, *cytochrome P450 27a1;* β-klotho, *beta-klotho;* Mrp2, *multidrug resistance protein 2;* Mrp3, *multidrug resistance protein 3;* Mrp4, *multidrug resistance protein 4;* Oatp1a1, *organic anion-transporting polypeptide 1a1;* Oatp1a4, *organic anion-transporting polypeptide 1a4;* Oatp1b2, *organic anion-transporting polypeptide 1b2;* Bsep, *bile acid export pump;* Asbt, *apical sodium dependent bile acid transporter;* Ntcp, *Na/taurocholate cotransporting polypeptide;* Ostα, *organic solute transporter alpha;* Ostβ, *organic solute transporter beta;* Fgf15, *fibroblast growth factor 15;* Fgfr4, *fibroblast growth factor receptor 4;* Abcb4, *ATP-binding cassette; subfamily B; member 4;* Fxr, *bile acid receptor;* Shp, *nuclear receptor subfamily 0 group B member 2;* Abcg5, *ATP-binding cassette subfamily G member 5;* Abcg8, *ATP-binding cassette subfamily G member 8;* Gapdh, *glyceraldehyde-3-phosphate dehydrogenase.*

A 38 min elution gradient was used: 0–4 min, 25% B; 4–9 min, 25–30% B; 9–14 min, 30–36% B; 14–18 min, 36–38% B; 18–24 min, 38–50% B; 24–32 min, 50–75% B; 32–35 min, 75–100% B; 35–38 min, and 100–25% B.

For gallbladder bile, a 10 μL bile sample was mixed with 500 μL of methanol (−20°C), vortex-mixed with oscillation for 1 min, and then centrifuged (12,000 × *g*, 10 min, 4°C). Twenty microliters of supernatant was transferred to a clean tube and diluted 2000-fold with methanol. After dilution, 300 μL of supernatant was ready for LC-MS/MS. The Hydrophobicity Index (HI) of gallbladder bile were calculated as reported previously (Heuman, 1989; Posa, 2014).

For ileum samples, the ileum was flushed with physiologic (0.9%) saline and soaked with gauze. Ileum tissue was weighed precisely (~50 mg), homogenized in 1 ml of methanol (−20°C), and centrifuged (12,000 × *g*, 10 min, 4°C). One-hundred microliters of supernatant was mixed with 900 μL of methanol, vortex-mixed with oscillation for 30 s, and passed through a 0.22-μm filter membrane. After centrifugation, the supernatant was ready for LC-MS/MS.

Histology of Liver Tissue

Liver sections were fixed in 4% neutral-buffered formaldehyde, embedded in paraffin, cut into slices (thickness, 4 μm), and then stained with hematoxylin and eosin (H&E). To determine lipid-droplet accumulation in the liver, Oil Red O (Servicebio, Wuhan, China) staining of frozen liver sections was undertaken. The corresponding positively stained area was quantified with Image-Pro Plus v6.0.0 (Media Cybernetics, Rockville, MD, United States) and results are expressed as a percentage of the total area of a high-power field.

Analyses of Hepatic Lipids

Hepatic lipids were extracted using the Folch method (Huang et al., 2019). Briefly, liver tissues were homogenized in a mixture of chloroform:methanol (2:1; *v/v*), followed by a series of dispersion, agitation, centrifugation, and resuspension steps. Levels of TC and TG were measured with assay kits following manufacturer instructions.

Real-Time Reverse Transcription-Quantitative Polymerase Chain Reaction

Total RNA in liver and ileum tissues was isolated using a tissue RNA purification kit (EZBioscience, Roseville, MN, United States). The total RNA of each sample was quantified by a spectrophotometer (NanoDrop™ 2000C; Thermo Fisher, Waltham, MA, United States). Complementary (c)DNA synthesis was done using HiScript™ III RT SuperMix for qPCR (Vazyme, Nanjing, China). RT-qPCR primers were designed and synthesized (Sangon Biotech, Shanghai, China) and the sequences are listed in **Table 1**. RT-qPCR was undertaken using AceQ Universal SYBR® qPCR Master Mix (Vazyme) on an ABI

QuantStudio seven Flex RT-PCR system (Applied Biosystems, Foster City, CA, United States). The values of the target genes were normalized to that of glyceraldehyde 3-phosphate dehydrogenase (*Gapdh*) and the $2^{-\Delta\Delta Ct}$ method was used to determine relative expression of target genes.

Western Blotting

Ileum and liver samples were homogenized in RIPA lysis buffer (Beyotime Institute of Biotechnology, Shanghai, China) containing protease and a phosphatase inhibitor cocktail (Beyotime Institute of Biotechnology). The protein extract was supplied with loading buffer (EpiZyme, Shanghai, China) and denatured by boiling at 100°C for 10 min. Equal amounts of total cellular proteins (40 μg) were separated by sodium dodecyl sulfate–polyacrylamide gel electrophoresis using 10% gels and transferred to Immobilon-P Transfer Membranes (Millipore, Tullagreen, Ireland). The latter were blocked with 5% nonfat milk in 0.1% TBS-Tween 20 for 1 h, incubated with primary antibodies overnight at 4°C, and then incubated with horseradish peroxidase-linked secondary antibody (catalog number, 7,074; Cell Signaling Technology, Danvers, MA, United States). Bands were visualized using SuperSignal West Pico Chemiluminescent Substrate (Thermo Scientific) with a ChemiDoc MP imaging system (Bio-Rad Laboratories, Hercules, CA, United States).

Gapdh was included as a loading control. The antibodies used (which were all raised in rabbits and the dilution was 1:1,000) were: anti-*Gapdh* (catalog number, 5174S; Cell Signaling Technology), anti-*Fgf15* (ab229630; Abcam, Cambridge, United Kingdom), anti-*Cyp7a1* (ab65596; Abcam), anti-*Abcg8* (DF6673; Affinity, Changzhou, China), anti-*Abcg5* (27722-1-AP; Proteintech, Rosemont, IL, United States), and anti-*Cyp7b1* (24889-1-AP; Affinity).

Preparation of 16S rRNA Gene Libraries, and Analyses of Sequencing and Diversity

16S rRNA-sequencing of cecal contents was carried out. Briefly, total genomic DNA from samples was extracted using the cetyltrimethylammonium-bromide method. 16S rRNA genes of distinct regions (V3–V4) were amplified using specific primers. The mixture of PCR products was purified with a gel extraction kit (Qiagen, Hilden, Germany). Sequencing libraries were generated using the TruSeq® DNA PCR-Free Sample Preparation kit (Illumina, San Diego, CA, United States) following manufacturer instructions, and index codes were added. A Qubit@2.0 fluorometer (Thermo Fisher) and bioanalyzer (2,100 system; Agilent Technologies, Santa Clara, CA, United States) were used to assess the quality of the library. The latter was sequenced on a NovaSeq platform (Illumina), and 250-bp paired-end reads were generated.

Sequencing was done using Uparse v7.0.1001 (http://drive5.com/uparse/) (Edgar, 2013). Operational taxonomic unit (OTU) analyses enabled clustering of sequences at a similarity level of 97%. Representative sequences for each OTU were screened for further annotation. The Silva Database (www.arb-silva.de/) (Quast et al., 2013) was used based on the Mothur algorithm to annotate taxonomic information. Information on OTU abundance was normalized using a standard sequence number corresponding to the sample with the fewest sequences. Alpha diversity was employed to analyze the complexity of species diversity and was calculated with QIIME 1.7.0 (http://qiime.org/). Beta-diversity analyses were used to evaluate differences in samples with regard to species complexity. Beta diversity on weighted UniFrac was calculated by QIIME 1.9.1. Principal coordinate analysis (PCoA) was undertaken to obtain principal coordinates and visualize complex, multidimensional data.

Statistical Analyses

Data are the mean ± standard deviation (SD). Appropriate statistical analyses were applied depending on data distribution. For data that showed a normal distribution, the two-tailed Student's *t*-test was used between two groups, and one-way analysis of variance followed by Tukey's test for multiple comparisons was used between three or four groups. For datasets with a skewed distribution, the Mann–Whitney test was used between two groups, and the Kruskal–Wallis test followed by Dunn's test for multiple comparisons was done between three or four groups. Statistical analyses were undertaken using Prism 8 (www.graphpad.com). Correlations between the level of BAs in the ileum and relative abundance of the microbiome were carried out using Spearman's correlation analysis followed by *p*-value correction of the false discovery rate, which was visualized using R 3.6.2 (R Institute for Statistical Computing, Vienna, Austria; www.r-project.org/). $p < 0.05$ was considered significant.

RESULTS

Astragalus polysaccharides Ameliorated Lithogenic Diet-Induced Cholesterol Gallstone Formation in Mice

Mice in the chow group did not have CG formation and had clear gallbladders. Ninety percent of mice in the LD group had CGs and "cloudy" gallbladders (**Figures 1A,C**). The color and morphology of CGs in mice are shown in **Figure 1B**. With APS supplementation, the prevalence of CG formation in the AL group and AH group was 60 and 30%, respectively, (**Figures 1A,C**). We graded CGs according to the method described by Akiyoshi and colleagues (Akiyoshi et al., 1986). The grade of CG formation in mice fed the LD was significantly higher than that of chow diet-fed mice, and was decreased significantly upon APS supplementation (**Figure 1D**). Bodyweight gain was not significantly different among the groups (**Figure 1E**). Compared with chow diet-fed mice, the ratio of liver weight-to-bodyweight was significantly higher in mice fed the LD, and APS could reverse these changes partially (**Figure 1F**).

Astragalus polysaccharides Altered Biliary Composition and the Cholesterol Saturation Index in Mice fed the Lithogenic Diet

We evaluated lipid profiles in gallbladder bile to understand the mechanism involved in the reduction of CG formation by APS.

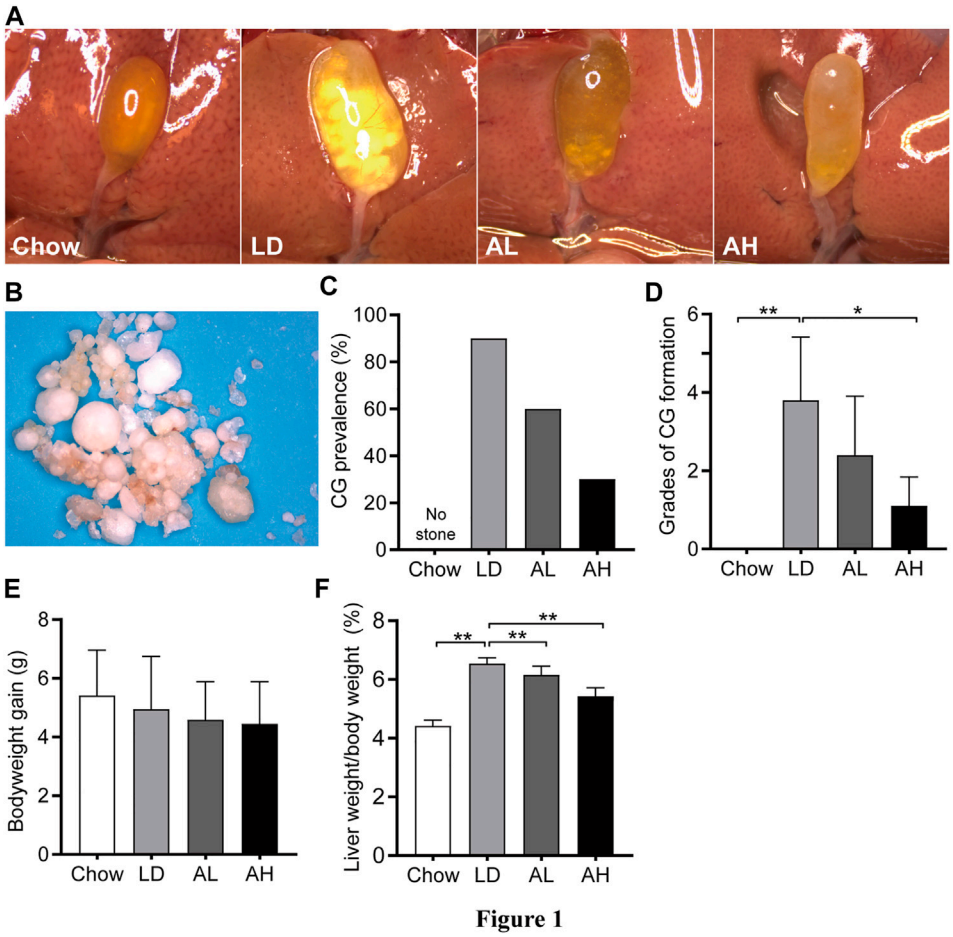

Figure 1

FIGURE 1 | Bodyweight, and liver weight, and cholesterol gallstone (CG) prevalence. **(A)** Representative gallbladders per group. **(B)** CGs from the LD group. **(C)** CG prevalence. **(D)** Grades of CG formation. **(E)** Bodyweight gain. **(F)** Ratio of liver weight-to-bodyweight. Data are the mean ± SD (n = 10). *p < 0.05, **p < 0.01. Chow, chow diet; LD, lithogenic diet; AL, low-dose APS; AH, high-dose APS.

Compared with that in the chow group, the TC level was increased significantly in the gallbladder bile of mice fed the LD, whereas APS decreased the TC level significantly (**Figure 2A**). However, total BAs and phospholipids in gallbladder bile was not altered significantly by APS supplementation (**Figure 2A**). The CSI in the LD group was higher than that in the chow group, and APS supplementation reduced it (**Figure 2B**).

The solubility and hydrophobicity of individual BAs were different. The rank order from hydrophobic to hydrophilic was: lithocholic acid (LCA) > DCA > chenodeoxycholic acid (CDCA) > CA > ursodeoxycholic acid (UDCA) > MCA (de Aguiar Vallim et al., 2013). We employed BA-targeted metabolomics analysis to determine the changes in individual BAs in gallbladder bile. Compared with that in the chow group, the level of CA, TDCA, GCA, α-MCA, and GDCA in gallbladder bile was increased significantly in the LD group. APS administration reduced the level of CA and α-MCA significantly, and increased the level of T-α-MCA, T-β-MCA, TUDCA, TCDCA, and β-MCA, in gallbladder bile (**Figure 2C**). The percentage of BAs in gallbladder bile is shown in **Supplementary Figure S1**. The HI of gallbladder-bile BAs in the LD group was significantly higher than that in the chow group, but APS supplementation reduced the HI (**Figure 2D**). Principal component analysis (PCA) of BAs in gallbladder bile showed clear separation among groups (**Supplementary Figure S2**, left). The level of total unconjugated BAs in bile was increased significantly in the LD group, whereas APS reversed these changes (**Figure 2E**). However, the level of total conjugated BAs in bile was not significantly different among the three groups (**Figure 2E**). These results indicated that APS could reduce the TC level and increase the level of hydrophilic BA, which might attenuate cholesterol hypersaturation in gallbladder bile.

Astragalus polysaccharides Ameliorated Lithogenic Diet-Induced Metabolic Disorders

LD administration resulted in significant hepatic steatosis (as revealed by H&E and Oil Red O staining), whereas APS

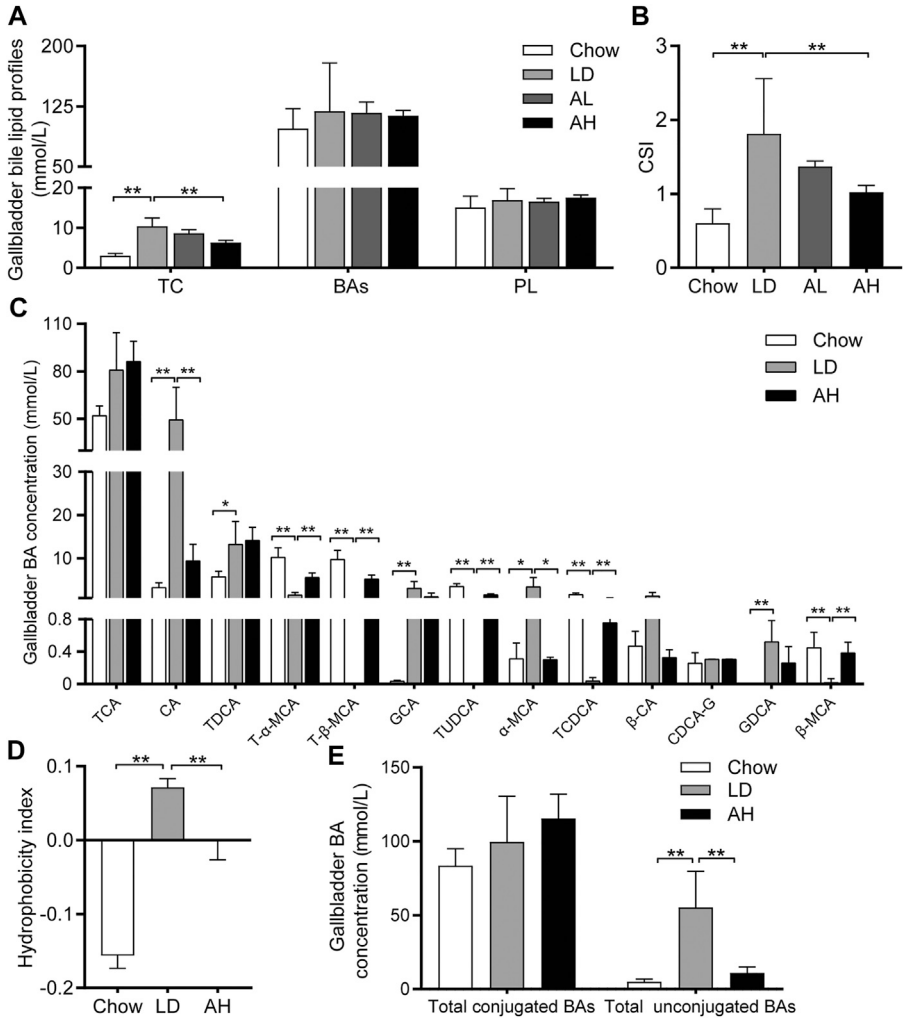

FIGURE 2 | Biliary Cholesterol Saturation Index (CSI) and Hydrophobicity Index (HI) of bile acids (BAs) in gallbladder bile. **(A)** Total cholesterol (TC), BAs and phospholipids (PL) (n = 8–10). **(B)** CSI (n = 8–10). **(C)** Analysis of BA species (n = 6). Top-13 most abundant BA species are shown. **(D)** HI of BAs (n = 6). **(E)** Total conjugated BAs and unconjugated BAs (n = 6). Data are the mean ± SD, $^{*}p < 0.05$, $^{**}p < 0.01$. Chow, chow diet; LD, lithogenic diet; AL, low-dose APS; AH, high-dose APS.

supplementation improved hepatic steatosis (**Figures 3A,B**). APS significantly reduced the hepatic TC level and serum level of TC and TG, which were increased by LD consumption (**Figures 3C,D**). The hepatic level of TG was not reduced significantly by APS (**Figure 3E**). These results indicated that APS could ameliorate LD-induced metabolic disorders in mice.

Astragalus polysaccharides Reduced the Cholic Acid in the Ileum and Downregulated Expression of the *Fxr–Fgf15* Axis

We analyzed the individual BA species in the ileum (where most BAs are reabsorbed) to explore the influence of APS on BA metabolism in the intestine (Huang et al., 2019; Jia et al., 2021). APS significantly reduced the CA level in the ileum, which was increased by LD consumption (**Figure 4A**). After APS supplementation, the level of T-β-MCA was increased significantly (Sayin et al., 2013) (**Figure 4A**). The level of total conjugated BAs and total unconjugated BAs was increased in mice fed the LD, whereas APS reduced the level of total unconjugated BAs significantly (**Figure 4B**).

Next, we analyzed expression of *Fgf15* and *Shp* in the ileum (both of which are target genes of *Fxr*) (Kong et al., 2012). APS decreased the mRNA expression of *Fgf15* and *Shp* in the ileum significantly, which was increased significantly by LD consumption (**Figure 4C**). Western blotting further confirmed the reduced protein expression of *Fgf15* in APS-treated mice (**Figure 4D**).

Astragalus polysaccharides Decreased the Canalicular Efflux of Cholesterol and Enhanced Bile Acids Synthesis

Consistent with the activation of intestinal *Fxr*, we found that hepatic mRNA expression of *Cyp7a1*, *Cyp8b1*, and *Cyp7b1* was

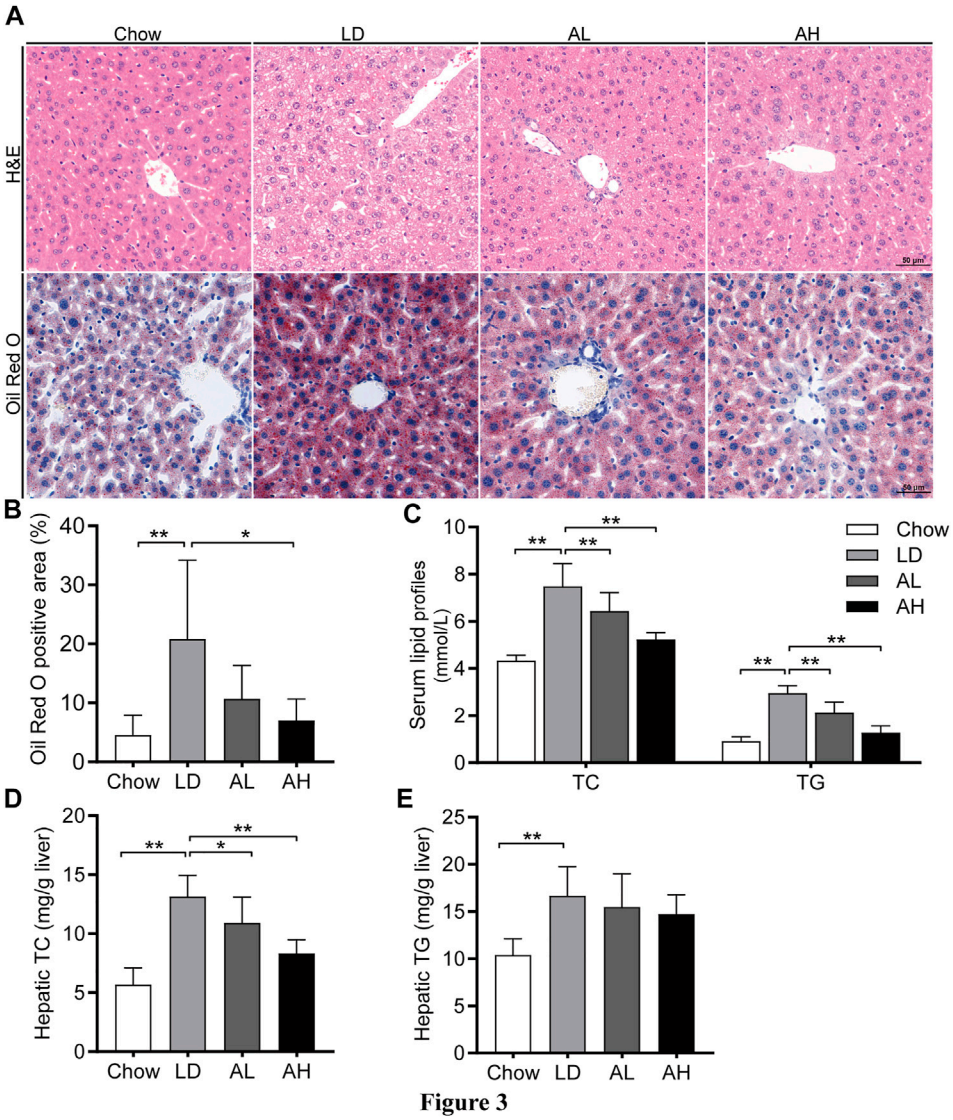

Figure 3

FIGURE 3 | APS attenuated LD-induced metabolic disorders. **(A)** Representative images of H&E and Oil Red O staining per group (scale bar: 50 μm). **(B)** Percentage of Oil Red O positive area. **(C)** Serum levels of total cholesterol (TC) and triglycerides (TG). **(D)** Hepatic level of TC. **(E)** Hepatic level of TG. Data are the mean ± SD (n = 10). *p < 0.05, **p < 0.01. Chow, chow diet; LD, lithogenic diet; AL, low-dose APS; AH, high-dose APS.

decreased significantly in mice fed the LD (**Figure 5A**). APS significantly increased hepatic mRNA expression of *Cyp7a1* and *Cyp7b1* (**Figure 5A**). Western blotting confirmed the increased protein level of *Cyp7a1* and *Cyp7b1* in APS-treated mice (**Figure 5B**). Consistent with the increased *de novo* synthesis of BAs from cholesterol, the hepatic level of cholesterol was reduced (**Figure 3D**). Compared with the LD group, expression of *Fgf* receptor 4 (*Fgfr4*) and its coreceptor *β-klotho* was unchanged in APS-treated mice (**Figure 5C**). Hepatic expression of *Fxr* and *Shp* was unchanged (**Supplementary Figure S3D**), which suggested that hepatic *Fxr* might not account for the increased expression of *Cyp7a1* and *Cyp7b1* in APS-treated mice. APS reduced mRNA and protein expression of *Abcg5* and *Abcg8* significantly, which were increased by LD consumption (**Figures 5D,E**). This finding was consistent with the reduced cholesterol level in gallbladder bile (**Figure 2A**). Taken together, these results indicated that increased expression of *Cyp7a1* and *Cyp7b1* might have resulted from the inhibition of intestinal *Fxr* and decreased *Fgf15* expression in the ileum.

Astragalus polysaccharides Changed Expression of the Genes Involved in Bile Acids Transport in the Liver and Ileum

Uptake and efflux of BAs are mediated by a series of efficient BA transporters in the liver. Sodium taurocholate cotransporting polypeptide (*Ntcp*) and organic anion-transporting polypeptides (*Oatps*) are responsible for transporting BAs

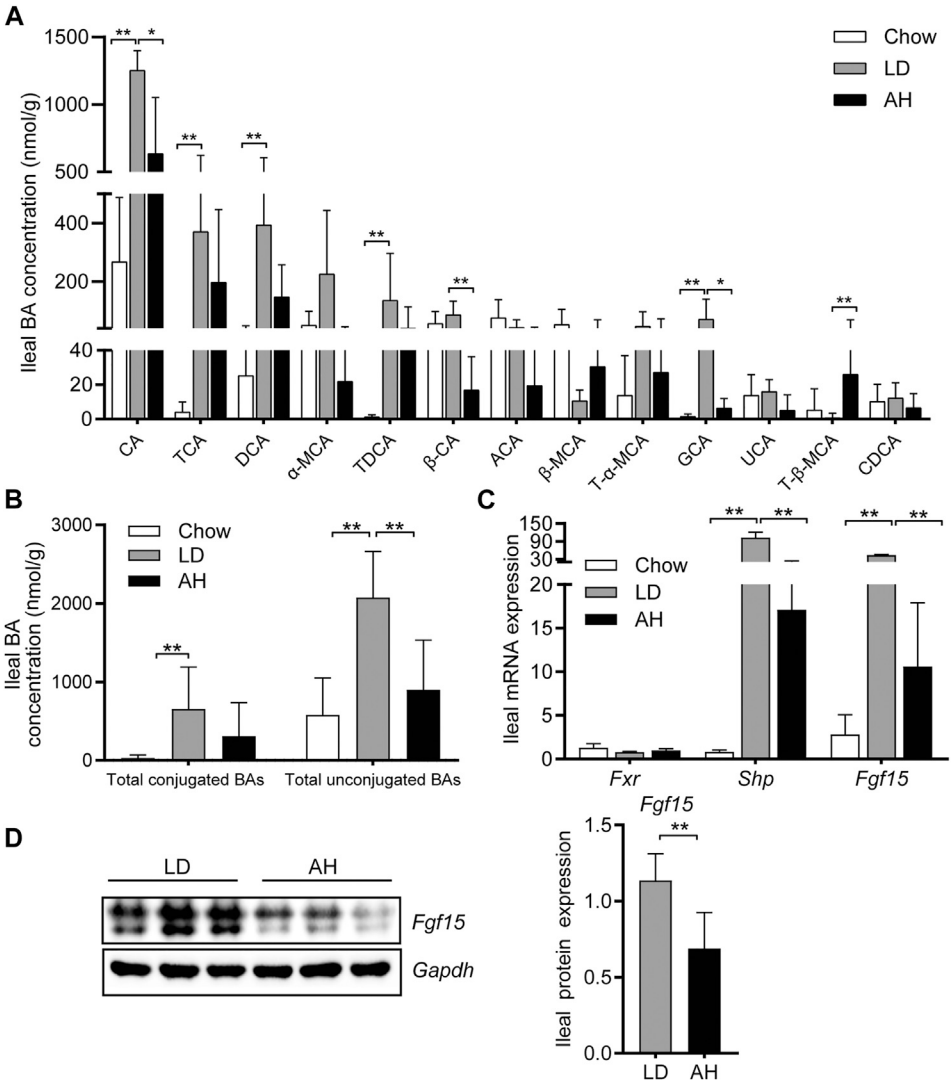

FIGURE 4 | Bile acid (BA) species in the ileum and *Fxr–Fgf15* axis. **(A)** Analyses of BA species (n = 10). Top-13 most abundant BA species are shown. **(B)** Total conjugated BAs and unconjugated BAs (n = 10). **(C)** Ileal mRNA expression of *Fxr*, *Shp*, and *Fgf15* (n = 8). **(D)** Ileal expression (left panel) and quantification (right panel) of *Fgf15* protein (n = 6). Data are the mean ± SD. *p < 0.05, **p < 0.01. Chow, chow diet; LD, lithogenic diet; AH, high-dose APS.

from portal blood into hepatocytes (Kunst et al., 2020). mRNA expression of *Oatp1a1* and *Oatp1a4* was decreased significantly and increased in mice fed the LD, respectively, whereas APS reversed these changes (**Supplementary Figure S3A**). mRNA expression of *Oatp1b2* and *Ntcp* did not change significantly in any group (**Supplementary Figure S3A**). For sinusoidal uptake transporters, increased mRNA expression of *Mrp3* and *Mrp4* in the LD group was decreased significantly by APS supplementation (**Supplementary Figure S3A**). *Bsep* and *Mrp2* pump bile salts out of hepatocytes into primary bile (Kunst et al., 2020). mRNA expression of *Bsep* was increased significantly in mice fed the LD, but APS had little effect on mRNA expression of *Bsep* and *Mrp2* (**Supplementary Figure S3A**). mRNA expression of *Abcb4*—a major phospholipid transporter (Poupon et al., 2013)—was not affected significantly (**Supplementary Figure S3C**).

Apical sodium-dependent bile acid transporter (*Asbt*) actively reabsorbs BAs in the distal ileum, and the reabsorbed BAs are then transported into the portal circulation by organic solute transporter α/β (*Ostα/β*) (Ticho et al., 2019). LD consumption decreased expression of *Asbt* mRNA and *Ostβ* mRNA in the ileum significantly, which might have been caused by activation of intestinal *Fxr* (Ticho et al., 2019), whereas APS normalized these changes partly (**Supplementary Figure S3B**).

Astragalus polysaccharides Reversed Lithogenic Diet-Induced Gut Dysbiosis in Mice

We further explored the influence of APS on the gut microbiota by 16S rRNA-sequencing. The Shannon Index and Simpson Index were reduced significantly in the LD group, and the

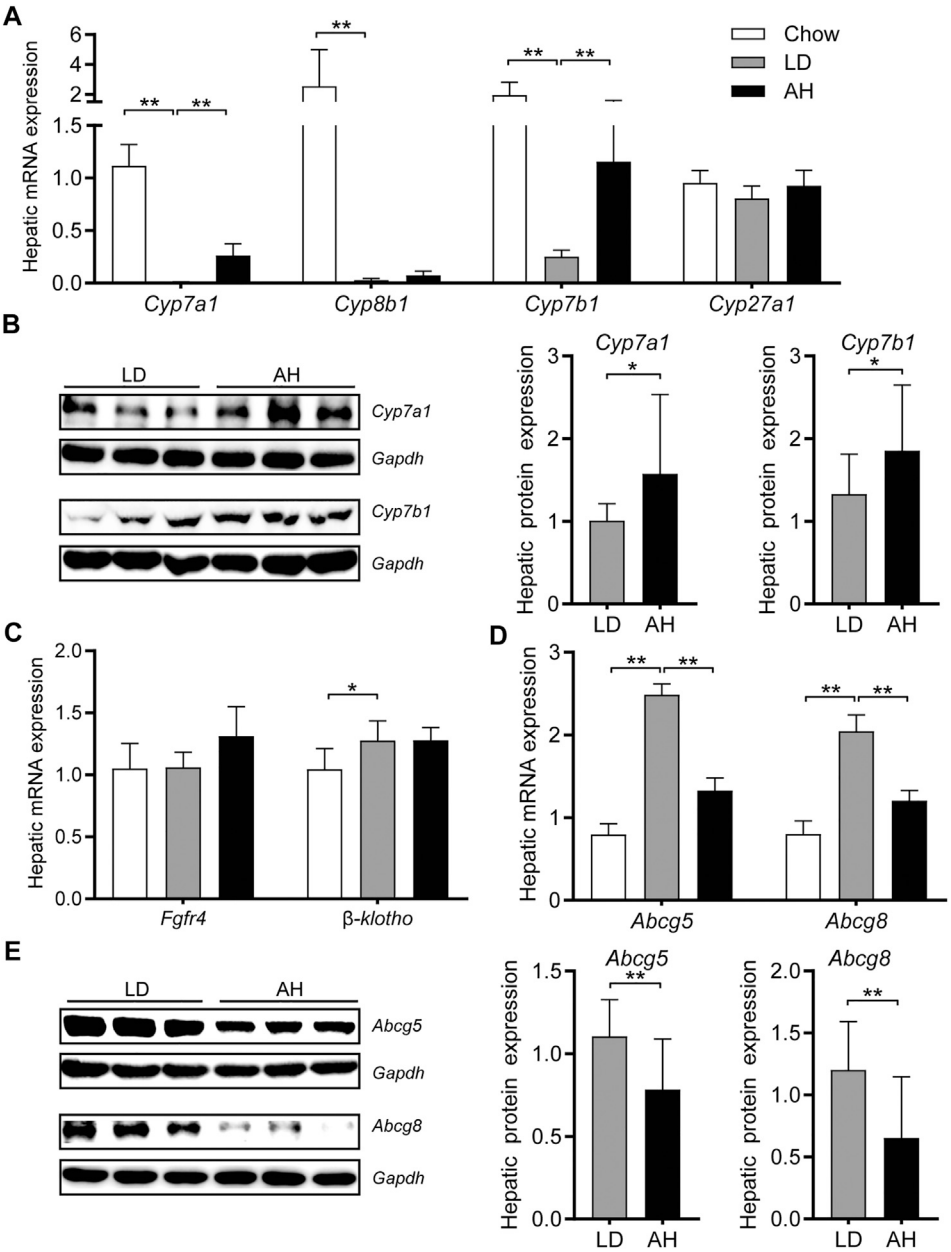

FIGURE 5 | Expression of the genes involved in cholesterol transport and bile-acid synthesis in the liver. **(A)** mRNA expression of *Cyp7a1*, *Cyp8b1*, *Cyp7b1*, and *Cyp27a1* ($n = 8$). **(B)** Protein expression (left panel) and quantification (middle and right panel) of *Cyp7a1* and *Cyp7b1* ($n = 6$). **(C)** mRNA expression of *Fgfr4* and *β-klotho* ($n = 8$). **(D)** mRNA expression of *Abcg5* and *Abcg8* ($n = 8$). **(E)** Protein expression (left panel) and quantification (middle and right panel) of *Abcg5* and *Abcg8* ($n = 6$). Data are the mean ± SD. $^{*}p < 0.05$, $^{**}p < 0.01$. Chow, chow diet; LD, lithogenic diet; AH, high-dose APS.

Simpson Index was increased significantly by APS supplementation, which suggested that APS could improve the diversity of the gut microbiota (**Figure 6A**). Weighted UniFrac PCoA showed clear separation among groups (**Figure 6B**). Taxonomic profiling of the top-nine most abundant phyla showed that LD consumption significantly increased the relative abundance of the phyla Verrucomicrobia, Proteobacteria and Cyanobacteria and reduced the relative abundance of the phylum Bacteroidetes, whereas APS reversed the changes in the abundance of Bacteroidetes and Verrucomicrobia (**Figures 6C,D**). Considering the intestinal crosstalk between BAs and microbiota, we undertook Spearman's correlation analysis between BAs in the ileum and the relative abundance of bacterial genera. In general, the abundance of *[Eubacterium]_fissicatena_group*, *Intestinimonas*, and *Negativibacillus* genera was correlated negatively with the level of β-MCA and T-β-MCA, whereas the abundance of the *Muribaculum* genus was correlated positively with the T-β-MCA level (**Supplementary Figure S4**).

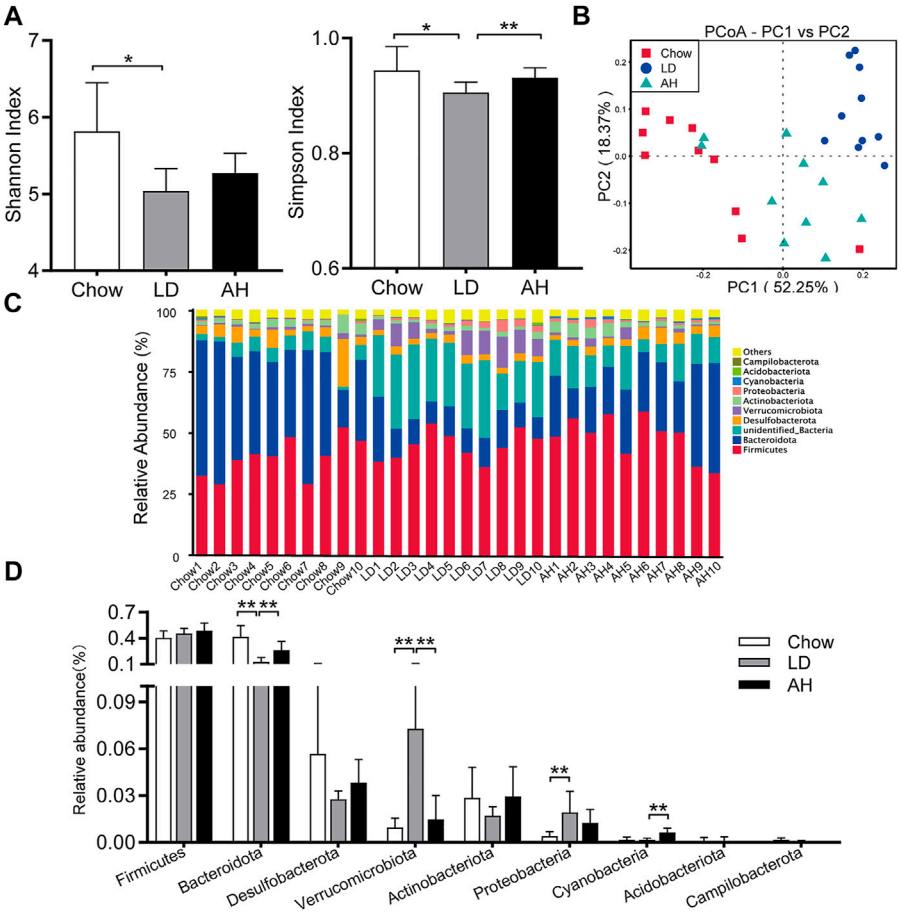

FIGURE 6 | APS changed the composition of the gut microbiota. **(A)** Shannon Index and Simpson Index. **(B)** Weighted Unifrac principal coordinate analysis (PCoA). **(C, D)** Multigroup difference analysis of the top-9 most abundant phyla. Data are the mean ± SD (n = 10). *p < 0.05, **p < 0.01. Chow, chow diet; LD, lithogenic diet; AH, high-dose APS.

DISCUSSION

We found that APS could ameliorate LD-induced CG formation in mice. APS supplementation decreased the level of TC, the HI of BAs and CSI in bile. The protective effect of APS might result from reduced absorption or reabsorption of CA in the intestine and increased BA synthesis in the liver. Increased expression of *Cyp7a1* and *Cyp7b1* might have resulted from inhibition of intestinal *Fxr* and decreased expression of *Fgf15* in the ileum. APS also improved LD-induced gut dysbiosis.

CG disease has relationships with several metabolic abnormalities: obesity, type-2 diabetes mellitus, atherosclerosis, and nonalcoholic fatty liver disease (Lammert et al., 2016; Di Ciaula et al., 2019). Recent studies have indicated that APS can ameliorate obesity, insulin resistance, hepatic steatosis, and hypercholesteremia in mice and cell lines (Huang et al., 2017; Ke et al., 2017; Hong et al., 2020). We found that APS could ameliorate LD-induced CG formation in mice. In addition, APS improved LD-induced hepatic steatosis and hypercholesterolemia.

Studies have shown that dietary fiber can protect against CG formation in prairie dogs, and this effect was associated with a decrease in the cholesterol level in bile (Schwesinger et al., 1999). Reduced reabsorption of BAs in the ileum is considered a major mechanism that explains the cholesterol-reducing effects of dietary fibers (Naumann et al., 2020). Several studies have reported that the viscous and adsorptive effects of dietary fibers can reduce BA reabsorption in the intestine (Naumann et al., 2018; Naumann et al., 2019; Naumann et al., 2020). In the intestine, BAs are absorbed in two ways: active and passive (Ticho et al., 2019). Active absorption relies on transepithelial transporters located on apical and basolateral sides, such as *Asbt* and *Ostα/β* in the ileum (Ticho et al., 2019). BAs can also diffuse passively through membranes, and passive absorption can occur in all regions of the small and large intestines (Ticho et al., 2019). We found that APS could inhibit BA absorption and reduce the CA level in the ileum, and that the level of T-β-MCA was increased. APS decreased the LD-induced expression of *Fgf15*, a target gene of *Fxr* (Kong et al., 2012). *Fgf15* reaches the liver through portal blood, where it binds to the *Fgfr4/β-klotho* heterodimer complex to inhibit BA synthesis in the liver (Wahlstrom et al., 2016).

Cholesterol hypersaturation is a prerequisite for CG formation, and excessive hepatic secretion of cholesterol is a

cause of supersaturated bile (Lammert et al., 2016). Hydrophilic BAs such as β-MCA and UDCA can act as biliary cholesterol-desaturating agents for the prevention and dissolution of CGs (Jazrawi et al., 1992; Wang and Tazuma, 2002). In the present study, in accordance with the relieved activation of intestinal *Fxr* and decreased *Fgf15* expression in the ileum, hepatic expression of *Cyp7a1*—the rate-limiting enzyme for BA synthesis (Wahlstrom et al., 2016)—and *Cyp7b1* was increased. Enhanced BA synthesis can increase cholesterol depletion. As a result, the cholesterol level in the bile and liver was reduced, and expression of *Abcg5* and *Abcg8* [which are responsible for biliary cholesterol secretion (Lammert et al., 2016)] was also decreased by APS. More hydrophilic BAs, such as T-α-MCA, T-β-MCA and TUDCA, were synthesized in mice, which decreased the HI of BAs and increased cholesterol solubility in bile. It has been reported that the biliary secretion of phospholipids and cholesterol is coupled to that of BAs under physiological conditions (Scherstén et al., 1971; Carulli et al., 1984; Gooijert et al., 2015). Several studies find that acute BAs infusion stimulates biliary secretion of phospholipids and cholesterol (Carulli et al., 1984; Gooijert et al., 2015). Whereas there is hypersaturation of the bile with cholesterol in mice fed LD, whether the correlation is altered or not still needs to be further explored. Hepatic *Shp* also regulates expression of *Cyp7a1* and *Cyp7b1* (Kong et al., 2012). However, a significant change in hepatic *Shp* expression was not observed, which suggested that hepatic *Fxr* might not account for the increased expression of *Cyp7a1* and *Cyp7b1* noted in APS-treated mice.

Recent studies have shown that CG formation is associated with alterations in the gut microbiota (Wang et al., 2017; Grigor'eva and Romanova, 2020; Wang et al., 2020b). APS is a type of prebiotic that can modulate the gut microbiome and host metabolism (Hong et al., 2020). We discovered that APS improved the diversity of the gut microbiota and increased the relative abundance of bacteria belonging to the Bacteroidetes phylum, data that are consistent with results from a study by Hong and coworkers (Hong et al., 2020).

Our study had two main limitations. First, the relative BA composition in BA pools in the humans and mice is different (de Aguiar Vallim et al., 2013). Mouse models of gallstones established with a combination of cholesterol and cholic acid are used widely (Wang et al., 2018; Munoz et al., 2019; Wang et al., 2020a), but the pathogenesis of CG formation in mice and humans is not identical. For example, humans do not ingest CA *via* the diet. When translating findings from mice to humans, these differences should be taken into account. Second, the hypotheses that lower CA absorption, enhanced BA synthesis, or microbial changes cause beneficial effects must be verified by additional mechanistic experiments, which we will do in the future.

CONCLUSION

Although cholecystectomy is efficacious treatment for CG disease, it has some limitations, such as surgical complications and high socioeconomic costs. More emphasis should be given to the prevention of CG disease. We found that the herbal polysaccharide APS demonstrated benefits against CG disease, which may be associated with enhanced BA synthesis and improved gut microbiota. Our study provides preliminary findings of APS preventing CG in a murine model. Future research is required to understand the underlying mechanism and the potential relevance to the prevention of human CG disease.

DATA AVAILABILITY STATEMENT

The data presented in the study are deposited in the NCBI BioProject repository, accession number PRJNA725334.

ETHICS STATEMENT

The animal study was reviewed and approved by the Affiliated Sixth People's Hospital within Shanghai Jiao Tong University.

AUTHOR CONTRIBUTIONS

QZ undertook most of the study, analyzed the data and drafted the manuscript. SS, XY, and JC helped in animal experiments and manuscript revision. YS and SW helped in H&E and Oil Red O staining of tissues. JX and MN helped in data analyses. ZD and XW supervised the project and revised the manuscript. All authors approved the final version of the manuscript.

FUNDING

This work was supported by the National Natural Science Foundation of China (No. 81870452) and grants from the Shanghai Science and Technology Program (No. 19411951500).

SUPPLEMENTARY MATERIAL

The Supplementary Material for this article can be found online at: https://www.frontiersin.org/articles/10.3389/fphar.2021.701003/full#supplementary-material

REFERENCES

Akiyoshi, T., Uchida, K., Takase, H., Nomura, Y., and Takeuchi, N. (1986). Cholesterol Gallstones in Alloxan-Diabetic Mice. *J. Lipid Res.* 27 (9), 915–924.

Carey, M. C. (1978). Critical Tables for Calculating the Cholesterol Saturation of Native Bile. *J. Lipid Res.* 19 (8), 945–955. doi:10.1016/s0022-2275(20)40677-7

Carulli, N., Loria, P., Bertolotti, M., Ponz de Leon, M., Menozzi, D., Medici, G., et al. (1984). Effects of Acute Changes of Bile Acid Pool Composition on Biliary Lipid Secretion. *J. Clin. Invest.* 74 (2), 614–624. doi:10.1172/jci111459

de Aguiar Vallim, T. Q., Tarling, E. J., and Edwards, P. A. (2013). Pleiotropic Roles of Bile Acids in Metabolism. *Cell Metab* 17 (5), 657–669. doi:10.1016/j.cmet.2013.03.013

Di Ciaula, A., Wang, D. Q.-H., and Portincasa, P. (2018). An Update on the Pathogenesis of Cholesterol Gallstone Disease. *Curr. Opin. Gastroenterol.* 34 (2), 71–80. doi:10.1097/MOG.0000000000000423

Di Ciaula, A., Wang, D. Q.-H., and Portincasa, P. (2019). Cholesterol Cholelithiasis: Part of a Systemic Metabolic Disease, Prone to Primary Prevention. *Expert Rev. Gastroenterol. Hepatol.* 13 (2), 157–171. doi:10.1080/17474124.2019.1549988

Edgar, R. C. (2013). UPARSE: Highly Accurate OTU Sequences from Microbial Amplicon Reads. *Nat. Methods* 10 (10), 996–998. doi:10.1038/nmeth.2604

Everhart, J. E., and Ruhl, C. E. (2009). Burden of Digestive Diseases in the United States Part III: Liver, Biliary Tract, and Pancreas. *Gastroenterology* 136 (4), 1134–1144. doi:10.1053/j.gastro.2009.02.038

Gooijert, K. E. R., Havinga, R., Wolters, H., Wang, R., Ling, V., Tazuma, S., et al. (2015). The Mechanism of Increased Biliary Lipid Secretion in Mice with Genetic Inactivation of Bile Salt export Pump. *Am. J. Physiology-Gastrointestinal Liver Physiol.* 308 (5), G450–G457. doi:10.1152/ajpgi.00391.2014

Grigor'eva, I. N., and Romanova, T. I. (2020). Gallstone Disease and Microbiome. *Microorganisms* 8 (6), 835. doi:10.3390/microorganisms8060835

Heuman, D. M. (1989). Quantitative Estimation of the Hydrophilic-Hydrophobic Balance of Mixed Bile Salt Solutions. *J. Lipid Res.* 30 (5), 719–730. doi:10.1016/s0022-2275(20)38331-0

Hong, Y., Li, B., Zheng, N., Wu, G., Ma, J., Tao, X., et al. (2020). Integrated Metagenomic and Metabolomic Analyses of the Effect of Astragalus Polysaccharides on Alleviating High-Fat Diet-Induced Metabolic Disorders. *Front. Pharmacol.* 11, 833. doi:10.3389/fphar.2020.00833

Huang, F., Zheng, X., Ma, X., Jiang, R., Zhou, W., Zhou, S., et al. (2019). Theabrownin from Pu-Erh tea Attenuates Hypercholesterolemia via Modulation of Gut Microbiota and Bile Acid Metabolism. *Nat. Commun.* 10 (1), 4971. doi:10.1038/s41467-019-12896-x

Huang, Y.-C., Tsay, H.-J., Lu, M.-K., Lin, C.-H., Yeh, C.-W., Liu, H.-K., et al. (2017). Astragalus Membranaceus-Polysaccharides Ameliorates Obesity, Hepatic Steatosis, Neuroinflammation and Cognition Impairment without Affecting Amyloid Deposition in Metabolically Stressed APPswe/PS1dE9 Mice. *Ijms* 18 (12), 2746. doi:10.3390/ijms18122746

Jazrawi, R. P., Pigozzi, M. G., Galatola, G., Lanzini, A., and Northfield, T. C. (1992). Optimum Bile Acid Treatment for Rapid Gall Stone Dissolution. *Gut* 33 (3), 381–386. doi:10.1136/gut.33.3.381

Jia, W., Wei, M., Rajani, C., and Zheng, X. (2021). Targeting the Alternative Bile Acid Synthetic Pathway for Metabolic Diseases. *Protein Cell* 12 (5), 411–425. doi:10.1007/s13238-020-00804-9

Ke, B., Ke, X., Wan, X., Yang, Y., Huang, Y., Qin, J., et al. (2017). Astragalus Polysaccharides Attenuates TNF-α-Induced Insulin Resistance via Suppression of miR-721 and Activation of PPAR-γ and PI3K/AKT in 3T3-L1 Adipocytes. *Am. J. Transl. Res.* 9 (5), 2195–2206.

Kong, B., Wang, L., Chiang, J. Y. L., Zhang, Y., Klaassen, C. D., and Guo, G. L. (2012). Mechanism of Tissue-specific Farnesoid X Receptor in Suppressing the Expression of Genes in Bile-Acid Synthesis in Mice. *Hepatology* 56 (3), 1034–1043. doi:10.1002/hep.25740

Kunst, R. F., Verkade, H. J., Oude Elferink, R. P. J., and Graaf, S. F. J. (2021). Targeting the Four Pillars of Enterohepatic Bile Salt Cycling; Lessons from Genetics and Pharmacology. *Hepatology* 73, 2577–2585. doi:10.1002/hep.31651

Lammert, F., Gurusamy, K., Ko, C. W., Miquel, J.-F., Méndez-Sánchez, N., Portincasa, P., et al. (2016). Gallstones. *Nat. Rev. Dis. Primers* 2, 16024. doi:10.1038/nrdp.2016.24

Muñoz, L. E., Boeltz, S., Bilyy, R., Schauer, C., Mahajan, A., Widulin, N., et al. (2019). Neutrophil Extracellular Traps Initiate Gallstone Formation. *Immunity* 51 (3), 443–450. doi:10.1016/j.immuni.2019.07.002

Naumann, S., Haller, D., Eisner, P., and Schweiggert-Weisz, U. (2020). Mechanisms of Interactions between Bile Acids and Plant Compounds-A Review. *Ijms* 21 (18), 6495. doi:10.3390/ijms21186495

Naumann, S., Schweiggert-Weisz, U., Bader-Mittermaier, S., Haller, D., and Eisner, P. (2018). Differentiation of Adsorptive and Viscous Effects of Dietary Fibres on Bile Acid Release by Means of *In Vitro* Digestion and Dialysis. *Ijms* 19 (8), 2193. doi:10.3390/ijms19082193

Naumann, S., Schweiggert-Weisz, U., Haller, D., and Eisner, P. (2019). Retention of Primary Bile Acids by Lupin Cell Wall Polysaccharides under *In Vitro* Digestion Conditions. *Nutrients* 11 (9), 2117. doi:10.3390/nu11092117

Posa, M. (2014). Heuman Indices of Hydrophobicity of Bile Acids and Their Comparison with a Newly Developed and Conventional Molecular Descriptors. *Biochimie* 97, 28–38. doi:10.1016/j.biochi.2013.09.010

Poupon, R., Rosmorduc, O., Boëlle, P. Y., Chrétien, Y., Corpechot, C., Chazouillères, O., et al. (2013). Genotype-phenotype Relationships in the Low-Phospholipid-Associated Cholelithiasis Syndrome: a Study of 156 Consecutive Patients. *Hepatology* 58 (3), 1105–1110. doi:10.1002/hep.26424

Quast, C., Pruesse, E., Yilmaz, P., Gerken, J., Schweer, T., Yarza, P., et al. (2013). The SILVA Ribosomal RNA Gene Database Project: Improved Data Processing and Web-Based Tools. *Nucleic Acids Res.* 41 (database issue), D590–D596. doi:10.1093/nar/gks1219

Sayin, S. I., Wahlström, A., Felin, J., Jäntti, S., Marschall, H.-U., Bamberg, K., et al. (2013). Gut Microbiota Regulates Bile Acid Metabolism by Reducing the Levels of Tauro-Beta-Muricholic Acid, a Naturally Occurring FXR Antagonist. *Cel Metab.* 17 (2), 225–235. doi:10.1016/j.cmet.2013.01.003

Scherstén, T., Nilsson, S., Cahlin, E., Filipson, M., and Brodin-Persson, G. (1971). Relationship between the Biliary Excretion of Bile Acids and the Excretion of Water, Lecithin, and Cholesterol in Man. *Eur. J. Clin. Invest.* 1 (4), 242–247. doi:10.1111/eci.1971.1.4.242

Schwesinger, W. H., Kurtin, W. E., Page, C. P., Stewart, R. M., and Johnson, R. (1999). Soluble Dietary Fiber Protects against Cholesterol Gallstone Formation. *Am. J. Surg.* 177 (4), 307–310. doi:10.1016/s0002-9610(99)00047-1

Sun, S., Wang, K., Sun, L., Cheng, B., Qiao, S., Dai, H., et al. (2020). Therapeutic Manipulation of Gut Microbiota by Polysaccharides of Wolfiporia Cocos Reveals the Contribution of the Gut Fungi-Induced PGE2 to Alcoholic Hepatic Steatosis. *Gut Microbes* 12 (1), 1830693. doi:10.1080/19490976.2020.1830693

Ticho, A. L., Malhotra, P., Dudeja, P. K., Gill, R. K., and Alrefai, W. A. (2019). Intestinal Absorption of Bile Acids in Health and Disease. *Compr. Physiol.* 10 (1), 21–56. doi:10.1002/cphy.c190007

Wahlström, A., Sayin, S. I., Marschall, H.-U., and Bäckhed, F. (2016). Intestinal Crosstalk between Bile Acids and Microbiota and its Impact on Host Metabolism. *Cel Metab.* 24 (1), 41–50. doi:10.1016/j.cmet.2016.05.005

Wang, D. Q.-H., and Tazuma, S. (2002). Effect of β-muricholic Acid on the Prevention and Dissolution of Cholesterol Gallstones in C57L/J Mice. *J. Lipid Res.* 43 (11), 1960–1968. doi:10.1194/jlr.m200297-jlr200

Wang, H. H., Bari, O., Arnatt, C. K., Liu, M., Portincasa, P., and Wang, D. Q. H. (2020a). Activation of Estrogen Receptor G Protein-Coupled Receptor 30 Enhances Cholesterol Cholelithogenesis in Female Mice. *Hepatology* 72 (6), 2077–2089. doi:10.1002/hep.31212

Wang, Q., Hao, C., Yao, W., Zhu, D., Lu, H., Li, L., et al. (2020b). Intestinal flora Imbalance Affects Bile Acid Metabolism and Is Associated with Gallstone Formation. *BMC Gastroenterol.* 20 (1), 59. doi:10.1186/s12876-020-01195-1

Wang, Q., Jiao, L., He, C., Sun, H., Cai, Q., Han, T., et al. (2017). Alteration of Gut Microbiota in Association with Cholesterol Gallstone Formation in Mice. *BMC Gastroenterol.* 17 (1), 74. doi:10.1186/s12876-017-0629-2

Wang, T. Y., Portincasa, P., Liu, M., Tso, P., and Wang, D. Q.-H. (2018). Mouse Models of Gallstone Disease. *Curr. Opin. Gastroenterol.* 34 (2), 59–70. doi:10.1097/MOG.0000000000000417

Wu, T.-R., Lin, C.-S., Chang, C.-J., Lin, T.-L., Martel, J., Ko, Y.-F., et al. (2019). Gut Commensal Parabacteroides Goldsteinii Plays a Predominant Role in the Anti-obesity Effects of Polysaccharides Isolated from Hirsutella Sinensis. *Gut* 68 (2), 248–262. doi:10.1136/gutjnl-2017-315458

Conflict of Interest: The authors declare that the research was conducted in the absence of any commercial or financial relationships that could be construed as a potential conflict of interest.

frontiers in Pharmacology

ORIGINAL RESEARCH
published: 21 July 2021
doi: 10.3389/fphar.2021.693298

Glycoproteins From *Rabdosia japonica* var. *glaucocalyx* Regulate Macrophage Polarization and Alleviate Lipopolysaccharide-Induced Acute Lung Injury in Mice *via* TLR4/NF-κB Pathway

An-qi Ren[1†], Hui-jun Wang[2†], Hai-yan Zhu[3], Guan Ye[4], Kun Li[4], Dao-feng Chen[5], Tao Zeng[6] and Hong Li[1]**

[1]Department of Pharmacology, School of Pharmacy, Fudan University, Shanghai, China, [2]The MOE Key Laboratory for Standardization of Chinese Medicines and the SATCM Key Laboratory for New Resources and Quality Evaluation of Chinese Medicines, Institute of Chinese Materia Medica, Shanghai University of Traditional Chinese Medicine, Shanghai, China, [3]Department of Biological Medicines and Shanghai Engineering Research Center of Immuno Therapeutics, School of Pharmacy, Fudan University, Shanghai, China, [4]Central Research Institute, Shanghai Pharmaceuticals Holding Co., Ltd., Shanghai, China, [5]Department of Pharmacognosy, School of Pharmacy, Fudan University, Shanghai, China, [6]Clinical Trial Institution, Obstetrics and Gynecology Hospital of Fudan University, Shanghai, China

OPEN ACCESS

Edited by:
Jing Zhao,
University of Macau, China

Reviewed by:
Lu-Yuan Peng,
Jilin University, China
Duanwu Zhang,
Fudan University, China

***Correspondence:**
Hong Li
lxzhang@shmu.edu.cn
Tao Zeng
zengtao1283@163.com

[†]These authors have contributed equally to this work

Specialty section:
This article was submitted to Inflammation Pharmacology, a section of the journal Frontiers in Pharmacology

Received: 10 April 2021
Accepted: 24 June 2021
Published: 21 July 2021

Citation:
Ren A-qi, Wang H-jun, Zhu H-yan, Ye G, Li K, Chen D, Zeng T and Li H (2021) Glycoproteins From Rabdosia japonica var. glaucocalyx Regulate Macrophage Polarization and Alleviate Lipopolysaccharide-Induced Acute Lung Injury in Mice via TLR4/NF-κB Pathway. Front. Pharmacol. 12:693298. doi: 10.3389/fphar.2021.693298

Background and Aims: *Rabdosia japonica* var. *glaucocalyx* is a traditional Chinese medicine (TCM) for various inflammatory diseases. This present work aimed to investigate the protective effects of *R. japonica* var. *glaucocalyx* glycoproteins on lipopolysaccharide (LPS)-induced acute lung injury (ALI) and the potential mechanism.

Methods: Glycoproteins (XPS) were isolated from *R. japonica* var. *glaucocalyx*, and homogeneous glycoprotein (XPS5-1) was purified from XPS. ANA-1 cells were used to observe the effect of glycoproteins on the secretion of inflammatory mediators by enzyme-linked immunosorbent assay (ELISA). Flow cytometry assay, immunofluorescence assay, and Western blot analysis were performed to detect macrophage polarization *in vitro*. The ALI model was induced by LPS via intratracheal instillation, and XPS (20, 40, and 80 mg/kg) was administered intragastrically 2 h later. The mechanisms of XPS against ALI were investigated by Western blot, ELISA, and immunohistochemistry.

Results: *In vitro*, XPS and XPS5-1 downregulated LPS-induced proinflammatory mediators production including tumor necrosis factor-α (TNF-α), interleukin-1β (IL-1β), IL-6, and nitric oxide (NO) and upregulated LPS-induced IL-10 secretion. The LPS-stimulated macrophage polarization was also modulated from M1 to M2. *In vivo*, XPS maintained pulmonary histology with significantly reducing protein concentration and numbers of mononuclear cells in bronchoalveolar lavage fluid (BALF). The level of IL-10 in BALF was upregulated by XPS treatment. The level of cytokines including TNF-α, IL-1β, and IL-6 was downregulated. XPS also decreased infiltration of macrophages and polymorphonuclear leukocytes (PMNs) in lung. XPS suppressed the expression of key proteins in the TLR4/NF-κB signal pathway.

Conclusion: XPS was demonstrated to be a potential agent for treating ALI. Our findings might provide evidence supporting the traditional application of *R. japonica* var. *glaucocalyx* in inflammation-linked diseases.

Keywords: *Rabdosia japonica* var *glaucocalyx*, glycoproteins, acute lung injury, macrophage polarization, inflammation, TLR4/NF-κB signal pathway

INTRODUCTION

Rabdosia genus is an important genus of the Labiatae family, with about 150 species worldwide (Huang et al., 2018). *Rabdosia japonica* (Burm. f.) Hara var. *glaucocalyx* (Maxim.) is a synonym of *Isodon japonicus* var. *glaucocalyx* (Maxim.) H.W.Li. *R. japonica* var. *glaucocalyx*, distributed mainly in northern China, is a traditional Chinese medicine (TCM) for hepatitis, gastritis, mastitis, and cough. It is recorded in Chinese Materia Medica (Hanson, 2011).

Previous studies focused a lot on organic extracts diterpenoids or phenolic compounds isolated from this plant. These active ingredients showed antioxidant, antitumor, and anti-inflammatory activities in treating neuroinflammation and gastritis (Hanson, 2011). Glycoproteins, as a kind of water-soluble compounds formed by carbohydrates and protein, possess the activities of modulating immunity (Fu et al., 2021) (Niu et al., 2020). The glycoproteins of *R. japonica* var. *glaucocalyx* (XPS) were isolated from the aqueous extracts of this plant, and two homogeneous glycoproteins (XPS5-1 and XPS10-1) were purified from XPS (Wang et al., 2020a). Our previous research found that XPS5-1 and XPS10-1 had antitumor activity *in vitro* (Wang et al., 2020a) but their anti-inflammatory effect remained unclear. According to our preliminary experiment, only XPS and XPS5-1 showed promising anti-inflammatory activity *in vitro*, and its anti-inflammatory mechanisms have not been reported yet.

Acute lung injury (ALI) is a kind of respiratory disorder with high mortality and calls for researches on effective drugs. The lung injury is characterized by excessive accumulation of inflammatory cells, uncontrolled secretion of cytokines, and damages of the alveolar-capillary membrane including epithelium and endothelium (Ge et al., 2020). Tentative clinical treatments including low tidal volume ventilation, modulation of immune defense, or fluid-conservative therapy are inefficient to ALI (Nieman et al., 2020). It was reported that lipopolysaccharide (LPS) could cause ALI (Ye and Liu, 2020) through the induction of innate immune response and inflammation (Huang et al., 2019). An animal model of ALI was established by intratracheal instillation of LPS in mice.

LPS activates TLR4, a member of the toll-like receptors (TLRs) family (Zhou et al., 2019). After recognizing LPS, the TLR4-linked nuclear transcription factor-κB (NF-κB) pathway can be activated through MyD88- and TRIF-dependent pathways (Wang et al., 2020c). The activated MyD88 pathway will upregulate the inflammatory cytokines (Han et al., 2018). High-level cytokines secreted by monocyte-macrophages in lungs severely affect pulmonary gas exchange and aggravate ALI by initiating, amplifying, and prolonging the inflammatory response (Liu J. et al., 2019). Reducing proinflammatory cytokines and increasing anti-inflammatory cytokines are at the heart of processes mediating lung inflammation (Watanabe et al., 2019).

The lung injury induced by LPS is associated with the lung excessive inflammation, which causes the activation of alveolar macrophage polarization homeostasis (Lin et al., 2020). Alveolar macrophages, as a kind of high heterogeneity and plasticity innate immunocyte, play an important role in the response to pneumonia and tissue repair (Zhou et al., 2020). Macrophages are generally grouped into classically activated (M1) macrophages and alternatively activated (M2) macrophages (Orecchioni et al., 2019). An increased M1 macrophage ratio, recruitment of neutrophils, and secretion of a large number of cytokines were observed in the acute inflammatory phase of ALI (Lin et al., 2020). M1 macrophages are found to exacerbate pathological inflammation, while M2 macrophages reduce autophagy and accelerate tissue repair (Su et al.). The dynamic changes of subsets balance and function of M1/M2 macrophages have a significant effect on inflammatory response (Zhou et al., 2020). Studies have indicated that compounds, which regulate the macrophages' polarization, may reduce the lung injury through anti-inflammatory effects (Lin et al., 2020).

Here, the anti-inflammatory activity of XPS and XPS5-1 was first elucidated in ANA-1 cells (a murine macrophage cell line). Then, the beneficial effect of XPS on ALI mice was explored to seek the effective drug for ALI.

MATERIALS AND METHODS

Materials and Reagents

The commercial herb of *R. japonica* var. *glaucocalyx* was obtained from Huqingyutang Pharmaceutical Co., Ltd. (Hangzhou, China) by Prof. L.H.Wu from the Institute of Chinese Materia Medica, Shanghai University of Traditional Chinese Medicine, serving to authenticate. Monosaccharide standards (l-rhamnose, d-arabinose, d-xylose, d-mannose, d-glucose, d-galactose, and d-galacturonic acid) were obtained from Sigma-Aldrich (St. Louis, MO, United States of America). Diethylaminoethyl (DEAE) cellulose column and Superdex-200 were purchased from GE Healthcare Bio-Sciences AB (Uppsala, Sweden).

LPS (*Escherichia coli* O127:B8), thiazolyl blue tetrazolium bromide (MTT), and dexamethasone (DEX) were purchased from Sigma, United States, for the *in vitro* experiments. RPMI 1640 and FBS were bought from Gibco, America. Dimethyl sulfoxide (DMSO) was purchased from Merck Millipore, Germany. Fluorescently labeled antibodies against mouse CD11b, F4/80, CD86, and CD206 were obtained from

Biolegend (San Diego, CA, United States). Arginase-1 (Cat. No. 93668), inducible nitric oxide synthase (iNOS) (Cat. No. 13120), and secondary antibodies (Cat. No. 4412 and 8889) were bought from CST Company (Beverly, MA, United States). DAPI was obtained from Dalian Meilun Biotechnology Co., Ltd. (China).

LPS (*Escherichia coli* O55:B5) was purchased from Sigma, United States, for the *in vivo* experiments. The ELISA kits were purchased from Boatman (China). Dexamethasone sodium phosphate injection (DEX) was purchased from Jiangxi Province Chuang Xin Pharmaceutical Group Co., Ltd. for the *in vivo* experiments. The ELISA kit for myeloperoxidase (MPO) was purchased from Lianke, Shanghai. Anti-mouse Ly-6G/Ly-6C (Cat. No. 108402) was purchased from Biolegend, United States. F4/80 (Cat. No. ab111101) was purchased from Abcam, Britain. Western blot kits were obtained from Beyotime (Shanghai, China). Antibody TLR4 (Cat. No. ab13556), TRAF6 (Cat. No. ab40675), and MyD88 (Cat. No. ab28763) were obtained from Abcam, Britain. GAPDH (Cat. No. AP0063) was purchased from Bioworld, China. Polyclonal antibodies NF-κB p65 (Cat. No. D14E12) and NF-κB p-p65 (Cat. No. S536) were bought from CST Company (Beverly, MA, United States).

Plant Material and Extract Preparation

Isolation and Purification of XPS

The overground part of *R. japonica* var. *glaucocalyx* (5.0 kg) was extracted with 50 L water at 100°C for 3 h and three times. The supernatant of water extract was combined and concentrated under reduced pressure. After centrifugation, four times 95% ethanol was added and the precipitates were collected and freeze-dried to obtain XPS (315 g, yield rate 6.3%) (Wang et al., 2020 b; Wang et al., 2020c). XPS (5 g) was dissolved in 40 ml water and centrifuged. The residue was collected and centrifuged. The supernatant was combined and fractionated on a DEAE-cellulose column (50 cm × 5 cm). The XPS was eluted stepwise with distilled water, 0.1, 0.2, 0.5, and 1.0 M NaCl, to give XPSW, XPS1, XPS2, XPS5, and XPS10. XPS5 was further separated on a column of superdex-75 and eluted with 0.2 M NaCl to give XPS5-1 (41 mg, yield rate 0.82% from XPS) (Wang et al., 2020a). The total carbohydrate and protein contents were determined by the phenol-sulfuric acid and bicinchoninic acid (BCA) methods, respectively.

Homogeneity and Molecular Weight

High-performance gel permeation chromatography (HPGPC) was performed with Agilent 1,260 instrument fitted with the GPC software and the determination of homogeneity and molecular weights of the glycoproteins sample. The system was linked to the series-connected serial column of Ultrahydrogel 1,000 and Ultrahydrogel 250, ID 7.8 mm, and length 300 mm (Waters, United States), and the sample was eluted with 0.2 M NaCl at a flow rate of 0.80 ml/min at 40.0 ± 0.1°C. The gel filtration column was calibrated by pullulans with known molecular weight. The column temperature was kept at 40.0 ± 0.1°C. NaCl (0.2 M) was used as an eluant and the flow rate was kept at 0.8 ml/min. The sample concentration upon injection was 2 mg/ml and approximately 10 μL was injected (Wang et al., 2015).

Monosaccharide Composition Analysis

The sample was hydrolyzed with 2.0 M trifluoroacetic acid (TFA) at 121°C for 2 h. TFA was completely removed by repeating evaporation with methanol. Water was added to dissolve the residue and reduced by $NaBH_4$ for 3 h at room temperature. After neutralization with acetic acid and evaporation to dryness, the residue was acetylated with acetic anhydride for 1 h at 100°C. The resulting alditol acetates were analyzed by GC-MS (Chaidedgumjorn et al., 2002).

In Vitro Anti-Inflammatory Activity of XPS and XPS5-1 in LPS-Stimulated ANA-1 Macrophage

Cell Culture and *In Vitro* Treatment

ANA-1 cells (ATCC, America) are a murine macrophage cell line for *in vitro* experiments. Cells were cultured in 10% FBS-RPMI 1640 medium (Geng et al., 2020). The cells were plated as 1×10^6 cells/mL, were cultured as 100 μL/well in a 96-well plate for 24 h, and then were treated with compounds with or without LPS for another 24 h (n = 3 for each group).

Cell Viability and Cytokines Assay

The cells were treated with XPS (25, 50, and 100 μg/ml) or XPS5-1 (100 μg/ml) for 24 h and were stimulated by LPS (0.5 μg/ml) simultaneously. DEX (20 μM) was administrated as a positive control. All the supernatant was collected for nitric oxide (NO) and other inflammatory cytokines' testing. The cell viability was tested by MTT and was presented as a percentage of viable cells to the control group (Su et al.).

The production of NO was represented by its end product, nitrite in the cell culture supernatant. The supernatant was mixed with Griess reagent and shook for 15 min. The absorbance was recorded at 540 nm. The levels of TNF-α, IL-10, IL-1β, and IL-6 in collected supernatants were tested by ELISA kits.

Western Blot Analysis

The ANA-1 cells were plated in a 6-well plate as 1×10^6 cells/well for 24 h. Cells were treated with XPS, XPS5-1 (both 100 μg/ml), and DEX (20 μM) for another 24 h after LPS (0.5 μg/ml) stimulation. Cells were collected to detect the expression of inflammation-related proteins (n = 4 for each group).

Total cell lysates were centrifuged at 4°C (2000 g, 15 min). Samples were loaded on 12% SDS-PAGE gel and were transferred to PVDF membranes. After blocking, the membranes were incubated with antibodies against iNOS, arginase-1, and GAPDH (all at 1:1,000 dilution) for 10 h at 4°C and secondary antibody HRP-conjugated IgG (1:2000) for 2 h at room temperature. The protein bands were visualized by the enhanced chemiluminescence (ECL) method and quantified by the ImageJ software. The GAPDH protein was served as internal control (Feng et al., 2019).

Immunofluorescence Confocal Microscopy

ANA-1 cells were cultured on a 24-well plate and then administrated with XPS, XPS5-1 (both 100 μg/ml), and DEX (20 μM) for another 24 h after LPS (0.5 μg/ml) was stimulated. Each representative experiment has three independent biological replicates.

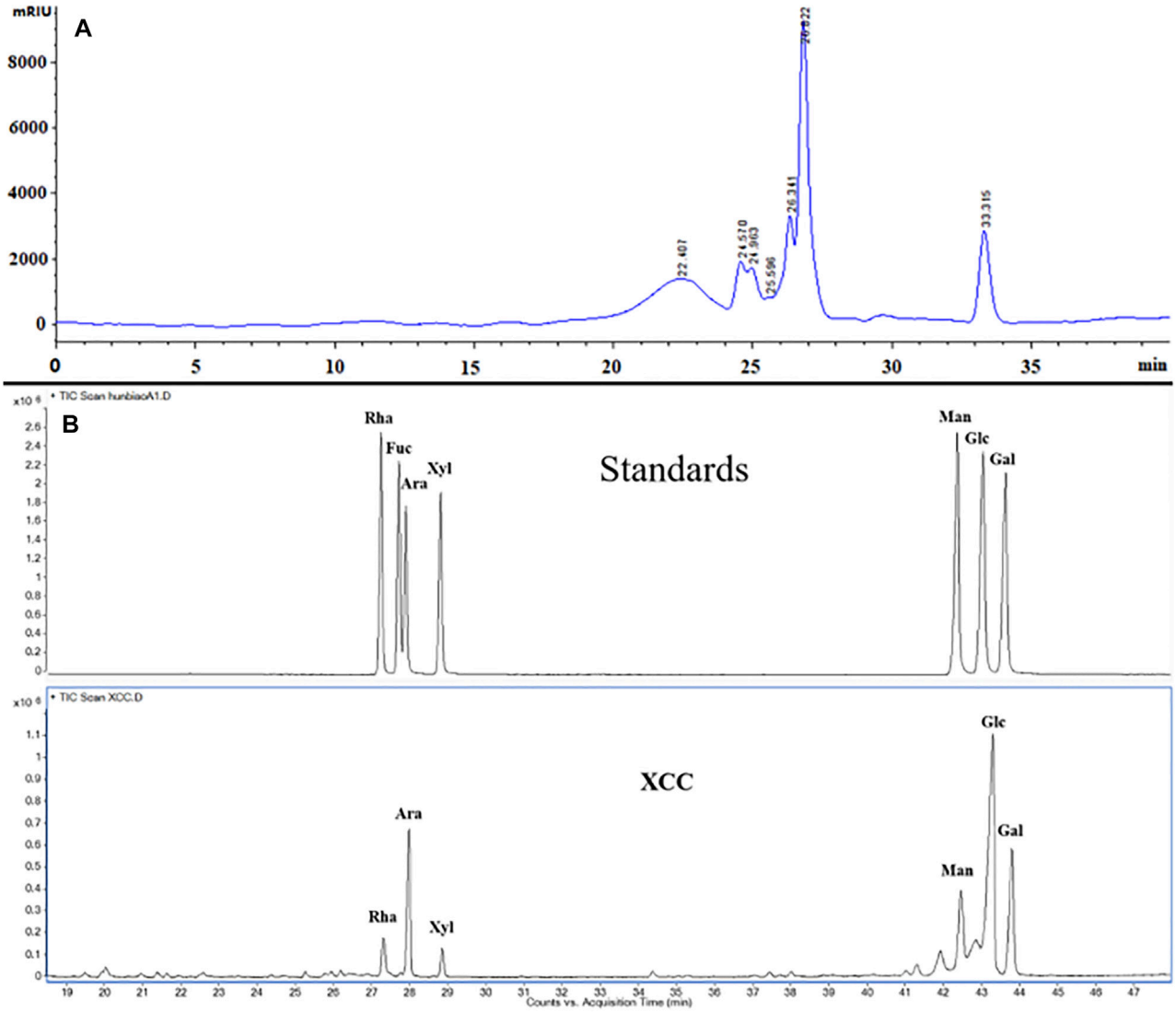

FIGURE 1 | Characterization of XPS by HPGPC chromatogram and monosaccharide composition. **(A)** HPGPC chromatogram of XPS. **(B)** Monosaccharide composition analysis of XPS by GC.

After being fixed in 4% paraformaldehyde and permeated with 0.3% Triton/PBS, the cells were incubated at 4°C with iNOS (1: 500) and arginase-1 (1:200) antibodies for 12 h. Then they were incubated with fluorescent dyes conjugated secondary antibodies (green for arginase-1 and red for iNOS) for 1 h at room temperature. Nuclei were observed after staining with DAPI at 10 μg/ml for 15 min. The cells were immediately observed by a fluorescence microscope (Leica EL6000 Microsystems) (He et al., 2020).

Flow Cytometry Analysis of Macrophages Phenotype *In Vitro*

ANA-1 cells were cultured as previously described and expression of $CD11b^+$, $F4/80^+$, $CD86^+$, and $CD206^+$ was detected (Wang B. et al., 2020). ANA-1 cells were all marked with fluorescently labeled antibodies targeting F4/80 and CD11b. To characterize the M1 phenotype, cells were marked with a CD86 antibody. To characterize the M2 phenotype, cells were marked with a CD206 antibody (Geng et al., 2020). Then the data ($n = 4$ for each group) were analyzed using the FlowJo software (Ashland, OR, United States).

Evaluation of *In Vivo* Anti-Inflammatory Activity of XPS

Animals and Ethics Statement

Six- to eight-week-old male BALB/C mice were obtained from the Shanghai SLAC Lab Animal Co. Ltd. All animal protocols in this experiment met the dictates of the National Animal Welfare Law of China and were in agreement with the Animal Ethical Committee of School of Pharmacy, Fudan University (approved identification: 2020-01-YL-LH-01).

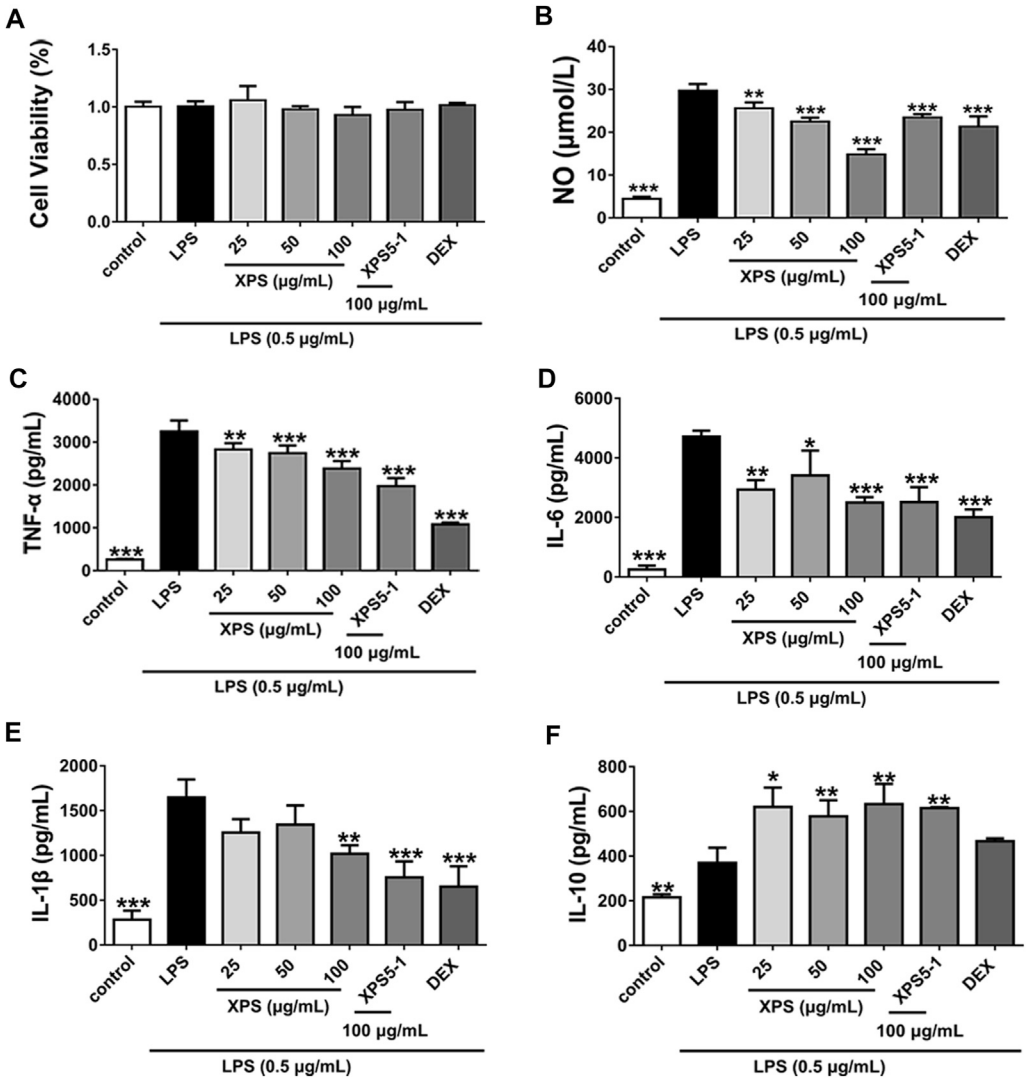

FIGURE 2 | Effects of XPS and XPS5-1 on LPS-induced inflammatory response in ANA-1 cells. Cells were stimulated by LPS (0.5 μg/ml) with the treatment of XPS (25, 50, and 100 μg/ml), XPS5-1 (100 μg/ml), and DEX (20 μM) for 24 h. The cell viability was measured **(A)**. The levels of NO **(B)**, TNF-α **(C)**, IL-6 **(D)**, IL-1β **(E)**, and IL-10 **(F)** in the supernatant were detected (n = 3, means ± SD). $^{*}p < 0.05$, $^{**}p < 0.01$, and $^{***}p < 0.001$ vs. the LPS-stimulated group, analyzed by ANOVA and Bonferroni *post hoc* test.

Experimental Design of LPS-Induced ALI Model

Mice were randomly divided into six groups (n = 6 for each group): sham, LPS-stimulated (LPS 3 mg/kg, model), LPS + XPS (20, 40, and 80 mg/kg), and LPS + DEX (4 mg/kg) groups. The mice were intratracheally instilled with normal saline (NS, the sham group) or LPS. ALI mice were treated 2 h after instillation. The mice in the sham and model group were given NS, and the mice in the LPS + XPS groups were administered with XPS intragastrically. DEX was administered intravenously as a positive control. All mice were sacrificed by an overdose of urethane 24 h after treatment (Xu et al., 2015).

Histopathologic Evaluation

The upper right lung lobe was chosen for histological examination. The tissues were fixed in 4% formaldehyde and embedded in paraffin. The embedded sections (5 μm thick) were stained with hematoxylin and eosin (H&E) solution to perform histopathological assessments (Wang et al., 2020d). The pathological ALI scoring system from the American Thoracic Association was used to score lung injury in a blinded manner (Matute-Bello et al., 2011). The scoring was assessed from 0 (normal) to 2 (severe) for the following categories: PMNs or monocytes in the interstitial space and alveolar septal thickening. The injury score was calculated according to the formula [(neutrophils in the interstitial space × 14) + (alveolar septal thickening × 2)]/(number of fields × 100) (Matute-Bello et al., 2011).

Bronchoalveolar Lavage Fluid Acquisition and Measurement of the Numbers of Mononuclear Cells and the Protein Level

After mice were sacrificed, trachea cannula was used to get the bronchoalveolar lavage fluid (BALF) from the left lungs.

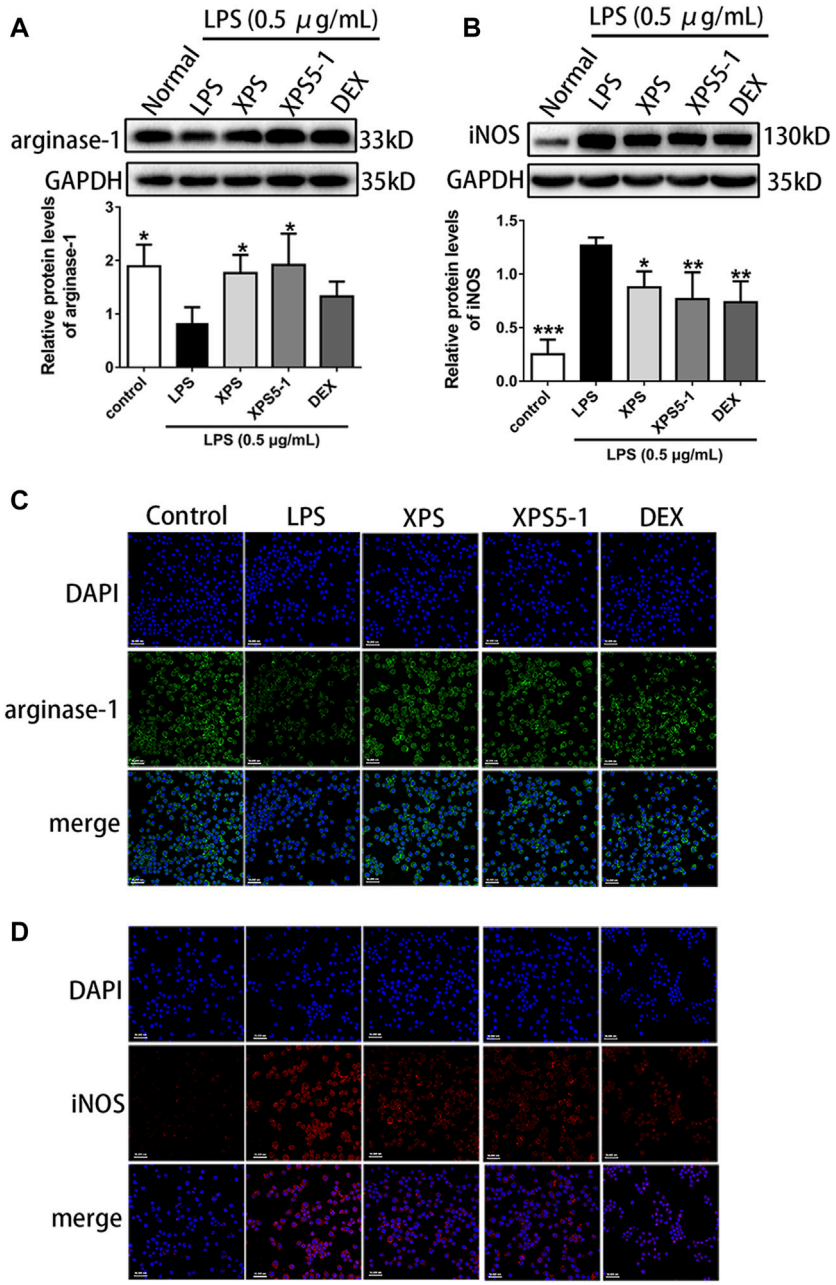

FIGURE 3 | Effects of XPS and XPS5-1 on protein expression in LPS-stimulated ANA-1 cells. Total cell lysates were collected for analyzing the expression of arginase-1 **(A)** and iNOS **(B)** by Western blot ($n = 4$, means ± SD). The effects of XPS, XPS5-1 (both 100 μg/ml), and DEX (20 μM) on the expression of arginase-1 (green) and iNOS (red) were detected by immunofluorescence, and cell nuclei were in blue **(C, D)**. $^{*}p < 0.05$, $^{**}p < 0.01$, and $^{***}p < 0.001$ vs. the LPS-stimulated group, analyzed by ANOVA and Bonferroni *post hoc* test.

Collected lavage was centrifuged at 80 g for 15 min and retained for subsequent tests at −80°C.

The protein concentration in BALF was tested by the BCA assay kit. The mononuclear cells were counted with a hemocytometer (Jia et al., 2014).

MPO and Inflammatory Cytokines Assay in Lung

MPO is a mark of neutrophils infiltration in the lungs (Ding et al., 2019). The MPO concentration in the BALF was assayed by the ELISA kit. The levels of cytokines in BALF such as IL-1β, TNF-α, IL-6, and IL-10 were detected by ELISA kits.

Immunohistochemistry

The detection of immunohistochemical staining was performed according to our previous research (Kang, 2018). The slices were incubated with F4/80 antibody (1:100) to detect lung macrophages or Ly-6G/Ly-6C (Gr-1) antibody (1:100) to label polymorphonuclear leukocytes for 12 h at 4°C. The next day,

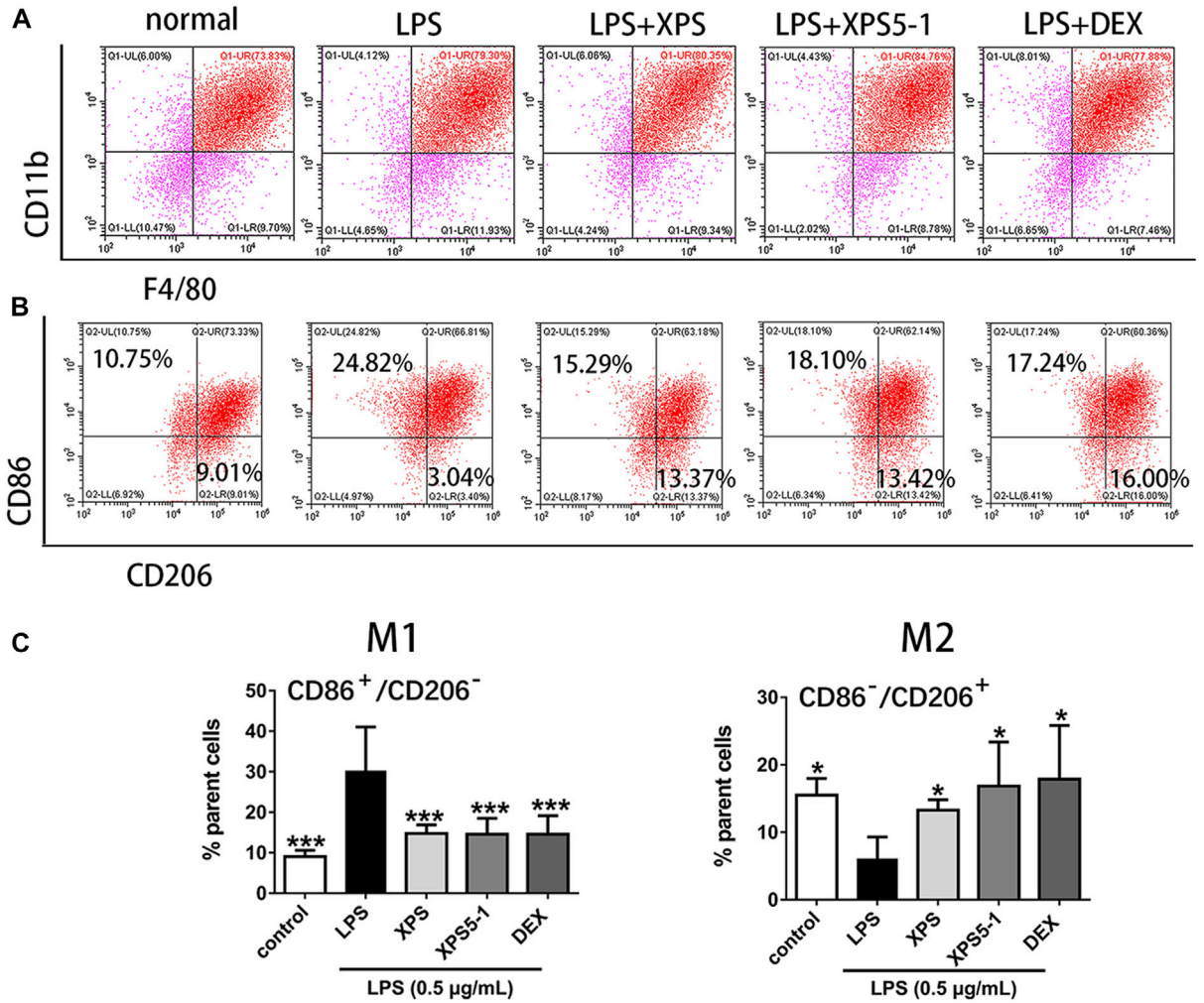

FIGURE 4 | Effect of XPS and XPS5-1 on LPS-induced macrophage polarization in ANA-1 cells. **(A)** Dot plots showing macrophages. **(B)** $CD86^+/CD206^-$ (upper left area representing M1) and $CD86^-/CD206^+$ (lower right area representing M2) by flow cytometry. **(C)** Graphs showing the radio of these two phenotypes. ANA-1 cells were stimulated by LPS (0.5 μg/ml) with XPS, XPS5-1 (both 100 μg/ml), and DEX (20 μM) for 24 h. The cells were incubated with fluorescently labeled antibodies. The expression ratio was detected by flow cytometry ($n = 4$, means ± SD). $^*p < 0.05$, $^{**}p < 0.01$, and $^{***}p < 0.001$ vs. the LPS-stimulated group, analyzed by ANOVA and Bonferroni *post hoc* test.

HRP-labeled secondary antibodies (1:2000) were added and incubated at 37°C for 1 h. The sections were stained with the DAB solution and hematoxylin. The average optical density (AOD) of the positive area in lung tissue was measured as previously described (Zheng et al., 2020). AOD = IOD (Integrated Optical Density)/Area.

Western Blot Analysis

Lung tissues were homogenized and extracted with RIPA lysis reagent. The samples were loaded on gel for electrophoresis and transformed to PVDF membranes. After blocking, the membranes were incubated with primary antibodies against TLR4, TRAF6, MyD88, NF-κB p65, NF-κB p-p65, iNOS, arginase-1, and GAPDH (all at 1:1,000 dilution) for 10 h at 4°C and anti-rabbit secondary antibody HRP-conjugated IgG (1:2,000) at room temperature for 2 h.

Statistics

Values were expressed as means ± SD. Multiple group comparisons were performed using one-way analysis of variance (ANOVA) followed by Bonferroni *post hoc* test using the software of SPSS. *p*-value of less than 0.05 ($p < 0.05$) was considered to be significant.

RESULTS

Extraction, Isolation, and Purification of Glycoproteins XPS and XPS5-1

315 g glycoproteins XPS (yield 6.3% of 5.0 kg dried material) were obtained from the overground part of *R. japonica* var. *glaucocalyx* by boiling water extraction and were characterized (**Figure 1**). XPS and XPS5 were isolated by a DEAE-cellulose column. XPS5 was further purified on a column of Superdex-75 to give XPS5-1.

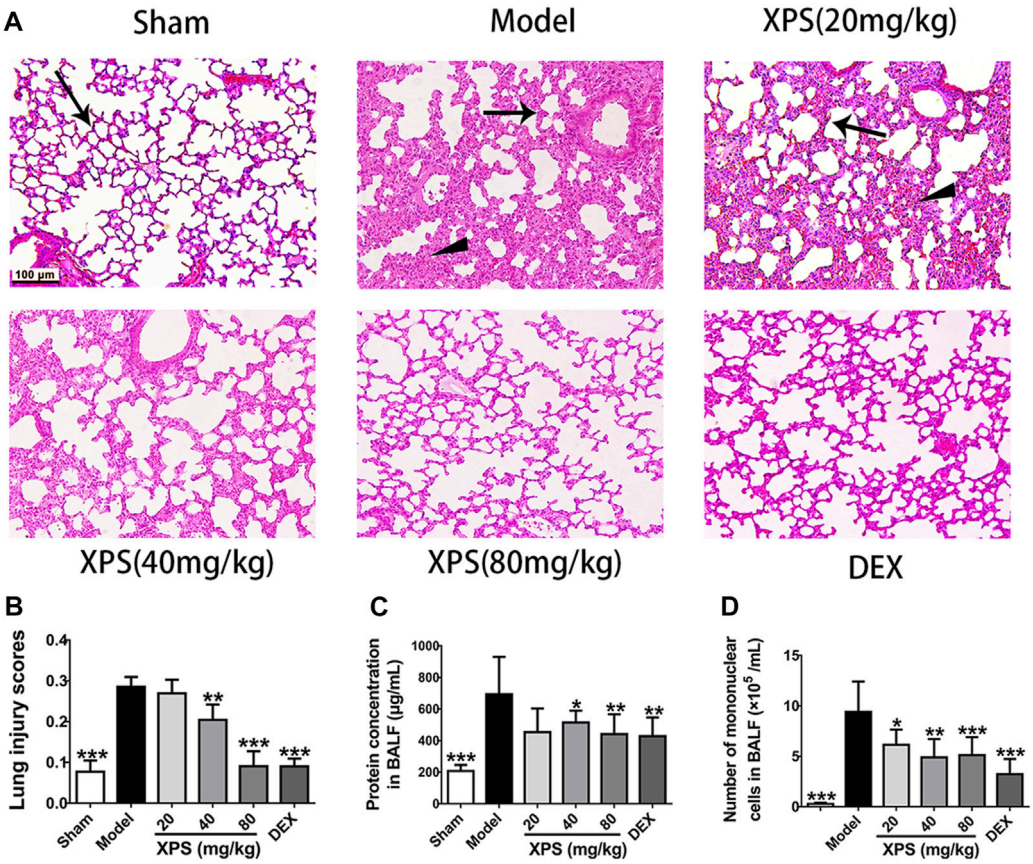

FIGURE 5 | XPS alleviated lung injury in ALI mice. H&E-stained lung tissues were observed under light microscopy 200× magnification. Wedge indicates accumulation of mononuclear cells, and black arrow indicates the alveolar wall **(A)**. Lung injury scores were assessed **(B)**. The protein concentration **(C)** and the numbers of mononuclear cells **(D)** in BALF were detected 24 h after XPS administration (n = 6, means ± SD). $^{*}p < 0.05$, $^{**}p < 0.01$, and $^{***}p < 0.001$ vs. the model group, analyzed by ANOVA and Bonferroni *post hoc* test.

The total carbohydrate content and protein content of XPS were 20.61 ± 0.38% and 60.08 ± 1.13%, respectively. XPS contained 10.96 ± 1.68% of uronic acid determined by the m-hydroxyl biphenyl method. Monosaccharide composition analysis showed that XPS had glucose, galactose, arabinose, mannose, rhamnose, and xylose with the molar ratio of 10.0, 3.8, 3.1, 1.2, and 0.6. XPS5-1, with Mw estimated to be 3.17×10^3 Da, and contained rhamnose, glucose, and arabinose with the molar ratio of 10.0:3.5:0.9, and amino acid of Glu:Ser:Gly = 30.2:21.6:48.2; the content of protein in XPS5-1 was 49.9% (Wang et al., 2020a). The profile of XPS5-1 had been published in another article (Wang et al., 2020a).

Anti-Inflammatory Activity *In Vitro*

Effects of XPS and XPS5-1 on Cell Viability and Production of Inflammatory Mediators *In Vitro*

XPS, XPS5-1, and DEX had no effect on cell viability after LPS stimulation (**Figure 2A**). Furthermore, stimulation with LPS observably increased the levels of NO, TNF-α, IL-6, and IL-1β ($p < 0.001$, **Figures 2B–E**). The level of inflammatory mediators, including NO, TNF-α, and IL-6, was significantly decreased by XPS treatment ($p < 0.05$). The level of IL-1β was reduced by 100 μg/ml XPS treatment ($p < 0.01$). The production of IL-10 distinctly rose by LPS stimulation ($p < 0.01$, **Figure 2F**), and XPS further elevated it ($p < 0.05$). DEX markedly decreased the level of NO, TNF-α, IL-6, and IL-1β ($p < 0.001$) but had less effect on IL-10 production. The effect of XPS5-1 (100 μg/ml) was similar to XPS.

Effects of XPS and XPS5-1 on Macrophage Polarization

The location and expression level of proteins were tested by immunofluorescence assay and Western blot. Arginase-1 was normally expressed in the control group, whereas LPS obviously reduced its expression. As an inducible synthase, iNOS was less expressed in resting cells. The expression of it increased after LPS stimulation ($p < 0.001$, **Figure 3**).

After administration, XPS and XPS5-1 markedly upregulated the level of arginase-1 ($p < 0.05$, **Figure 3A**), but DEX only had a mild effect on arginase-1 expression. The intracellular green fluorescence (represented arginase-1) was bright in the XPS and XPS5-1 groups.

XPS, XPS5-1, and DEX distinctly downregulated the expression of iNOS ($p < 0.05$, **Figure 3B**). The intracellular red fluorescence (labeled iNOS) was dim in the XPS, XPS5-1, and DEX groups.

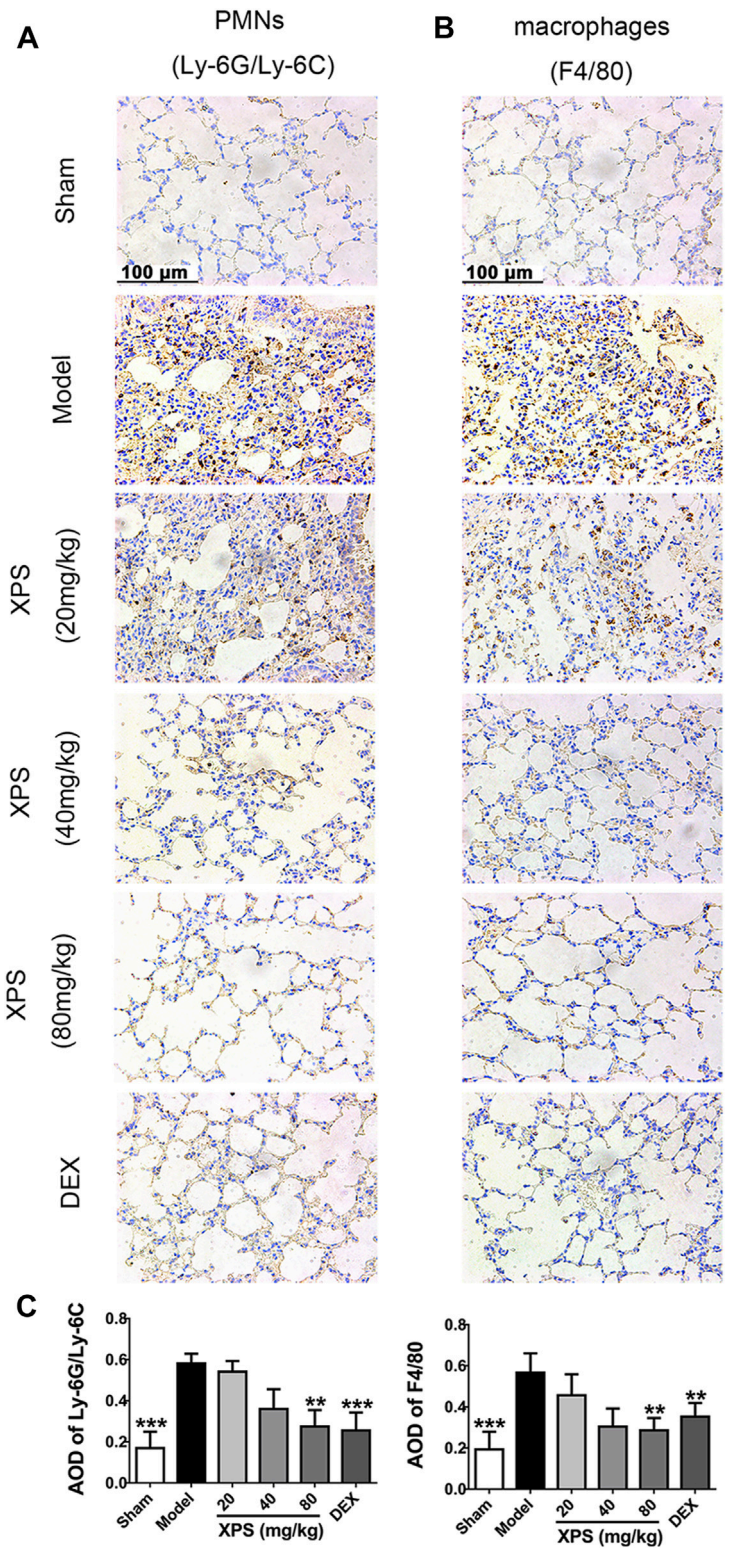

FIGURE 6 | XPS inhibited inflammatory cells infiltration in lung tissue of ALI mice. The PMNs **(A)** and macrophages' **(B)** infiltration were observed under light microscopy (400×) by immunohistochemistry analysis. A semiquantitative analysis of the images **(C)** was performed by measuring the AOD (n = 4, means ± SD). $^{*}p < 0.05$, $^{**}p < 0.01$, and $^{***}p < 0.001$ vs. the model group, analyzed by ANOVA and Bonferroni *post hoc* test.

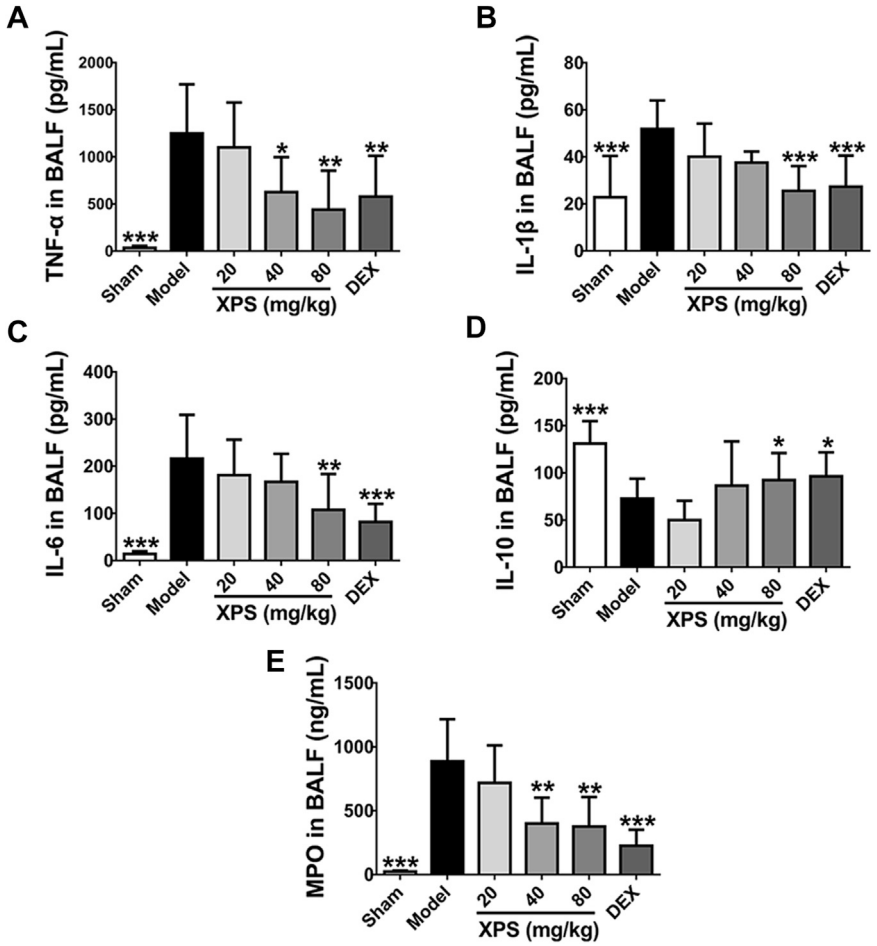

FIGURE 7 | XPS regulated the level of inflammatory cytokines and MPO in BALF. The levels of TNF-α **(A)**, IL-1β **(B)**, IL-6 **(C)**, IL-10 **(D)**, and MPO **(E)** in BALF were tested by ELISA (n = 6, means ± SD). $^{*}p < 0.05$, $^{**}p < 0.01$, and $^{***}p < 0.001$ vs. the model group, analyzed by ANOVA and Bonferroni *post hoc* test.

After LPS stimulation, the macrophage phenotype of ANA-1 cells was detected by flow cytometry. Double-positive of F4/80 and CD11b indicated that they belong to the macrophage lineage (**Figure 4A**).

After 24 h of culture, LPS stimulation promoted a proinflammatory (M1) phenotype of macrophages, characterized by the increased events of $CD86^{+}/CD206^{-}$ (M1) in ANA-1 ($p < 0.001$). XPS and XPS5-1 obviously reversed the LPS-promoted M1 subtype ($p < 0.001$). The cells stimulated by LPS expressed less $CD86^{-}/CD206^{+}$ events (M2) ($p < 0.001$). XPS and XPS5-1 administration skewed the LPS simulated ANA-1 to an anti-inflammatory (M2) phenotype, characterized by the increased events of $CD86^{-}/CD206^{+}$ ($p < 0.05$, **Figures 4B,C**).

Anti-Inflammatory Effects of XPS *In Vivo*

Effects of XPS on LPS-Induced ALI

To estimate the effect of XPS treatment in LPS-stimulated mice at histological level, the lung tissues were tested by H&E staining. The sham group showed only mild changes caused by intratracheal instillation of NS. However, pulmonary congestion, alveolar wall thickness, and edema were observed in the model group. XPS or DEX administration obviously alleviated these damages (**Figure 5A**). The LPS group had the highest lesion scores and the XPS or DEX group had lower scores, which reflected the levels of lung injury (**Figure 5B**).

To further assess the extent of alveolus damage, the BALF was collected to test the protein concentration and the mononuclear cell counts. In comparison with the sham group, dramatic increases were observed in protein concentration and cell counts after LPS instillation ($p < 0.001$). XPS (40 and 80 mg/kg) and DEX (4 mg/kg) treatment significantly restrained these phenomena ($p < 0.05$, **Figures 5C, D**).

XPS Attenuated Accumulation of Inflammatory Cells in the Lung

The effect of XPS on attenuating the accumulation of macrophages (expressing F4/80) and PMNs (expressing Ly-6G/Ly-6C (Gr-1)) in lung tissue was evaluated (**Figures 6A,B**). The results showed a high level of PMNs and macrophages in the model group. The XPS and DEX groups exhibited lower levels of staining in lung tissue compared with the model group. These observations were also supported by the semiquantitative

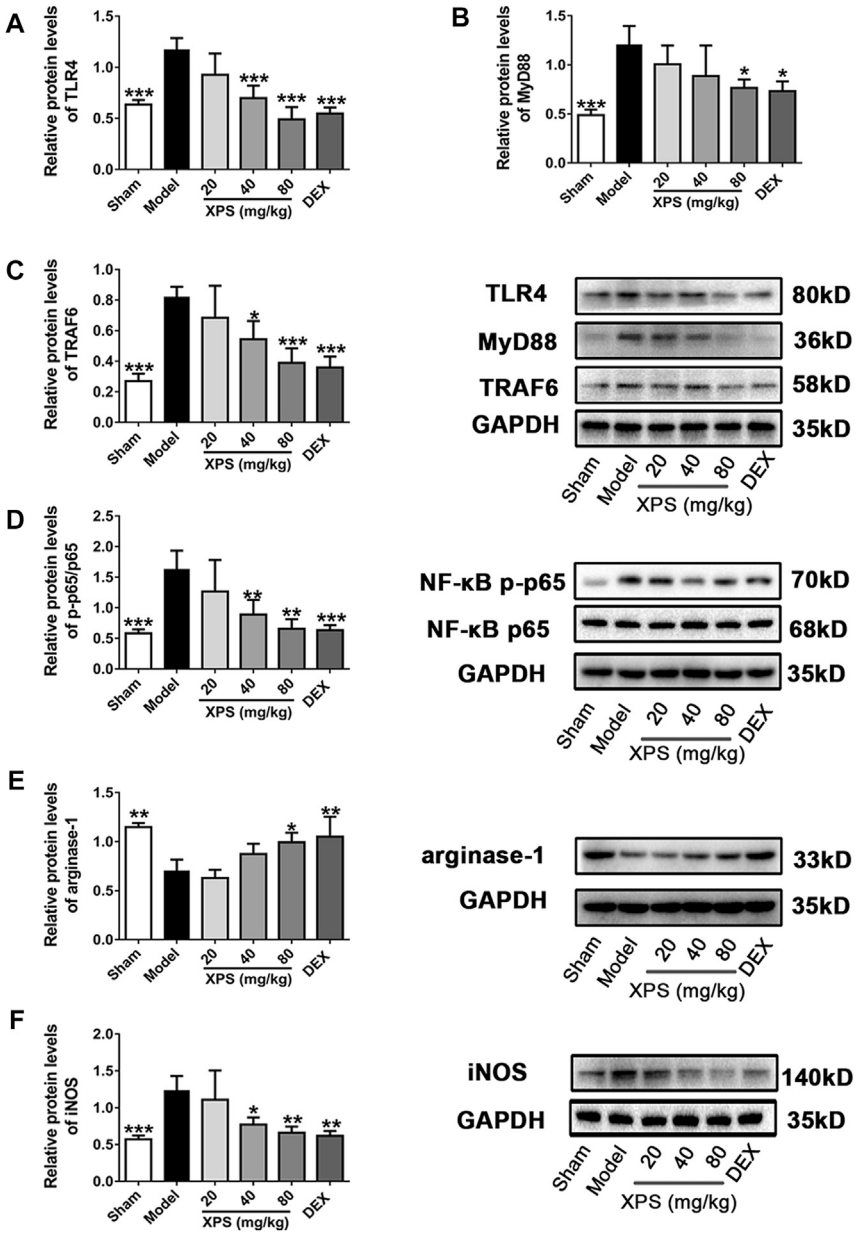

FIGURE 8 | XPS downregulated the TLR4/MyD88 signaling pathway in the lung. Lung tissues were harvested for Western blot analysis (n = 4, means ± SD). The protein expression of TLR4 **(A)**, MyD88 **(B)**, and TRAF6 **(C)** and the ratio of NF-κB p-p65 to NF-κB p65 **(D)** were shown. The level of arginase-1 **(E)** and iNOS **(F)** was detected. $^{*}p < 0.05$, $^{**}p < 0.01$, and $^{***}p < 0.001$ vs. the model group, analyzed by ANOVA and Bonferroni *post hoc* test.

analysis. XPS (40 and 80 mg/kg) and DEX (4 mg/kg) obviously reduced the infiltration of inflammatory cells ($p < 0.01$, **Figure 6C**).

XPS Regulated the Levels of Inflammatory Cytokines and MPO in BALF

Compared with the sham group, the level of TNF-α, IL-1β, and IL-6 was obviously elevated in the model group ($p < 0.001$, **Figures 7A–C**). XPS (80 mg/kg) and DEX significantly attenuated the levels of these proinflammatory cytokines ($p < 0.01$). XPS (40 mg/kg) only markedly inhibited the expression of TNF-α ($p < 0.05$). XPS 20 mg/kg mildly inhibited the release of cytokines with no significance. The production of IL-10 distinctly decreased in the model group ($p < 0.001$, **Figure 7D**). XPS (80 mg/kg) and DEX significantly increased the level of IL-10 ($p < 0.05$). Treatment of XPS in 20 and 40 mg/kg only showed an upward tendency with no significance.

MPO is a reliable marker for neutrophils infiltration and catalyzes oxidants generation (Lei et al., 2020). Compared with the sham group, MPO level was obviously increased in the model group ($p < 0.001$), while XPS (40 and 80 mg/kg) and DEX markedly reduced such elevations ($p < 0.01$, **Figure 7E**).

XPS Inhibited the Expression of Proteins in TLR4/MyD88 Signaling Pathway

LPS obviously augmented the expression of TLR4, MyD88, and TRAF6 in the model group compared with the sham group ($p < 0.001$, **Figures 8A–C**). XPS (40 and 80 mg/kg) decreased the protein content of TLR4 and TRAF6 ($p < 0.05$), while only XPS 80 mg/kg significantly reduced MyD88 expression ($p < 0.05$).

The phosphorylation level of NF-κB p65 in the cytosol was expressed by the ratio of NF-κB p-p65 to NF-κB p65. The ratio (**Figure 8D**) was markedly elevated in the model group ($p < 0.001$) and was downregulated by XPS (40 and 80 mg/kg, $p < 0.01$). Arginase-1 expression reduced markedly in the model group ($p < 0.01$, **Figure 8E**) but was elevated by XPS (80 mg/kg, $p < 0.05$). Moreover, iNOS (**Figure 8F**) expression was consistent with the phosphorylation level of NF-κB. Similarly, XPS (40 and 80 mg/kg) decreased the expression of iNOS ($p < 0.05$).

DISCUSSION

R. japonica var. *glaucocalyx* is a TCM prescribed to treat inflammatory diseases. The terpenoid and flavonoid in *R. japonica* var. *glaucocalyx* show the anti-inflammatory activity (Wang et al., 2020a), but the effect of macromolecules in this plant is unclear. In recent years, lots of researches have focused on the anti-inflammatory and antitumor effects of glycoproteins due to their remarkable therapeutic effects and relatively low toxicity (Fu et al., 2021).

XPS was glycoproteins isolated from *R. japonica* var. *glaucocalyx*. XPS5-1 and XPS10-1 were glycoproteins purified from XPS. XPS5-1 showed an inhibitory effect *in vitro* on tryptophan 2,3-dioxygenase (TDO) (Wang et al., 2020a), an enzyme that subsequently mediates the immune response to cancers. XPS10-1 is an inhibitor of indoleamine 2,3-dioxygenase (IDO) (Wang et al., 2020b). However, our preliminary experiment found that only XPS and XPS5-1 had anti-inflammatory activity. The present work demonstrated that XPS and XPS5-1 inhibited inflammatory response *in vitro* through modulating macrophage polarization with the reduction of inflammatory mediators.

Macrophages have been widely studied as the center of inflammatory response in recent years (Anders et al., 2018). Macrophages can be grouped into two main phenotypes, M1 or M2, depending on the various stimuli and specific microenvironment of tissue (Ye W. et al., 2020). The activated M1 phenotype is associated with the ability to release IL-1β, TNF-α, IL-6, and NO (Askari and Shafiee-Nick, 2019). Additionally, M2 macrophages upregulate the immune-suppressive factors and anti-inflammatory cytokines, including arginase-1 and IL-10 (Su et al.).

Arginase-1 and iNOS are involved in two opposite macrophage phenotypes, M1 and M2 (Orecchioni et al., 2019). Both enzymes utilize L-arginine (L-Arg) as a substrate and are mutually downregulated (Liu L. L. et al., 2019). The iNOS is typically elevated in inflammatory states and catalyzes the production of NO (Wang et al., 2017). The excessive production of NO not only is helpful for fighting pathogens but also leads to inflammation and organs injury (Cinelli et al., 2020).

LPS as bacteria endotoxin polarized macrophage to M1 with more expression of $CD86^+$ and less $CD206^+$ (Anders et al., 2018). It also increased iNOS expression but decreased the level of arginase-1. XPS and XPS5-1 treatment significantly reversed these phenomena. The LPS-induced proinflammatory cytokine (TNF-α, IL-1β, and IL-6) production and anti-inflammatory cytokine (IL-10) level were adjusted by XPS and XPS5-1 treatment. All the results suggested that the anti-inflammatory effects of XPS and XPS5-1 might be mediated by promoting macrophage polarization from M1 to M2 *in vitro*.

According to our results, XPS accounted for 6.3% of the plants, and XPS5-1 yield rate from XPS was 0.82%. XPS was easier to obtain considering the isolation and purification process. XPS5-1 has similar anti-inflammatory effects as XPS *in vitro*; it may be established as the quality control indicator of XPS. The anti-inflammation effect of XPS was further detected in LPS-induced ALI mice.

Immune cells in the lung such as alveolar macrophages and PMNs further cause a proinflammatory microenvironment and aggravate lung injury (Mantovani et al., 2019). The superfluous recruitment of PMNs into lung tissues is a hallmark of ALI (Peng et al., 2019; Ye S. et al., 2020). MPO is an enzyme present only in PMNs and involves oxidative stress (Ye S. et al., 2020). A high level of MPO in the lung represents the infiltration of PMNs, which could accelerate the development of ALI (Ding et al., 2019).

XPS administration obviously decreased the number of mononuclear cells in BALF and inhibited PMN infiltration with the reduction of MPO level. The results in the immunohistochemical analysis also demonstrated that XPS treatment inhibited neutrophils and monocytes infiltration.

Enhanced macrophage M1 polarization relates to the inflammation in the lungs. When M1 phenotype macrophages are constantly activated, the proinflammatory cytokines, such as TNF-α, IL-1β, and IL-6, are released. Activated M2 phenotype macrophages produce IL-10, a potentially immunosuppressive cytokine, to terminate inflammatory responses and participate in tissue repair (Su et al.).

After LPS stimulation, TNF-α is produced first and upregulates the secretion of IL-1β (Zhao et al., 2019). As an amplifier in the inflammatory response, IL-1β increases pulmonary vascular permeability and is widely accepted as an important molecular marker for the ALI (Mantovani et al., 2019). The high level of IL-1β and TNF-α increases the expression of IL-6, a pleiotropic cytokine involved in chronic inflammation, which may promote the migration of neutrophils and contribute to organ damage (Fields et al., 2019). IL-10 production decreased in the ALI model group, which also represents a hyperinflammatory state (Su et al.).

XPS administration obviously decreased the production of TNF-α, IL-1β, and IL-6 with the increased production of IL-10 in the lung of ALI mice. XPS treatment alleviated the damages of the lung caused by excessive inflammation.

LPS-TLR4/NF-κB signaling pathway is essential in inflammatory response (Liu J. et al., 2019). The myD88-dependent pathway is important in pulmonary inflammation and is required for the infiltration of neutrophils (Wang et al., 2020b). LPS activates TRAF6 via TLR4 and MyD88 and then phosphorylates NF-κB. Subsequently, large amounts of inflammatory cytokines mentioned above are released (Zhou et al., 2019).

The expression of iNOS is motivated by the activation of the TLR4/NF-κB pathway (Zhou et al., 2019). A large amount of NO produced by iNOS in the lung accelerates the recruitment and infiltration of mononuclear cells in the lung of ALI (Hu et al., 2020).

Our testing results indicated that LPS stimulation upregulated the expression of TLR4, MyD88, TRAF6, and p-NF-κB. XPS administration decreased the expression of key proteins. The excessive iNOS and proinflammatory cytokines were reduced by XPS treatment. XPS might alleviate ALI by downregulating the LPS-TLR4/NF-κB signaling pathway.

R. japonica var. *glaucocalyx* has been traditionally used in numerous inflammatory diseases. Our research suggested that the activity of *R. japonica* var. *glaucocalyx* might partly come from glycoproteins (XPS), an important ingredient in herbs. As homogeneous glycoproteins purified from XPS, XPS5-1 had similar activity *in vitro*. Consistent with the traditional application of *R. japonica* var. *glaucocalyx*, XPS might be a promising candidate for inflammatory diseases, especially for treating ALI.

CONCLUSION

In vitro, XPS and its purified ingredients (XPS5-1) inhibited the secretion of proinflammatory mediators and polarized LPS-stimulated macrophages from M1 to M2. *In vivo,* XPS ameliorated LPS-induced ALI by reducing the inflammatory response and inhibiting macrophages and PMNs accumulation in lung tissues. These phenomena were related to the inhibition of the TLR4/NF-κB pathway. Glycoproteins from *R. japonica* var. *glaucocalyx* could be a potential agent for ALI.

DATA AVAILABILITY STATEMENT

The original contributions presented in the study are included in the article/supplementary material; further inquiries can be directed to the corresponding authors.

ETHICS STATEMENT

The animal study was reviewed and approved by the Animal Experiment Committee of Fudan University (Shanghai, China). All animal protocols in this experiment met the dictates of the National Animal Welfare Law of China and were in agreement with the Animal Ethical Committee of School of Pharmacy, Fudan University (approved identification: 2020-01-YL-LH-01).

AUTHOR CONTRIBUTIONS

AR, HZ, HL, and GY conceived and designed the experiments. AR, HW, and KL performed the experiments. AR, DC, TZ, and HL analyzed and interpreted the data. All authors read and approved the manuscript.

FUNDING

This work was funded by the Ministry of Science and Technology of China (Grants Nos. 2019ZX09735001), Natural Science Foundation of Shanghai (No. 20ZR1458100), and Science and Technology Commission of Shanghai Municipality (No. 15DZ1900104).

ACKNOWLEDGMENTS

All authors would like to show our deepest gratitude to the Ministry of Science and Technology of China, Natural Science Foundation of Shanghai and Science and Technology Commission of Shanghai Municipality.

REFERENCES

Anders, H.-J., Suarez-Alvarez, B., Grigorescu, M., Foresto-Neto, O., Steiger, S., Desai, J., et al. (2018). The Macrophage Phenotype and Inflammasome Component NLRP3 Contributes to Nephrocalcinosis-Related Chronic Kidney Disease Independent from IL-1-mediated Tissue Injury. *Kidney Int.* 93 (3), 656–669. doi:10.1016/j.kint.2017.09.022

Askari, V. R., and Shafiee-Nick, R. (2019). The Protective Effects of β-caryophyllene on LPS-Induced Primary Microglia M1/M2 Imbalance: A Mechanistic Evaluation. *Life Sci.* 219, 40–73. doi:10.1016/j.lfs.2018.12.059

Chaidedgumjorn, A., Toyoda, H., Woo, E. R., Lee, K. B., Kim, Y. S., Toida, T., et al. (2002). Effect of (1→3)- and (1→4)-linkages of Fully Sulfated Polysaccharides on Their Anticoagulant Activity. *Carbohydr. Res.* 337 (10), 925–933. doi:10.1016/s0008-6215(02)00078-2

Cinelli, M. A., Do, H. T., Miley, G. P., and Silverman, R. B. (2020). Inducible Nitric Oxide Synthase: Regulation, Structure, and Inhibition. *Med. Res. Rev.* 40 (1), 158–189. doi:10.1002/med.21599

Ding, H., Ci, X., Cheng, H., Yu, Q., and Li, D. (2019). Chicoric Acid Alleviates Lipopolysaccharide-Induced Acute Lung Injury in Mice through Anti-inflammatory and Anti-oxidant Activities. *Int. Immunopharmacol.* 66, 169–176. doi:10.1016/j.intimp.2018.10.042

Feng, Y., Weng, H., Ling, L., Zeng, T., Zhang, Y., Chen, D., et al. (2019). Modulating the Gut Microbiota and Inflammation Is Involved in the Effect of *Bupleurum* Polysaccharides against Diabetic Nephropathy in Mice. *Int. J. Biol. Macromol.* 132, 1001–1011. doi:10.1016/j.ijbiomac.2019.03.242

Fields, J. K., Günther, S., and Sundberg, E. J. (2019). Structural Basis of IL-1 Family Cytokine Signaling. *Front. Immunol.* 10, 1412. doi:10.3389/fimmu.2019.01412

Fu, Y. W., Peng, Y. F., Huang, X. D., Yang, Y., Huang, L., Xi, Y., et al. (2021). *Lycium Barbarum* Polysaccharide-Glycoprotein Preventative Treatment Ameliorates Aversive. *Neural Regen. Res.* 16 (3), 543–549. doi:10.4103/1673-5374.293156

Ge, P., Luo, Y., Okoye, C. S., Chen, H., Liu, J., Zhang, G., et al. (2020). Intestinal barrier Damage, Systemic Inflammatory Response Syndrome, and Acute Lung Injury: A Troublesome Trio for Acute Pancreatitis. *Biomed. Pharmacother.* 132, 110770. doi:10.1016/j.biopha.2020.110770

Geng, P., Zhu, H., Zhou, W., Su, C., Chen, M., Huang, C., et al. (2020). Baicalin Inhibits Influenza A Virus Infection via Promotion of M1 Macrophage Polarization. *Front. Pharmacol.* 11, 1298. doi:10.3389/fphar.2020.01298

Han, X.-Z., Ma, R., Chen, Q., Jin, X., Jin, Y.-Z., An, R.-B., et al. (2018). Anti-inflammatory Action of Athyrium Multidentatum Extract Suppresses the LPS-

Induced TLR4 Signaling Pathway. *J. Ethnopharmacol.* 217, 220–227. doi:10.1016/j.jep.2018.02.031

Hanson, J. R. (2011). Diterpenoids of Terrestrial Origin. *Nat. Prod. Rep.* 28 (10), 1755–1772. doi:10.1039/c1np90021h

He, Y., Zhao, Y., Feng, Y., Ren, A., Zhang, Y., Wang, Y., et al. (2020). Therapeutic Effect and Mechanism Study of *L-Cysteine* Derivative 5P39 on LPS-Induced Acute Lung Injury in Mice. *Eur. J. Pharmacol.* 869, 172893. doi:10.1016/j.ejphar.2019.172893

Hu, X., Qin, H., Li, Y., Li, J., Fu, L., Li, M., et al. (2020). Biochanin A Protect against Lipopolysaccharide-Induced Acute Lung Injury in Mice by Regulating TLR4/NF-Kb and PPAR-γ Pathway. *Microb. Pathogenesis* 138, 103846. doi:10.1016/j.micpath.2019.103846

Huang, W., Guan, X., and Lv, Y. (2018). Simultaneous Determination of Glaucocalyxin A and Glaucocalyxin B in Rat Plasma by LC-MS/MS and its Application to a Pharmacokinetic Study after Oral Administration of *Rabdosia Japonica* Extract. *Biomed. Chromatogr.* 32 (2), e4089. doi:10.1002/bmc.4089

Huang, Y., Huang, L., Zhu, G., Pei, Z., and Zhang, W. (2019). Downregulated microRNA-27b Attenuates Lipopolysaccharide-Induced Acute Lung Injury via Activation of NF-E2-Related Factor 2 and Inhibition of Nuclear Factor κB Signaling Pathway. *J. Cel Physiol.* 234 (5), 6023–6032. doi:10.1002/jcp.27187

Jia, Y., Chen, K., Lin, P., Lieber, G., Nishi, M., Yan, R., et al. (2014). Treatment of Acute Lung Injury by Targeting MG53-Mediated Cell Membrane Repair. *Nat. Commun.* 5, 4387. doi:10.1038/ncomms5387

Kang, H. (2018). Anti-inflammatory Mechanism of *Isodon Japonicas (Burm) Hara* on Lipopolysaccharide-Induced Neuroinflammation. *Trop. J. Pharm. Res.* 17 (1), 85–89. doi:10.4314/tjpr.v17i1.13

Lei, J., Shen, Y., Xv, G., Di, Z., Li, Y., and Li, G. (2020). Aloin Suppresses Lipopolysaccharide-Induced Acute Lung Injury by Inhibiting NLRP3/NF-Kb via Activation of SIRT1 in Mice. *Immunopharmacol. Immunotoxicol.* 42 (4), 306–313. doi:10.1080/08923973.2020.1765373

Lin, F., Song, C., Zeng, Y., Li, Y., Li, H., Liu, B., et al. (2020). Canagliflozin Alleviates LPS-Induced Acute Lung Injury by Modulating Alveolar Macrophage Polarization. *Int. Immunopharmacol.* 88, 106969. doi:10.1016/j.intimp.2020.106969

Liu, J., Chang, G., Huang, J., Wang, Y., Ma, N., Roy, A.-C., et al. (2019). Sodium Butyrate Inhibits the Inflammation of Lipopolysaccharide-Induced Acute Lung Injury in Mice by Regulating the Toll-like Receptor 4/Nuclear Factor κB Signaling Pathway. *J. Agric. Food Chem.* 67 (6), 1674–1682. doi:10.1021/acs.jafc.8b06359

Liu, L.-L., Li, J.-M., Su, W.-J., Wang, B., and Jiang, C.-L. (2019). Sex Differences in Depressive-like behaviour May Relate to Imbalance of Microglia Activation in the hippocampus. *Brain Behav. Immun.* 81, 188–197. doi:10.1016/j.bbi.2019.06.012

Mantovani, A., Dinarello, C. A., Molgora, M., and Garlanda, C. (2019). Interleukin-1 and Related Cytokines in the Regulation of Inflammation and Immunity. *Immunity* 50 (4), 778–795. doi:10.1016/j.immuni.2019.03.012

Matute-Bello, G., Downey, G., Moore, B. B., Groshong, S. D., Matthay, M. A., Slutsky, A. S., et al. (2011). An Official American Thoracic Society Workshop Report: Features and Measurements of Experimental Acute Lung Injury in Animals. *Am. J. Respir. Cel Mol. Biol.* 44 (5), 725–738. doi:10.1165/rcmb.2009-0210ST

Nieman, G. F., Gatto, L. A., Andrews, P., Satalin, J., Camporota, L., Daxon, B., et al. (2020). Prevention and Treatment of Acute Lung Injury with Time-Controlled Adaptive Ventilation: Physiologically Informed Modification of Airway Pressure Release Ventilation. *Ann. Intensive Care* 10 (1), 3. doi:10.1186/s13613-019-0619-3

Niu, X., Zang, L., Li, W., Xiao, X., Yu, J., Yao, Q., et al. (2020). Anti-inflammatory Effect of Yam Glycoprotein on Lipopolysaccharide-Induced Acute Lung Injury via the NLRP3 and NF-Kb/tlr4 Signaling Pathway. *Int. Immunopharmacol.* 81, 106024. doi:10.1016/j.intimp.2019.106024

Orecchioni, M., Ghosheh, Y., Pramod, A. B., and Ley, K. (2019). Macrophage Polarization: Different Gene Signatures in M1(LPS+) vs. Classically and M2(LPS-) vs. Alternatively Activated Macrophages. *Front. Immunol.* 10, 1048. doi:10.3389/fimmu.2019.01084

Peng, L.-Y., Yuan, M., Song, K., Yu, J.-L., Li, J.-H., Huang, J.-N., et al. (2019). Baicalin Alleviated APEC-Induced Acute Lung Injury in Chicken by Inhibiting NF-Kb Pathway Activation. *Int. Immunopharmacol.* 72, 467–472. doi:10.1016/j.intimp.2019.04.046

Su, B., Han, H., Gong, Y., Li, X., Ji, C., Yao, J., et al. (2021). Let-7d Inhibits Intratumoral Macrophage M2 Polarization and Subsequent Tumor Angiogenesis by Targeting IL-13 and IL-10. *Cancer Immunol. Immunother.* 70, 1619–1634. doi:10.1007/s00262-020-02791-6

Wang, B., Kasper, M., Laffer, B., Meyer zu Hörste, G., Wasmuth, S., Busch, M., et al. (2020). Increased Hydrostatic Pressure Promotes Primary M1 Reaction and Secondary M2 Polarization in Macrophages. *Front. Immunol.* 11,573955. doi:10.3389/fimmu.2020.573955

Wang, G., Hu, Z., Fu, Q., Song, X., Cui, Q., Jia, R., et al. (2017). Resveratrol Mitigates Lipopolysaccharide-Mediated Acute Inflammation in Rats by Inhibiting the TLR4/NF-κBp65/MAPKs Signaling cascade. *Sci. Rep.* 7. doi:10.1038/srep45006

Wang, H. J., Han, J. Q., and Tian, H. W. (2020a). Bioactivity Guide Isolation of TDO Inhibitory Constituents from *Rabdosia Japonica*. *Lishizhen Med. Materia Med. Res.* 31 (06), 1339–1341. doi:10.1016/j.micpath.2019.103846

Wang, H. J., Zhu, J., Han, J., Tian, H., Chen, W., and Ye, G. (2020b). Isolation and Purification of Indoleamine 2,3-dioxygenase (Ido) Inhibitory Constituents from *Rabdosia Japonica*. *Chin. Traditional Herbal Drugs* 51 (17), 4419–4424. doi:10.7501/j.issn.02532670.2020.17.008

Wang, H., Shi, S., Bao, B., Li, X., and Wang, S. (2015). Structure Characterization of an Arabinogalactan from green tea and its Anti-diabetic Effect. *Carbohydr. Polym.* 124, 98–108. doi:10.1016/j.carbpol.2015.01.070

Wang, J., Gao, Y., Lin, F., Han, K., and Wang, X. (2020c). Omentin-1 Attenuates Lipopolysaccharide (LPS)-induced U937 Macrophages Activation by Inhibiting the TLR4/MyD88/NF-Kb Signaling. *Arch. Biochem. Biophys.* 679, 108187. doi:10.1016/j.abb.2019.108187

Wang, J., Li, R., Peng, Z., Hu, B., Rao, X., and Li, J. (2020d). HMGB1 Participates in LPS-induced Acute Lung Injury by activating the AIM2 Inflammasome in Macrophages and Inducing Polarization of M1 Macrophages via TLR2, TLR4, and RAGE/NF-κB Signaling Pathways. *Int. J. Mol. Med.* 45 (1), 61–80. doi:10.3892/ijmm.2019.4402

Watanabe, S., Alexander, M., Misharin, A. V., and Budinger, G. R. S. (2019). The Role of Macrophages in the Resolution of Inflammation. *J. Clin. Invest.* 129 (7), 2619–2628. doi:10.1172/jci124615

Xu, Y.-Y., Zhang, Y.-Y., Ou, Y.-Y., Lu, X.-X., Pan, L.-Y., Li, H., et al. (2015). *Houttuynia Cordata Thunb.* Polysaccharides Ameliorates Lipopolysaccharide-Induced Acute Lung Injury in Mice. *J. Ethnopharmacol.* 173, 81–90. doi:10.1016/j.jep.2015.07.015

Ye, R., and Liu, Z. (2020). ACE2 Exhibits Protective Effects against LPS-Induced Acute Lung Injury in Mice by Inhibiting the LPS-TLR4 Pathway. *Exp. Mol. Pathol.* 113, 104350. doi:10.1016/j.yexmp.2019.104350

Ye S., S., Yang, X., Wang, Q., Chen, Q., and Ma, Y. (2020). Penehyclidine Hydrochloride Alleviates Lipopolysaccharide-Induced Acute Lung Injury by Ameliorating Apoptosis and Endoplasmic Reticulum Stress. *J. Surg. Res.* 245, 344–353. doi:10.1016/j.jss.2019.07.080

Ye, W., Wang, J., Lin, D., and Ding, Z. (2020). The Immunomodulatory Role of Irisin on Osteogenesis via AMPK-Mediated Macrophage Polarization. *Int. J. Biol. Macromolecules* 146, 25–35. doi:10.1016/j.ijbiomac.2019.12.028

Zhao, Y., Cooper, D. K. C., Wang, H., Chen, P., He, C., Cai, Z., et al. (2019). Potential Pathological Role of Pro-inflammatory Cytokines (IL-6, TNF-α, and IL-17) in Xenotransplantation. *Xenotransplantation* 26 (3), e12502. doi:10.1111/xen.12502

Zheng, J., He, Q., Tang, H., Li, J., Xu, H., Mao, X., et al. (2020). Overexpression of miR-455-5p Affects Retinol (Vitamin A) Absorption by Downregulating STRA6 in a Nitrofen-induced CDH with Lung Hypoplasia Rat Model. *Pediatr. Pulmonol* 55 (6), 1433–1439. doi:10.1002/ppul.24739

Zhou, J., Deng, Y., Li, F., Yin, C., Shi, J., and Gong, Q. (2019). Icariside II Attenuates Lipopolysaccharide-Induced Neuroinflammation through Inhibiting TLR4/MyD88/NF-Kb Pathway in Rats. *Biomed. Pharmacother.* 111, 315–324. doi:10.1016/j.biopha.2018.10.201

Zhou, P., Yang, X.-L., Wang, X.-G., Hu, B., Zhang, L., Zhang, W., et al. (2020). A Pneumonia Outbreak Associated with a New Coronavirus of Probable bat Origin. *Nature* 579 (7798), 270–273. doi:10.1038/s41586-020-2012-7

Conflict of Interest: GY and KL were employed by Shanghai Pharmaceuticals Holding Co., Ltd.

The remaining authors declare that the research was conducted in the absence of any commercial or financial relationships that could be construed as a potential conflict of interest.

frontiers in Pharmacology

ORIGINAL RESEARCH
published: 10 September 2021
doi: 10.3389/fphar.2021.734394

Polysaccharides Extracted From *Panax* Ginseng C.A. Mey Enhance Complement Component 4 Biosynthesis in Human Hepatocytes

Shuang Liu[1†], Fangbing Liu[1†], Tingting Wang[1], Jianzeng Liu[2], Cheng Hu[1], Liwei Sun[3] and Guan Wang[1]**

[1]National Engineering Laboratory for AIDS Vaccine, Key Laboratory for Molecular Enzymology and Engineering, School of Life Sciences, Jilin University, Changchun, China, [2]Jilin Ginseng Academy, Changchun University of Chinese Medicine, Changchun, China, [3]Research Center of Traditional Chinese Medicine, The Affiliated Hospital of Changchun University of Chinese Medicine, Key Laboratory of Active Substances and Biological Mechanisms of Ginseng Efficacy, Changchun University of Chinese Medicine, Changchun, China

OPEN ACCESS

Edited by:
Jing Zhao,
University of Macau, China

Reviewed by:
Wang Lingchong,
Nanjing University of Chinese Medicine, China
Lin Sun,
Northeast Normal University, China

***Correspondence:**
Liwei Sun
sunnylilwei@163.com
Guan Wang
wg10@jlu.edu.cn

†These authors have contributed equally to this work

Specialty section:
This article was submitted to Ethnopharmacology, a section of the journal Frontiers in Pharmacology

Received: 01 July 2021
Accepted: 30 August 2021
Published: 10 September 2021

Citation:
Liu S, Liu F, Wang T, Liu J, Hu C, Sun L and Wang G (2021) Polysaccharides Extracted From Panax Ginseng C.A. Mey Enhance Complement Component 4 Biosynthesis in Human Hepatocytes. Front. Pharmacol. 12:734394. doi: 10.3389/fphar.2021.734394

Panax ginseng C.A. Mey (ginseng) is a classic medicinal plant which is well known for enhancing immune capacity. Polysaccharides are one of the main active components of ginseng. We isolated water-soluble ginseng polysaccharides (WGP) and analyzed the physicochemical properties of WGP including molecular weight, monosaccharide composition, and structural characteristics. WGP had minimal effect on the growth of hepatocytes. Interestingly, WGP significantly increased the mRNA and protein levels of complement component 4 (C4), one of the core components of the complement system. Promoter reporter gene assays revealed that WGP significantly enhanced activity of the *C4* gene promoter. Deletion analyses determined that the E-box1 and Sp1 regions play key roles in WGP-induced *C4* transcription. Taken together, our results suggest that WGP promotes C4 biosynthesis through upregulation of transcription. These results provide new explanation for the intrinsic mechanism by which ginseng boosts human immune capacity.

Keywords: ginseng, water-soluble ginseng polysaccharides, complement component 4, C4 transcription, C4 promoter

INTRODUCTION

For *Panax* ginseng C.A. Mey (ginseng), a perennial plant belonging to genus Panax, is one of the most appreciated medicinal plants (Yun, 2001). Regulation of the immune response is one of the main biological activities of ginseng extracts (Wang et al., 2001; Senchina et al., 2009; Kang and Min, 2012; Kachur and Suntres, 2016; Yun and Yi, 2020). The reason for long-lasting usage of ginseng is that it contains numerous natural regulatory compounds, such as polysaccharides, ginsenoside, phytosterols, and peptides (Dai et al., 2017).

As an important active component of ginseng, water-soluble ginseng polysaccharides (WGP) have been proved playing an important role in the modulation of immunity (Lim et al., 2004; Kim et al., 2007; Sun, 2011; Yu et al., 2017; Li et al., 2019). Human immune system is an elaborate and layered defense system against infections through gradual increase of specificity to invading organisms (Medzhitov, 2007). Among the components of immune response, the complement system plays an important role in organismal defense. Complements can lower the B-cell

activating threshold and promote antigen retention on the surface of dendritic cells (Janssen et al., 2006; Gros et al., 2008; Carter and Fearon, 2010; Carroll and Isenman, 2012). Interaction between the effector components and the complement receptors can alter the secretion of cytokines and regulate the direction of T cell differentiation by influencing the microenvironment, thereby affecting the outcome of inflammation (Lalli et al., 2008; Amsen et al., 2009; Kolev et al., 2013).

The *C4* gene product, fourth component of human complement (C4), is an important component of the complement system (Galibert et al., 1997). C4 together with C2 forms the classical complement which activates C3 convertase (Dodds and Law, 1990). C4 is an important effector for both innate and adaptive immune systems among vertebrate animals. C4 is mainly expressed in the liver and induced during acute inflammation or tissue injury (Zhang et al., 2009).

Until now, little is known about the effects of ginseng on the production of complement components. In this study, we investigated the effect of WGP on C4 biosynthesis and explored the underlying molecular mechanism. We demonstrate that WGP enhances C4 production by promoting *C4* gene transcription via the E-box1 and Sp1 regions in the promoter. Our results provide more clues to fully understand the mechanism by which ginseng enhances human immunity.

MATERIALS AND METHODS

Preparation of Water-Soluble Ginseng Polysaccharides

Ginseng powder (400 g) was boiled in deionized water (4 L) for 3 h. After filtration, the solid phase was boiled in deionized water at the same ratio (g/ml) two more times. The filtrate was combined, centrifuged, and concentrated. The concentrated solution was mixed with anhydrous ethanol at a volume ratio of 1:3 and left overnight at 4°C. Discard the supernatant by centrifugation and the precipitate was successively washed with 75% ethanol, 95% ethanol, anhydrous ethanol, and ether. The crude ginseng polysaccharides were obtained after drying and subsequently redissolved in deionized water. After removal of proteins using a Sevage reagent, a 3 KD molecular sieve was used to remove small molecules to obtain WGP. The content of sugar was tracked and monitored by the phenol sulfuric acid method (Wang et al., 2020).

Molecular Weight Analysis of Water-Soluble Ginseng Polysaccharides

WGP (5 mg/ml) was filtered *via* 0.45 μm microfiltration membrane. The filtered sample (20 μL) was loaded into a TSK-Gel G4000PWXL column (Tosoh, Shanghai branch, China) controlled by LC-10Avp system (Shimadzu, Shanghai branch, China). High performance gel permeation chromatography (HPGPC) was performed using 0.2 M NaCl as mobile phase at flow rate of 0.5 ml/min. T-series Dextran standards were used for reference standards.

Monosaccharide Composition Analysis of Water-Soluble Ginseng Polysaccharides

Monosaccharide composition analysis was performed as previously described (Wang et al., 2020). Briefly, WGP (200 g) was hydrolysed in anhydrous methanol solution (1 ml) containing hydrochloric acid in nitrogen. Then, the sample was dried and hydrolysed in 2 M trifluoroacetate acid. After dried, the sample was dissolved using 0.3 M sodium hydroxide and added an equal volume of 0.5 M PMP (1-phenyl-3-methyl-5-pyrazolone) with thoroughly blending using pipettor. Placed the mixture (0.2 ml) for 30 min at 70°C, added 0.1 ml hydrochloric acid and 0.7 ml dichloromethane for extraction. The aqueous phase was filtered *via* 0.22 μm organic membrane. Conversion of monosaccharides with PMP were detected *via* high-performance liquid chromatography (HPLC). The sample (10 μL) was injected into a 4.6 mm × 250 mm COSMOSIL 5C18-PAQ column (Nacalai Tesque, Shanghai branch, China) controlled by an LC-20AT system (Shimadzu, Shanghai branch, China). HPLC was performed using a mobile phase composed of 19.5% Acetonitrile and 80.5% 0.1 M PBS (pH 7.0) at flow rate of 1 ml/min. The absorbance values at wavelength 245 nm were compared with those of monosaccharide standards including arabinose, fucose, galactose, galacturonic acid, glucose, glucuronic acid, mannose, rhamnose, and xylose to determine the monosaccharide composition of WGP.

Fourier Transform-Infrared Spectroscopy Analysis

Fourier transform-infrared spectroscopy (FT-IR) spectra of WGP was acquired *via* Tenor 27 spectrophotometer (Shimadzu, Shanghai branch, China). WGP was ground with KBr powder at a mass ratio of 3:1 and compressed into a pellet. The FT-IR spectra were recorded in range of 400–4,000 cm^{-1}.

Nuclear Magnetic Resonance Analysis

The lyophilized WGP was dissolved in D_2O. The ^{1}H and ^{13}C nuclear magnetic resonance (NMR) spectrum were performed on AV-500, 600, and 800 instruments (Bruker, Germany) using tetramethylsilane as the internal standard.

Cell Culture

Human hepatic cell line L-O2 was purchased from the American Type Culture Collection (Manassas, VA, United States). Cells were cultured using DMEM media containing 100 U/ml penicillin, 100 μg/ml streptomycin, 2 mM L-glutamine (Thermo Fisher Scientific, Shanghai branch, China) and 10% (V/V) fetal bovine serum (Abwbio, Guangzhou, China) and incubated in HERAcell150i incubator (Thermo Fisher Scientific) set to 5%CO2/95% air and 37°C. Cells were tested for *mycoplasma* monthly by the PCR method described by Uphoff and Drexler (Uphoff and Drexler, 2005).

In Vitro Cytotoxicity Assays

The L-O2 cells were treated with a series of equal ratio gradient concentrations of WGP for 72 h in a 96-well plate. MTT [3-(4, 5-dimethyl-thiazol-2yl)-2, 5-diphenyl tetrazolium bromide]

TABLE 1 | Primers used in *C4* promoter luciferase assay (5'—3').

Full length-forward	CCCTCGAGAGATTCTGCTCATCATTGCTCAGC
Segment 1- forward	CCCTCGAGCCACAACTCTGGGCCTGA
Segment 2- forward	CCCTCGAGAGGCCAGTTGCACTTCTTGG
Segment 3- forward	CCCTCGAGCACTTCTTGGCTGTCACGTG
Segment 4- forward	CCCTCGAGGTTTCCCAGCTTAGCTGG
Segment 5- forward	CCCTCGAGGGAGGAGCAAGGTCCAGAGT
Reverse	GGAAGCTTGGATCCAAGAGAGGTTAGATCC

(Sigma-Aldrich, Shanghai branch, China) was added at the final concentration of 0.5 mg/ml and incubated for 4 h in incubator. Then, the cells were lysed in 10% SDS containing 10 mM HCl overnight. The absorbance values at wavelength 590 nm were measured *via* a microplate reader.

Western Blotting

Whole cell lysates were obtained *via* ultrasonic cell disruption and subjected to SDS-polyacrylamide gel electrophoresis. Proteins were electrophoretically transferred onto PVDF (polyvinylidene difluoride) membrane (Thermo Fisher Scientific), and subsequently immunoblotted utilizing anti-β-actin (Proteintech, Rosemont, IL, United States) and -C4 (Abcam, Cambridge, MA, United States) antibodies. Visualization of immunoreactive proteins was conducted using the Odyssey Infrared Imaging System (LiCor, Lincoln, NE, United States). Densitometry measurements were performed using Odyssey V3.0 software (LiCor).

Real-Time PCR

Total RNA was extracted by TRIZOL method and used to make cDNAs *via* reverse transcription PCR Kit (Thermo Fisher Scientific), as described previously (Edwards et al., 2009). The LightCycler 480 real-time PCR meter (Roche, Indianapolis, IN, United States) and TaqMan probe Hs00246758_m1 (Thermo Fisher Scientific) were used to quantify *C4* transcripts. Comparative Ct method was used to calculate the fold changes (Livak and Schmittgen, 2001). *C4* transcripts were normalized to GAPDH transcripts measured by TaqMan probe (Hs02786624_g1).

Construction of C4 Promoter-Luciferase Reporter Plasmids

The C4 promoter region was PCR amplified from human genomic DNA *via* full length-forward and reverse primers (**Table 1**). Then, the PCR product was cloned into pGEM-T-Easy vector (Promega, Madison, WI, United States). A single clone of *C4* promoter was identified and digested by XhoI and HindIII (Promega). The *C4* promoter was then subcloned into reporter gene vector pGL4.19 basic (Promega) at the XhoI and HindIII restriction sites to generate pC4-1,007/+44. To generate the 5'-deletion constructs, pC4-119/+44, pC4-102/+44, pC4-92/+44, pC4-72/+44, and pC4-48/+44, genomic DNA fragments were PCR amplified from the pGL4.19 plasmid using forward (segment 1 to segment 5) and reverse primers (**Table 1**). Then, the PCR product was digested by HindIII and XhoI, and subcloned into pGL4.19 basic.

Statistical Analysis

Statistical analyses were performed using GraphPad Prism (GraphPad Software, San Diego, CA, United States). Differences were compared *via* the non-pair-wised two-sample *t*-test.

RESULTS

Isolation and Physicochemical Characterization of Water-Soluble Ginseng Polysaccharides

WGP were obtained *via* hot-water extraction and alcohol precipitation from ginseng powder. The yield of WGP was 0.85%. Carbohydrate content of WGP was over 98% and protein impurity was less than 0.1%. HPGPC was used for molecular weight analysis of WGP. We obtained two overlapping peaks and a single symmetric peak indicating that the molecular weight range of the WGP was from 1 kD to 79.4 kD (**Figure 1A**). The peak at 1 kD is due to incomplete interception of molecular sieve. Then, monosaccharide compositions analysis of WGP hydrolysate was performed using HPLC and nine monosaccharide reference standards. Monosaccharide profile was obtained by comparing retention times of nine standards under the same analytical conditions (**Figures 1B,C**). Chromatographic results demonstrated that WGP was composed of galacturonic acid, galactose, glucose, arabinose, rhamnose, glucuronic acid, and mannose in molar proportions of 28.9: 24.4: 23.0: 13.9: 6.7: 2.6: 0.6, respectively. Xylose and fucose were not detected. Consistent with published studies, glucose, galacturonic acid, and galactose are the most common monosaccharide compositions of WGP (Shi et al., 2017; Shin et al., 2017; Chen et al., 2018; Song et al., 2018; Zhao et al., 2019; Park et al., 2020). However, the specific proportion of these monosaccharides has varied widely across these studies, which may be due to the different origins of ginseng.

The FT-IR spectrum of WGP showed characteristic hydroxyl and C-H stretching vibration peak at 3,416.51 and 2,929.93 cm^{-1}, respectively. The absorption peaks at 1,625.99 and 1735.68 cm^{-1} were caused by bound water and C=O stretching vibration of uronic acid, respectively. The absorption peaks at 1,414.96 and 1,241.87 cm^{-1} represented C-H angular vibrations of carbohydrate. In addition, 1,153.18, 1,080.52, and 1,023.91 cm^{-1} were assigned to C-O-H and C-O-C stretching vibration peaks of pyran, indicated that WGP was connected by α-pyranoside bond. The absorption peaks at 936.61 and 851.02 cm^{-1} were the characteristic absorption peaks of α-Glc*p* (**Figure 2A**).

WGP ^{1}H NMR spectrum exhibited seven anomeric proton signals at δ5.32, 5.31, 5.14, 5.13, 5.06, 5.02, and 5.00 ppm, suggesting that the analyte was made up of seven monosaccharides. Intense signals within δ3.10–4.20 ppm represented CH-O and CH_2-O groups of carbohydrate. The chemical shift from δ3.15–4.13 ppm was contributed by H-2 to H-6 protons. Meanwhile, no signal was observed at δ5.50 ppm

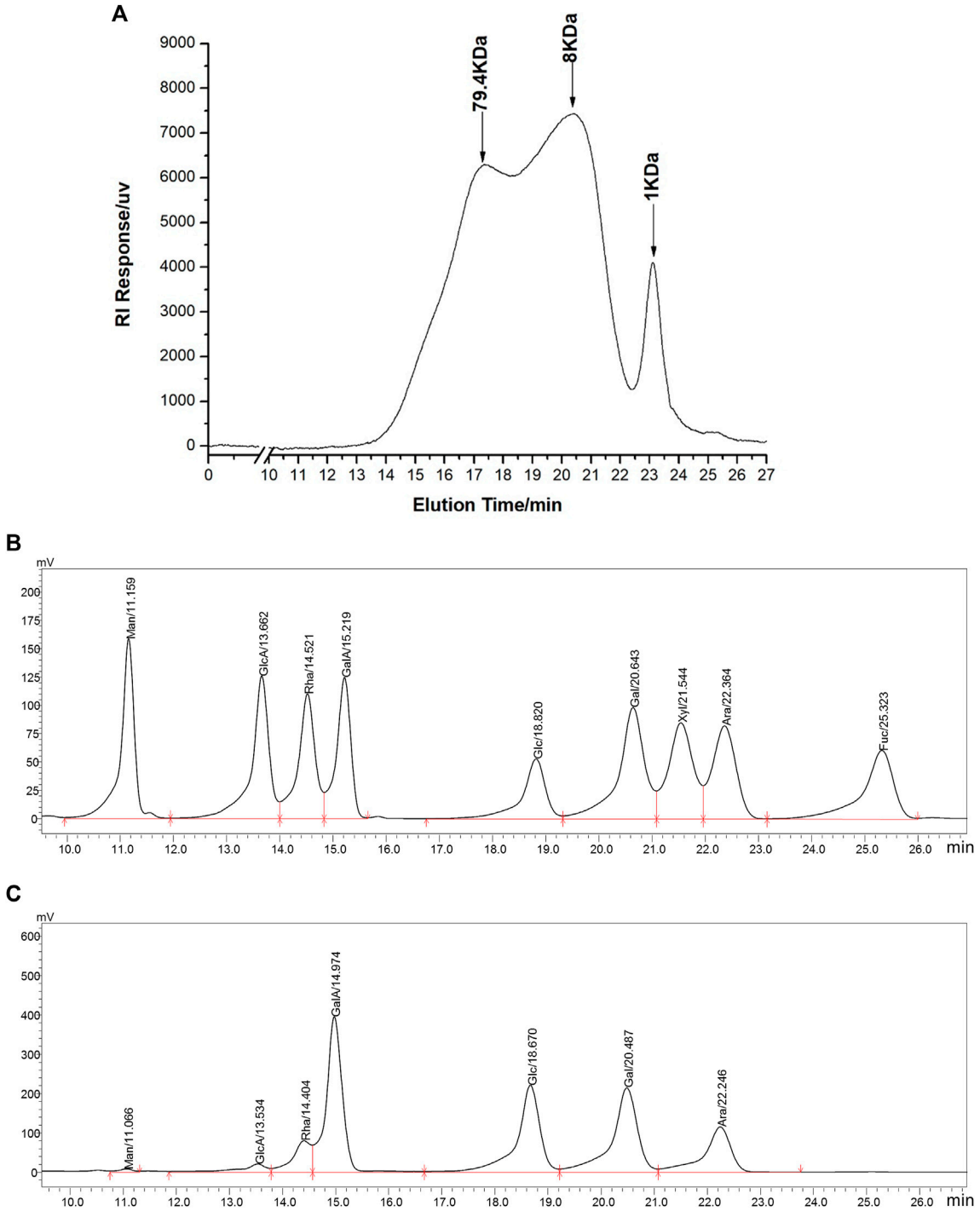

FIGURE 1 | Chromatographic analysis of WGP. HPGPC was used to determine WGP molecular weight distribution **(A)**. HPLC was used to separate monosaccharide standards **(B)** and analysis the monosaccharides composition in WGP **(C)**. Man, GlcA, Rha, GalA, Glc, Gal, Xyl, Ara, and Fuc represent mannose, glucuronic acid, rhamnose, galacturonic acid, glucose, galactose, xylose, arabinose, and fucose, respectively.

indicating that WGP contained glucopyranose, consistent with the FT-IR result (**Figure 2B**). The structure of WGP was further analyzed by ^{13}C NMR spectroscopy. β-1,4-Linked Gal residues exhibited six signals at δ105.15, 70.70, 73.05, 75.44, 74.05, and 61.58 ppm, corresponding to their C-1 to C-6. Signals at δ105.13 and 82.84 ppm were attributed to C-1 and C-3 of β-1,3-Gal, respectively. Furthermore, δ101.42 ppm was the heterocephalic carbon position of α-Glc*p*. Peak at δ78.04 ppm indicated

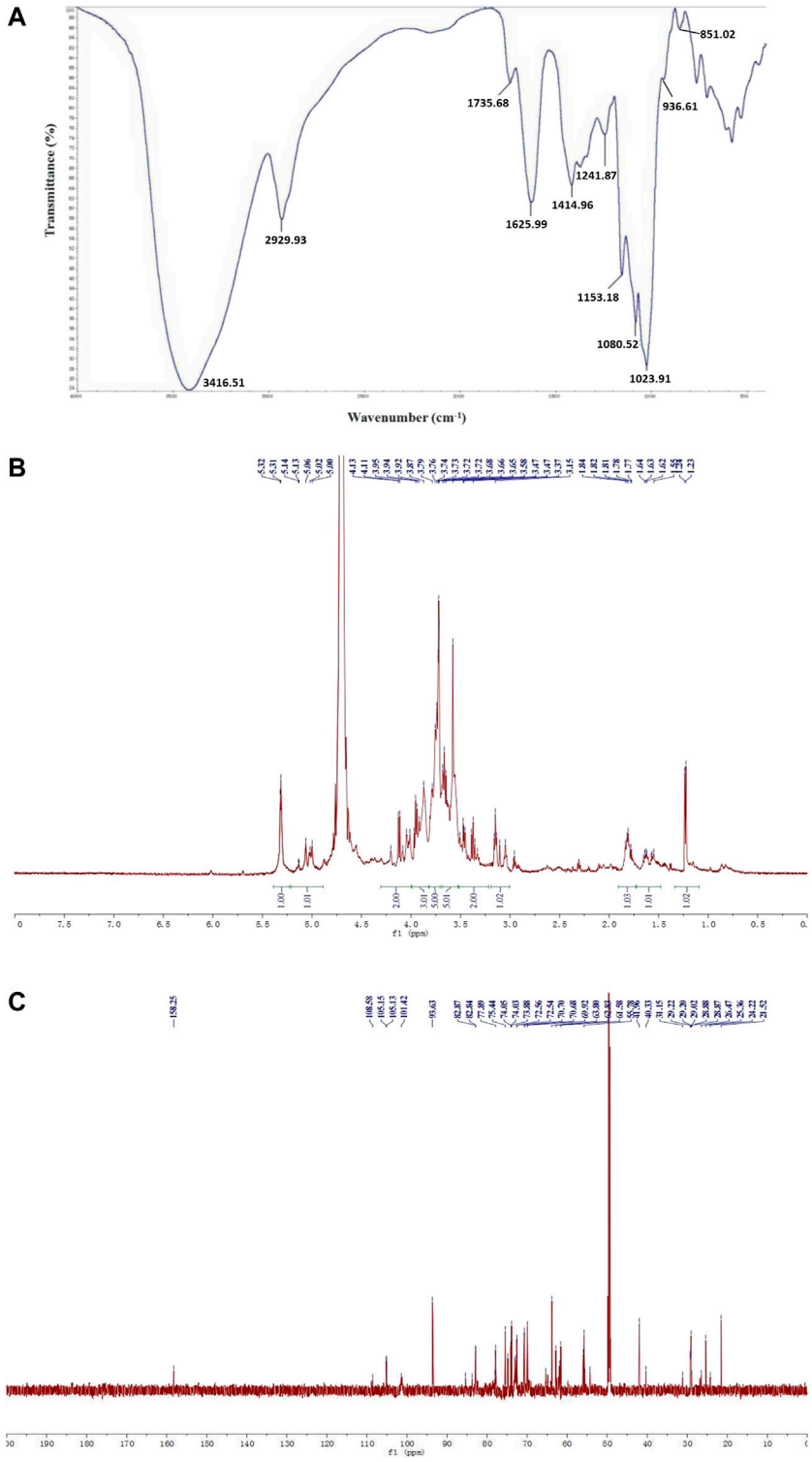

FIGURE 2 | Structural characterization of WGP. FT-IR spectrum with the range of 4,000–400 cm^{-1} **(A)** and ^{1}H NMR **(B)**, ^{13}C NMR **(C)** spectra were used to characterize WGP structure.

that C-4 of *α*-Glc*p* had been replaced. δ73.07, 74.81, 72.54, and 62.83 ppm were the positions of C-2, C-3, C-5, and C-6 of *α*-1,4-Glc*p*, respectively. The anomeric signals at δ108.58 and 83.72 ppm were due to C-1 and C-3 carbons of *α*-1,3,5-Ara (**Figure 2C**). These results were consistent with the monosaccharide composition analysis and FT-IR spectrum of WGP.

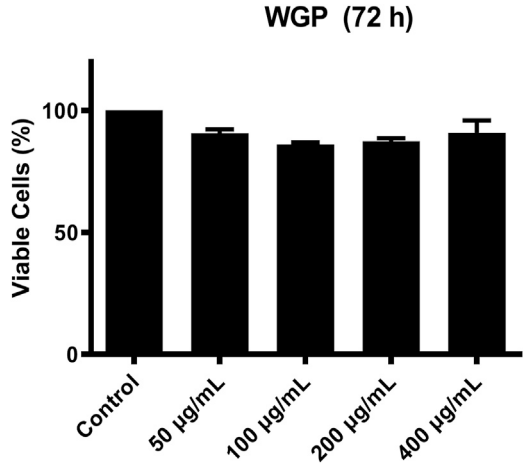

FIGURE 3 | WGP have minimal effect on the growth of hepatocytes. L-O2 cells were treated with WGP at a series of equal ratio gradient concentrations for 72 h and then subjected to MTT assay. Data are presented as mean ± standard errors of the mean (SEM) from 3 independent experiments.

Water-Soluble Ginseng Polysaccharides Induce C4 Expression in Hepatocytes

C4 is mostly synthesized in the liver (Galibert et al., 1997). Therefore, we chose human normal hepatocyte L-O2 cells as model. First, we investigated the cytotoxic effect of WGP on L-O2 cells by treating the L-O2 cells with WGP for 72 h. The results obtained from MTT assays showed that WGP treatment had minimal effect on viable cells, with the inhibition rate of viable cells less than 14% (**Figure 3**). Then, we determined the effect of WGP on the protein levels of C4 by western blotting. As shown in **Figure 4**, WGP increased C4 protein levels as early as 24 h and lasted for 72 h in a dose dependent way. These results show that WGP increase C4 production in hepatocytes.

Effect of Water-Soluble Ginseng Polysaccharides on C4 Gene Transcription

To determine if WGP enhance C4 production through transcriptional mechanisms, we treated L-O2 cells with WGP for 24, 48, and 72 h, and then measured *C4* mRNA levels by real-time PCR. Treatment of L-O2 cells with WGP for 48 and 72 h significantly increased levels of *C4* mRNA, indicating WGP enhances *C4* gene transcription (**Figure 5A**). To determine if WGP truly enhances *C4* gene transcription, pGL4.19 reporter plasmid consisting of −1,007 to +44 region of the C4 promoter (designated FL) was used to confirm the effect of WGP on *C4* transcription. Transient transfection of pC4-1,007/+44 into L-O2 cells was performed first, then the cells were treated with WGP for 72 h. The p-C4-1,007/+44 construct showed significant reporter activity compared to pGL4.19 basic in the absence or presence of WGP. Interestingly, treatment of the cells with WGP for 72 h significantly enhanced the C4 promoter reporter gene activity (**Figure 5B**). Taken together, these results demonstrate that WGP increase the production of C4 by promoting *C4* gene transcription.

Water-Soluble Ginseng Polysaccharides Enhance C4 Transcription Potentially *via* the E-box1 and Sp1 Elements

C4 promoter contains three E-boxes (positions −137 to −132, −98 to −93, and −78 to −73; designated E-box1, E-box2, and E-box3), one NF1 binding site (positions −110 to −97), and one Sp1 (positions −57 to −49) binding element (**Figure 6A**). To determine which Cis-acting element(s) is (are) vital to the enhancing effect of WGP, a series of 5' deletion constructs (designated S1-S5; **Figure 6A**) were generated by using the −1,007 to +144 region of the *C4* promoter as the template. As shown in **Figures 6B,C**, deletion from −1,007 to −119 significantly decreased *C4* promoter activity and significantly decreased the enhancing effect of WGP on *C4* promoter activity compared to the FL construct, indicating the E-box1 element in this region plays an important role in mediating the enhancing effect of WGP on *C4* promoter. In contrast, further deletions from −119 to −102, −102 to −92, and −92 to −72 did not significantly affect the enhancing effect of WGP on *C4* promoter. Interestingly, deletion from −72 to −48 completely abolished the enhancing effect of WGP, indicating the Sp1 element in this region also plays an important role in mediating the WGP effect on C4 promoter. Taken together, results from our deletion analyses suggest that the E-box1 and Sp1 cis-elements play vital roles in mediating the enhancing effect of WGP on *C4* gene transcription.

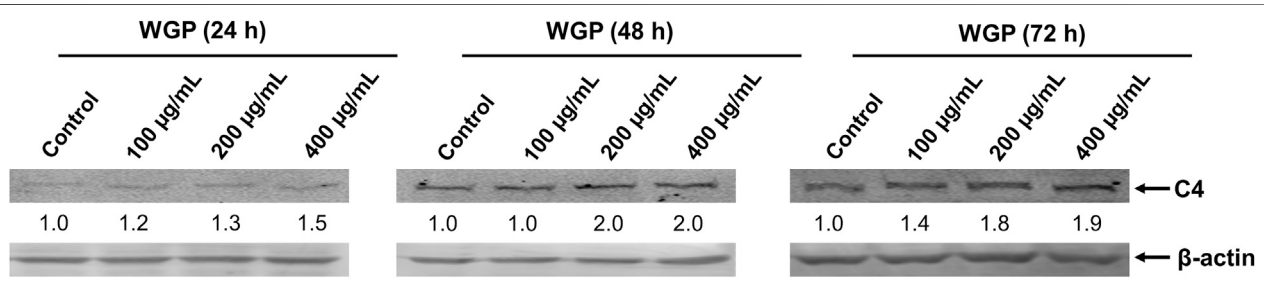

FIGURE 4 | WGP increase C4 production in hepatocytes. L-O2 cells were treated with WGP at a series of equal ratio gradient concentrations for 24, 48 or 72 h. Protein levels of C4 were determined using western blotting. The fold changes of C4 densitometry measurements were compared to β-actin and then normalized to the vehicle control.

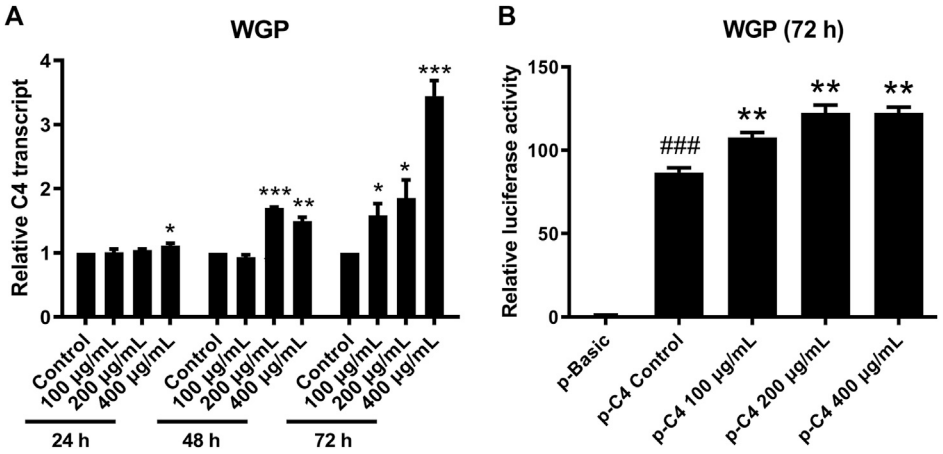

FIGURE 5 | WGP promote C4 gene transcription. L-O2 cells were treated with WGP at a series of equal ratio gradient concentrations for up to 72 h. Real-time PCR method was used to detect the levels of C4 transcripts **(A)**. L-O2 cells was transiently transfected with the full-length pC4 -1,007/+75 (p-C4) plasmid and then treated with WGP or vehicle control for 72 h. Luciferase assays were performed to determine the C4 promoter activity **(B)**. Data are presented as mean of triplicates ±SEM from one representative experiment. * indicates $p < 0.05$, ** indicates $p < 0.005$, and *** indicates $p < 0.001$ compared to vehicle control. ### indicates $p < 0.001$ compared to the basic vector control.

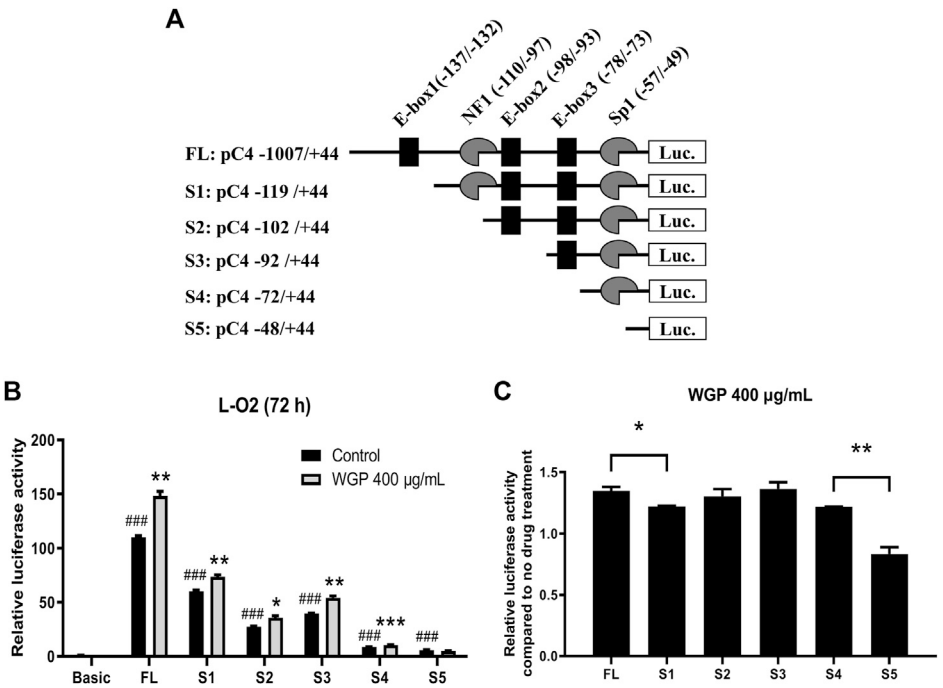

FIGURE 6 | WGP enhance C4 transcription via the E-box1 and Sp1 elements. **(A)** The critical cis-regulatory elements (NF-1, E-box1~3, Sp1) on the plus (+) and minus (-) DNA strand are shown. Numbering is relative to the C4 translation start site. A series of 5'-deletion constructs were generated by PCR amplification and subcloning into the pGL4.19 basic vector. **(B)** The C4 promoter constructs were transiently transfected into L-O2 cells. Luciferase assay was used to measure the activity of C4 promoter. * indicates $p < 0.05$, ** indicates $p < 0.005$, and *** indicates $p < 0.001$ compared to no drug treatment control. ### indicates $p < 0.001$ compared to basic vector control. **(C)** Fold changes of WGP treatment compared to vehicle control are graphed. * indicates $p < 0.05$ and ** indicates $p < 0.005$. Data are presented as mean of triplicates ±SEM from one representative experiment.

DISCUSSION

Immunomodulatory activity is one of the main functions of ginseng polysaccharides (Guo et al., 2021). The immune system orchestrated by immune organs, immune cells, and immunoreactive substances has the functions of surveillance, defense, and regulation. In the modern world, increasing stress has shifted humans' lifestyle leading to various health issues, such as cardiovascular disorders, hypertension, diabetes, and hypoimmunity (Parkin and Cohen, 2001). Hypoimmunity predisposes people to infection and cancer. In this study, we explored the immunomodulatory effect of ginseng polysaccharides from the perspective of C4, an important component of the complement system. Here, we demonstrate that WGP possess a strong and significant inductive effect on both protein and mRNA levels of C4 in hepatocyte. Complement deficiency including C4 has been associated with susceptibility to infection. C4 has been shown to inhibit adenoviral infections by inactivating viral capsids (Schröder-Braunstein and Kirschfink, 2019). Reduced levels of complement system components can cause autoimmune diseases due to the lacking of clearance of immunocomplexes (Conigliaro et al., 2019). In these scenarios, taking ginseng polysaccharide or ginseng extract is a potential adjuvant therapy.

C4 is composed of two isotypes, C4A and C4B. Both of them are encoded 10 kb apart in the major histocompatibility complex (MHC) class III area on the sixth human chromosome. *C4A* and *C4B* genes have similarly sequences located separately and closely (Carroll et al., 1984a; Carroll et al., 1984b). *C4* promoter lacks a canonical TATA-box which is commonly found at promoters of genes transcribed by RNA polymerase II (Roeder, 1991). *C4* promoter contains a nuclear factor 1 (NF-1) site at −110 to −97, an Sp1 site at −57 to −49, and three basic helix-loop-helix -like transcription factor sites at −137 to −132, −98 to −93, and −78 to −73, respectively referred to as E-box1, E-box2, and E-box3. These regions appear to be critical for the transcript activity of *C4* gene (Vaishnaw et al., 1998). Thus, we performed deletion analyses within the *C4* gene promoter. We found that E-box1 and Sp1 elements play key roles in WGP-regulated *C4* transcription. A previous study has shown that the E-box motif of *C4* promoter can be recognized by one of the many basic helix-loop-helix (bHLH) or basic helix-loop-helix-leucine zipper (bHLH-LZ) transcription factor family members (Littlewood and Evan, 1995). Moreover, IFN-γ could increase transcription of *C4 via* the E-box sequence at −78 to −73 (Banerjee et al., 2011). Thus, additional studies are warranted to determine the factors modulated by WGP in hepatocytes. However, these studies are not in the scope of this paper.

In conclusion, our results demonstrate that polysaccharides derived from ginseng can significantly increase production of C4 through transcriptional mechanisms. These results provide a molecular explanation for the immunity enhancing function of ginseng extracts.

DATA AVAILABILITY STATEMENT

The original contributions presented in the study are included in the article/Supplementary Material, further inquiries can be directed to the corresponding authors.

AUTHOR CONTRIBUTIONS

GW: conceptualization, project administration, investigation, funding acquisition, and writing the original draft; LS: conceptualization, project administration, and supervision; SL, FL, JL, TW, and CH: investigation and data curation.

FUNDING

This work was supported by a grant from National Key Research and Development Program of China (2017YFC1702103). This study was supported by the Key Laboratory for Molecular Enzymology and Engineering, the Ministry of Education, National Engineering Laboratory for AIDS Vaccine, School of Life Sciences, Jilin University, and Jilin Ginseng Academy, Research Center of Traditional Chinese Medicine, the Affiliated Hospital of Changchun University of Chinese Medicine, Key Laboratory of Active Substances and Biological Mechanisms of Ginseng Efficacy, the Ministry of Education, Changchun University of Chinese Medicine.

REFERENCES

Amsen, D., Antov, A., and Flavell, R. A. (2009). The Different Faces of Notch in T-Helper-Cell Differentiation. *Nat. Rev. Immunol.* 9 (2), 116–124. doi:10.1038/nri2488

Banerjee, A., Mazumdar, B., Meyer, K., Di Bisceglie, A. M., Ray, R. B., and Ray, R. (2011). Transcriptional Repression of C4 Complement by Hepatitis C Virus Proteins. *J. Virol.* 85 (9), 4157–4166. doi:10.1128/JVI.02449-10

Carroll, M. C., Belt, T., Palsdottir, A., and Porter, R. R. (1984a). Structure and Organization of the C4 Genes. *Philos. Trans. R. Soc. Lond. B Biol. Sci.* 306 (1129), 379–388. doi:10.1098/rstb.1984.0098

Carroll, M. C., Campbell, R. D., Bentley, D. R., and Porter, R. R. (1984b). A Molecular Map of the Human Major Histocompatibility Complex Class III Region Linking Complement Genes C4, C2 and Factor B. *Nature* 307 (5948), 237–241. doi:10.1038/307237a0

Carroll, M. C., and Isenman, D. E. (2012). Regulation of Humoral Immunity by Complement. *Immunity* 37 (2), 199–207. doi:10.1016/j.immuni.2012.08.002

Carter, R. H., and Fearon, D. T. (2010). Pillars Article: CD19: Lowering the Threshold for Antigen Receptor Stimulation of B Lymphocytes. Science, 1992. 256: 105-107. *J. Immunol.* 184 (5), 2233–2235.

Chen, Q. L., Chen, Y. J., Zhou, S. S., Yip, K. M., Xu, J., Chen, H. B., et al. (2018). Laser Microdissection Hyphenated with High Performance Gel Permeation Chromatography-Charged Aerosol Detector and Ultra Performance Liquid Chromatography-Triple Quadrupole Mass Spectrometry for Histochemical Analysis of Polysaccharides in Herbal Medicine: Ginseng, a Case Study. *Int. J. Biol. Macromol* 107, 332–342. doi:10.1016/j.ijbiomac.2017.08.162

Conigliaro, P., Triggianese, P., Ballanti, E., Perricone, C., Perricone, R., and Chimenti, M. S. (2019). Complement, Infection, and Autoimmunity. *Curr. Opin. Rheumatol.* 31 (5), 532–541. doi:10.1097/bor.0000000000000633

Dai, C., Heemers, H., and Sharifi, N. (2017). Androgen Signaling in Prostate Cancer. *Cold Spring Harb Perspect. Med.* 7 (9). doi:10.1101/cshperspect.a030452

Dodds, A. W., and Law, S. K. (1990). The Complement Component C4 of Mammals. *Biochem. J.* 265 (2), 495–502. doi:10.1042/bj2650495

Edwards, H., Xie, C., LaFiura, K. M., Dombkowski, A. A., Buck, S. A., Boerner, J. L., et al. (2009). RUNX1 Regulates Phosphoinositide 3-kinase/AKT Pathway: Role in Chemotherapy Sensitivity in Acute Megakaryocytic Leukemia. *Blood* 114 (13), 2744–2752. doi:10.1182/blood-2008-09-179812

Galibert, M. D., Boucontet, L., Goding, C. R., and Meo, T. (1997). Recognition of the E-C4 Element from the C4 Complement Gene Promoter by the Upstream Stimulatory Factor-1 Transcription Factor. *J. Immunol.* 159 (12), 6176–6183.

Gros, P., Milder, F. J., and Janssen, B. J. (2008). Complement Driven by Conformational Changes. *Nat. Rev. Immunol.* 8 (1), 48–58. doi:10.1038/nri2231

Guo, M., Shao, S., Wang, D., Zhao, D., and Wang, M. (2021). Recent Progress in Polysaccharides from Panax Ginseng C. A. Meyer. *Food Funct.* 12 (2), 494–518. doi:10.1039/d0fo01896a

Janssen, B. J., Christodoulidou, A., McCarthy, A., Lambris, J. D., and Gros, P. (2006). Structure of C3b Reveals Conformational Changes that Underlie Complement Activity. *Nature* 444 (7116), 213–216. doi:10.1038/nature05172

Kachur, K., and Suntres, Z. E. (2016). The Antimicrobial Properties of Ginseng and Ginseng Extracts. *Expert Rev. Anti Infect. Ther.* 14 (1), 81–94. doi:10.1586/14787210.2016.1118345

Kang, S., and Min, H. (2012). Ginseng, the 'Immunity Boost': The Effects of Panax Ginseng on Immune System. *J. Ginseng Res.* 36 (4), 354–368. doi:10.5142/jgr.2012.36.4.354

Kim, H. J., Kim, M. H., Byon, Y. Y., Park, J. W., Jee, Y., and Joo, H. G. (2007). Radioprotective Effects of an Acidic Polysaccharide of Panax Ginseng on Bone Marrow Cells. *J. Vet. Sci.* 8 (1), 39–44. doi:10.4142/jvs.2007.8.1.39

Kolev, M., Le Friec, G., and Kemper, C. (2013). The Role of Complement in CD4$^+$ T Cell Homeostasis and Effector Functions. *Semin. Immunol.* 25 (1), 12–19. doi:10.1016/j.smim.2013.04.012

Lalli, P. N., Strainic, M. G., Yang, M., Lin, F., Medof, M. E., and Heeger, P. S. (2008). Locally Produced C5a Binds to T Cell-Expressed C5aR to Enhance Effector T-Cell Expansion by Limiting Antigen-Induced Apoptosis. *Blood* 112 (5), 1759–1766. doi:10.1182/blood-2008-04-151068

Li, B., Zhang, N., Feng, Q., Li, H., Wang, D., Ma, L., et al. (2019). The Core Structure Characterization and of Ginseng Neutral Polysaccharide with the Immune-Enhancing Activity. *Int. J. Biol. Macromol* 123, 713–722. doi:10.1016/j.ijbiomac.2018.11.140

Lim, T. S., Na, K., Choi, E. M., Chung, J. Y., and Hwang, J. K. (2004). Immunomodulating Activities of Polysaccharides Isolated from Panax Ginseng. *J. Med. Food* 7 (1), 1–6. doi:10.1089/109662004322984626

Littlewood, T. D., and Evan, G. I. (1995). Transcription Factors 2: helix-loop-helix. *Protein Profile* 2 (6), 621–702.

Livak, K. J., and Schmittgen, T. D. (2001). Analysis of Relative Gene Expression Data Using Real-Time Quantitative PCR and the 2(-Delta Delta C(T)) Method. *Methods* 25 (4), 402–408. doi:10.1006/meth.2001.1262

Medzhitov, R. (2007). Recognition of Microorganisms and Activation of the Immune Response. *Nature* 449 (7164), 819–826. doi:10.1038/nature06246

Park, D. H., Han, B., Shin, M. S., and Hwang, G. S. (2020). Enhanced Intestinal Immune Response in Mice after Oral Administration of Korea Red Ginseng-Derived Polysaccharide. *Polymers (Basel)* 12 (10), 2186. doi:10.3390/polym12102186

Parkin, J., and Cohen, B. (2001). An Overview of the Immune System. *Lancet* 357 (9270), 1777–1789. doi:10.1016/S0140-6736(00)04904-7

Roeder, R. G. (1991). The Complexities of Eukaryotic Transcription Initiation: Regulation of Preinitiation Complex Assembly. *Trends Biochem. Sci.* 16 (11), 402–408. doi:10.1016/0968-0004(91)90164-q

Schröder-Braunstein, J., and Kirschfink, M. (2019). Complement Deficiencies and Dysregulation: Pathophysiological Consequences, Modern Analysis, and Clinical Management. *Mol. Immunol.* 114, 299–311. doi:10.1016/j.molimm.2019.08.002

Senchina, D. S., Shah, N. B., Doty, D. M., Sanderson, C. R., and Hallam, J. E. (2009). Herbal Supplements and Athlete Immune Function-Wwhat's Proven, Disproven, and Unproven? *Exerc. Immunol. Rev.* 15, 66–106.

Shi, H., Yu, L., Shi, Y., Lu, J., Teng, H., Zhou, Y., et al. (2017). Structural Characterization of a Rhamnogalacturonan I Domain from Ginseng and its Inhibitory Effect on Galectin-3. *Molecules* 22 (6), 1016. doi:10.3390/molecules22061016

Shin, M. S., Hwang, S. H., Yoon, T. J., Kim, S. H., and Shin, K. S. (2017). Polysaccharides from Ginseng Leaves Inhibit Tumor Metastasis via Macrophage and NK Cell Activation. *Int. J. Biol. Macromol* 103, 1327–1333. doi:10.1016/j.ijbiomac.2017.05.055

Song, Y. R., Sung, S. K., Jang, M., Lim, T. G., Cho, C. W., Han, C. J., et al. (2018). Enzyme-assisted Extraction, Chemical Characteristics, and Immunostimulatory Activity of Polysaccharides from Korean Ginseng (Panax Ginseng Meyer). *Int. J. Biol. Macromol* 116, 1089–1097. doi:10.1016/j.ijbiomac.2018.05.132

Sun, Y. (2011). Structure and Biological Activities of the Polysaccharides from the Leaves, Roots and Fruits of Panax Ginseng C.A. Meyer: An Overview. *Carbohydr. Polym.* 85 (3), 490–499. doi:10.1016/j.carbpol.2011.03.033

Uphoff, C. C., and Drexler, H. G. (2005). Detection of Mycoplasma Contaminations. *Methods Mol. Biol.* 290, 13–23. doi:10.1385/1-59259-838-2:013

Vaishnaw, A. K., Mitchell, T. J., Rose, S. J., Walport, M. J., and Morley, B. J. (1998). Regulation of Transcription of the TATA-Less Human Complement Component C4 Gene. *J. Immunol.* 160 (9), 4353–4360.

Wang, J., Zhang, Y., Xu, X., Jin, W., Jing, C., Leng, X., et al. (2020). ASP2-1, a Polysaccharide from Acorus Tatarinowii Schott, Inhibits Osteoclastogenesis via Modulation of NFATc1 and Attenuates LPS-Induced Bone Loss in Mice. *Int. J. Biol. Macromol* 165 (Pt B), 2219–2230. doi:10.1016/j.ijbiomac.2020.10.077

Wang, M., Guilbert, L. J., Ling, L., Li, J., Wu, Y., Xu, S., et al. (2001). Immunomodulating Activity of CVT-E002, a Proprietary Extract from North American Ginseng (Panax Quinquefolium). *J. Pharm. Pharmacol.* 53 (11), 1515–1523. doi:10.1211/0022357011777882

Yu, X. H., Liu, Y., Wu, X. L., Liu, L. Z., Fu, W., and Song, D. D. (2017). Isolation, Purification, Characterization and Immunostimulatory Activity of Polysaccharides Derived from American Ginseng. *Carbohydr. Polym.* 156, 9–18. doi:10.1016/j.carbpol.2016.08.092

Yun, M., and Yi, Y. S. (2020). Regulatory Roles of Ginseng on Inflammatory Caspases, Executioners of Inflammasome Activation. *J. Ginseng Res.* 44 (3), 373–385. doi:10.1016/j.jgr.2019.12.006

Yun, T. K. (2001). Brief Introduction of Panax Ginseng C.A. Meyer. *J. Korean Med. Sci.* 16, S3–S5. doi:10.3346/jkms.2001.16.S.S3

Zhang, J., Koh, J., Lu, J., Thiel, S., Leong, B. S., Sethi, S., et al. (2009). Local Inflammation Induces Complement Crosstalk Which Amplifies the Antimicrobial Response. *Plos Pathog.* 5 (1), e1000282. doi:10.1371/journal.ppat.1000282

Zhao, J. L., Zhang, M., and Zhou, H. L. (2019). Microwave-Assisted Extraction, Purification, Partial Characterization, and Bioactivity of Polysaccharides from Panax Ginseng. *Molecules* 24 (8), 1605. doi:10.3390/molecules24081605

Conflict of Interest: The authors declare that the research was conducted in the absence of any commercial or financial relationships that could be construed as a potential conflict of interest.

frontiers in Pharmacology

ORIGINAL RESEARCH
published: 22 October 2021
doi: 10.3389/fphar.2021.766737

Mori Fructus Polysaccharides Attenuate Alcohol-Induced Liver Damage by Regulating Fatty Acid Synthesis, Degradation and Glycerophospholipid Metabolism in Mice

Liang Bian[1,2,3], *Hua-Guo Chen*[1,2,3], *Xiao-Jian Gong*[1,2,3], *Chao Zhao*[1,2,3] *and Xin Zhou*[1,2,3]*

[1]*Key Laboratory for Information System of Mountainous Areas and Protection of Ecological Environment, Guizhou Normal University, Guiyang, China,* [2]*Guizhou Engineering Laboratory for Quality Control and Evaluation Technology of Medicine, Guizhou Normal University, Guiyang, China,* [3]*Research Center for Quality Control of Natural Medicine, Guizhou Normal University, Guiyang, China*

Mori Fructus polysaccharides (MFP) are macromolecules extracted from Mori Fructus (MF), which has the biological activity of anti-liver damage. Our group found that MFP maybe down regulate the serum triglyceride level in mice with alcohol-induced liver damage, suggesting that MFP can regulate lipid metabolism, but its specific mechanism is still not clear. Fifty SPF-ICR male mice weighing 18–22 g were randomly divided into five groups, blank group, model group, bifendate group, MFPA1 group and MFPB1 group. The blood and liver tissues were taken from mice for nontargeted lipidomic analysis and histopathological examination after 7 day's treatment. The histopathological changes indicated that the normal liver cells were intact and regular, with orderly arrangement and distinct cell boundaries; the liver of model mice showed inflammatory infiltration, ballooning degeneration in the cells and small lipid drops; the liver of mice in the bifendate, MFPA1 and MFPB1 groups showed similar symptoms to those of model mice, but the lesions were less severe and the ballooning degeneration were reduced. Multivariate analysis of all lipids in the serum of five groups of mice showed there were obvious differences in lipid metabolism between the model group and the blank group. At the same time, seven kinds of differential lipids were precisely identified after screening, including prostaglandins, long-chain fatty acids, glycerophospholipids, acyl carnitines. In summary, alcohol intake and MFP intervention have significant effects on fatty acid synthesis, degradation and glycerophospholipid metabolism.

Keywords: nontargeted lipidomics, *Mori fructus* polysaccharide, lipid metabolism, protective effect, hematoxylin and eosin staining

OPEN ACCESS

Edited by:
SP Li,
University of Macau, China

Reviewed by:
Xuan Qin,
Baylor College of Medicine, United States
Hongxia Zhao,
Shanghai University, China
Sylwia Chojnowska,
Lomza State University of Applied Sciences, Poland

***Correspondence:**
Xin Zhou
Alice9800@sina.com

Specialty section:
This article was submitted to Ethnopharmacology, a section of the journal Frontiers in Pharmacology

Received: *30 August 2021*
Accepted: *11 October 2021*
Published: *22 October 2021*

Citation:
Bian L, Chen H-G, Gong X-J, Zhao C and Zhou X (2021) Mori Fructus *Polysaccharides Attenuate Alcohol-Induced Liver Damage by Regulating Fatty Acid Synthesis, Degradation and Glycerophospholipid Metabolism in Mice. Front. Pharmacol. 12:766737. doi: 10.3389/fphar.2021.766737*

INTRODUCTION

Ethanol is metabolized in the liver to produce toxic substances such as acetaldehyde, which increases the intracellular NADH/NAD^+ ratio, inhibits the β-oxidation of fatty acids, increases the esterification rate of fatty acids and causes the accumulation of triglycerides in the liver, ultimately causing a fatty liver (Ramachandran et al., 2019). World Health Organization released the Global status report on alcohol and health in 2018, which states that approximately 3 million people die from alcohol-induced liver disease each year worldwide, accounting for nearly 5.3% of all deaths (World Health Organization, 2018). The current treatment of alcohol-induced liver disease is mainly drug therapy and surgical operation, but most drug therapy have side effects and high recurrence rate, for example, glucocorticoids and phosphatidylcholine cause disorders of lipid metabolism, while taurine and bile salts place a high burden on the gastrointestinal tract, so the search for a low toxicity and high efficiency drug has become a hot spot in the field of alcohol-induced liver disease.

Mori Fructus (*Morus alba L.* fruit, mulberry) is a kind of effective Chinese herbs for the treatment of alcoholic intoxication and has a long history of use. MFP is a kind of low side effect macromolecule which is used to treat alcohol-induced liver disease (Zhou et al., 2017). Many researches indicate that MFP can treat alcohol-induced liver disease, but the mechanism of MFP against alcohol-induced liver disease has not been elucidated. Studies have shown that alcohol could induce lipid peroxidation in the liver, leading to steatosis (Kotronen et al., 2010). Therefore, the present study explores the lipid metabolism mechanism of MFP against acute alcohol-induced liver damage.

Lipidomics can detect the composition and content of lipids in organism, and discover the connection between specific signaling pathways of lipid metabolism and disease (Lam and Shui, 2013). At present, mass spectrometry (MS) is the core tool for lipidomics, and liquid chromatography-mass spectrometry (LC-MS) and shotgun are mainstream in the MS method (Murphy and Nicolaou, 2013). The UPLC-Q-Orbitrap-HRMS method can extract the accurate mass of the target compound in the full scan mode, automatically trigger the acquisition of the tandem mass spectrum, reduce the probability of false positive results, and improve the accuracy of qualitative (Jiang et al., 2020). Therefore, a non-targeted lipidomics approach by using UPLC-Q-Orbitrap-HRMS was used for qualitative and semi-quantitative analysis of differential lipids.

In our work, H&E staining was performed and the histopathological changes were detected under microscope. The nontargeted lipidomics analysis of the serum of the mice was carried out to obtain the biomarkers of alcohol-induced liver damage, and to explore the mechanism of alcoholic liver damage and lipid metabolism of MFP against acute alcohol-induced liver damage.

MATERIALS AND METHODS

Chemicals and Reagents

CH_2Cl_2, methanol, acetonitrile, isopropyl alcohol, and formic acid are HPLC grade from Sinopharm Chemical Reagent Co. (Shanghai, China). Ethanol, trinitrophenol, xylene, n-butanol, and formaldehyde are AR grade from FUYU Chemical Co. (Tianjin, China).

Extraction, Purification and Characterization of *Mori Fructus* polysaccharides

Fresh MF was purchased from Beijing Tongrentang Co., Chengdu City, Sichuan Province, China. Fresh MF were pulverized, defatted, extracted by maceration in 90°C water and deproteinized to obtain an extract of MFP, then continued to precipitate with 30 and 50% ethanol to finally obtain crude polysaccharides (MFPA, MFPB). 20 ml of 6 mg mL^{-1} MFPA and MFPB solution was prepared and gradient eluted with 300 ml of distilled water and 300 ml of 0.05 mol L^{-1} NaCl on a DEAE-52 cellulose column (3 × 50 cm) at a flow rate of 2.5 ml min^{-1}. Each eluate was monitored by the phenol-sulphuric acid method until no polysaccharide was present. MFPA1 and MFPB1 were obtained by combining the different fractions of MFP according to the absorption peaks, concentrating, dialyzing and freeze-drying under vacuum. The polysaccharide content, protein content, uronic acid content, molecular weight and monosaccharide composition of MFPA1 and MFPB1 were determined by sulfuric acid-phenol method, coomassie brilliant blue G-250 method, sulfuric acid-carbazole method, high performance gel chromatography and PMP pre-column derivatization high performance liquid chromatography, respectively. The results show that the contents of MFPA1 and MFPB1 were 93.44 and 89.68%, the specific experimental results are as described in the reference (Tan et al., 2021).

Induction of Alcohol-Induced Liver Damage in Mice and Treatments

50 SPF-ICR mice (4–6 weeks, 18–22 g, males) were purchased from Changsha Tianqin Biotechnology Co., Ltd. All mice take food and drank water freely with standard environmental conditions. The mice were fed adaptively for a week and randomly divided into five groups, blank group, model group, bifendate group, MFPA1 group and MFPB1 group. At 10 o'clock every day, the blank group was given with saline (10 mg/kg), and other groups were administered intragastrically by 56% ethanol (10 ml/kg). At 12 o'clock every day, the bifendate group, MFPA1 group and MFPB1 group were administered by bifendate (220 mg/kg), MFPA1 (50 mg/kg), MFPB1 (50 mg/kg), and the blank group and model group were given with saline (10 mg/kg). After 7 day's treatment, the blood and liver were collected for histopathological examination and nontargeted lipidomic analysis after the last administration.

Histopathology Examination

The freshly dissected mice livers were cleaned, placed in a 10% neutral formalin solution for 36 h and stored at room temperature. The mice livers were removed, rinsed under running water for 5 min, cut into pieces, and dehydrated in

TABLE 1 | Chromatographic parameters for nontargeted lipidomics analysis.

	Chromatographic parameters
Column	Phenomenex ACE Excel 1.7 C18-AR UPLC PR column (100 mm × 2.1 mm, 1.7 μm)
Column temp	4°C
Injection volume	4 μL
Flow rate	0.3 ml/min
Run time	30 min
Mobile phase	A: 60:40 (v/v) acetonitrile/water containing 10 mM ammonium formate and 0.1% (v/v) formic acid
	B: 90:10 (v/v) isopropanol/acetonitrile containing 10 mM ammonium formate and 0.1% (v/v) formic acid
Gradient	0–2 min, 40%-43%B
	2–2.1 min, 43%-50%B
	2.1–12 min, 50%-54%B
	12–25 min, 54%-99%B
	25–25.1 min, 99%-40%B
	25.1–30 min, 40%B

increasing grades of ethanol, then cleared in xylene, finally embedded in paraffin. The paraffin blocks containing the liver tissue were cut into 4 μm thick pieces, stained with hematoxylin and eosin and the histological section continued to be sealed with neutral balsam and observed by optical microscope.

Nontargeted Lipidomic Investigations

Extraction of Lipids in Serum

Our groups have adapted the Folch's method, which is based on the theory of "the like dissolves like," and successfully extracted lipids from serum samples (Folch et al., 1957). Briefly, whole blood of mice was collected in a 1.5 ml centrifuge tube and allowed to stand at room temperature for 30 min, followed by centrifugation at 3,000 rpm, 4°Cfor 10 min, and finally aspirated the upper layer of the yellow transparent serum in the centrifuge tube. 150 μL serum was placed in a 5 ml centrifuge tube and 600 μL of methanol, 300 μL of water and 450 μL of dichloromethane were added sequentially. The sample was mixed, homogenized, vortexed for 1 min and centrifuged at 12,000 rpm, 4°C for 15 min. The lower organic phase was taken and dried with nitrogen to obtain dried lipid extracts. The 200 μL of acetonitrile/isopropanol/water (65:30:5, V: V: V) mixture was added to dried lipid extracts, centrifuged at 8,000 rpm, 4°C for 5 min and the supernate was aspirated for nontargeted lipidomic analysis.

UPLC-Q-Orbitrap-HRMS Analysis

The serum nontargeted lipidomics method was used on a Q Exactive Focus quadrupole orbitrap high resolution mass spectrometry (Thermo Fisher Scientific, Shanghai, China) coupled with an Ultimate 3000 RSLC (HPG) ultra-performance liquid chromatography (Dionex, Beijing, China), with a HESI ionization source. The chromatographic parameters are shown in **Table 1**. All MS/MS data for serum lipids were collected in positive ion mode and negative ion mode by full scan mode. The optimized parameter settings for ESI were: spray voltage, 3.5 kV/3.2 kV; sheath gas, 35; auxiliary gas, 10 (both high-purity nitrogen); capillary temperature, 320°C; sphere-lens, 60 V; mass scan range, 100–1,000 m/z; resolution, 70,000; collision energy, 20,40 and 60 eV (Bian et al., 2021).To verify the stability of the instrument during operation, 20 μL from each serum lipid samples were taken, placed in the same tube and then evenly divided into five quality control (QC) samples. During the mass spectrometer analysis, one quality control sample was detected after every five serum lipid samples to test the stability of the experimental method.

Statistical Analysis

The data obtained by statistical analysis are all expressed as mean ± SD. A one-way ANOVA was performed using Graphpad prism 8.0.2, with a significant difference between the two groups when $p < 0.05$. Pairwise comparison in five groups was conducted with HSD method. The raw data is processed by noise filtering, baseline correction and peak matching to obtain two-dimensional data consisting of m/z and peak area. After processing the missing values, the above data was standardized and conversion, and imported into SIMCA14.1 software for multivariate statistical analysis. Analysis of the results of the Principal component analysis (PCA) and Orthogonal partial least squares-discriminant analysis (OPLS-DA) showed differences in lipid metabolism between the groups. With VIP>1, $p < 0.05$, FC ≥ 1.5 or FC ≤ 0.67 as the screening conditions, the difference variables were obtained. By comparing the MS/MS spectrum of the difference variable with the standard MS/MS spectrum of the candidate lipid in the HMDB database, the differential lipid is finally obtained. The HMDB database IDs of candidate lipid were imported into MetaboAnalyst 5.0, and finally found signal pathways related to liver damage and MFP against liver damage.

RESULTS

Effect of *Mori Fructus* polysaccharides on Alcohol-Induced Liver Damage

The body weight changes of the five groups of mice are shown in **Figure 1**. After a week of intragastric infusion with alcohol, the body weight of mice in the model group were significantly lower than those in other groups. After 3 days of intragastric infusion with alcohol, model mice began to lose weight, while the remaining four groups continued to gain weight until the end of the experiment, indicating that alcohol inhibited weight gain

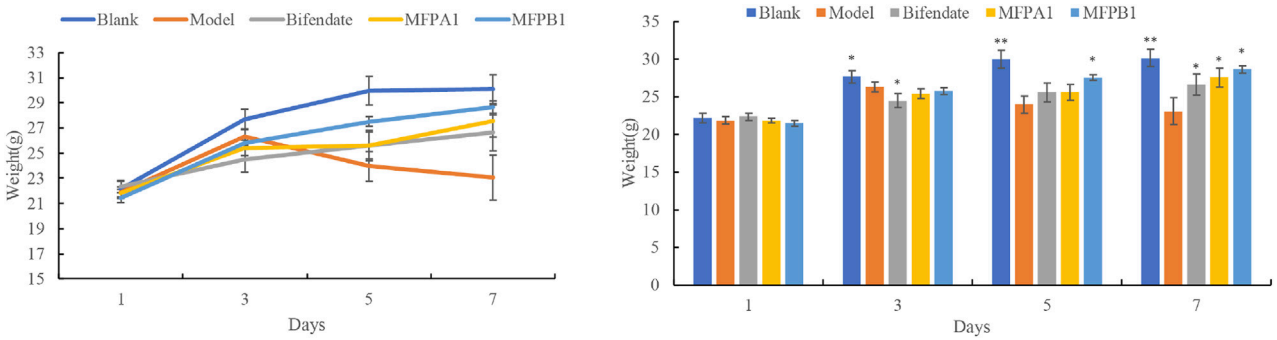

FIGURE 1 | Body weight changes of mice, value are means ± SD (n = 10, g). *: $p < 0.05$, **:$p < 0.01$, blank, bifendate, MFPA1, MFPB1 group vs model group.

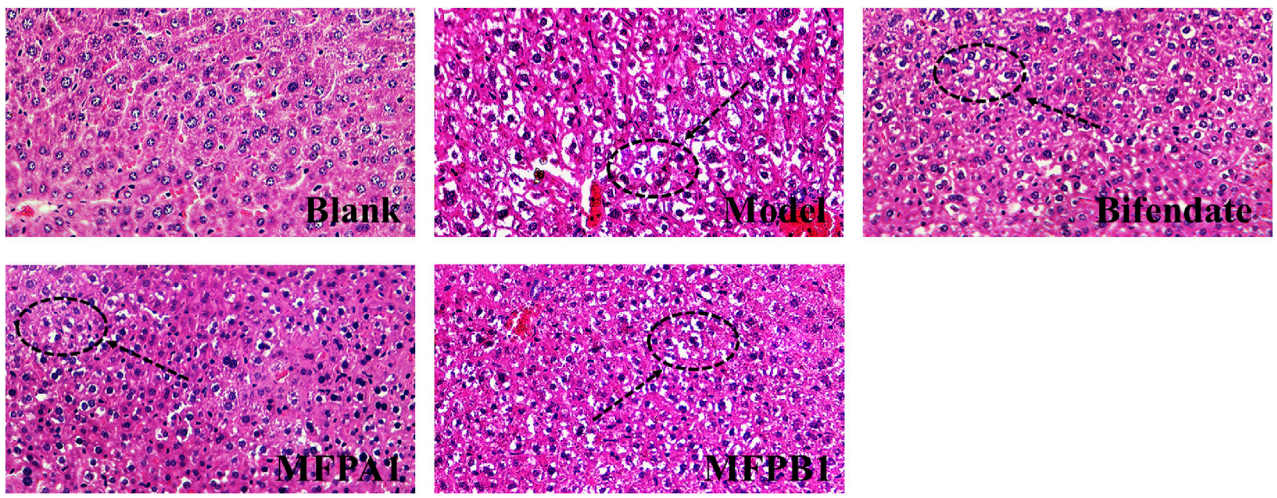

FIGURE 2 | Histopathological changes of liver tissue in mice. Liver cells with lipid droplets are marked with black arrows.

and bifendate, MFPA1 and MFPB1 were effective in improving this situation.

The histopathological changes in the liver of the five groups of mice are shown in **Figure 2**. By using image pro plus 6.0 to count, the area ratios of hepatocyte ballooning degeneration of mice in the blank, model, bifendate, MFPA1 and MFPB1 groups were 1.95, 14.20, 4.76, 2.39 and 8.29% respectively. The liver cells of mice in the normal group were intact and regular, with orderly arrangement and obvious cell boundaries; the liver of mice in the model group showed inflammatory infiltration, ballooning degeneration in the cells and small lipid drops; the liver of mice in the bifendate, MFPA1 and MFPB1 groups showed similar symptoms to those of mice in the model group, but the lesions were less severe and the ballooning degeneration were reduced. The above results confirmed that MFP maybe attenuate alcohol-induced steatosis.

Stability Detection of Experimental Method

To test the stability of the mass spectrometry method, a QC sample was run every five serum lipid samples. The total ion chromatogram of the five QC samples is shown in **Figure 3A**. The number, time, and value of the chromatographic peaks are almost the same, indicating that the method was stable during lipid analysis. At the same time, PCA analysis found that the deviation of the five QC samples during operation was within 2std according to the results of lipid determination, which also confirmed that the mass spectrometry method was stable (**Figures 3B,C**).

Multivariate Analysis of all Serum Lipids

Multivariate analysis of all lipids in the serum of five groups of mice can show the differences in lipid metabolism between groups and to obtain variable important to projection values (VIP) for all lipids in OPLS-DA.

In the positive ion mode, PCA showed R2X = 0.994 and Q2 = 0.949, while OPLS-DA showed R2X = 0.893 and Q2 = 0.578. The result of 200 permutation tests confirmed that the OPLS-DA was not overfitted. The above results confirm that both models have good explanatory and predictive ability. As shown in **Figures 4A,C,E**, the mice in the model group were clearly separated from

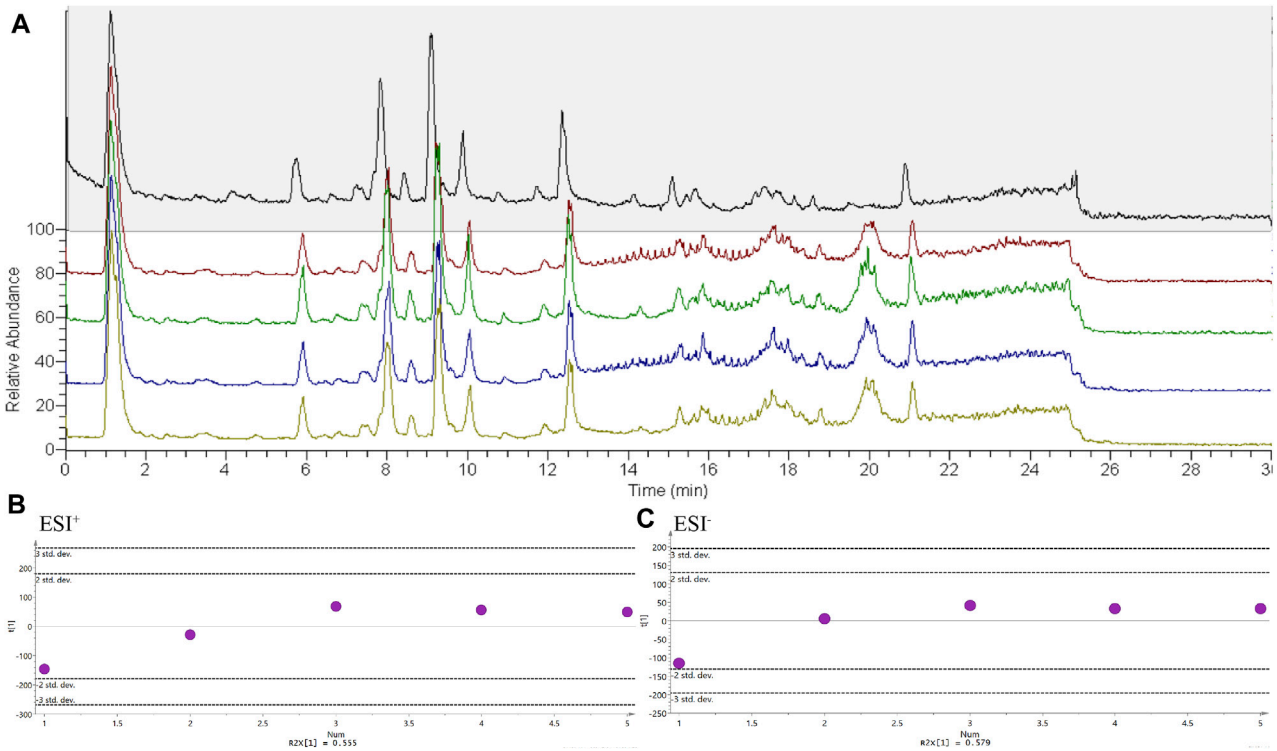

FIGURE 3 | The stability detection of experimental method. *n* = 5. **(A)** Chromatograms of QC samples, **(B)** PCA score charts of QC samples in positive ion mode, **(C)** PCA score charts of QC samples in negative ion mode.

the mice in the blank group, implying that alcohol can cause disruption of lipid metabolism in mice serum, resulting in different lipid accumulation in the serum of the model and blank mice.

In the negative ion mode, PCA showed R2X = 0.958, Q2 = 0.837 and OPLS-DA showed R2X = 0.893, Q2 = 0.76. The result of 200 permutation tests confirmed that OPLS-DA did not overfit, indicating that both models had good explanatory and predictive ability. As shown in **Figures 4B,D,F**, there was a good separation between the blank group and the model group in the score of PCA and OPLS-DA, and the MFPA1 and MFPB1 groups were positioned closer to the blank group, implying that alcohol caused abnormal lipid accumulation in the serum of mice, and MFPA1 and MFPB1 maybe regulate the abnormal lipid accumulation and restore the levels of differential lipids to normal, resulting in the improvement of alcohol-induced liver damage.

Screening and Identification of Differential Lipids

After data processing, the calculation of FC and one-way ANOVA were performed to finally obtain the P and FC values between the model and blank groups. With VIP>1, $p < 0.05$, FC ≥ 1.5 or FC ≤ 0.67 as the screening conditions, the difference variables were obtained. By comparing the MS/MS spectrum of the difference variable with the standard MS/MS spectrum of the candidate lipid in the HMDB database, seven kinds of differential lipids were precisely identified, including prostaglandins, long-chain fatty acids, glycerophospholipids, acyl carnitines. As shown in **Table 2**, the m/z of the measured molecular ions deviated from the m/z of the theoretical molecular ions within ±15 ppm; the concentrations of serum Palmitoylcarnitine, LPC(17:0), Palmitic acid, Vaccenic acid, Stearic acid, and Prostaglandin J2 in mice of the model group were lower than those in the blank group, while the concentration of LPC(18:3) in the serum of mice in the model group was higher than that in the blank group.

Effect of Alcohol on Serum Lipid in Mice

In our work, heatmap, correlation heatmap and bubble chart were presented based on the content of differential lipids and the ID of the HMDB database. As depicted in **Figures 5**, **6** the clustering algorithm classified the differential lipids into up-regulated and down-regulated lipids based on the results of changes in the content of the seven differential lipids, which showed that alcohol intake resulted in higher LPC(18:3) concentrations and lower Palmitoylcarnitine, LPC(17:0), Palmitic acid, Vaccenic acid, Stearic acid, and Prostaglandin J2 concentrations in mice serum. In order to explore the correlation between seven different lipids in alcohol-induced liver damage, the correlation analysis on seven different lipids in mice serum

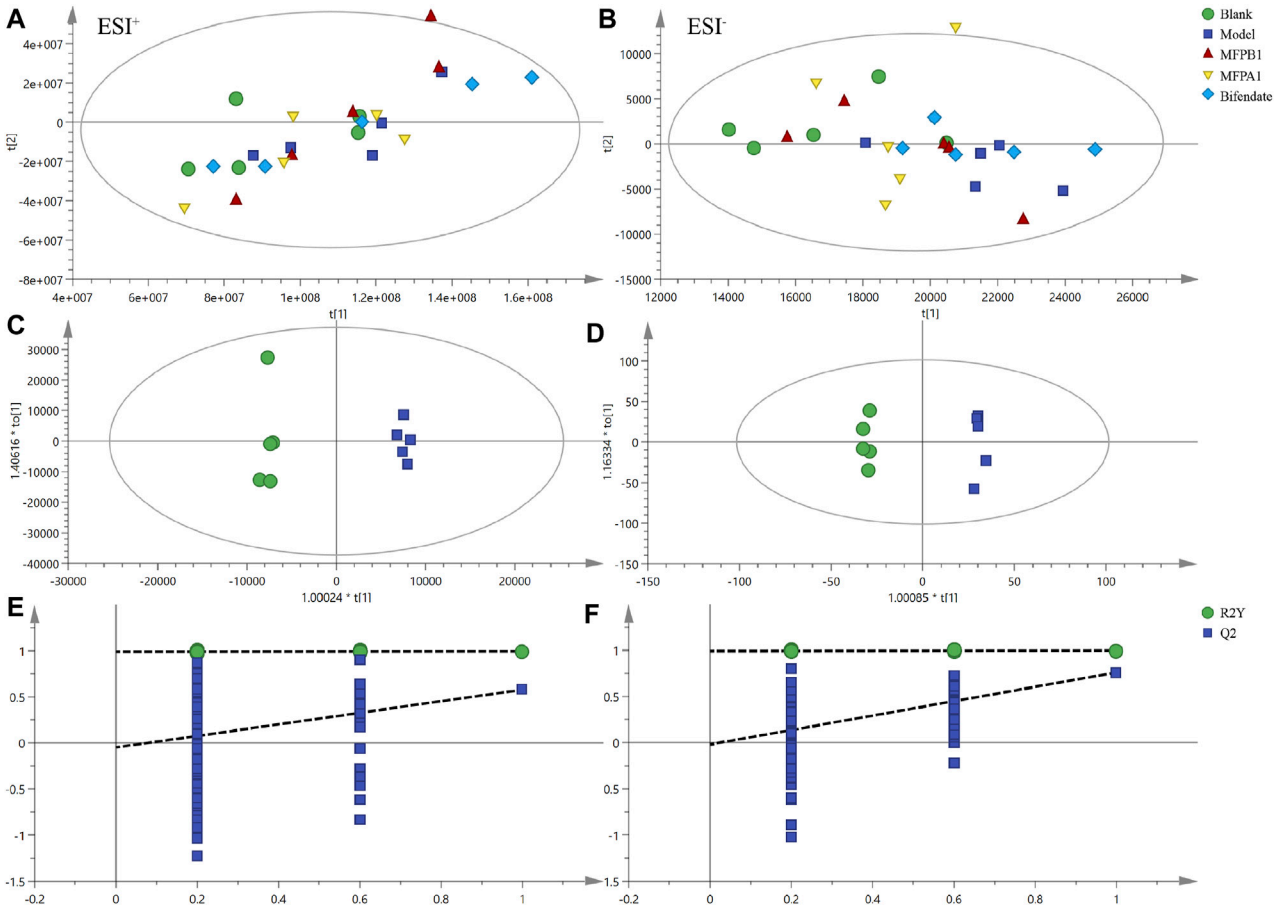

FIGURE 4 | PCA score charts of serum lipid analysis of each experimental group are shown for positive ion mode **(A)** and negative ion mode **(B)**, OPLS-DA score charts of serum lipid analysis of each experimental group are shown for positive ion mode **(C)** and negative ion mode **(D)**, and permutation tests are shown for positive ion mode **(E)** and negative ion mode **(F)**. *n* = 5.

TABLE 2 | Specific information of Palmitoylcarnitine, LPC (17:0), Palmitic acid, Vaccenic acid, Stearic acid, Prostaglandin J2 and LPC (18:3).

Metabolite	Species	ESI mode	Retention time (min)	Measured m/z	Mass accuracy (ppm)	MS/MS fragments	Blank	Model	Bifendate	MFPA1	MFPB1
Palmitoylcarnitine	CAR	+	11.76	400.3417	−1	85.0290; 400.3421	↑	—	—	↑	↑
Palmitic acid	FA	-	17.57	255.2328	2.35	205.7752; 255.2332	↑	—	—	↑	↑
Vaccenic acid	FA	-	18.42	281.2486	−0.71	281.2489	↑	—	—	↑	↑
Stearic acid	FA	-	20.13	283.2641	1.77	283.2641	↑	—	—	—	—
Prostaglandin J2	PG	-	26.05	333.2072	0.3	271.2066; 191.1437	↑	—	—	—	↓
LPC (18:3)	PC	-	6.46	562.315	0.89	277.2173; 502.2940	↓	—	—	—	—
LPC (17:0)	PC	+	10.89	510.3553	−1.37	184.0733	↑	—	↑	↑	↑

Using the content of differential lipids in the model group as benchmark, and marked as "—". The up arrows (or down arrows) represented the relative up-regulation (or down-regulation) of the differential lipids, p < *0.05; "—" represented no change of the differential lipids content,* p > *0.05. blank, bifendate, MFPA1, MFPB1 group vs model group.* n = *5.*

was performed. The results showed that Palmitoylcarnitine was significantly and positively correlated with Palmitic acid and Vaccenic acid, and Palmitic acid was significantly and negatively correlated with LPC(18:3), which implies that alcohol-induced Palmitoylcarnitine acted synergistically with Palmitic acid and Vaccenic acid during hepatic steatosis, while

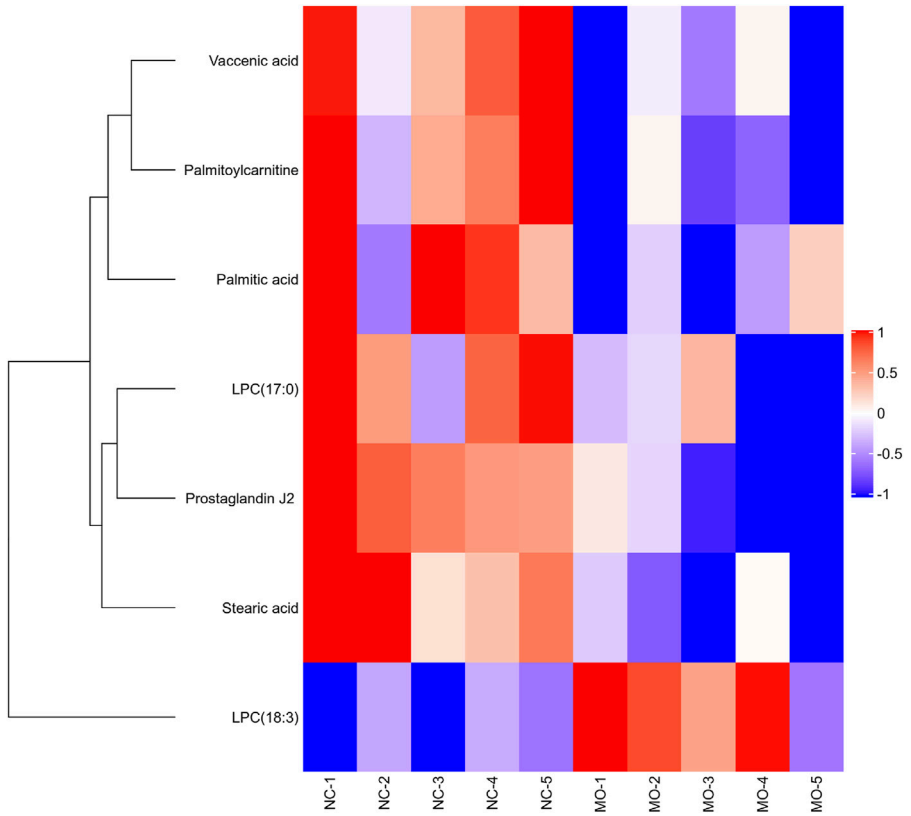

FIGURE 5 | Overview of Matrix heatmap using fold-changes between groups.

Palmitic acid acted antagonistically with LPC(18:3) during alcohol-induced liver damage.

In order to elucidate the mechanism of alcohol-induced liver damage, the HMDB database IDs of Palmitoylcarnitine, LPC (17:0), Palmitic acid, Vaccenic acid, Stearic acid, Prostaglandin J2 and LPC (18:3) were imported into MetaboAnalyst 5.0 that can explain the influence of alcohol on different lipid metabolism pathways. Present result indicated alcohol-induced liver damage may be related to the mechanism of fatty acid degradation, fatty acid biosynthesis, glycerophospholipid (**Figure 7**).

Protective Effect of *Mori Fructus* polysaccharides in Mice With Alcohol-Induced Liver Damage

The action mechanism of MFPA1 and MFPB1 against acute alcohol-induced liver damage was finally obtained by one-way ANOVA on the content of seven differential lipids among five groups of mice. As shown in **Figure 8**, the contents of Palmitoylcarnitine, LPC(17:0), Palmitic acid, and Vaccenic acid in the serum of mice decreased significantly after ingesting alcohol, but the contents of the above four lipids quickly returned to normal levels after 7 days of MFPA1 and MFPB1 administration. The statistical results showed that compared with the model group, the content of Palmitoylcarnitine in the serum of MFPA1 group and MFPB1 mice increased by 260.26 and 345.05%, respectively; the content of LPC(17:0) increased by 154.18 and 93.26%, respectively; the content of Palmitic acid increased by 94.51 and 131.55%, respectively; the content of Vaccenic acid increased by 239.32 and 320.81%, respectively.

Pathway analysis of almitoylcarnitine, LPC (17:0), Palmitic acid, and Vaccenic acid showed that MFPA1 and MFPB1 may regulate fatty acid degradation, fatty acid biosynthesis, and glycerophospholipid metabolism to reduce alcohol-induced liver damage (**Figure 9**).

DISCUSSION

Studies have shown that saturated fatty acids have a therapeutic effect on alcohol-induced liver damage, and Palmitic acid is one of the most common saturated fatty acids found in animals (Sveinbjrnsson and Baldursdóttir, 2020). Chronic alcohol consumption increases the levels of sterol regulatory element binding protein-1 (SREBP-1) and Acetyl CoA carboxylase (ACC), leading to the accumulation of triacylglycerols in the liver, while saturated fatty acids inhibit the activity of SREBP-1 and also increase the transport ability of triacylglycerols, thereby reducing the liver damage caused by alcohol consumption

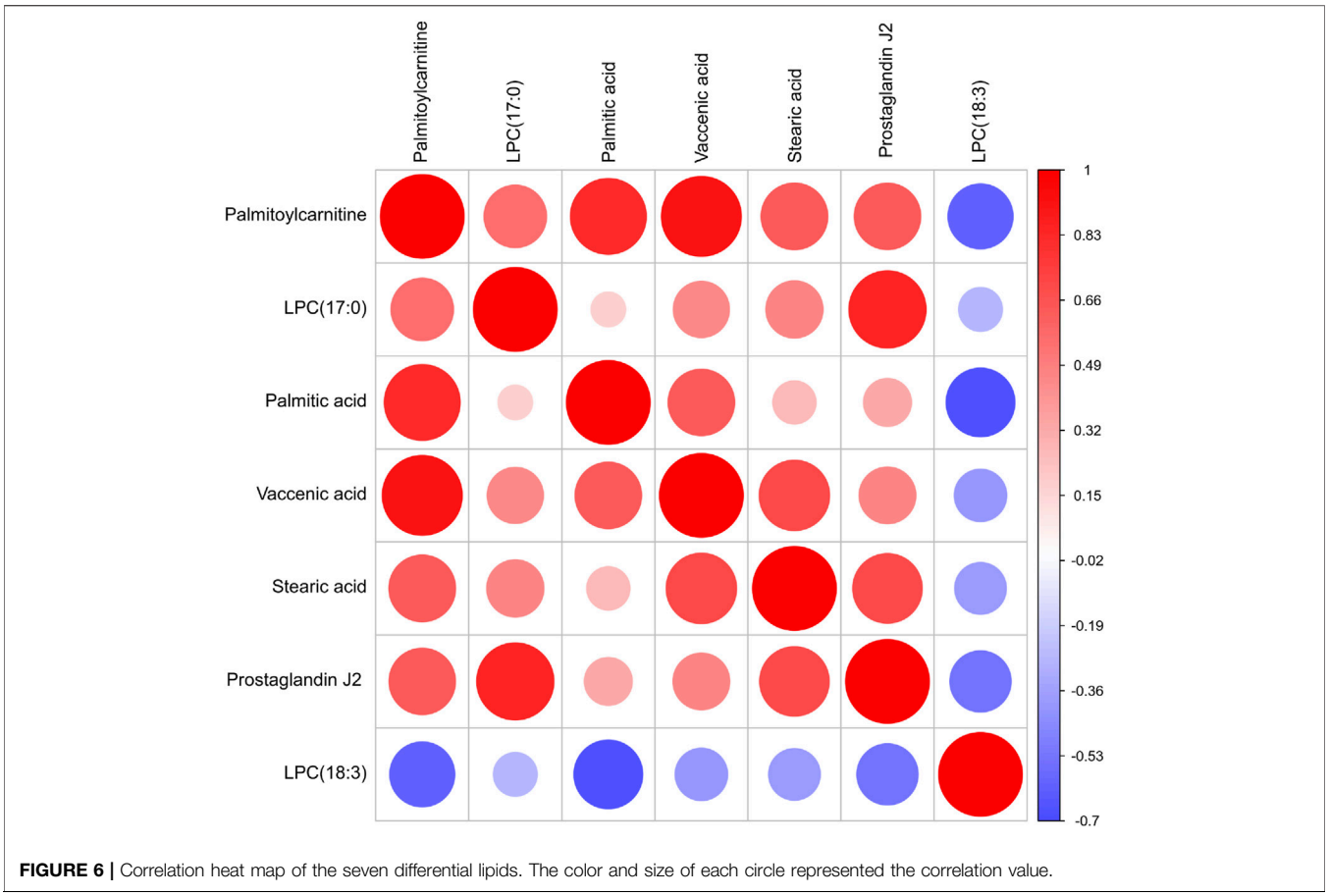

FIGURE 6 | Correlation heat map of the seven differential lipids. The color and size of each circle represented the correlation value.

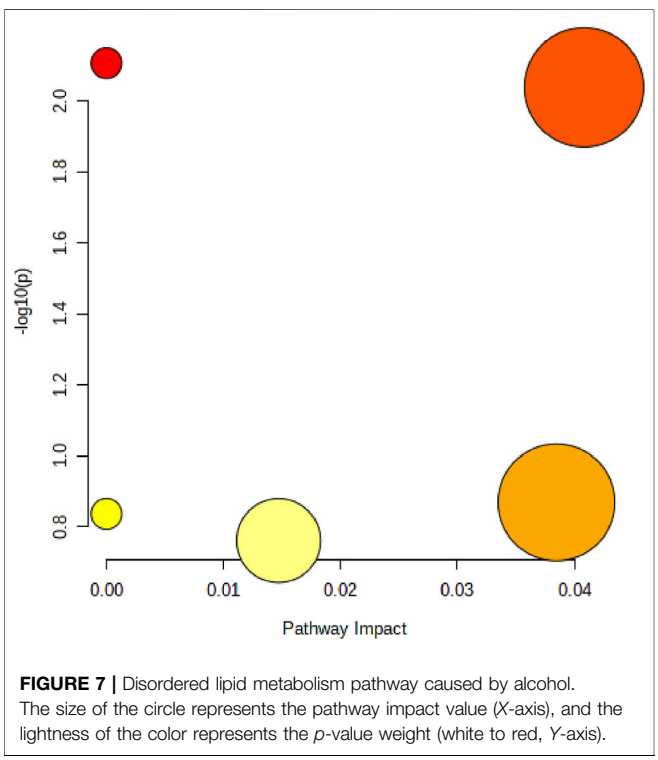

FIGURE 7 | Disordered lipid metabolism pathway caused by alcohol. The size of the circle represents the pathway impact value (*X*-axis), and the lightness of the color represents the *p*-value weight (white to red, *Y*-axis).

(Cheng and Kaplowitz, 2003; You, 2002; Park et al., 2002). Saturated fatty acids can reduce liver lipid peroxidation by affecting cytochrome P450 2E1 and non-heme iron, and reduce the expression of inflammatory factors and cytokines such as Cyclooxygenase-2 and TNF-α by down-regulating NF-κB (Ming et al., 1999; Lawler et al., 1998). At the same time, the concentration of lysophosphatidylcholine containing polyunsaturated fatty acids in the serum of alcohol-induced liver damage mice is higher than that of normal mice, while the content of saturated lysophosphatidylcholine is lower than that of normal mice (Li et al., 2011).Alcohol intake increases the liver's uptake of exogenous palmitic acid and subsequently incorporates palmitic acid into the liver's triglycerides or total lipids. The upregulation of fatty acid transporters (FATP), especially CD36/FAT, FATP1 and FATP5, promotes fatty acid uptake, fat accumulation and steatosis in mice (Nie et al., 2020). At the same time, both SREBP-1 and ChREBP may be activated under alcohol intake, which further promotes the production of fatty acids.

Effect on Fatty Acid Degradation Metabolism

Palmitic acid is one of the most common fatty acids in animals, its concentration in serum is related to synthesis and degradation. As

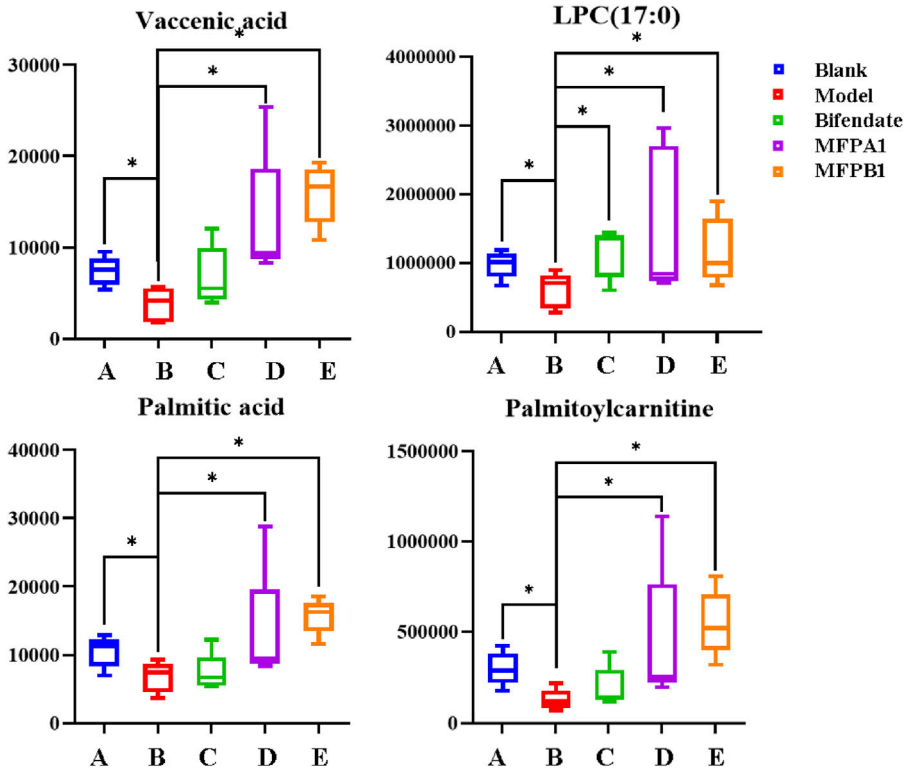

FIGURE 8 | The content of the four differential lipids. *: $p < 0.05$, **:$p < 0.01$, blank, bifendate, MFPA1, MFPB1 group vs model group. $n = 5$.

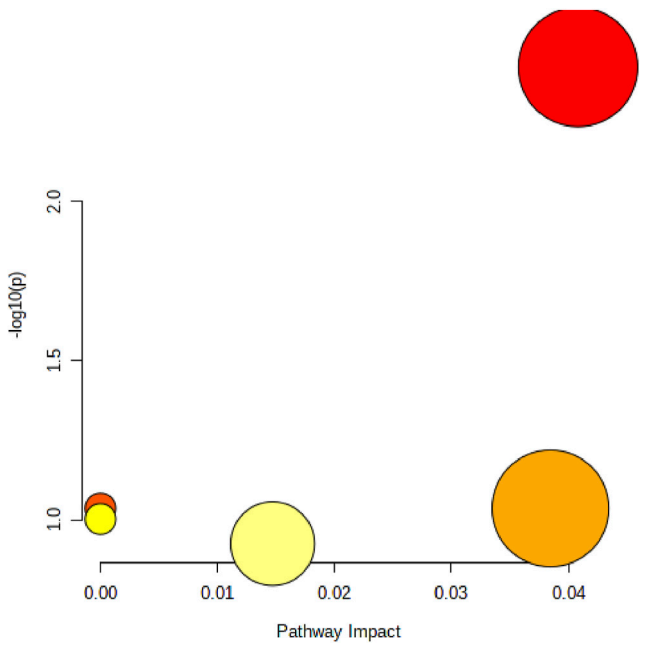

FIGURE 9 | Abnormal lipid metabolism pathway that MFP may be attenuate. The size of the circle represents the pathway impact value (*X*-axis), and the lightness of the color represents the *p*-value weight (white to red, *Y*-axis).

a long-chain fatty acid, Palmitic acid is activated by the catalysis of CoA synthase to become fatty acyl CoA, which is transported by carnitine to the mitochondria, where it is finally β-oxidised to produce acetyl CoA (Fromenty and Pessayre, 1994; Hu et al., 2016). Palmitoylcarnitine is an acylcarnitine, formed from carnitine transported by the carnitine transporter, which facilitates the transfer of long-chain fatty acids from the cytoplasm to the mitochondria (Serviddio et al., 2011). In our work, the levels of Palmitic acid and Palmitoylcarnitine in the alcohol-induced liver damage mice decreased, while the levels of Palmitic acid and Palmitoylcarnitine in the mice of the MFPA1 and MFPB1 groups increased, which means that both alcohol and MFP may affect the degradation of fatty acids by regulating the concentration of palmitic acid and palmitoylcarnitine.

Effect on Glycerophospholipid Metabolism

Lysophosphatidylcholine (LPC), which accounts for approximately 8–12% of plasma, is a class of compounds produced by the hydrolysis of phospholipids and the loss of one molecule of fatty acid. The synthesis and catabolism of LPC takes place mainly in the liver, and its concentration in plasma fluctuated greatly. Numerous liver diseases have been found to cause changes in plasma LPC levels, making LPC a potential biomarker for liver disease (Takahashi et al., 2002; Tanaka et al., 2012). In this study, the level of LPC(18:3) was increased and the level of LPC(17:0) was decreased in mice of the model group,

while the level of LPC(18:3) was decreased and the level of LPC(17:0) was increased in mice of the MFPA1 and MFPB1 groups. This result is consistent with a previous study reporting an increased polyunsaturated LPC and decreased saturated LPC measured by metabolomics study in alcoholic fatty liver mice (Li et al., 2011). Meanwhile, MFP may affect glycerophospholipid metabolism by regulating the concentration of LPC (17:0).

Effect on Fatty Acid Biosynthesis Metabolism

Palmitic acid is the first fatty acid produced during fatty acid synthesis, as well as being a precursor to many long-chain fatty acids. Acetyl CoA in the mitochondria crosses the mitochondrial membrane into the cytoplasm, where Palmitic acid is generated under the combined effect of acetyl CoA carboxylase and fatty acid synthase (Foster., 2012). In our study, the serum Palmitic acid level of model group mice decreased, indicating that alcohol affected the synthesis of Palmitic acid. MFP could restore the level of Palmitic acid to normal, indicating that MFP promoted the synthesis of citric acid.

CONCLUSION

In this work, histopathological examination of the livers of mice with acute alcohol--induced liver damage showed that alcohol caused lipid droplets to appear in the liver cells, leading to steatosis and ballooning degeneration. Compared with the model group, the liver cell structure of the MFP group was more complete and the cytoplasm was more evenly distributed. These results suggest that the model was successfully induced and that MFP had a protective effect on the liver. Nontargeted lipidomic analysis have shown that alcohol causes disruption of lipid metabolism in serum, and alcohol intake and MFP intervention have significant effects on fatty acid synthesis, degradation and glycerophospholipid metabolism.

DATA AVAILABILITY STATEMENT

The original contributions presented in the study are included in the article/Supplementary Material, further inquiries can be directed to the corresponding author.

ETHICS STATEMENT

The animal study was reviewed and approved by Institutional Animal Ethics Committee of Guizhou Medical University, Guiyang, China.

AUTHOR CONTRIBUTIONS

LB completed the majority of experiments, performed the statistical analysis and wrote the manuscript; XZ and HC conceived this study and polished the language; XG and CZ assisted all the experiments.

FUNDING

This work was financially supported in part by the National Natural Science Foundation of China (82160786), High level innovative talents training project of Guizhou Province (20154033), and 2018 Special project for young academic talent cultivation and innovation exploration of Guizhou Normal University (20185769-27), China.

ACKNOWLEDGMENTS

We thank Dao-Ping Wang and En-Ming Hu from The Key Laboratory of Natural Product Chemistry of the Chinese Academy of Sciences in Guizhou Province for assistance to lipid analysis.

REFERENCES

Bian, L., Chen, H., and Zhou, X. (2021). Untargeted Lipidomics Analysis of Mori Fructus Polysaccharide on Acute Alcoholic Liver Injury in Mice Using Ultra Performance Liquid Chromatography-Quadrupole-Orbitrap-High Resolution Mass Spectrometry. *Int. Immunopharmacol* 97, 107521. doi:10.1016/j.intimp.2021.107521

Cheng, J., and Kaplowitz, N. (2003). Betaine Decreases Hyperhomocysteinemia, Endoplasmic Reticulum Stress, and Liver Injury in Alcohol-Fed Mice. *Gastroenterology* 124 (5), 1488–1499. doi:10.1016/S0016-5085(03)00276-2

Folch, J., Lees, M., and Sloane, S. G. H. (1957). A Simple Method for the Isolation and Purification of Total Lipides from Animal Tissues. *J. Biol. Chem.* 226 (1), 497–509.

Foster, D. W. (2012). Malonyl-CoA: the Regulator of Fatty Acid Synthesis and Oxidation. *J. Clin. Invest.* 122 (6), 1958–1959. doi:10.1172/JCI63967

Fromenty, B., and Pessayre, D. (1994). Inhibition of Mitochondrial Beta-Oxidation as a Mechanism of Hepatotoxicity. *Pharmacol. Ther.* 67 (1), 101–154. doi:10.1016/0163-7258(95)00012-6

Hu, X., Jogasuria, A., Wang, J., Kim, C., Han, Y., Shen, H., et al. (2016). MitoNEET Deficiency Alleviates Experimental Alcoholic Steatohepatitis in Mice by Stimulating Endocrine Adiponectin-Fgf15 Axis. *J. Biol. Chem.* 291 (43), 22482–22495. doi:10.1074/jbc.M116.737015

Jiang, Y., Yao, X., Fan, S., Gao, Y., Zhang, H., Huang, M., et al. (2021). Lipidomic Profiling Reveals Triacylglycerol Accumulation in the Liver during Pregnane X Receptor Activation-Induced Hepatomegaly. *J. Pharm. Biomed. Anal.* 195 (1), 113851. doi:10.1016/j.jpba.2020.113851

Kotronen, A., Seppälä-Lindroos., A., Vehkavaara, S., Bergholm, R., Frayn, K. N., Fielding, B. A., et al. (2010). Liver Fat and Lipid Oxidation in Humans. *Liver Int.* 29 (9), 1439–1446. doi:10.1111/j.1478-3231.2009.02076.x

Lam, S. M., and Shui, G. (2013). Lipidomics as a Principal Tool for Advancing Biomedical Research. *J. Genet. Genomics* 40 (08), 375–390. doi:10.1016/j.jgg.2013.06.007

Lawler, J. F., Yin, M., Diehl, A. M., Roberts, E., and Chatterjee, S. (1998). Tumor Necrosis Factor-Alpha Stimulates the Maturation of Sterol Regulatory Element Binding Protein-1 in Human Hepatocytes through the Action of Neutral Sphingomyelinase. *J. Biol. Chem.* 273 (9), 5053–5059. doi:10.1074/jbc.273.9.5053

Li, S., Liu, H., Jin, Y., Lin, S., Cai, Z., and Jiang, Y. (2011). Metabolomics Study of Alcohol-Induced Liver Injury and Hepatocellular Carcinoma Xenografts in Mice. *J. Chromatogr. B Analyt Technol. Biomed. Life Sci.* 879 (24), 2369–2375. doi:10.1016/j.jchromb.2011.06.018

Murphy, S. A., and Nicolaou, A. (2013). Lipidomics Applications in Health, Disease and Nutrition Research. *Mol. Nutr. Food Res.* 57, 1336–1346. doi:10.1002/mnfr.201200863

Nie, J., Ngokana, L. D., Kou, J., Zhao, Y., Tu, J., Ji, H., et al. (2020). Low-dose Ethanol Intake Prevents High-Fat Diet-Induced Adverse Cardiovascular Events in Mice. *Food Funct.* 11 (4), 3549–3562. doi:10.1039/C9FO02645B

Park, S. H., Gammon, S. R., Knippers, J. D., Paulsen, S. R., Rubink, D. S., and Winder, W. W. (2002). Phosphorylation-activity Relationships of AMPK and Acetyl-CoA Carboxylase in Muscle. *J. Appl. Physiol. (1985)* 92 (6), 2475–2482. doi:10.1152/japplphysiol.00071.2002

Ramachandran, P., Dobie, R., Wilson-Kanamori, J. R., Dora, E. F., Henderson, B. E. P., Luu, N. T., et al. (2019). Resolving the Fibrotic Niche of Human Liver Cirrhosis at Single-Cell Level. *Nature* 575 (7783), 512–518. doi:10.1038/s41586-019-1631-3

Serviddio, G., Giudetti, A. M., Bellanti, F., Priore, P., Rollo, T., Tamborra, R., et al. (2011). Oxidation of Hepatic Carnitine Palmitoyl Transferase-I (Cpt-i) Impairs Fatty Acid Beta-Oxidation in Rats Fed a Methionine-Choline Deficient Diet. *Plos One* 6 (9), e24084. doi:10.1371/journal.pone.0024084

Sveinbjörnsson, J., and Baldursdóttir, H. (2020). Effect of a High-Palmitic Acid Fat Supplement on Milk Production in Icelandic Dairy Cows Fed Grass Silage-Based Diet. *Ias* 2020, 15–24. doi:10.16886/IAS.2020.02

Takahashi, M., Okazaki, H., Ogata, Y., Takeuchi, K., Ikeda, U., and Shimada, K. (2002). Lysophosphatidylcholine Induces Apoptosis in Human Endothelial Cells through a P38-Mitogen-Activated Protein Kinase-dependent Mechanism. *Atherosclerosis* 161 (2), 387–394. doi:10.1016/s0021-9150(01)00674-8

Tan, X., Chen, H., and Zhou, X. (2021). Study on the Activity of Mori Fructus Polysaccharides and its Derivatives against Acute Alcoholic Liver Injury in Mice. *J. Carbohydr. Chem.* 39 (6), 450–471. doi:10.1080/07328303.2021.1895194

Tanaka, N., Matsubara, T., Krausz, K. W., Patterson, A. D., and Gonzalez, F. J. (2012). Disruption of Phospholipid and Bile Acid Homeostasis in Mice with Nonalcoholic Steatohepatitis. *Hepatology* 56 (1), 118–129. doi:10.1002/hep.25630

World Health Organization (2018). Global Status Report on Alcohol and Health. Available at: https://apps.who.int/iris/bitstream/handle/10665/274603/9789241565639-eng.pdf?ua=1 (Accessed September 21, 2018).

Yin, M., Wheeler., M. D., Kono, H., Bradford, B. U., Gallucci, R. M., Luster, M. I., et al. (1999). Essential Role of Tumor Necrosis Factor Alpha in Alcohol-Induced Liver Injury in Mice. *Gastroenterology* 117 (4), 942–952. doi:10.1016/S0016-5085(99)70354-9

You, M., Fischer, M., Deeg, M. A., and Crabb, D. W. (2002). Ethanol Induces Fatty Acid Synthesis Pathways by Activation of Sterol Regulatory Element-Binding Protein (SREBP). *J. Biol. Chem.* 277 (32), 29342–29347. doi:10.1074/jbc.M202411200

Zhou, X., Deng, Q., Chen, H., Hu, E., Zhao, C., and Gong, X. (2017). Characterizations and Hepatoprotective Effect of Polysaccharides from Mori Fructus in Rats with Alcoholic-Induced Liver Injury. *Int. J. Biol. Macromol* 102, 60–67. doi:10.1016/j.ijbiomac.2017.03.083

Conflict of Interest: The authors declare that the research was conducted in the absence of any commercial or financial relationships that could be construed as a potential conflict of interest.

Publisher's Note: All claims expressed in this article are solely those of the authors and do not necessarily represent those of their affiliated organizations, or those of the publisher, the editors and the reviewers. Any product that may be evaluated in this article, or claim that may be made by its manufacturer, is not guaranteed or endorsed by the publisher.

frontiers in Pharmacology

MINI REVIEW
published: 18 November 2021
doi: 10.3389/fphar.2021.783641

Cardiovascular Protective Effects of Plant Polysaccharides: A Review

Xinli Dong[1,2†], *Mengze Zhou*[1†], *Yehong Li*[1,2], *Yuxin Li*[1,2], *Hui Ji*[1,2*] *and Qinghua Hu*[1,2*]

[1]State Key Laboratory of Natural Medicines, China Pharmaceutical University, Nanjing, China, [2]School of Pharmacy, China Pharmaceutical University, Nanjing, China

Cardiovascular disease is a kind of heart, brain, and blood vessel injury disease by the interaction of various pathological factors. The pathogenesis of cardiovascular disease is complex with various risk factors, including abnormally elevated blood pressure, glucose, and lipid metabolism disorders, atherosclerosis, thrombosis, etc. Plant polysaccharides are a special class of natural products derived from plant resources, which have the characteristics of wide sources, diverse biological activities, and low toxicity or side effects. Many studies have shown that plant polysaccharides improve cardiovascular diseases through various mechanisms such as anti-oxidative stress, restoring the metabolism of biological macromolecules, regulating the apoptosis cascade to reduce cell apoptosis, and inhibiting inflammatory signal pathways to alleviate inflammation. This article reviews the pharmacological effects and protective mechanisms of some plant polysaccharides in modulating the cardiovascular system, which is beneficial for developing more effective drugs with low side effects for management of cardiovascular diseases.

Keywords: plant polysaccharides, cardiovascular diseases, pharmacological effects, protective mechanisms, low side effects

OPEN ACCESS

Edited by:
Jing Zhao,
University of Macau, China

Reviewed by:
Zunpeng Shu,
Guangdong Pharmaceutical University, China
Ming Lu,
Nanjing Medical University, China
Guo Chen,
Jinan University, China

***Correspondence:**
Qinghua Hu
huqh@cpu.edu.cn
Hui Ji
Huijicpu@163.com

[†]*These authors have contributed equally to this work*

Specialty section:
This article was submitted to Ethnopharmacology, a section of the journal Frontiers in Pharmacology

Received: *26 September 2021*
Accepted: *25 October 2021*
Published: *18 November 2021*

Citation:
Dong X, Zhou M, Li Y, Li Y, Ji H and Hu Q (2021) Cardiovascular Protective Effects of Plant Polysaccharides: A Review. Front. Pharmacol. 12:783641. doi: 10.3389/fphar.2021.783641

INTRODUCTION

Cardiovascular disease (CVD) is a type of chronic non-infectious disease caused by circulatory system damage (Abe et al., 2017), with the characteristics of high incidence and large mortality. In recent years, owing to human lifestyle changes, the prevalence of CVD has been on an upward trend, and its fatality rate far exceeds that of cancer and other diseases. Statistically, more than two-fifths of deaths are attributed to CVD, in the rural and urban Chinese death population in 2016 (Ma et al., 2020), which makes CVD become the number one killer that affects human health. With the increasing understanding of the pathogenesis of CVD, the level of medical care of CVD has made great progress. Still, there are some shortcomings in the clinical treatment of CVD that remain to be resolved. In terms of drugs, most of small molecule chemicals commonly used in clinical treatment of CVD have many adverse reactions, insignificant efficacy, low patient compliance and other disadvantages. Consequently, in the process of seeking new drugs, plant polysaccharides with multiple targets, good biocompatibility and low toxicity have gradually become a hot spot in the research of anti-CVD drugs.

As a kind of natural macromolecule polymer extracted from various parts of plants, plant polysaccharides are composed of ten or more monosaccharides through polymerization with glycosidic linkages (Yu et al., 2018). A large number of studies have shown that plant polysaccharides have various bioactivities such as anti-tumor, immunomodulation, antioxidant, radioprotection, hepatoprotection, anti-virus (Xie et al., 2016; Yu et al., 2018), which play an important role in regulating human physiological functions. More importantly, several studies have

also shown other functions of plant polysaccharides such as antioxidant, anti-hyperglycemic, anti-hypertensive, anti-atherosclerosis, anti-myocardial ischemia etc. (Zaporozhets and Besednova, 2016). These pharmacological effects provide a theoretical basis for plant polysaccharides to treat CVD. This article reviews reported mechanisms by which plant polysaccharides protect CVD from the perspective of multiple pharmacological effects.

PROTECTIVE EFFECTS OF PLANT POLYSACCHARIDES ON CARDIOVASCULAR SYSTEM

Globally, CVD is not only the leading cause of the decline in people's quality of life, but a primary reason for death. The pathogenesis of CVD is complicated, including glucose or lipid metabolism disorders, endothelial dysfunction, oxidative stress, and inflammation response. Till now, atherosclerosis, myocardial ischemia, abnormally elevated blood pressure, and thrombosis are recognized as the main risk factors for inducing CVD (Benjamin et al., 2019). Plant polysaccharides from natural sources play a cardiovascular protective effect by improving these series of risk factors.

The Effect of Plant Polysaccharides on Hypertension

Hypertension characterized by an uncontrolled increase in blood pressure leads to arteriosclerosis and myocardial injury, which has been regarded as one of the major factors to induce a series of refractory CVDs including coronary heart disease, cerebrovascular disease (stroke) and heart failure (Huang et al., 2013). The occurrence and development of hypertension is related to quite a few factors, among them, the dysfunction of endothelial and vascular smooth muscle is one of the primary causes of hypertension. Previous studies have shown that administration of low-molecular-weight fucoidan (LMWF) extracted from brown algae promoted the phosphorylation of endothelial nitric oxide synthase (eNOS) at Ser1177 and up-regulated the eNOs/NO signal of vascular endothelial cells, which significantly improved the vasodilation disorder induced by endothelial dysfunction and robustly reduced basal hypertension in Goto-Kakizaki type 2 diabetic rats (Cui et al., 2014). Additionally, the subsequent findings by the research group suggested that LMWF also alleviated the hyper-responsiveness of vascular smooth muscle caused by diabetes and effectively improved diabetes induced hypertension. The effect of anti-vascular smooth muscle hyper-responsiveness of LMWF is mainly achieved by restoring the activity of antioxidant enzymes to inhibit the production of ROS, and inhibiting COX-2 to reduce the level of vasoconstrictor TXA2 in vascular smooth muscle (Liang et al., 2016). Consistently, mean arterial blood pressure in both normal blood pressure rats and hypertensive rats were appreciably lowered by white mulberry fruit polysaccharides, which is also related to the increase of the release of NO in vascular endothelial cells (Wang et al., 2019). In this study, the production of NO may be related to the activation of intracellular Ca^{2+} signaling and PI3K/AKT signaling pathway. In addition, Astragalus polysaccharides treatment also reduced the mean pulmonary artery pressure in rats with monocrotaline-induced pulmonary arterial hypertension by activating eNOS/NO signaling pathway (Yuan et al., 2017). Interestingly, several studies have demonstrated that plant polysaccharides can also reduce high blood pressure by inhibiting angiotension-converting enzyme (ACE), including acidic polysaccharides from gastrodia rhizome (Lee et al., 2012), Chickpea water-soluble polysaccharide (Mokni Ghribi et al., 2015), Cymodocea nodosa sulfated polysaccharide (Kolsi et al., 2016), Momordica charantia polysaccharide (Tan and Gan, 2016), as well as water-soluble polysaccharides from Ephedra alata (Soua et al., 2020) and Almond and Pistachio (Sila et al., 2014). They can not only alleviate vasoconstriction by inhibiting the formation of angiotensin II, but also reduce metabolism of vasodilator bradykinin through the inhibition of kininase II, thereby dilating blood vessels and lowering blood pressure. **Figure 1** summarizes plant polysaccharides with anti-hypertension activities.

The Effect of Plant Polysaccharides on Atherosclerosis

Atherosclerosis (AS) is a lipid-driven vascular inflammatory disease accompanied by gradually formation of vascular occlusive plaques and thrombus at the lesion site, which in turn induces CVDs including myocardial and cerebral infraction. Polysaccharides from Nitraria retusa fruits (Rjeibi et al., 2019) improved the atherosclerosis index (AI) of hyperlipidemia mice induced by TritonX-100 by reducing the level of serum triglycerides (TG), total cholesterol (TC), low-density lipoprotein cholesterol (LDL-C), and increasing the level of high-density lipoprotein cholesterol (HDL-C). Treatment with Gastrodia rhizomes crude and acidic polysaccharides (Kim et al., 2012) also markedly reduced the content of serum TC, LDL-C and AI of high-fat diet rats, but had no effect on serum TG and HDL-C levels. Furthermore, Enteromorpha prolifera polysaccharide (Tang et al., 2013; Guo et al., 2021), polysaccharides from Porphyra yezoensis (Qian et al., 2014) also reversed abnormal serum lipid concentrations in rats or hamsters with high-fat feeding, which is beneficial to alleviate atherogenesis. Fan et al. (Fan et al., 2013) found that the effect of Okra polysaccharide in lowering the serum lipid contents of obese mice was related to the regulation of the expression of lipid metabolism-related genes. Likewise, administration of polysaccharides from Rosae laevigatae fruits (Yu et al., 2013; Zhang et al., 2020), the sulfated polysaccharide from Ulva pertusa (Qi and Sheng, 2015; Li et al., 2020) and Ophiopogon polysaccharide (Wang et al., 2017) decreased blood lipids also by affecting the expression of these genes. Surprisingly, the Ophiopogon polysaccharide (Shi et al., 2016) also lowered the blood lipid level of hyperlipidemia mice by combining with the cholesterol metabolite bile acid then promoting the excretion of cholesterol through feces. Cyclocarya paliurus polysaccharide improved the blood lipid levels of hyperlipidemia rats by up-

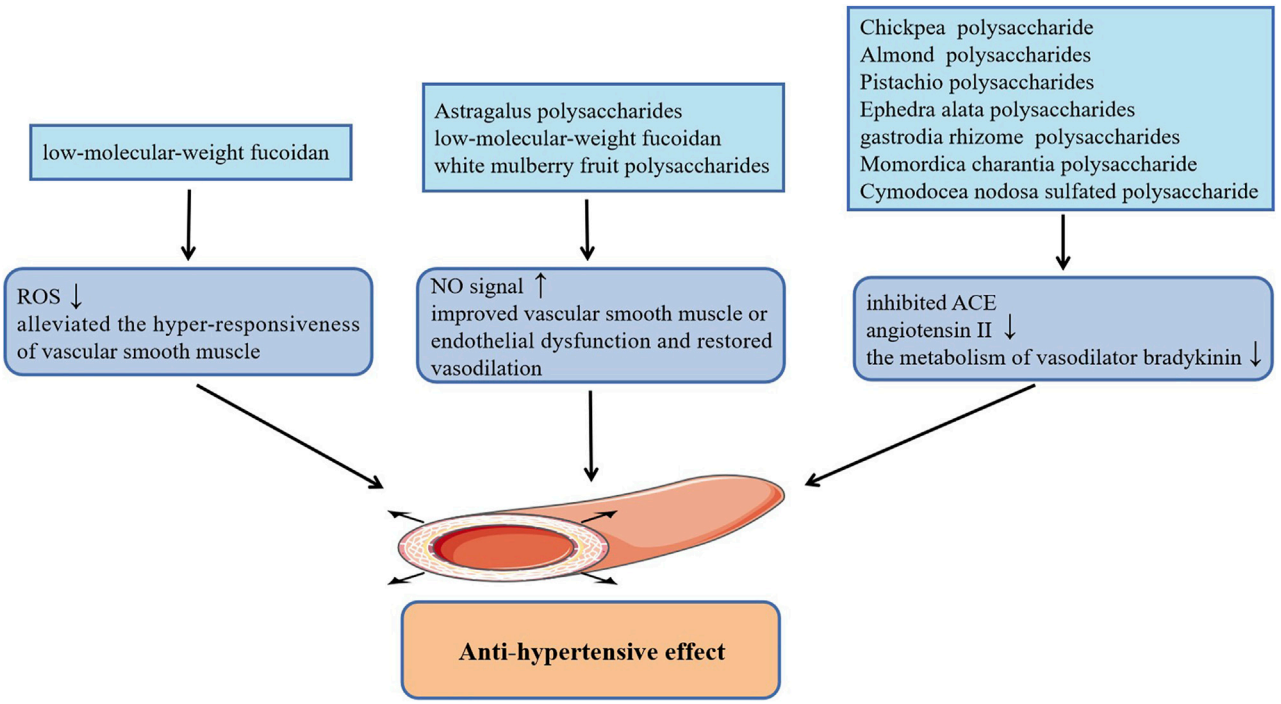

FIGURE 1 | Plant polysaccharides with anti-hypertension activities.

regulating the level of lipoprotein lipase, hormone-sensitive lipase as well as adipose triglyceride lipase, which promote lipid metabolism by down-regulating the level of acetyl-CoA carboxylase, fatty acid synthase as well as hydroxy methylglutaryl coenzyme A reductase (HMG-CoA) involved in lipid synthesis (Yang et al., 2016; Hu et al., 2017). Yang et al. also reported that Cyclocarya paliurus polysaccharide can regulate the expression of lipid metabolism enzymes by affecting the methylation level of related genes, thereby reducing blood lipids (Yang et al., 2019; Yang et al., 2021). Besides, fucoidan not only promoted lipid metabolism by regulating the expression of cholesterol metabolism-related genes, but inhibited the expression of aortic α-smooth muscle actin (α-SMA), CD11b and vascular endothelial growth factor (VEGF), fibroblast growth factor-2 (FGF-2), P-SAPK as well as inflammatory cytokines, which alleviated atherosclerotic lesions in apolipoprotein E-deficient (apoE-/-) mice with high fat diet (Xu et al., 2019; Yin et al., 2019).

On the other hand, in atherosclerosis progression, macrophages can not only release inflammatory mediators to promote inflammatory response in the site of lesion, but excessively ingest lipids to transform into foam cells that are one of the components of atherosclerotic plaque. Remarkably, the administration of sulphated galactan isolated from the Acanthophora muscoides decreased the content of macrophages and tissue factor in the atherosclerotic plaques of apoE-/- mice with high-cholesterol diet by directly interferes with the chemotactic function of macrophages (GomesQuindere et al., 2015). In cholesterol crystals-pretreated macrophage-like THP-1 cells, treatment with Chayote polysaccharides reduced intracellular lipids levels by up-regulating the expression of liver X receptor alpha (LXRα), and also inhibited the activation of inflammasome NLRP3 (Castro-Alves et al., 2019). Additionally, Red alga polysaccharides inhibited the activation of NF-κB and the up-regulation of intercellular vascular cell adhesion molecule-1 (VCAM-1) as well as adhesion molecule-1 (ICAM-1) in human coronary artery endothelial cells (HCAECs) induced by angiotensin II (Hamias et al., 2018) or TNF-α (Levy-Ontman et al., 2017), which is helpful for alleviating inflammatory atherosclerosis progression. In addition, Opuntia dillenii Haw. Polysaccharides (Zhao et al., 2012) improved the aortic injury of hyperlipidemia rats by inhibiting the expression of VCAM-1 in the vascular endothelial and smooth muscle cells, which alleviated the process of AS. **Figure 2** shows plant polysaccharides with anti-atherosclerosis actions.

The Effect of Plant Polysaccharides on Thrombus

Thrombus is a blood clot formed by the aggregation of insoluble fibrin, activated platelets, and other cells on the internal surface of blood vessels at the site of injury, including arterial thrombosis and venous thrombosis (Chan and Weitz, 2019). Several plant polysaccharides have the biological activity of anticoagulant and inhibiting platelet aggregation, which could effectively depress the thrombosis. Guar gum hydrolysate delayed the time to arterial blood flow decreases to zero, which is beneficial to depress arterial thrombosis induced by $FeCl_3$ in hamster with high-fat diet (Kuo

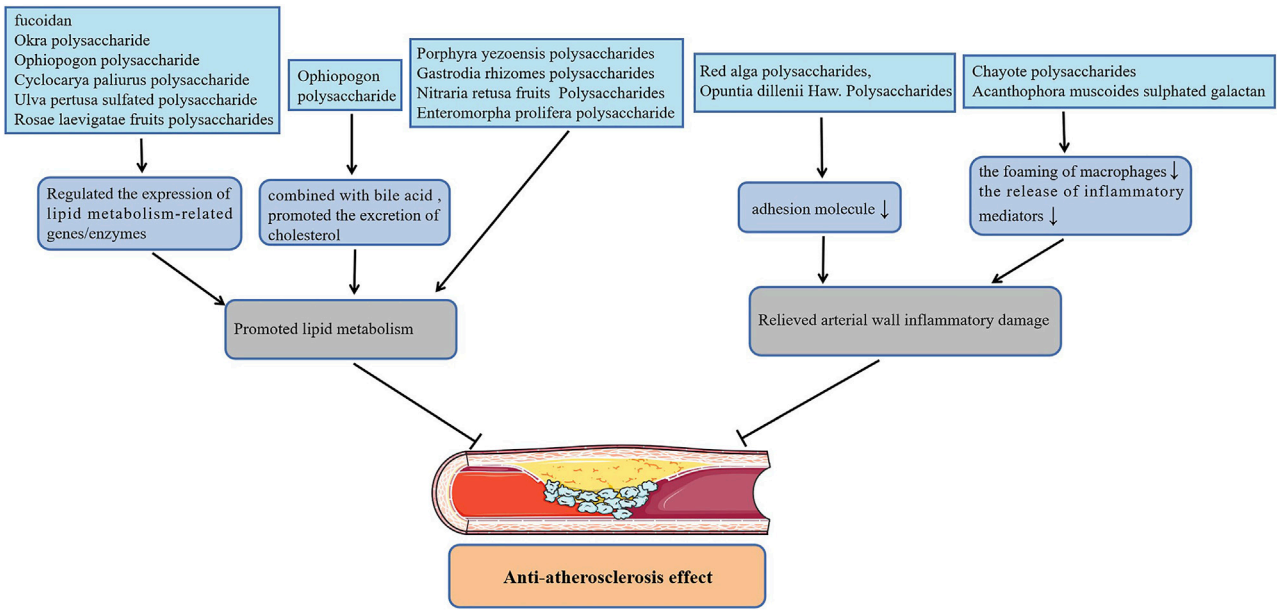

FIGURE 2 | Plant polysaccharides with anti-atherosclerosis actions.

et al., 2009). Consistently, chemically sulfated guar gum exhibited anticoagulant and antithrombotic effects in rats (de Oliveira Barddal et al., 2020). Similarly, sodium alginate sulfates inactivated α-thrombin and coagulation factor Xa through the interaction between negative charges in the sulfate groups and the positively charges of anti-thrombin amino acid residues, exerting anticoagulant effect (Fan et al., 2011). Differently, sulfated Citrus pectin fractions inhibited coagulation factor Xa and platelet aggregation by directly inhibiting α-thrombin, which attenuated venous thrombosis in rats (Cipriani et al., 2009). Additionally, sulfated rhamnan from Monostroma angicava (Liu D. et al., 2018), sulfated Pumpkin polysaccharide (Liang et al., 2018), sulfated Ginger polysaccharide (Wang et al., 2020), sulfated polysaccharides from Codium dwarkense børgesen (Golakiya et al., 2017), other sulfated polysaccharides extracted from seaweeds (Glauser et al., 2013; Chagas et al., 2020), as well as tea polysaccharides from Camellia sinensis (Cai et al., 2013) have been reported to have anticoagulant effects. On the other hand, Caesalpinia ferrea polysaccharides (de Araujo et al., 2021), polysaccharides of Geoffroea spinosa (Souza et al., 2015) and Lycium barbarum L. leaves polysaccharides (Lin et al., 2019) not only have anticoagulant activity but inhibit platelet aggregation, which exhibit depression effects on the formation of thrombus.

The Effect of Plant Polysaccharides on Myocardial Ischemia and Myocardial Ischemia-Reperfusion Injury

In recent years, persistent myocardial ischemia has becoming the primary cause of myocardial infarction (Thomes et al., 2010). As a classical approach, ischemia reperfusion could effectively restore the blood supply of ischemic myocardium, however, the production of a large amount of reactive oxygen species (ROS) and the infiltration of inflammatory cells caused by ischemia-reperfusion can also cause irreversible damage to the heart tissue (Hou et al., 2017). The biological activities of plant polysaccharides including anti-oxidant stress, anti-apoptosis, and anti-myocardial ischemia are beneficial to slow the progression of ischemic heart disease. Dendrobium officinale polysaccharides supplementation elevated serum SOD levels, up-regulated the expression of meis1, inhibited cardiomyocyte apoptosis, which significantly improved myocardial ischemic injury induced by coronary artery ligation in mice (Dou et al., 2016). Anti-oxidant and anti-apoptosis effects of Dendrobium officinale polysaccharide on cardiomyocytes were discovered using H9C2 cells damage model induced by H_2O_2 (Zhao et al., 2017). Ophiopogon japonicus polysaccharide promoted angiogenesis in myocardial ischemic tissue by activating SPHK/S1P/bFGF/AKT/ERK and eNOS/NO signaling pathways, which decreased the myocardial infarct size in rats with acute myocardial ischemia (Wang et al., 2012). It also increased endogenous antioxidants contents, Na^+-K^+-ATPase and Ca^{2+}-Mg^{2+}-ATPase activities in rats with isoproterenol (ISO)-induced myocardial ischemia (Fan et al., 2020). Momordica charantia polysaccharides protected rats against ISO-induced cardiomyocytes damage attributed to the depression of NF-κB, the increase of myocardial antioxidants levels and the decrease of pro-inflammatory factors (Raish, 2017). For rats with myocardial injury caused by cardiac ischemia or I/R, fucoidan plays a cardioprotective effect by improving oxidative stress, reducing the release of inflammatory factors and normalizing the Na^+-K^+-ATPase and Ca^{2+}-Mg^{2+}-ATPase levels (Li et al., 2011; Krishnamurthy et al., 2012). Notably, in cardiac I/R injury rats, Tamarind xyloglucan inhibited MAPK/bax/caspase-3 apoptosis cascade by up-regulated the expression of

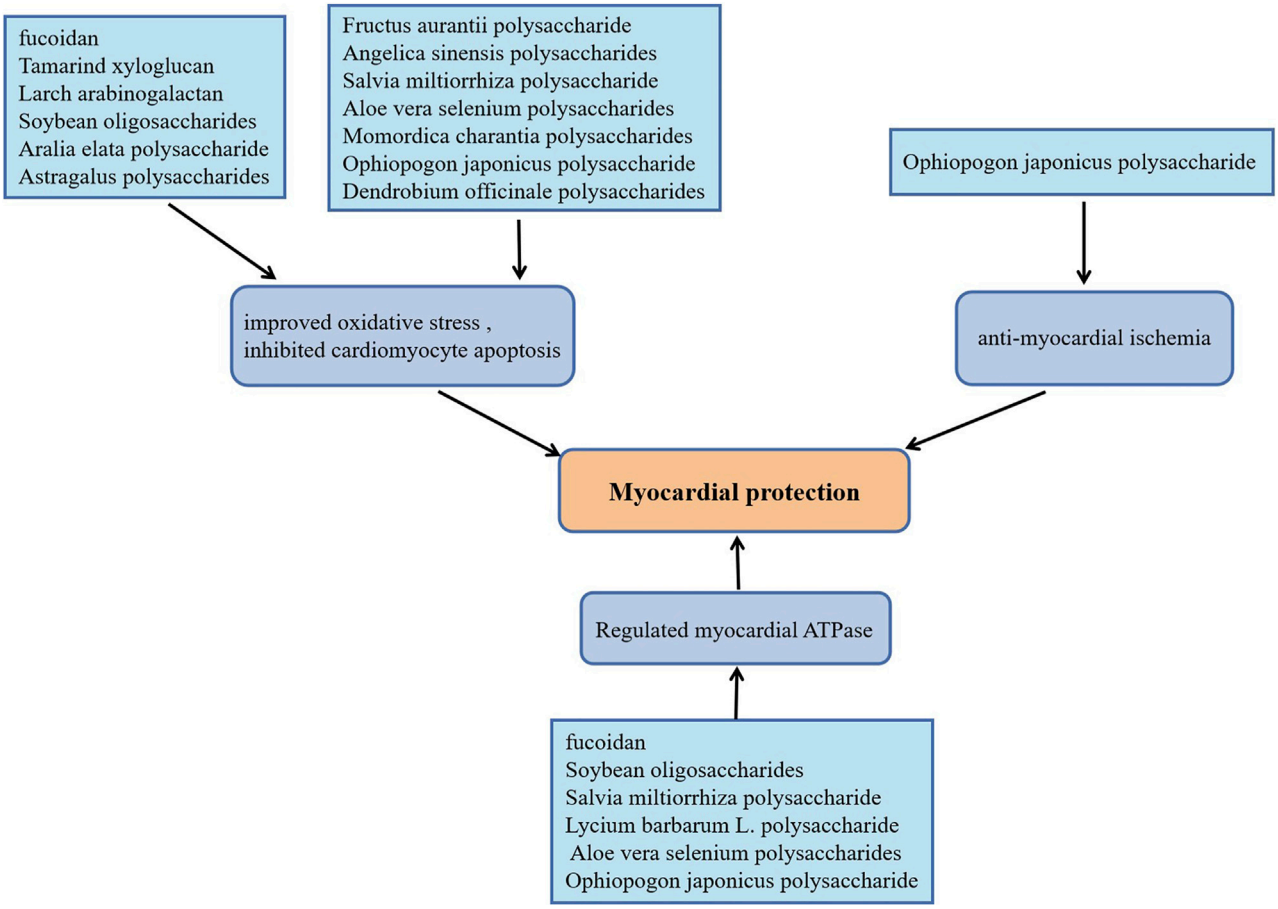

FIGURE 3 | Plant polysaccharides with myocardial protective effects.

fatty acid-binding protein (Lim and Lee, 2017), while Larch arabinogalactan depressed the cardiomyocytes apoptosis by inhibiting gelsolin/MAPK p38 and gelsolin/HIF-1α signals, which effectively alleviated myocardial damage (Lim, 2017). Moreover, Astragalus polysaccharides (Liu X. et al., 2018), Angelica sinensis polysaccharides (Zhang et al., 2010), Aralia elata polysaccharide (Zhang et al., 2013), Aloe vera selenium polysaccharides (Yang et al., 2017), Salvia miltiorrhiza polysaccharide (Song et al., 2013; Geng et al., 2015) as well as Soybean oligosaccharides (Zhang et al., 2015) have been reported to the effects of anti-oxidation and reduce myocardial cell apoptosis in cardiac I/R model rats. More strikingly, Aloe vera selenium polysaccharides, Salvia miltiorrhiza polysaccharide and Soybean oligosaccharides also elevated the activities of Na^+-K^+-ATPase and Ca^{2+}-Mg^{2+}-ATPase, which is consistent with the effect of Lycium barbarum L. polysaccharide on cardiomyocytes in cardiac I/R rats (Hou et al., 2017). In the experiment of hypoxia-reoxygenation treatment of H9C2 cells, Fructus aurantii polysaccharide inhibited bax/caspase-mediated cells apoptosis and promoted the antioxidant effect mediated by Nrf2/HO-1 signal by activating the PI3K/AKT signaling pathway (Shu et al., 2020). Yang et al. also proved that Fructus aurantii polysaccharide has a protective effect on ISO-induced myocardial ischemia injury in rats by exerting antioxidant and anti-apoptotic effects (Yang et al., 2020). **Figure 3** exhibits plant polysaccharides with myocardial protective effects.

DISCUSSION

In recent years, with the rise of botanical medicine, the active ingredients in traditional herbs have gradually attracted people's attention. As one of the main active ingredients in most plant extracts, polysaccharides are widely used in research on the treatment of cardiovascular diseases. Nevertheless, most of the reports focus on the extraction, isolation, physical, and chemical properties of plant polysaccharides, but the pharmacological research of plant polysaccharides is relatively simple. We believe that the exact target of plant polysaccharides *in vivo*, and the cardiovascular protective mechanism at the molecular level need to be studied in depth in the future. On the other hand, although we generally accepted that plant polysaccharides had low toxicity or side effects, the structural uncertainty of plant polysaccharide monomers and individual differences might still lead to serious adverse events, so that the identification of plant

polysaccharide molecular structure and adverse reactions clarification are necessary.

AUTHOR CONTRIBUTIONS

XD and MZ wrote the manuscript. YeL and YuL contributed to reviewing the manuscript. QH and HJ provided guidance on the framework of the review. All authors contributed to the editing and submission of the review.

FUNDING

This research was supported by Natural Science Foundation of China (Grants 81773745, 81872867).

REFERENCES

Abe, H., Semba, H., and Takeda, N. (2017). The Roles of Hypoxia Signaling in the Pathogenesis of Cardiovascular Diseases. *J. Atheroscler. Thromb.* 24, 884–894. doi:10.5551/jat.RV17009

Benjamin, E. J., Muntner, P., Alonso, A., Bittencourt, M. S., Callaway, C. W., Carson, A. P., et al. (2019). Heart Disease and Stroke Statistics-2019 Update: A Report from the American Heart Association. *Circulation* 139, e56–e528. doi:10.1161/CIR.0000000000000659

Cai, W., Xie, L., Chen, Y., and Zhang, H. (2013). Purification, Characterization and Anticoagulant Activity of the Polysaccharides from green tea. *Carbohydr. Polym.* 92, 1086–1090. doi:10.1016/j.carbpol.2012.10.057

Castro-Alves, V. C., Shiga, T. M., and Nascimento, J. R. O. D. (2019). Polysaccharides from Chayote Enhance Lipid Efflux and Regulate NLRP3 Inflammasome Priming in Macrophage-like THP-1 Cells Exposed to Cholesterol Crystals. *Int. J. Biol. Macromol* 127, 502–510. doi:10.1016/j.ijbiomac.2019.01.048

Chagas, F. D. D. S., Lima, G. C., Dos Santos, V. I. N., Costa, L. E. C., de Sousa, W. M., Sombra, V. G., et al. (2020). Sulfated Polysaccharide from the Red Algae Gelidiella Acerosa: Anticoagulant, Antiplatelet and Antithrombotic Effects. *Int. J. Biol. Macromol* 159, 415–421. doi:10.1016/j.ijbiomac.2020.05.012

Chan, N. C., and Weitz, J. I. (2019). Antithrombotic Agents. *Circ. Res.* 124, 426–436. doi:10.1161/circresaha.118.313155

Cipriani, T. R., Gracher, A. H., de Souza, L. M., Fonseca, R. J., Belmiro, C. L., Gorin, P. A., et al. (2009). Influence of Molecular Weight of Chemically Sulfated Citrus Pectin Fractions on Their Antithrombotic and Bleeding Effects. *Thromb. Haemost.* 101, 860–866. doi:10.1160/th08-08-0556

Cui, W., Zheng, Y., Zhang, Q., Wang, J., Wang, L., Yang, W., et al. (2014). Low-molecular-weight Fucoidan Protects Endothelial Function and Ameliorates Basal Hypertension in Diabetic Goto-Kakizaki Rats. *Lab. Invest.* 94, 382–393. doi:10.1038/labinvest.2014.12

de Araujo, D. F., Madeira, J. D. C., Cunha, A. P., Ricardo, N. M. P. S., Bezerra, F. F., Mourão, P. A. S., et al. (2021). Structural Characterization of Anticoagulant and Antithrombotic Polysaccharides Isolated from Caesalpinia Ferrea Stem Barks. *Int. J. Biol. Macromol* 175, 147–155. doi:10.1016/j.ijbiomac.2021.01.177

de Oliveira Barddal, H. P., Faria, F. A. M., Nogueira, A. V., Iacomini, M., and Cipriani, T. R. (2020). Anticoagulant and Antithrombotic Effects of Chemically Sulfated Guar Gum. *Int. J. Biol. Macromol* 145, 604–610. doi:10.1016/j.ijbiomac.2019.12.210

Dou, M. M., Zhang, Z. H., Li, Z. B., Zhang, J., and Zhao, X. Y. (2016). Cardioprotective potential of Dendrobium officinale Kimura et Migo against myocardial ischemia in mice. *Mol. Med. Rep.* 14, 4407–4414. doi:10.3892/mmr.2016.5789

Fan, L., Jiang, L., Xu, Y., Zhou, Y., Shen, Y., Xie, W., et al. (2011). Synthesis and Anticoagulant Activity of Sodium Alginate Sulfates. *Carbohydr. Polym.* 83, 1797–1803. doi:10.1016/j.carbpol.2010.10.038

Fan, S., Guo, L., Zhang, Y., Sun, Q., Yang, B., and Huang, C. (2013). Okra Polysaccharide Improves Metabolic Disorders in High-Fat Diet-Induced Obese C57BL/6 Mice. *Mol. Nutr. Food Res.* 57, 2075–2078. doi:10.1002/mnfr.201300054

Fan, S., Zhang, J., Xiao, Q., Liu, P., Zhang, Y., Yao, E., et al. (2020). Cardioprotective Effect of the Polysaccharide from Ophiopogon Japonicus on Isoproterenol-Induced Myocardial Ischemia in Rats. *Int. J. Biol. Macromol* 147, 233–240. doi:10.1016/j.ijbiomac.2020.01.068

Geng, Z. H., Huang, L., Song, M. B., and Song, Y. M. (2015). Protective Effect of a Polysaccharide from Salvia Miltiorrhiza on Isoproterenol (ISO)-induced Myocardial Injury in Rats. *Carbohydr. Polym.* 132, 638–642. doi:10.1016/j.carbpol.2015.06.086

Glauser, B. F., Mourão, P. A., and Pomin, V. H. (2013). Marine Sulfated Glycans with Serpin-Unrelated Anticoagulant Properties. *Adv. Clin. Chem.* 62, 269–303. doi:10.1016/b978-0-12-800096-0.00007-x

Golakiya, H. N., Naik, V. N., Hirapara, H. N., Mody, K. H., Goswami, A. P., and Tripathi, C. (2017). Evaluation of Anticoagulant Effect of Sulfated Polysaccharide (Sps) from Codium Dwarkense Borgesen in κ-Carrageenan Induced Hypercoagulable State in Wistar Albino Rats. *Acta Pol. Pharm.* 74, 987–994.

Gomes Quinderé, A. L., Barros Benevides, N. M., Pelli, G., Lenglet, S., Burger, F., Carbone, F., et al. (2015). Treatment with Sulphated Galactan Inhibits Macrophage Chemotaxis and Reduces Intraplaque Macrophage Content in Atherosclerotic Mice. *Vascul Pharmacol.* 71, 84–92. doi:10.1016/j.vph.2015.02.015

Guo, F., Han, M., Lin, S., Ye, H., Chen, J., Zhu, H., et al. (2021). Enteromorpha Prolifera Polysaccharide Prevents High- Fat Diet-Induced Obesity in Hamsters: A NMR-Based Metabolomic Evaluation. *J. Food Sci.* 86, 3672–3685. doi:10.1111/1750-3841.15818

Hamias, R., Wolak, T., Huleihel, M., Paran, E., and Levy-Ontman, O. (2018). Red Alga Polysaccharides Attenuate Angiotensin II-Induced Inflammation in Coronary Endothelial Cells. *Biochem. Biophys. Res. Commun.* 500, 944–951. doi:10.1016/j.bbrc.2018.04.206

Hou, Y. M., Wang, J., and Zhang, X. Z. (2017). Lycium Barbarum Polysaccharide Exhibits Cardioprotection in an Experimental Model of Ischemia-Reperfusion Damage. *Mol. Med. Rep.* 15, 2653–2658. doi:10.3892/mmr.2017.6294

Hu, W.-B., Zhao, J., Chen, H., Xiong, L., and Wang, W.-J. (2017). Polysaccharides from Cyclocarya Paliurus: Chemical Composition and Lipid-Lowering Effect on Rats Challenged with High-Fat Diet. *J. Funct. Foods* 36, 262–273. doi:10.1016/j.jff.2017.07.020

Huang, W. Y., Davidge, S. T., and Wu, J. (2013). Bioactive Natural Constituents from Food Sources-Potential Use in Hypertension Prevention and Treatment. *Crit. Rev. Food Sci. Nutr.* 53, 615–630. doi:10.1080/10408398.2010.550071

Kim, K. J., Lee, O. H., Han, C. K., Kim, Y. C., and Hong, H. D. (2012). Acidic Polysaccharide Extracts from Gastrodia Rhizomes Suppress the Atherosclerosis Risk index through Inhibition of the Serum Cholesterol Composition in Sprague Dawley Rats Fed a High-Fat Diet. *Int. J. Mol. Sci.* 13, 1620–1631. doi:10.3390/ijms13021620

Kolsi, R. B. A., Fakhfakh, J., Krichen, F., Jribi, I., Chiarore, A., Patti, F. P., et al. (2016). Structural Characterization and Functional Properties of Antihypertensive Cymodocea Nodosa Sulfated Polysaccharide. *Carbohydr. Polym.* 151, 511–522. doi:10.1016/j.carbpol.2016.05.098

Krishnamurthy, M., Selvaraju, M., and Tamilarasan, M. (2012). Turbinaria Conoides (J. Agardh) Sulfated Polysaccharide Protects Rat's Heart against Myocardial Injury. *Int. J. Biol. Macromol* 50, 1275–1279. doi:10.1016/j.ijbiomac.2012.03.012

Kuo, D. C., Hsu, S. P., and Chien, C. T. (2009). Partially Hydrolyzed Guar Gum Supplement Reduces High-Fat Diet Increased Blood Lipids and Oxidative Stress and Ameliorates FeCl3-Induced Acute Arterial Injury in Hamsters. *J. Biomed. Sci.* 16, 15. doi:10.1186/1423-0127-16-15

Lee, O. H., Kim, K. I., Han, C. K., Kim, Y. C., and Hong, H. D. (2012). Effects of Acidic Polysaccharides from Gastrodia Rhizome on Systolic Blood Pressure and Serum Lipid Concentrations in Spontaneously Hypertensive Rats Fed a High-Fat Diet. *Int. J. Mol. Sci.* 13, 698–709. doi:10.3390/ijms13010698

Levy-Ontman, O., Huleihel, M., Hamias, R., Wolak, T., and Paran, E. (2017). An Anti-inflammatory Effect of Red Microalga Polysaccharides in Coronary Artery

Endothelial Cells. *Atherosclerosis* 264, 11–18. doi:10.1016/j.atherosclerosis.2017.07.017

Li, B., Xu, H., Wang, X., Wan, Y., Jiang, N., Qi, H., et al. (2020). Antioxidant and Antihyperlipidemic Activities of High Sulfate Content Purified Polysaccharide from Ulva Pertusa. *Int. J. Biol. Macromol* 146, 756–762. doi:10.1016/j.ijbiomac.2019.11.061

Li, C., Gao, Y., Xing, Y., Zhu, H., Shen, J., and Tian, J. (2011). Fucoidan, a Sulfated Polysaccharide from Brown Algae, against Myocardial Ischemia-Reperfusion Injury in Rats via Regulating the Inflammation Response. *Food Chem. Toxicol.* 49, 2090–2095. doi:10.1016/j.fct.2011.05.022

Liang, L., Ao, L., Ma, T., Ni, Y., Liao, X., Hu, X., et al. (2018). Sulfated Modification and Anticoagulant Activity of Pumpkin (Cucurbita Pepo, Lady Godiva) Polysaccharide. *Int. J. Biol. Macromol* 106, 447–455. doi:10.1016/j.ijbiomac.2017.08.035

Liang, Z., Zheng, Y., Wang, J., Zhang, Q., Ren, S., Liu, T., et al. (2016). Low Molecular Weight Fucoidan Ameliorates Streptozotocin-Induced Hyper-Responsiveness of Aortic Smooth Muscles in Type 1 Diabetes Rats. *J. Ethnopharmacol* 191, 341–349. doi:10.1016/j.jep.2016.06.054

Lim, S. H. (2017). Larch Arabinogalactan Attenuates Myocardial Injury by Inhibiting Apoptotic Cascades in a Rat Model of Ischemia-Reperfusion. *J. Med. Food* 20, 691–699. doi:10.1089/jmf.2016.3886

Lim, S. H., and Lee, J. (2017). Xyloglucan Intake Attenuates Myocardial Injury by Inhibiting Apoptosis and Improving Energy Metabolism in a Rat Model of Myocardial Infarction. *Nutr. Res.* 45, 19–29. doi:10.1016/j.nutres.2017.07.003

Lin, S., Al-Wraikat, M., Niu, L., Zhou, F., Zhang, Y., Wang, M., et al. (2019). Degradation Enhances the Anticoagulant and Antiplatelet Activities of Polysaccharides from Lycium Barbarum L. Leaves. *Int. J. Biol. Macromol* 133, 674–682. doi:10.1016/j.ijbiomac.2019.04.147

Liu, D., Chen, L., Zhao, J., and Cui, K. (2018a). Cardioprotection Activity and Mechanism of Astragalus Polysaccharide *In Vivo* and *In Vitro*. *Int. J. Biol. Macromol* 111, 947–952. doi:10.1016/j.ijbiomac.2018.01.048

Liu, X., Wang, S., Cao, S., He, X., Qin, L., He, M., et al. (2018b). Structural Characteristics and Anticoagulant Property *In Vitro* and *In Vivo* of a Seaweed Sulfated Rhamnan. *Mar. Drugs* 16, 243. doi:10.3390/md16070243

Ma, L. Y., Chen, W. W., Gao, R. L., Liu, L. S., Zhu, M. L., Wang, Y. J., et al. (2020). China Cardiovascular Diseases Report 2018: an Updated Summary. *J. Geriatr. Cardiol.* 17, 1–8. doi:10.11909/j.issn.1671-5411.2020.01.001

Mokni Ghribi, A., Sila, A., Maklouf Gafsi, I., Blecker, C., Danthine, S., Attia, H., et al. (2015). Structural, Functional, and ACE Inhibitory Properties of Water-Soluble Polysaccharides from Chickpea Flours. *Int. J. Biol. Macromol* 75, 276–282. doi:10.1016/j.ijbiomac.2015.01.037

Qi, H., and Sheng, J. (2015). The Antihyperlipidemic Mechanism of High Sulfate Content Ulvan in Rats. *Mar. Drugs* 13, 3407–3421. doi:10.3390/md13063407

Qian, L., Zhou, Y., and Ma, J. X. (2014). Hypolipidemic Effect of the Polysaccharides from Porphyra Yezoensis. *Int. J. Biol. Macromol* 68, 48–49. doi:10.1016/j.ijbiomac.2014.04.004

Raish, M. (2017). Momordica Charantia Polysaccharides Ameliorate Oxidative Stress, Hyperlipidemia, Inflammation, and Apoptosis during Myocardial Infarction by Inhibiting the NF-Kb Signaling Pathway. *Int. J. Biol. Macromol* 97, 544–551. doi:10.1016/j.ijbiomac.2017.01.074

Rjeibi, I., Feriani, A., Hentati, F., Hfaiedh, N., Michaud, P., and Pierre, G. (2019). Structural Characterization of Water-Soluble Polysaccharides from Nitraria Retusa Fruits and Their Antioxidant and Hypolipidemic Activities. *Int. J. Biol. Macromol* 129, 422–432. doi:10.1016/j.ijbiomac.2019.02.049

Shi, L., Wang, J., Wang, Y., and Feng, Y. (2016). MDG-1, an Ophiopogon Polysaccharide, Alleviates Hyperlipidemia in Mice Based on Metabolic Profile of Bile Acids. *Carbohydr. Polym.* 150, 74–81. doi:10.1016/j.carbpol.2016.05.008

Shu, Z., Yang, Y., Ding, Z., Wang, W., Zhong, R., Xia, T., et al. (2020). Structural Characterization and Cardioprotective Activity of a Novel Polysaccharide from Fructus Aurantii. *Int. J. Biol. Macromol* 144, 847–856. doi:10.1016/j.ijbiomac.2019.09.162

Sila, A., Bayar, N., Ghazala, I., Bougatef, A., Ellouz-Ghorbel, R., and Ellouz-Chaabouni, S. (2014). Water-soluble Polysaccharides from Agro-Industrial By-Products: Functional and Biological Properties. *Int. J. Biol. Macromol* 69, 236–243. doi:10.1016/j.ijbiomac.2014.05.052

Song, M., Huang, L., Zhao, G., and Song, Y. (2013). Beneficial Effects of a Polysaccharide from Salvia Miltiorrhiza on Myocardial Ischemia-Reperfusion Injury in Rats. *Carbohydr. Polym.* 98, 1631–1636. doi:10.1016/j.carbpol.2013.08.020

Soua, L., Koubaa, M., Barba, F. J., Fakhfakh, J., Ghamgui, H. K., and Chaabouni, S. E. (2020). Water-Soluble Polysaccharides from Ephedra Alata Stems: Structural Characterization, Functional Properties, and Antioxidant Activity. *Molecules* 25, 2210. doi:10.3390/molecules25092210

Souza, R. O., Assreuy, A. M., Madeira, J. C., Chagas, F. D., Parreiras, L. A., Santos, G. R., et al. (2015). Purified Polysaccharides of Geoffroea Spinosa Barks Have Anticoagulant and Antithrombotic Activities Devoid of Hemorrhagic Risks. *Carbohydr. Polym.* 124, 208–215. doi:10.1016/j.carbpol.2015.01.069

Tan, H. F., and Gan, C. Y. (2016). Polysaccharide with Antioxidant, α-amylase Inhibitory and ACE Inhibitory Activities from Momordica Charantia. *Int. J. Biol. Macromol* 85, 487–496. doi:10.1016/j.ijbiomac.2016.01.023

Tang, Z., Gao, H., Wang, S., Wen, S., and Qin, S. (2013). Hypolipidemic and Antioxidant Properties of a Polysaccharide Fraction from Enteromorpha Prolifera. *Int. J. Biol. Macromol* 58, 186–189. doi:10.1016/j.ijbiomac.2013.03.048

Thomes, P., Rajendran, M., Pasanban, B., and Rengasamy, R. (2010). Cardioprotective Activity of Cladosiphon Okamuranus Fucoidan against Isoproterenol Induced Myocardial Infarction in Rats. *Phytomedicine* 18 (1), 52–57. doi:10.1016/j.phymed.2010.06.006

Wang, C., Cheng, W., Bai, S., Ye, L., Du, J., Zhong, M., et al. (2019). White mulberry Fruit Polysaccharides Enhance Endothelial Nitric Oxide Production to Relax Arteries *In Vitro* and Reduce Blood Pressure *In Vivo*. *Biomed. Pharmacother.* 116, 109022–022. doi:10.1016/j.biopha.2019.109022

Wang, C., He, Y., Tang, X., and Li, N. (2020). Sulfation, Structural Analysis, and Anticoagulant Bioactivity of Ginger Polysaccharides. *J. Food Sci.* 85, 2427–2434. doi:10.1111/1750-3841.15338

Wang, S., Lin, X., Wang, L. Y., Ruan, K. F., Feng, Y., and Li, X. Y. (2012). A Polysaccharides MDG-1 Augments Survival in the Ischemic Heart by Inducing S1P Release and S1P1 Expression. *Int. J. Biol. Macromol* 50, 734–740. doi:10.1016/j.ijbiomac.2011.12.005

Wang, X., Shi, L., Joyce, S., Wang, Y., and Feng, Y. (2017). MDG-1, a Potential Regulator of PPARα and PPARγ, Ameliorates Dyslipidemia in Mice. *Int. J. Mol. Sci.* 18, 1930. doi:10.3390/ijms18091930

Xie, J. H., Jin, M. L., Morris, G. A., Zha, X. Q., Chen, H. Q., Yi, Y., et al. (2016). Advances on Bioactive Polysaccharides from Medicinal Plants. *Crit. Rev. Food Sci. Nutr.* 56 (Suppl. 1), S60–S84. doi:10.1080/10408398.2015.1069255

Xu, Y., Zhu, W., Wang, T., Jin, L., Liu, T., Li, X., et al. (2019). Low Molecule Weight Fucoidan Mitigates Atherosclerosis in ApoE (-/-) Mouse Model through Activating Multiple Signal Pathway. *Carbohydr. Polym.* 206, 110–120. doi:10.1016/j.carbpol.2018.10.097

Yang, Y., Ding, Z., Zhong, R., Xia, T., Wang, W., Zhao, H., et al. (2020). Cardioprotective Effects of a Fructus Aurantii Polysaccharide in Isoproterenol-Induced Myocardial Ischemic Rats. *Int. J. Biol. Macromol* 155, 995–1002. doi:10.1016/j.ijbiomac.2019.11.063

Yang, Y., Yang, M., Ai, F., and Huang, C. (2017). Cardioprotective Effect of Aloe Vera Biomacromolecules Conjugated with Selenium Trace Element on Myocardial Ischemia-Reperfusion Injury in Rats. *Biol. Trace Elem. Res.* 177, 345–352. doi:10.1007/s12011-016-0896-8

Yang, Z., Zhao, J., Li, J., Wang, J., and Wang, W. (2021). Genome-wide DNA Methylation Profiling of High-Fat Emulsion-Induced Hyperlipidemia Mice Intervened by a Polysaccharide from Cyclocarya Paliurus (Batal) Iljinskaja. *Food Chem. Toxicol.* 152, 112230. doi:10.1016/j.fct.2021.112230

Yang, Z., Zhao, J., Wang, J., Li, J., Ouyang, K., and Wang, W. (2019). Effects of Cyclocarya Paliurus Polysaccharide on Lipid Metabolism-Related Genes DNA Methylation in Rats. *Int. J. Biol. Macromol* 123, 343–349. doi:10.1016/j.ijbiomac.2018.11.110

Yang, Z. W., Ouyang, K. H., Zhao, J., Chen, H., Xiong, L., and Wang, W. J. (2016). Structural Characterization and Hypolipidemic Effect of Cyclocarya Paliurus Polysaccharide in Rat. *Int. J. Biol. Macromol* 91, 1073–1080. doi:10.1016/j.ijbiomac.2016.06.063

Yin, J., Wang, J., Li, F., Yang, Z., Yang, X., Sun, W., et al. (2019). The Fucoidan from the Brown Seaweed Ascophyllum Nodosum Ameliorates Atherosclerosis in Apolipoprotein E-Deficient Mice. *Food Funct.* 10, 5124–5139. doi:10.1039/c9fo00619b

Yu, C. H., Dai, X. Y., Chen, Q., Zang, J. N., Deng, L. L., Liu, Y. H., et al. (2013). Hypolipidemic and Antioxidant Activities of Polysaccharides from Rosae

Laevigatae Fructus in Rats. *Carbohydr. Polym.* 94, 56–62. doi:10.1016/j.carbpol.2013.01.006

Yu, Y., Shen, M., Song, Q., and Xie, J. (2018). Biological Activities and Pharmaceutical Applications of Polysaccharide from Natural Resources: A Review. *Carbohydr. Polym.* 183, 91–101. doi:10.1016/j.carbpol.2017.12.009

Yuan, L. B., Hua, C. Y., Gao, S., Yin, Y. L., Dai, M., Meng, H. Y., et al. (2017). Astragalus Polysaccharides Attenuate Monocrotaline-Induced Pulmonary Arterial Hypertension in Rats. *Am. J. Chin. Med.* 45, 773–789. doi:10.1142/S0192415X17500410

Zaporozhets, T., and Besednova, N. (2016). Prospects for the Therapeutic Application of Sulfated Polysaccharides of Brown Algae in Diseases of the Cardiovascular System: Review. *Pharm. Biol.* 54, 3126–3135. doi:10.1080/13880209.2016.1185444

Zhang, J., Wang, H., and Zheng, Q. (2013). Cardioprotective Effect of Aralia Elata Polysaccharide on Myocardial Ischemic Reperfusion (IR) Injury in Rats. *Int. J. Biol. Macromol* 59, 328–332. doi:10.1016/j.ijbiomac.2013.04.060

Zhang, M., Cai, S., and Ma, J. (2015). Evaluation of Cardio-Protective Effect of Soybean Oligosaccharides. *Gene* 555, 329–334. doi:10.1016/j.gene.2014.11.027

Zhang, S., He, B., Ge, J., Li, H., Luo, X., Zhang, H., et al. (2010). Extraction, Chemical Analysis of Angelica Sinensis Polysaccharides and Antioxidant Activity of the Polysaccharides in Ischemia-Reperfusion Rats. *Int. J. Biol. Macromol* 47, 546–550. doi:10.1016/j.ijbiomac.2010.07.012

Zhang, X., Hu, Y., Jin, C., and Wu, W. (2020). Extraction and Hypolipidemic Activity of Low Molecular Weight Polysaccharides Isolated from Rosa Laevigata Fruits. *Biomed. Res. Int.* 2020, 2043785. doi:10.1155/2020/2043785

Zhao, L. Y., Huang, W., Yuan, Q. X., Cheng, J., Huang, Z. C., Ouyang, L. J., et al. (2012). Hypolipidaemic Effects and Mechanisms of the Main Component of Opuntia Dillenii Haw. Polysaccharides in High-Fat Emulsion-Induced Hyperlipidaemic Rats. *Food Chem.* 134, 964–971. doi:10.1016/j.foodchem.2012.03.001

Zhao, X., Dou, M., Zhang, Z., Zhang, D., and Huang, C. (2017). Protective Effect of Dendrobium Officinale Polysaccharides on H2O2-Induced Injury in H9c2 Cardiomyocytes. *Biomed. Pharmacother.* 94, 72–78. doi:10.1016/j.biopha.2017.07.096

Conflict of Interest: The authors declare that the research was conducted in the absence of any commercial or financial relationships that could be construed as a potential conflict of interest.

Publisher's Note: All claims expressed in this article are solely those of the authors and do not necessarily represent those of their affiliated organizations, or those of the publisher, the editors and the reviewers. Any product that may be evaluated in this article, or claim that may be made by its manufacturer, is not guaranteed or endorsed by the publisher.

frontiers in Pharmacology

ORIGINAL RESEARCH
published: 03 December 2021
doi: 10.3389/fphar.2021.704486

Effects of Different Molecular Weight Polysaccharides From *Dendrobium officinale* Kimura & Migo on Human Colorectal Cancer and Transcriptome Analysis of Differentially Expressed Genes

Shengchang Tao[1,2], *Zhiyao Ren*[3,4,5], *Zerui Yang*[1], *Shuna Duan*[1,6], *Zhongxian Wan*[1], *Jiahui Huang*[1,6], *Chenxing Liu*[1,6] *and Gang Wei*[1]*

[1]*School of Pharmaceutical Sciences, Guangzhou University of Chinese Medicine, Guangzhou, China,* [2]*Department of Pharmacy, Affiliated Dongguan Hospital, Southern Medical University, Dongguan, China,* [3]*Department of Systems Biomedical Sciences, School of Medicine, Jinan University, Guangzhou, China,* [4]*NHC Key Laboratory of Male Reproduction and Genetics, Guangzhou, China,* [5]*Department of Central Laboratory, Family Planning Research Institute of Guangdong Province, Guangzhou, China,* [6]*Shaoguan Institute of Danxia Dendrobium Officinale, Shaoguan, China*

OPEN ACCESS

Edited by:
Sp Li,
University of Macau, China

Reviewed by:
Prashant Kaushik,
University of Valencia, Spain
Xiuping Chen,
University of Macau, China

***Correspondence:**
Gang Wei
weigang021@outlook.com

Specialty section:
This article was submitted to Ethnopharmacology, a section of the journal Frontiers in Pharmacology

Received: *03 May 2021*
Accepted: *27 October 2021*
Published: *03 December 2021*

Citation:
Tao S, Ren Z, Yang Z, Duan S, Wan Z, Huang J, Liu C and Wei G (2021) Effects of Different Molecular Weight Polysaccharides From Dendrobium officinale *Kimura & Migo on Human Colorectal Cancer and Transcriptome Analysis of Differentially Expressed Genes. Front. Pharmacol. 12:704486. doi: 10.3389/fphar.2021.704486*

We investigated the antitumor effects of four fractions of *Dendrobium officinale* Kimura & Migo (*D. officinale*) polysaccharides with different molecular weights (Mw), *Astragalus membranaceus* polysaccharides (APS) and *Lentinus edodes* polysaccharides (LNT) on colorectal cancer (CRC) using a zebrafish xenograft model. Transcriptome sequencing was performed to further explore the possible antitumor mechanisms of *D. officinale* polysaccharides. Fractions of *D. officinale* polysaccharides, LNT, and APS could significantly inhibit the growth of HT-29 cells in a zebrafish xenograft model. One fraction of *D. officinale* polysaccharides called DOPW-1 (Mw of 389.98 kDa) exhibited the strongest tumor inhibition. Compared with the control group, RNA-seq revealed that the DOPW-1–treated experimental group had 119 differentially expressed genes (DEGs), of which 45 had upregulated expression and 74 had downregulated expression. Analyses using Gene Ontology and Kyoto Encyclopedia of Genes and Genomes suggested that the pathway "apoptosis-multiple species" was the most significantly enriched. Our data indicated that 1) fractions of *D. officinale* polysaccharides of Mw 389.98 kDa were most suitable against CRC; 2) DOPW-1 could be developed into a clinical agent against CRC; and 3) an apoptosis pathway is important for DOPW-1 to inhibit the proliferation of HT-29 cells.

Keywords: ***Dendrobium officinale*** **Kimura & Migo, polysaccharide, molecular weight, colorectal cancer,** ***Astragalus membranaceus*** **polysaccharides,** ***Lentinus edodes*** **polysaccharides, RNA sequencing**

INTRODUCTION

Dendrobium officinale Kimura & Migo (*D. officinale*) is a perennial herb in the Orchidaceae family. It possesses high pharmacological value and nutritional value. *D. officinale* has been used in traditional Chinese medicine formulations and a functional food in China for more than 1,000 years (Ng et al., 2012).

D. officinale polysaccharides possess anticancer (Yu et al., 2018a; Zhang et al., 2019; Zhang et al., 2020; Tao et al., 2021), immunomodulation (Huang et al., 2016; Tao et al., 2019), antioxidant (Luo et al., 2016), hypoglycemic (Wang et al., 2018; Kuang et al., 2020) and antifatigue (Wei et al., 2017) activities. However, few studies have focused on the activity of *D. officinale* polysaccharides against colorectal cancer (CRC).

The molecular weight (Mw) of polysaccharides has been considered to have a close relationship with the biological activities of polysaccharides (Wasser, 2002). Wang et al. (2014) showed that high-Mw polysaccharides (524 kDa) from *Lentinus edodes* displayed robust antitumor effects. Ren et al. (2016) revealed that a high-Mw polysaccharide (463 kDa) from *Pleurotus eryngii* had antitumor effects against HepG2 cells. However, Xu et al. (2016) revealed that medium-Mw polysaccharides (rather than high-Mw polysaccharides) from *Camellia*-species seed cake displayed excellent antioxidant activity. Bhadja et al. (2016) revealed that polysaccharides from seaweed with low Mw had a repairing effect on damaged HK-2 cells. Unfortunately, the relationship between the Mw and biological activity of *D. officinale* polysaccharides has not been investigated deeply. Zhang et al. (2019) explored the suitable Mw range of polysaccharides from *D. officinale* on inducing the apoptosis of HeLa cells, but was studied *in vitro* only. Therefore, for CRC, the Mw of *D. officinale* polysaccharides that are most suitable *in vivo* is still unknown.

In China and Japan, lentinan injection (which contains the main active ingredients of *Lentinus edodes* polysaccharides (LNT)) has been approved as adjuvant therapy for malignant tumors (Sun et al., 2020). *Astragalus membranaceus* polysaccharides (APS) have been applied widely in the clinic due to their immunomodulatory and antitumor activities (Zhou et al., 2017). Therefore, comparing the anticancer effects of *D. officinale* polysaccharides with those of APS and LNT could help provide a scientific basis for developing the polysaccharides of *D. officinale* as pharmacological agents.

Zebrafish (*Danio rerio*) is regarded as an "ideal" model organism for assessing human diseases because it possesses several orthologs with human genes and drug targets (Gunnarsson et al., 2008; Howe et al., 2013; Kim et al., 2013; Dai et al., 2014). Hence, zebrafish could be used to test the effects of *D. officinale* polysaccharides.

Transcriptome studies provide a promising perspective for exploring the molecular mechanisms of drug functions and investigating the underlying pathogenesis of diseases and modes of drug action (Wang et al., 2008; Li et al., 2011; Chen et al., 2012). Transcriptome abundance is measured by RNA sequencing (RNA-seq) (Hao et al., 2018). Some transcriptome analyses that aimed at elucidating the molecular mechanisms related to the antitumor effects of polysaccharides have been undertaken. For example, Kang et al. (2016) revealed the underlying antitumor mechanism of marine algae (*Gracilariopsis lemaneiformis*) polysaccharides by transcriptome profiling. Ren et al. (2019) uncovered the underlying antitumor mechanism of the action of polysaccharides from dandelions in inhibiting a specific pathway: phosphoinositide 3-kinase/protein kinase B/mammalian target of rapamycin. Qi et al. (2020) exposed the underlying anti-CRC mechanism of *Cordyceps sinensis* polysaccharides. Wang et al. (2019) revealed the underlying antitumor mechanism of the polysaccharides of Taishan *Pinus massoniana* pollen. All these research teams used RNA-seq to provide these observations.

We compared the effects of *D. officinale* polysaccharides of different Mw, as well as LNT and APS, on the growth of HT-29 cells in a zebrafish xenograft model. Also, we evaluated the changes in the gene-expression profile induced by treatment with *D. officinale* polysaccharides on HT-29 cells by RNA-seq to explore the underlying anti-CRC mechanism.

MATERIALS AND METHODS

Ethical Approval of the Study Protocol

Animal care and experimental protocols were approved (IACUC-2019-194, IACUC-2020-097) by the Animal Ethics Committee at Hunter Biotechnology (Hangzhou, China) and were conducted in accordance with the Chinese Association for Laboratory Animal Sciences guidelines.

Materials

5-Fluorouracil (5-Fu) was purchased from Sigma-Aldrich (Saint Louis, MO, United States). APS was obtained from Tianjin Cinorch Pharmaceuticals (Tianjin, China). LNT was purchased from Jinling Pharmaceuticals (Jinling, China). Also, 5× All-In-One RT MasterMix (with AccuRT Genomic DNA Removal Kit) and EvaGreen 2× quantitative polymerase chain reaction (qPCR) MasterMix-LOW ROX were purchased from Applied Biological Materials (Vancouver, Canada). The TRIzol® reagent was obtained from CoWin Biosciences (Beijing, China).

Cell Lines

A human CRC cell line (HT-29) was purchased from the Cell Line Bank of the Chinese Academy of Sciences (Shanghai, China). HT-29 cells were cultured in McCoy's 5A medium (Gibco, Grand Island, NY, United States) containing 10% fetal bovine serum (Gibco), penicillin (100 $U \cdot ml^{-1}$), and streptomycin (100 $\mu g \cdot ml^{-1}$) at 37°C in a humidified atmosphere with 5% CO_2.

Zebrafish

Wild-type AB zebrafish maintained at Hunter Biotechnology was incubated at 28°C with E3 medium (pH 7.2) under a 14 h: 10 h light-dark cycle according to a standard zebrafish breeding protocol (Kimmel et al., 1995). The embryos were obtained by natural spawning.

TABLE 1 | Primer sequences used in RT-qPCR.

Genes	Direction	Sequence (from 5′to 3′)
β-actin	Forward	TGGCACCCAGCACAATGAA
	Reverse	CTAAGTCATAGTCCGCCTAGAAGCA
Caspase-3	Forward	GACTCTGGAATATCCCTGGACAACA
	Reverse	AGGTTTGCTGCATCGACATCTG
Bcl-2	Forward	AACATCGCCCTGTGGATGAC
	Reverse	AGAGTCTTCAGAGACAGCCAGGAG
P53	Forward	TCGAGATGTTCCGAGAGCTGAAT
	Reverse	GTCTGAGTCAGGCCCTTCTGTCTT
Bax	Forward	TTGCTTCAGGGTTTCATCCA
	Reverse	CTTGAGACACTCGCTCAGCTTC
Cytochrome C	Forward	GGAGCGAGTTTGGTTGCACTTAC
	Reverse	TGTGGCACTGGGAACACTTCATA

Polysaccharides From *Dendrobium officinale* Kimura & Migo

Three polysaccharide fractions, DOP2 (D2), DOP8 (D8), and DOP122 (D122), with a Mw (in kDa) of 24.89, 80.32, and 1,224.54, respectively, were obtained from the stems of *D. officinale*, as described previously (Zhang et al., 2020). In brief, after hot water extraction, a *D. officinale*–extracting solution was precipitated with ethanol followed by oxidative degradation with a Vc–H_2O_2–$FeCl_2{\cdot}4H_2O$ system. Then, D2, D8, and D122 were obtained by freeze-drying.

Another polysaccharide, DOPW-1, of Mw 389.98 kDa, was isolated from the stems of *D. officinale* according to a method described previously (Tao et al., 2019). In brief, after hot water extraction, a *D. officinale*–extracting solution was precipitated with ethanol followed by purification using a DEAE cellulose-52 column and Sephadex G-300 HR column. Then, DOPW-1 was obtained by freeze-drying.

Effects of Polysaccharides of Different Molecular Weight in a Zebrafish Xenograft Model

A zebrafish xenograft model was established according to the method described by Hamilton et al. (2016). In brief, zebrafish xenografts were generated by microinjection of ~200 chloromethylbenz-amino derivatives of 1,1′-dioctadecyl-3,3,3′,3′-tetramethylindocarbocyanine perchlorate (CM-Dil)–labeled HT-29 cells into the yolk sac of zebrafish embryos 2 days post fertilization (dpf).

After establishing the zebrafish xenograft model, the embryos (3 dpf) were placed into six groups randomly: model; 5-Fu (50 ng/zebrafish); D2 (250 $\mu g{\cdot}ml^{-1}$); D8 (250 $\mu g{\cdot}ml^{-1}$); DOPW-1 (250 $\mu g{\cdot}ml^{-1}$); D122 (250 $\mu g{\cdot}ml^{-1}$). The embryos were transferred into six-well plates (30 embryos/well). The dose of 5-Fu was selected based on the study by Xu et al. (2019), and the dose of experimental groups was selected based on our previous study (Tao et al., 2021), where we explored the maximum tolerance concentration (MTC) of polysaccharides from *D. officinale* and determined the effect of polysaccharides from *D. officinale* (27.8, 83.3, 250 $\mu g{\cdot}ml^{-1}$) in the zebrafish xenograft model. The results indicated that the concentration of 250 $\mu g{\cdot}ml^{-1}$ is determined as MTC and it has the most significant inhibitory effect on CRC. Subsequently, 5-Fu was administered through caudal vein microinjection. D2, D8, DOPW-1, and D122 were dissolved in the embryo medium. 2 days after administration, fluorescence images were captured using a fluorescence microscope (AZ100; Nikon, Japan). The fluorescence intensity was quantified with NIS-Elements D 3.10 (Nikon). The inhibition of tumor growth was calculated according to the following formula:

$$\text{Inhibition of tumor growth (\%)} = \left(1 - \frac{\text{fluorescence intensity of experimental group}}{\text{fluorescence intensity of model group}}\right) \times 100\%.$$

Effects of *Astragalus membranaceus* Polysaccharides, *Dendrobium officinale* Kimura & Migo Polysaccharide-1, and *Lentinus edodes* Polysaccharides in a Zebrafish Xenograft Model

After establishing the zebrafish xenograft model, the embryos (3 dpf) were divided randomly into five groups: model; 5-Fu (50 ng/zebrafish); APS (250 $\mu g{\cdot}ml^{-1}$); DOPW-1 (250 $\mu g{\cdot}ml^{-1}$); LNT (250 $\mu g{\cdot}ml^{-1}$). The embryos were transferred into six-well plates (30 embryos/well). Subsequently, 5-Fu was administered through caudal vein microinjection. APS, DOPW-1, and LNT were dissolved in the embryo medium. 2 days after administration, and fluorescence images were captured using a fluorescence microscope (AZ100). The fluorescence intensity was quantified with NIS-Elements D 3.10 (Nikon). Inhibition of tumor growth was calculated as described in the previous section.

RNA Extraction, Library Preparation, and Transcriptome Sequencing

In our previous study, cell proliferation assay was conducted (Tao et al., 2021), and the results demonstrated that the concentration of 400 $\mu g{\cdot}ml^{-1}$ possess the most significant inhibitory effect on HT-29 cells. Therefore, 400 $\mu g{\cdot}ml^{-1}$ was selected as the intervention dosage in this experiment. In brief, HT-29 cells were seeded in six-well plates ($1{\times}10^6$ cells/well) for 24 h, and treated/ untreated with DOPW-1 (400 $\mu g{\cdot}ml^{-1}$) for an additional 48 h. After cell harvesting, total RNA was extracted using the TRIzol reagent at 4°C, and the concentration and purity (optical density at 260 nm (OD_{260})/$OD_{280} \geq 1.8$, $OD_{260}/OD_{230} \geq 1.5$) were tested using a spectrophotometer (NanoDrop™ 2000; Thermo Fisher Scientific, Wilmington, DE, United States). The RNA Nano 6000 Assay Kit of the Bioanalyzer 2,100 system (Agilent Technologies, Santa Clara, CA, United States) was used to evaluate RNA integrity to ensure that the RNA integrity number ≥8.0. Finally, extracted RNA samples were frozen immediately at −80°C until use.

According to the manufacturer's recommendations, the NEBNext® Ultra™ RNA Library Prep Kit for Illumina® (New

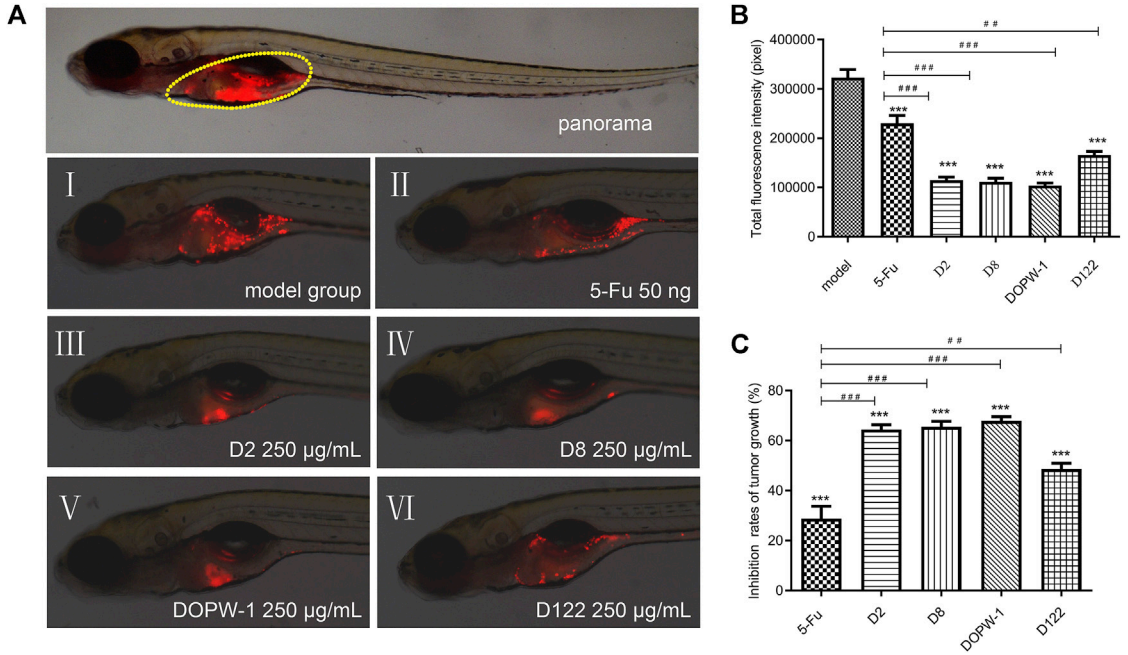

FIGURE 1 | Inhibitory effect of polysaccharides of different Mw derived from *D. officinale* stems in a zebrafish xenograft model. **(A)** Red fluorescence represents a tumor area. **(B)** Fluorescence intensity of the tumor xenograft model. **(C)** Quantification of the inhibition of tumor growth. Data are expressed as the mean ± SEM. ***$P < 0.001$ for each group *vs*. the model group; $^{\#\#}P < 0.01$ and $^{\#\#\#}P < 0.001$ for each group *vs*. the 5-Fu group.

TABLE 2 | Effects of *D. officinale* polysaccharides of different Mw on a zebrafish xenograft model.

Group	Mean ± SEM	
	Fluorescence intensity (Pixels)	Inhibition (%)
Model	323075.80 ± 16458.07	0 ± 5.09
5-Fu (50 ng)	230121.44 ± 16011.40[a]	28.77 ± 4.96[a]
D2 (250 μg·ml^{-1})	114979.79 ± 6147.02[a,b]	64.41 ± 1.90[a,b]
D8 (250 μg·ml^{-1})	111484.58 ± 7199.76[a,b]	65.49 ± 2.23[a,b]
DOPW-1 (250 μg·ml^{-1})	103675.11 ± 5448.93[a,b]	67.91 ± 1.69[a,b]
D122 (250 μg·ml^{-1})	165928.09 ± 7214.14[a,c]	48.64 ± 2.23[a,c]

Data are expressed as the mean ± SEM.
[a]*P < 0.001 for each group vs. the model group.*
[b]*P < 0.001 for each group vs. 5-Fu group.*
[c]*P < 0.01 for each group vs. 5-Fu group.*

England Biolabs, Ipswich, MA, United States) was used to construct the sequencing libraries. This was achieved using 1 μg of total RNA from each sample, and then index codes were added to attribute sequences to each sample. Clustering of the index-coded samples was performed using the TruSeq PE Cluster Kit v4-cBot-HS (Illumina, San Diego, CA, United States) on a cBot Cluster Generation System in accordance with the manufacturer's (Illumina) directions. After cluster generation, sequencing of libraries was performed on an Illumina platform, and paired-end reads were generated (Chao et al., 2019).

Bioinformatics Analysis

Raw data with the "fastq" format were analyzed using in-house Perl scripts. In this step, the adapter sequence, poly-N-containing reads, and low-quality reads in raw data were discarded to obtain clean data. Meanwhile, Q20, Q30, GC-content, and sequence duplication in clean data were measured for quality control. Then, the filtered clean data of high quality were used for further analyses.

After the raw sequences had been processed and converted to clean reads, the latter were mapped to the reference genome sequence using HISAT2. Only reads with perfect matches or single mismatches were utilized further for this analysis based on the reference genome.

Several databases were used to annotate gene function: Nr (National Center for Biotechnology Information non-redundant protein sequences, ftp://ftp.ncbi.nih.gov/blast/db/); Pfam (Protein Family, http://pfam.xfam.org/); COG (Clusters of Orthologous Groups of Proteins, www.ncbi.nlm.nih.gov/COG/); KOG (Clusters of Protein Homology, www.ncbi.nlm.nih.gov/KOG/); SWISS-PROT (manually annotated and reviewed protein sequences, http://www.expasy.ch/sprot); KO (Kyoto Encyclopedia of Genes and Genomes (KEGG) Ortholog, http://www.genome.jp/kegg/); GO (Gene Ontology, www.geneontology.org/).

Fragments per kilobase of transcript per million mapped (FPKM) values were used to estimate gene expression. FPKM was calculated using the following formula:

$$\mathrm{FPKM} = \frac{\text{cDNA Fragments}}{\text{Mapped Fragments (Millions)*TranscriptLength (kb)}}.$$

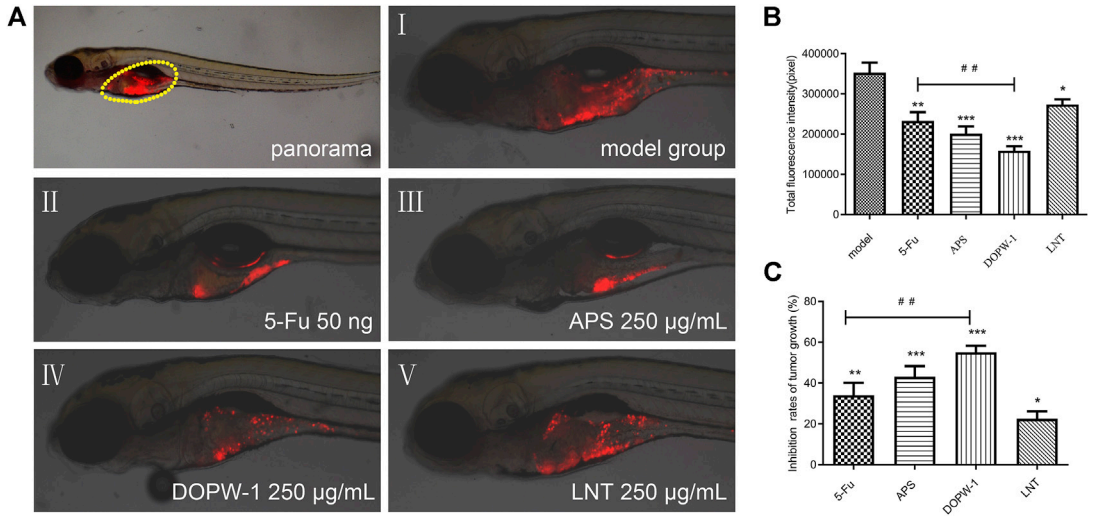

FIGURE 2 | Tumor inhibition elicited by APS, DOPW-1, and LNT in a zebrafish xenograft model. **(A)** HT-29 cells (red) after xenotransplantation. **(B)** Fluorescence intensity of the tumor xenograft. **(C)** Quantification of the inhibition of tumor growth. Data are expressed as the mean ± SEM. $^{*}P < 0.05$, $^{**}P < 0.01$, and $^{***}P < 0.001$ for each group *vs*. the model group; $^{\#\#}P < 0.01$ for the DOPW-1 group *vs*. the 5-Fu group.

TABLE 3 | Effects of APS, DOPW-1, and LNT on a zebrafish xenograft model.

Group	Mean ± SEM	
	Fluorescence intensity (Pixels)	Inhibition (%)
Model	352981.93 ± 24936.72	0 ± 3.89
5-Fu (50 ng)	232871.15 ± 21488.43[a]	34.03 ± 6.09[a]
APS (250 μg·ml^{-1})	200902.50 ± 18346.50[b]	43.08 ± 5.19[b]
DOPW-1 (250 μg·ml^{-1})	158395.32 ± 11137.22[b,c]	55.13 ± 3.16[b,c]
LNT (250 μg·ml^{-1})	273619.86 ± 12819.40[d]	22.48 ± 3.65[d]

Data are expressed as the mean ± SEM.
[a]P < *0.01.*
[b]P < *0.001 for each group vs. the model group.*
[c]P < *0.01 for the DOPW-1 group vs. the 5-Fu group.*
[d]P < *0.05 for each group vs. the model group.*

Analysis of differential expression of the two groups was executed using edgeR (Robinson et al., 2010). Differentially expressed genes (DEGs) with $P < 0.05$ and fold change ≥2 were screened for further analysis. Analysis of the functional enrichment of DEGs using the GO database was performed using GOseq within R (R Institute for Statistical Computing, Vienna, Austria) based on Wallenius' noncentral hyper-geometric distribution (Young et al., 2010), which can adjust for bias in gene length in DEGs. KOBAS (Mao et al., 2005) was applied for the analysis of pathway enrichment of DEGs using the KEGG database.

Analysis of Gene Expression by Real-Time Reverse Transcription-Quantitative Polymerase Chain Reaction

HT-29 cells were seeded in six-well plates at 1×10^6 cells/well for 24 h, and then treated or not treated with DOPW-1 (400 μg·ml^{-1}) for an additional 48 h. After cell harvesting, total RNA was extracted using the TRIzol reagent. The quantity and quality of cells were evaluated using a spectrophotometer (NanoDrop 2000). RNA was transcribed into complementary DNA using the 5× All-In-One RT MasterMix (with AccuRT Genomic DNA Removal Kit) according to the manufacturer's instructions. Expression of apoptosis-related genes (Bax, B-cell lymphoma (Bcl)-2, P53, caspase-3, cytochrome C) was detected using a real-time PCR instrument (ABI 7500; Applied Biosystems, Foster City, CA, United States) with EvaGreen 2× qPCR MasterMix-LOW ROX™ following the manufacturer's instructions. β-actin was used as an internal standard to normalize gene targets. Relative RNA expression was calculated using the $2^{-\Delta\Delta CT}$ method (Rieu and Powers 2009). The primers used were designed by Takara Biotechnology (Shiga, Japan) and are listed in **Table 1**. RT-qPCR experiments were carried out in triplicate.

Statistical Analyses

Statistical analyses were undertaken using SPSS 19.0 (IBM, Armonk, NY, United States) applying a two-tailed independent Student's *t*-test or one-way ANOVA followed by Dunnett's *t*-test. Data are expressed as the mean ± standard error of the mean (SEM). $P < 0.05$ was considered statistically significant.

RESULTS

Effects of Polysaccharides of Different Molecular Weights in a Zebrafish Xenograft Model

To determine the antitumor effects of *D. officinale* polysaccharides of different Mw on tumorigenesis *in vivo*, we established a novel zebrafish xenograft model by transplanting

TABLE 4 | Summary of RNA-seq alignment.

Sample	Clean reads	Mapped reads	Uniquely mapped	Multiply mapped
Control-1	63,262,836	61,388,655 (97.04%)	59,818,229 (94.59%)	1,570,426 (2.48%)
Control-2	50,902,230	49,507,501 (97.26%)	48,243,322 (94.78%)	1,264,179 (2.48%)
Control-3	52,359,808	50,903,021 (97.22%)	49,597,105 (94.72%)	1,305,916 (2.49%)
DOPW-1-1	54,529,350	52,995,672 (97.19%)	51,623,823 (94.67%)	1,371,849 (2.52%)
DOPW-1-2	46,143,896	44,829,360 (97.15%)	43,666,343 (94.63%)	1,163,017 (2.52%)
DOPW-1-3	47,175,218	45,878,612 (97.25%)	44,744,159 (94.85%)	1,134,453 (2.40%)

Note: Control represents HT-29 cells without DOPW-1 treatment; DOPW-1 represents HT-29 cells with DOPW-1 treatment for 48 h.

TABLE 5 | Functional annotation of genes using protein databases.

Database	Number of genes annotated
GO	12,006 (51.75%)
KEGG	13,660 (58.88%)
KOG	13,749 (59.26%)
All annotations	22,478 (96.88%)
Total number of genes annotated	23201

HT-29 cells. Zebrafish embryos (3 dpf) were treated with 5-Fu, D2, D8, DOPW-1, or D122.

The fluorescence intensity reflected the tumor volume. The inhibitory effect was revealed by reduced fluorescence intensity (**Figure 1A**). Notably, all treatments exhibited antitumor effects in the HT-29 xenograft model (**Figures 1B,C**). Compared with the model group, the inhibition of the tumor xenograft treated with 5-Fu, D2, D8, DOPW-1, or D122 was 28.77 ± 4.96%, 64.41 ± 1.90%, 65.49 ± 2.23%, 67.91 ± 1.69%, and 48.64 ± 2.23%, respectively (**Table 2**). Tumor growth was inhibited potently and significantly by 5-Fu, D2, D8, DOPW-1, and D122 (**Figure 1**). DOPW-1, with a Mw of 389.98 kDa, exhibited the strongest tumor inhibition.

Effects of *Astragalus membranaceus* Polysaccharides, *Dendrobium officinale* Kimura & Migo Polysaccharide-1, and *Lentinus edodes* Polysaccharides in a Zebrafish Xenograft Model

The zebrafish model (created by implanting HT-29 cells) was also applied to determine the antitumor effects of APS, DOPW-1, and LNT on tumorigenesis *in vivo*. Zebrafish embryos (3 dpf) were treated with 5-Fu, APS, DOPW-1, or LNT. Growth inhibition was determined by capturing the fluorescence images using a fluorescence microscope. **Figure 2A** shows the tumor-inhibitory effect, which was indicated by reduced fluorescence

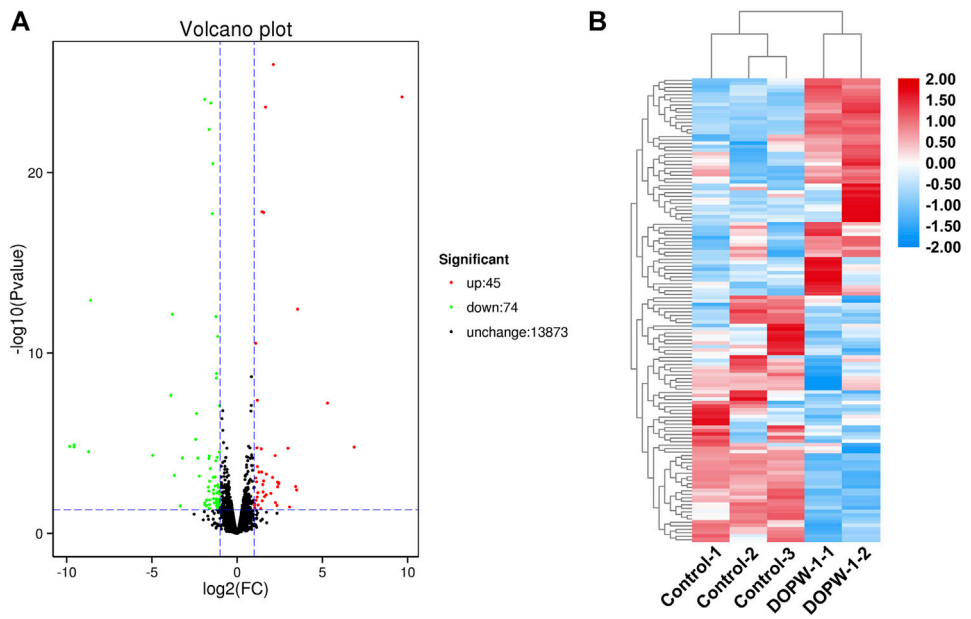

FIGURE 3 | (A) Volcano map of DEGs between the DOPW-1 and control groups. Black, red, and green dots represent genes with no significant change in expression, significantly upregulated expression, and significantly downregulated expression in DEGs, respectively. **(B)** Hierarchical clustering of DEGs for the DOPW-1 group *vs*. the control group. Different colors represent different gene expressions in the DOPW-1 and control groups.

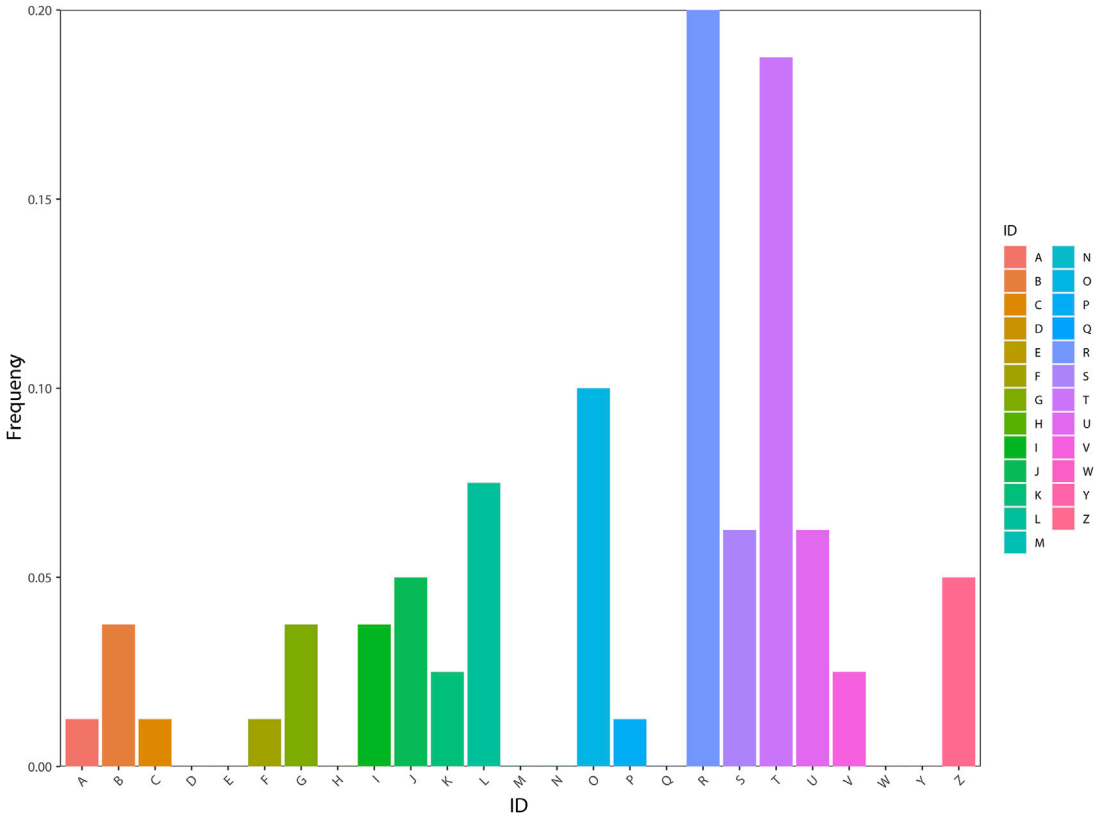

FIGURE 4 | Functional classification of genes using the KOG database. **(A)** RNA processing and modification [1-1.25%]; **(B)** Chromatin structure and dynamics [3-3.75%]; **(C)** Energy production and conversion [1-1.25%]; **(D)** Cell cycle control, cell division, and chromosome partitioning [0-0%]; **(E)** Amino acid transport and metabolism [0-0%]; **(F)** Nucleotide transport and metabolism [1-1.25%]; **(G)** Carbohydrate transport and metabolism [3-3.75%]; **(H)** Coenzyme transport and metabolism [0-0%]; **(I)** Lipid transport and metabolism [3-3.75%]; **(J)** Translation, ribosomal structure, and biogenesis [4-5%]; **(K)** Transcription [2-2.5%]; **(L)** Replication, recombination, and repair [6-7.5%]; **(M)** Cell wall/membrane/envelope biogenesis [0-0%]; **(N)** Cell motility [0-0%]; **(O)** Posttranslational modification, protein turnover, and chaperones [8-10%]; **(P)** Inorganic ion transport and metabolism [1-1.25%]; **(Q)** Secondary metabolite biosynthesis, transport, and catabolism [0-0%]; **(R)** General function prediction only [16-20%]; **(S)** Function unknown [5-6.25%]; **(T)** Signal transduction mechanisms [15-18.75%]; **(U)** Intracellular trafficking, secretion, and vesicular transport [5-6.25%]; **(V)** Defense mechanisms [2-2.5%]; **(W)** Extracellular structures [0-0%]; **(Y)** Nuclear structure [0-0%]; **(Z)** Cytoskeleton [4-5%].

intensity. **Figures 2B,C** show that all treatments exhibited antitumor effects in the zebrafish xenograft model. Compared with the model group, the inhibition of the tumor xenograft model treated with 5-Fu, APS, DOPW-1, or LNT was 34.03 ± 6.09%, 43.08 ± 5.19%, 55.13 ± 3.16%, and 22.48 ± 3.65%, respectively (**Table 3**). 5-Fu, APS, DOPW-1, and LNT inhibited tumor growth potently and significantly when compared with that in the model group (**Figure 2**). The inhibition of tumor growth elicited by DOPW-1 was significantly greater than that in the 5-Fu group. Moreover, compared with the APS and LNT groups, the DOPW-1 group exhibited the strongest tumor inhibition.

Mapping of Reads

The strongest inhibitory effect on the growth of HT-29 cells was elicited by DOPW-1. Hence, DOPW-1 was selected as the experimental group to explore the difference in transcriptomes between it and the control group. All six constructed libraries (named control-1, control-2, control-3, DOPW-1-1, DOPW-1-2, and DOPW-1-3) were sequenced with raw reads.

An average of 52.39 (range, 46.14–63.26) million clean reads was obtained after discarding the adaptor sequence, poly-N–containing reads, and low-quality raw reads. HISAT2 was used to map clean reads to the human reference genome. A summary of the detailed mapping output is listed in **Table 4**. The ratio of mapping for the control and DOPW-1 groups was 94.69 and 94.71%, respectively, which demonstrated high gene expression in both groups.

Functional Annotation and Differentially Expressed Genes Analysis

Analysis of gene function was performed using gene annotation. The genes were aligned against the publicly available protein databases KEGG, KOG, and GO. In total, 22,478 (96.88%) genes were annotated (**Table 5**). Most of the genes were annotated by gene functions using KOG (59.26%), KEGG (58.88%), and GO (51.75%) databases.

Hierarchical clustering was undertaken, and volcano plots were created to visualize the differential expression of genes

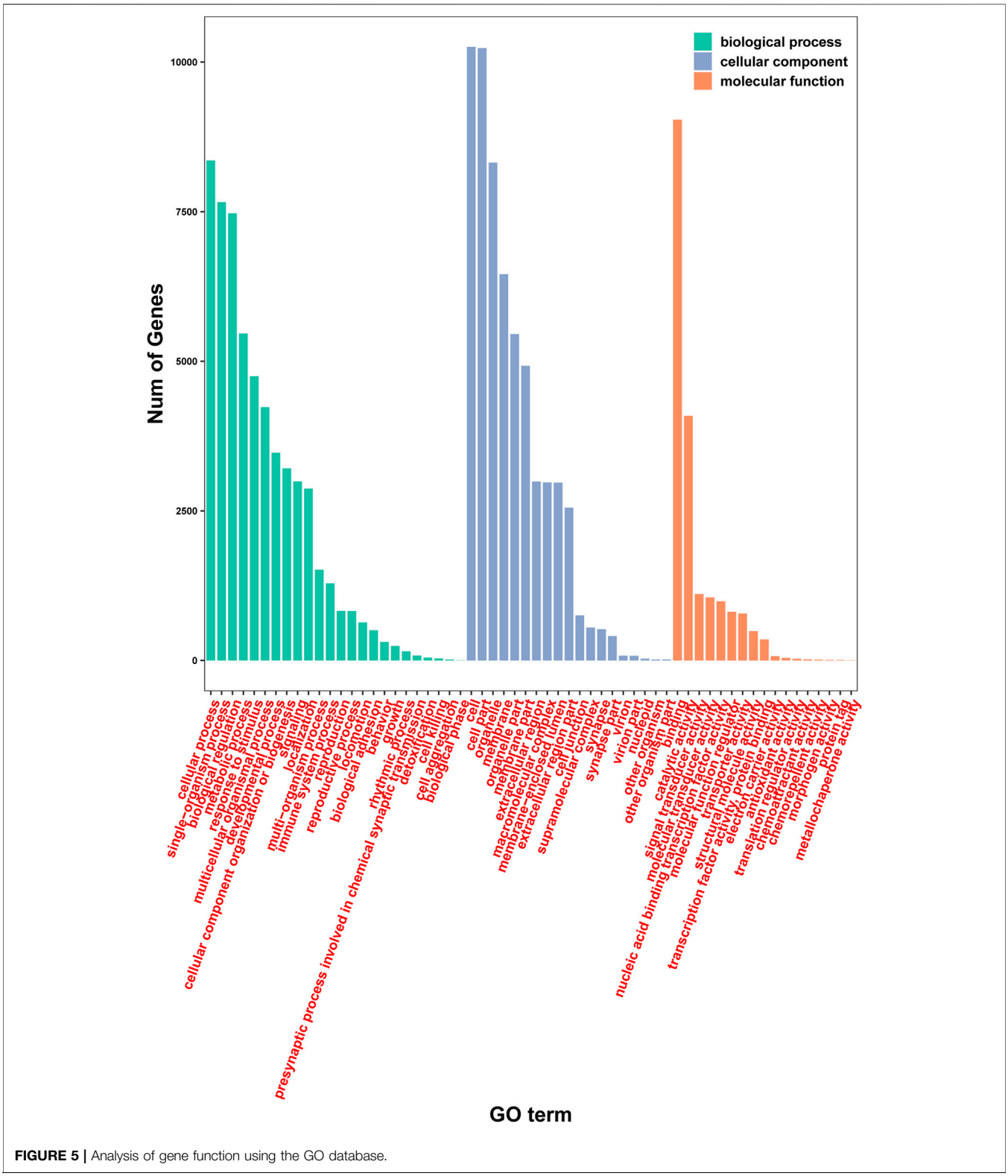

FIGURE 5 | Analysis of gene function using the GO database.

(**Figure 3A**). We identified 119 genes with significant differential expression in the DOPW-1 group compared with that in the control group. Forty-five genes had upregulated expression and 74 genes had downregulated expression, which was likely due to activation of HT-29 cells after DOPW-1 treatment. Agglomerative hierarchical clustering was used to identify the number of clusters from the cluster dendrogram (**Figure 3B**).

FIGURE 6 | Analysis of pathway enrichment of genes using the KEGG database.

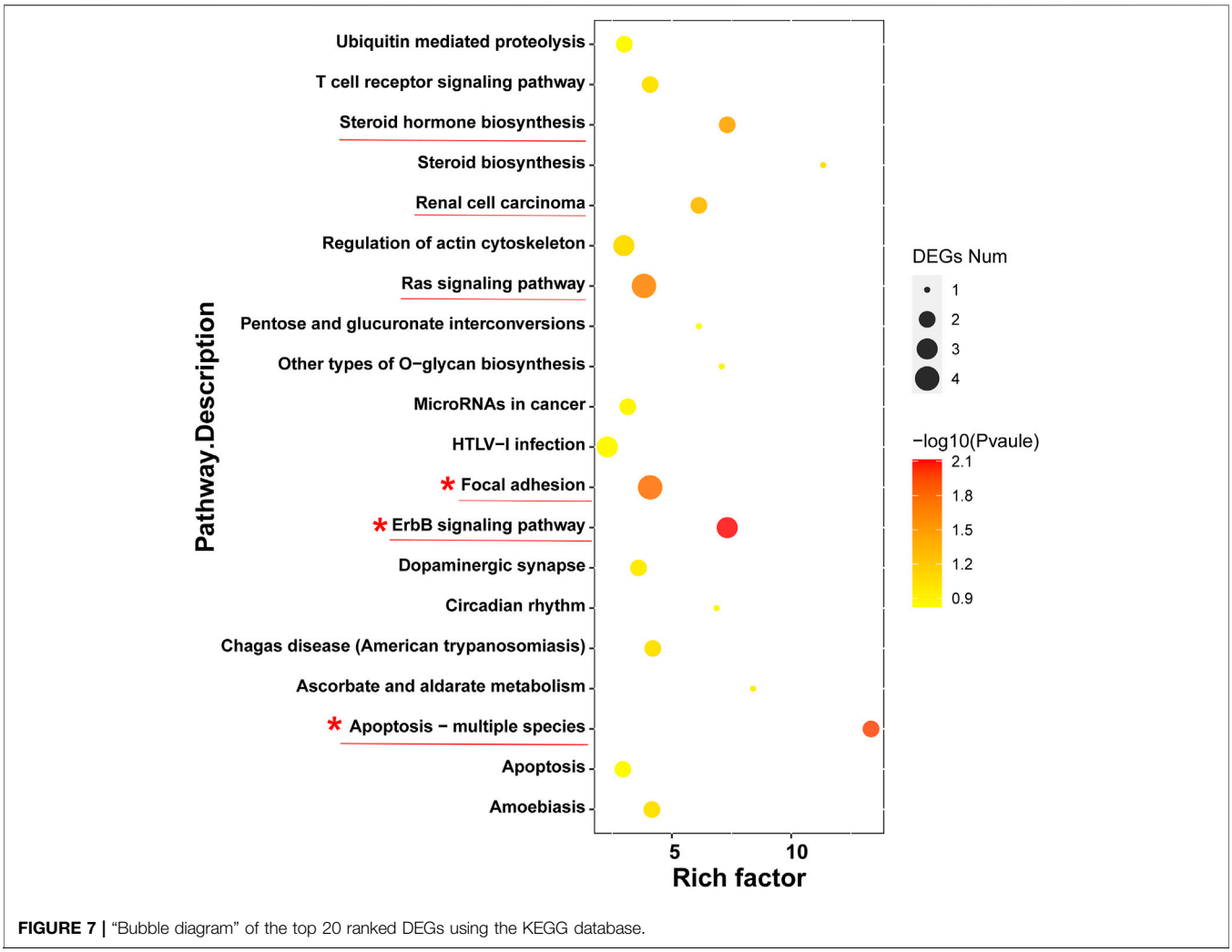

FIGURE 7 | "Bubble diagram" of the top 20 ranked DEGs using the KEGG database.

Functional Analysis of Genes Using Clusters of Protein Homology and Gene Ontology Databases

To evaluate and categorize the possible functions of genes, all unigenes were aligned to the KOG database. Orthologous genes were classified in the KOG database.

According to the KOG database, the genes were distributed in 17 orthologous clusters (**Figure 4**). Most of the genes were assigned to "general function prediction only" (16–20%), followed by "signal transduction mechanisms" (15–18.75%), "posttranslational modification, protein turnover, and chaperones" (8–10%), "replication, recombination, and repair" (6–7.5%), and "intracellular trafficking, secretion, and vesicular transport" (5–6.25%).

Further analysis of gene function was performed using the GO database employing the categories of biological process, cell component, and molecular function. A total of 12,006 genes were mapped using the GO database (**Figure 5**). Specifically, 10,434, 11,381, and 10,623 genes were assigned to biological process, cell component, and molecular function, respectively. Importantly, several different GO terms may be assigned to the same gene.

Analysis of Pathway Enrichment Using the Kyoto Encyclopedia of Genes and Genomes Database

Analysis of pathway enrichment revealed most genes to be assigned to "apoptosis and apoptosis-multiple species" (12.5%), "focal adhesion" (12.5%), and "ras signaling pathway" (12.5%) followed by "regulation of actin cytoskeleton" (9.38%) and "ErbB signaling pathway" (9.38%) (**Figure 6**).

To further investigate the anticancer signaling pathways of HT-29 cells treated with DOPW-1, we conducted enrichment analysis of DEGs using the KEGG database. The top 20 enriched pathways were selected (**Figure 7**). "Apoptosis-multiple species," "ErbB signaling pathway," "focal adhesion," "ras signaling pathway," "renal cell carcinoma," and "steroid hormone biosynthesis" were the top six enriched pathways. Among them, "apoptosis-multiple species" was the most significantly enriched pathway. Hence, an apoptosis pathway is one of the

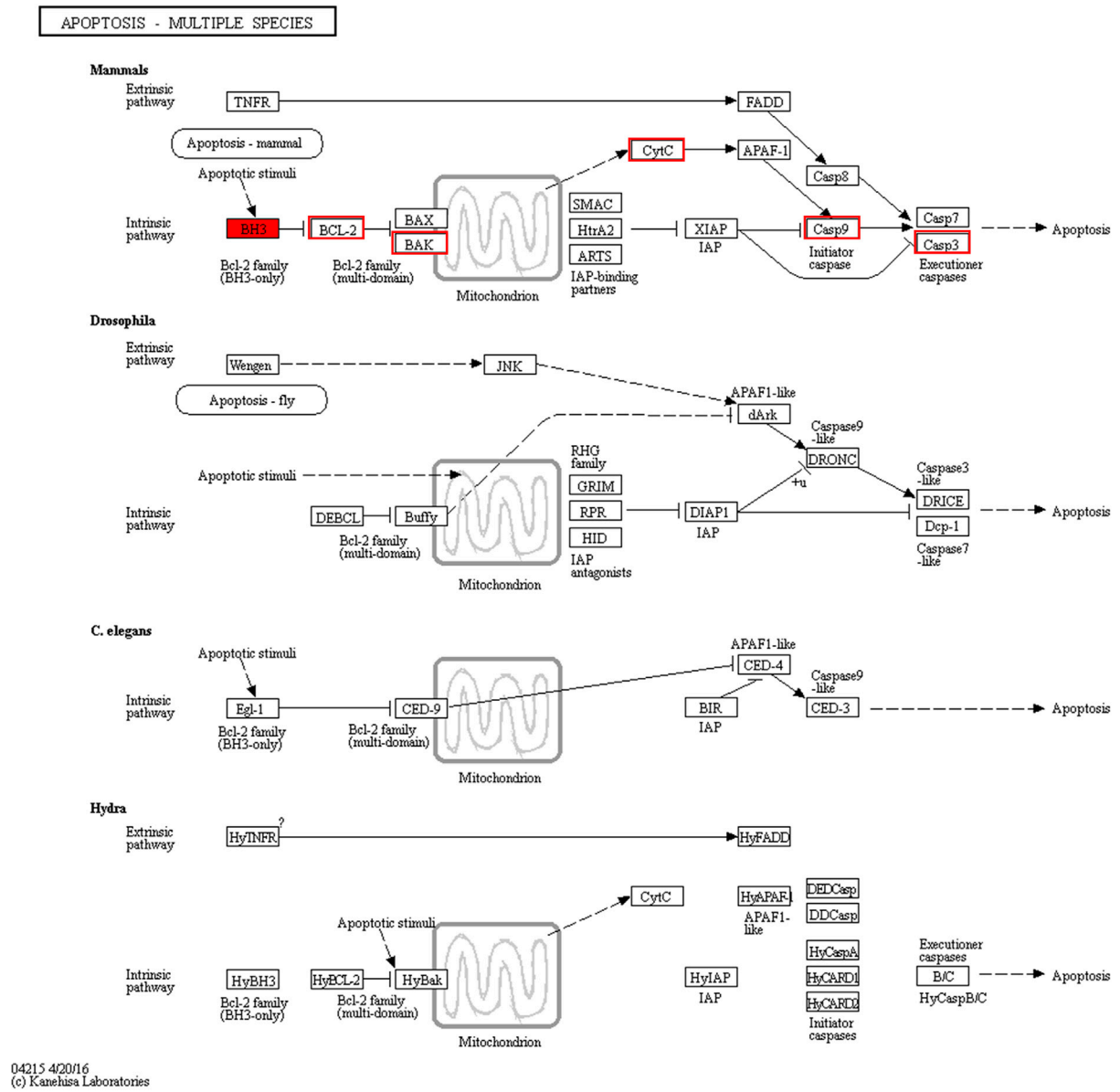

FIGURE 8 | "Apoptosis-multiple species" pathway.

most important pathways to consider if DOPW-1 inhibits the proliferation of HT-29 cells. This finding is consistent with an observation in our previous report (Tao et al., 2021).

Transcriptome Analysis of "Apoptosis-Multiple Species"

We discovered a close relationship among Bcl-2 family proteins, P53 protein, cytochrome C protein, caspase-3 protein, and apoptosis (**Figure 8**). In addition, the intrinsic pathway of apoptosis analyzed using RT-qPCR has been further verified by our previous study using Western blotting (Tao et al., 2021).

The apoptosis-related gene expression of P53, Bax, Bcl-2, cytochrome C, and caspase-3 was evaluated using RT-qPCR. Treatment with DOPW-1 (400 $\mu g \cdot ml^{-1}$) significantly increased the corresponding gene expression of P53, cytochrome C, and caspase-3 (**Figure 9**). Interestingly, the ratio of the expression of Bax/Bcl-2 in the DOPW-1 group was not significantly higher than that of the control group ($P > 0.05$). In our previous study, we calculated the ratio of the expression of Bak/Mcl-1 (anti- and pro-apoptotic factors, respectively) using Western blotting (Tao et al., 2021). Those results showed that the expression of Bak increased and that of Mcl-1 decreased after DOPW-1 treatment, which led to an increase in the Bak/Mcl-1 ratio when compared with that in the control group.

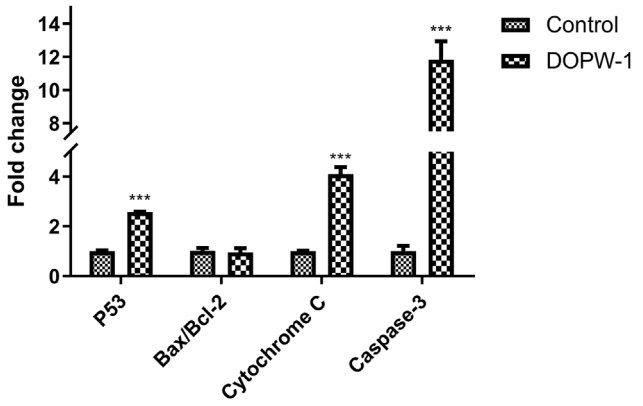

FIGURE 9 | Effect of different treatments on gene expression. ***$P < 0.001$ for the DOPW-1 group *vs*. the control group.

DISCUSSION

D. officinale polysaccharides possess anti-CRC activities (Tao et al., 2021). The Mw of polysaccharides is closely related to their antitumor activities (Huang et al., 2020). The side effects of chemotherapeutics warrant the development of nature-derived drugs based on polysaccharides. We investigated the effect of *D. officinale* polysaccharides of different Mw and currently used medicines based on polysaccharides (APS and LNT) in inhibiting tumor growth in a zebrafish xenograft model. We also studied the mechanism of action of *D. officinale* polysaccharides on the growth of HT-29 cells by RNA-seq.

In the study, the dose of *D. officinale* polysaccharides were selected based on our previous study (Tao et al., 2021), where we explored the MTC of polysaccharides from *D. officinale* and determined the effect of *D. officinale* polysaccharides (27.8, 83.3, 250 $\mu g \cdot ml^{-1}$) in a zebrafish xenograft model. The results indicated that the concentration of 250 $\mu g \cdot ml^{-1}$ is determined as the MTC and has the most significant inhibitory effect on CRC. *D. officinale* polysaccharides with a Mw ranging between 24.89 and 1,224.54 kDa exhibited significant antitumor activity, among which *D. officinale* polysaccharides of Mw 389.98 kDa exhibited the strongest tumor inhibition. This finding is in accordance with that of scholars who reported that lentinan of Mw 400–600 kDa exhibits strong antitumor activity (Wasser, 2002; Zhang et al., 2011). Also, Chen et al. (2009) postulated that polysaccharides of relatively high Mw may have more opportunity to "collide effectively". Furthermore, long-chain polysaccharides have more repeating units and higher valency to bind to more receptors than that of short-chain polysaccharides. In addition, Zhang et al. (2016) reported that most polysaccharides of Mw from 10 kDa to 10^3 kDa exhibited a marked antitumor effect. In the present study, D2 (24.89 kDa) and D8 (80.32 kDa) showed a strong antitumor effect, whereas D122 (1,224.54 kDa) showed a relatively weaker effect. One reason may be that polysaccharides of low Mw could enter tumor cells more readily than polysaccharides of high Mw. Yu et al. (2015) showed that high-Mw polysaccharides from *Porphyra yezoensis* were not conducive to inhibiting gastric cancer cells. Huang et al. (2020) revealed that high-Mw polysaccharides from *Dendrobium densiflorum* could not exert biological effects by breaking through membranes to enter cells. In general, the degradation of high-Mw polysaccharides to low-Mw polysaccharides can improve their biological activity significantly. Nevertheless, a too low Mw of polysaccharides will inhibit the formation of an active polymer structure.

Naturally derived polysaccharides have been widely used as medicines in China, thanks to their low toxicity and efficacy. For example, polysaccharides from *Astragalus* species, *Poria cocos*, *Ginseng* species, and *L. edodes* have been approved for clinical use by the National Medical Products Administration of China (Yu et al., 2018b). In the present study, the effect of DOPW-1 on CRC was more robust than that of the medicinal polysaccharides APS and LNT. Hence, DOPW-1 could be a promising potential agent against CRC. The effect of LNT on CRC was weaker than that of APS and DOPW-1, and the dose plays an important role in this result. Jeff et al. (2013) reported that the efficacious dose of LNT against the proliferation of HCT-116 cells and HT-29 cell was 5 $mg \cdot ml^{-1}$, whereas we employed an LNT dose of 250 $\mu g \cdot ml^{-1}$. Therefore, the anti-CRC activity of DOPW-1 was better than that of LNT at the same dose (250 $\mu g \cdot ml^{-1}$).

Transcriptome studies are used to explore the underlying molecular mechanisms of drug actions (Zhang et al., 2017). RNA-seq was undertaken to investigate how DOPW-1 inhibited the growth of HT-29 cells. Use of the KEGG database showed that the DEGs mainly encoded proteins involved in "apoptosis-multiple species," "ErbB signaling pathway," "focal adhesion," "ras signaling pathway," "renal cell carcinoma," and "steroid hormone biosynthesis". Among them, "apoptosis-multiple species" was the most significantly enriched. It is known that polysaccharides of *D. officinale* possess pharmacological activities of anticancerous nature (Yu et al., 2018a; Liang et al., 2019; Zhang et al., 2019), and this study might supply valuable information for DOPW-1 anti-CRC.

Apoptosis as an important molecular mechanism for polysaccharides in inhibiting colon cancer has been reported (Feregrino-Pérez et al., 2008; Di et al., 2017). For example, Di et al. (2017) reported that exopolysaccharides produced by *Lactobacillus casei* SB27 from yak milk induced the apoptosis of HT-29 cells. Feregrino-Pérez et al. (2008) revealed that a polysaccharide extract from common beans (*Phaseolus vulgaris* L.) could induce apoptosis via mitochondria-based mechanisms. In the present study, RT-qPCR demonstrated that gene expression of P53, cytochrome C, and caspase-3 was increased significantly after DOPW-1 treatment. However, the ratio of the expression of Bax/Bcl-2 in the DOPW-1 group was not significantly higher than that in the control group. Western blotting in our previous study showed that the expression of Bak increased and that of Mcl-1 decreased after DOPW-1 treatment, which led to an increase in the Bak/Mcl-1 ratio compared with that in the control group (Tao et al., 2021). Taken together, these results suggested that DOPW-1–triggered apoptosis of HT-29 cells was associated with the upregulation of the intrinsic p53 signaling pathway through caspase activation and, finally, led to apoptosis through the mitochondrial pathway (intrinsic pathway of apoptosis).

CONCLUSION

Fractions of *D. officinale* polysaccharides with a Mw of 389.98 kDa may be the most suitable for antitumor effects against CRC. The antitumor effect of DOPW-1 on CRC was stronger than that of currently available alternatives: APS and LNT. RNA-seq revealed that an apoptosis pathway was important for DOPW-1 to inhibit the proliferation of HT-29 cells. We revealed that the pathway DOPW-1 induces the apoptosis of HT-29 cells and provided a scientific basis for use of DOPW-1 as a naturally occurring medicine against CRC. However, there are some limitations in this study. We merely performed the experiments in a zebrafish xenograft model, and clinical trials are needed to verify our data. On the other hand, a deeper understanding about the transcellular transport and subcellular location of *D. officinale* polysaccharides in CRC cells is yet to be gained. In the following studies, we will conduct further research to explore the transport and absorption of *D. officinale* polysaccharides in CRC cells by using labeling technology.

DATA AVAILABILITY STATEMENT

The datasets presented in this study can be found in online repositories. The names of the repository/repositories and accession number(s) can be found below: https://www.ncbi.nlm.nih.gov/bioproject/PRJNA727088 PRJNA727088.

ETHICS STATEMENT

All animal care and experimental protocols were approved by the Animal Ethics Committee at Hunter Biotechnology, Inc. (No. IACUC-2019-194, No. IACUC-2020-097) and were conducted in accordance with the Chinese Association for Laboratory Animal Sciences guidelines.

AUTHOR CONTRIBUTIONS

Conceptualization: GW and ST. Methodology: ST, ZR, ZW and JH. Software: ST and ZY. Validation: ST and SD. Data analysis: ST, ZR and CL. Resources: GW. Data curation: ST. Writing (preparation of original draft and revised the manuscript): ST. Supervision: GW. Project administration: GW. Funding acquisition: GW.

FUNDING

This work was supported by the 2018 Shaoguan City Science and Technology Plan Project: Special Project of Industry-University-Research Cooperation (2018CS11919) and 2019 Guangdong Province Special Fund for Science and Technology ('Big project + task list') Project: Ecological Cultivation and Sustainable Utilization of Danxia Dendrobium officinale, a rare Southern Medicine in Guangdong Province (no. 2019gdskjzxzj-zt3-2).

REFERENCES

Bhadja, P., Tan, C. Y., Ouyang, J. M., and Yu, K. (2016). Repair Effect of Seaweed Polysaccharides with Different Contents of Sulfate Group and Molecular Weights on Damaged HK-2 Cells. *Polymers (Basel)*. 8:188. doi:10.3390/polym8050188

Chao, Q., Gao, Z. F., Zhang, D., Zhao, B. G., Dong, F. Q., Fu, C. X., et al. (2019). The Developmental Dynamics of the *Populus* Stem Transcriptome. *Plant Biotechnol. J.* 17:206–219. doi:10.1111/pbi.12958

Chen, R., Mias, G. I., Li-Pook-Than, J., Jiang, L., Lam, H. Y., Chen, R., et al. (2012). Personal Omics Profiling Reveals Dynamic Molecular and Medical Phenotypes. *Cell.* 148:1293–1307. doi:10.1016/j.cell.2012.02.009

Chen, X., Xu, X., Zhang, L., and Zeng, F. (2009). Chain Conformation and Anti-tumor Activities of Phosphorylated (1→3)-β-D-Glucan from *Poria Cocos*. *Carbohydr. Polym.* 78:581–587. doi:10.1016/j.carbpol.2009.05.019

Dai, Y. J., Jia, Y. F., Chen, N., Bian, W. P., Li, Q. K., Ma, Y. B., et al. (2014). Zebrafish as a Model System to Study Toxicology. *Environ. Toxicol. Chem.* 33:11–17. doi:10.1002/etc.2406

Di, W., Zhang, L., Wang, S., Yi, H., Han, X., Fan, R., et al. (2017). Physicochemical Characterization and Antitumour Activity of Exopolysaccharides Produced by *Lactobacillus Casei* SB27 from Yak Milk. *Carbohydr. Polym.* 171:307–315. doi:10.1016/j.carbpol.2017.03.018

Feregrino-Pérez, A. A., Berumen, L. C., García-Alcocer, G., Guevara-Gonzalez, R. G., Ramos-Gomez, M., Reynoso-Camacho, R., et al. (2008). Composition and Chemopreventive Effect of Polysaccharides from Common Beans (*Phaseolus vulgaris L.*) on Azoxymethane-Induced colon Cancer. *J. Agric. Food Chem.* 56: 8737–8744. doi:10.1021/jf8007162

Gunnarsson, L., Jauhiainen, A., Kristiansson, E., Nerman, O., and Larsson, D. G. (2008). Evolutionary Conservation of Human Drug Targets in Organisms Used for Environmental Risk Assessments. *Environ. Sci. Technol.* 42, 5807–5813. doi:10.1021/es8005173

Hamilton, L., Astell, K. R., Velikova, G., and Sieger, D. (2016). A Zebrafish Live Imaging Model Reveals Differential Responses of Microglia toward Glioblastoma Cells *In Vivo*. *Zebrafish.* 13:523–534. doi:10.1089/zeb.2016.1339

Hao, S., Li, S., Wang, J., Zhao, L., Yan, Y., Cao, Q., et al. (2018). Transcriptome Analysis of Phycocyanin-Mediated Inhibitory Functions on Non-small Cell Lung Cancer A549 Cell Growth. *Mar. Drugs.* 16:511. doi:10.3390/md16120511

Howe, K., Clark, M. D., Torroja, C. F., Torrance, J., Berthelot, C., Muffato, M., et al. 2013). The Zebrafish Reference Genome Sequence and its Relationship to the Human Genome. *Nature*. 496:498–503. doi:10.1038/nature12111

Huang, K., Li, Y., Tao, S., Wei, G., Huang, Y., Chen, D., et al. (2016). Purification, Characterization and Biological Activity of Polysaccharides from *Dendrobium officinale*. *Molecules.* 21:701. doi:10.3390/molecules21060701

Huang, S., Chen, F., Cheng, H., and Huang, G. (2020). Modification and Application of Polysaccharide from Traditional Chinese Medicine Such as *Dendrobium officinale*. *Int. J. Biol. Macromol.* 157:385–393. doi:10.1016/j.ijbiomac.2020.04.141

Jeff, I. B., Yuan, X., Sun, L., Kassim, R. M., Foday, A. D., and Zhou, Y. (2013). Purification and *In Vitro* Anti-proliferative Effect of Novel Neutral Polysaccharides from *Lentinus Edodes*. *Int. J. Biol. Macromol.* 52:99–106. doi:10.1016/j.ijbiomac.2012.10.007

Kang, Y., Li, H., Wu, J., Xu, X., Sun, X., Zhao, X., et al. (2016). Transcriptome Profiling Reveals the Antitumor Mechanism of Polysaccharide from Marine Algae *Gracilariopsis lemaneiformis*. *Plos One*. 11:e0158279. doi:10.1371/journal.pone.0158279

Kim, J. Y., Kim, H. H., and Cho, K. H. (2013). Acute Cardiovascular Toxicity of Sterilizers, PHMG, and PGH: Severe Inflammation in Human Cells and Heart Failure in Zebrafish. *Cardiovasc. Toxicol.* 13:148–160. doi:10.1007/s12012-012-9193-8

Kimmel, C. B., Ballard, W. W., Kimmel, S. R., Ullmann, B., and Schilling, T. F. (1995). Stages of Embryonic Development of the Zebrafish. *Dev. Dyn.* 203: 253–310. doi:10.1002/aja.1002030302

Kuang, M. T., Li, J. Y., Yang, X. B., Yang, L., Xu, J. Y., Yan, S., et al. (2020). Structural Characterization and Hypoglycemic Effect via Stimulating Glucagon-like Peptide-1 Secretion of Two Polysaccharides from

Dendrobium officinale. *Carbohydr. Polym.* 241: 116326. doi:10.1016/j.carbpol.2020.116326

Li, M., Wang, I. X., Li, Y., Bruzel, A., Richards, A. L., Toung, J. M., et al. (2011). Widespread RNA and DNA Sequence Differences in the Human Transcriptome. *Science*. 333:53–58. doi:10.1126/science.1207018

Liang, J., Li, H., Chen, J., He, L., Du, X., Zhou, L., et al. (2019). *Dendrobium Officinale* Polysaccharides Alleviate colon Tumorigenesis via Restoring Intestinal Barrier Function and Enhancing Anti-tumor Immune Response. *Pharmacol. Res.* 148:104417. doi:10.1016/j.phrs.2019.104417

Luo, Q. L., Tang, Z. H., Zhang, X. F., Zhong, Y. H., Yao, S. Z., Wang, L. S., et al. (2016). Chemical Properties and Antioxidant Activity of a Water-Soluble Polysaccharide from *Dendrobium officinale*. *Int. J. Biol. Macromol.* 89: 219–227. doi:10.1016/j.ijbiomac.2016.04.067

Mao, X., Cai, T., Olyarchuk, J. G., and Wei, L. (2005). Automated Genome Annotation and Pathway Identification Using the KEGG Orthology (KO) as a Controlled Vocabulary. *Bioinformatics*. 21:3787–3793. doi:10.1093/bioinformatics/bti430

Ng, T. B., Liu, J., Wong, J. H., Ye, X., Wing Sze, S. C., Tong, Y., et al. (2012). Review of Research on *Dendrobium*, a Prized Folk Medicine. *Appl. Microbiol. Biotechnol.* 93:1795–1803. doi:10.1007/s00253-011-3829-7

Qi, W., Zhou, X., Wang, J., Zhang, K., Zhou, Y., Chen, S., et al. (2020). *Cordyceps Sinensis* Polysaccharide Inhibits colon Cancer Cells Growth by Inducing Apoptosis and Autophagy Flux Blockage via mTOR Signaling. *Carbohydr. Polym.* 237:116113. doi:10.1016/j.carbpol.2020.116113

Ren, D., Wang, N., Guo, J., Yuan, L., and Yang, X. (2016). Chemical Characterization of *Pleurotus Eryngii* Polysaccharide and its Tumor-Inhibitory Effects against Human Hepatoblastoma HepG-2 Cells. *Carbohydr. Polym.* 138:123–133. doi:10.1016/j.carbpol.2015.11.051

Ren, F., Li, J., Yuan, X., Wang, Y., Wu, K., Kang, L., et al. (2019). Dandelion Polysaccharides Exert Anticancer Effect on Hepatocellular Carcinoma by Inhibiting PI3K/AKT/mTOR Pathway and Enhancing Immune Response. *J. Funct. Foods.* 55:263–274. doi:10.1016/j.jff.2019.02.034

Rieu, I., and Powers, S. J. (2009). Real-time Quantitative RT-PCR: Design, Calculations, and Statistics. *Plant Cell*. 21:1031–1033. doi:10.1105/tpc.109.066001

Robinson, M. D., McCarthy, D. J., and Smyth, G. K. (2010). edgeR: a Bioconductor Package for Differential Expression Analysis of Digital Gene Expression Data. *Bioinformatics*. 26:139–140. doi:10.1093/bioinformatics/btp616

Sun, M., Bu, R., Zhang, B., Cao, Y., Liu, C., and Zhao, W. (2020). Lentinan Inhibits Tumor Progression by Immunomodulation in a Mouse Model of Bladder Cancer. *Integr. Cancer Ther.* 19, 1–7. doi:10.1177/1534735420946823

Tao, S., Huang, C., Tan, Z., Duan, S., Zhang, X., Ren, Z., et al. (2021). Effect of the Polysaccharides Derived from *Dendrobium Officinale* Stems on Human HT-29 Colorectal Cancer Cells and a Zebrafish Model. *Food Biosci.* 41:100995. doi:10.1016/j.fbio.2021.100995

Tao, S., Lei, Z., Huang, K., Li, Y., Ren, Z., Zhang, X., et al. (2019). Structural characterization and immunomodulatory activity of two novel polysaccharides derived from the stem of *Dendrobium officinale* Kimura et Migo. *J. Funct. Foods.* 57:121–134. doi:10.1016/j.jff.2019.04.013

Wang, E. T., Sandberg, R., Luo, S., Khrebtukova, I., Zhang, L., Mayr, C., et al. (2008). Alternative Isoform Regulation in Human Tissue Transcriptomes. *Nature*. 456:470–476. doi:10.1038/nature07509

Wang, K.-p., Wang, J., Li, Q., Zhang, Q.-l., You, R.-x., Cheng, Y., et al. (2014). Structural Differences and Conformational Characterization of Five Bioactive Polysaccharides from *Lentinus edodes*. *Food Res. Int.* 62:223–232. doi:10.1016/j.foodres.2014.02.047

Wang, K., Wang, H., Liu, Y., Shui, W., Wang, J., Cao, P., et al. (2018). *Dendrobium Officinale* Polysaccharide Attenuates Type 2 Diabetes Mellitus via the Regulation of PI3K/Akt-Mediated Glycogen Synthesis and Glucose Metabolism. *J. Funct. Foods.* 40:261–271. doi:10.1016/j.jff.2017.11.004

Wang, Q., Miao, Y., Xu, Y., Meng, X., Cui, W., Wang, Y., et al. (2019). Taishan *Pinus Massoniana* Pollen Polysaccharide Inhibits the Replication of Acute Tumorigenic ALV-J and its Associated Tumor Growth. *Vet. Microbiol.* 236: 108376. doi:10.1016/j.vetmic.2019.07.028

Wasser, S. P. (2002). Medicinal Mushrooms as a Source of Antitumor and Immunomodulating Polysaccharides. *Appl. Microbiol. Biotechnol.* 60: 258–274. doi:10.1007/s00253-002-1076-7

Wei, W., Li, Z. P., Zhu, T., Fung, H. Y., Wong, T. L., Wen, X., et al. (2017). Anti-Fatigue Effects of the Unique Polysaccharide Marker of *Dendrobium Officinale* on BALB/c Mice. *Molecules*. 22:155. doi:10.3390/molecules22010155

Xu, Z., Hu, C., Chen, S., Zhang, C., Yu, J., Wang, X., et al. (2019). Apatinib Enhances Chemosensitivity of Gastric Cancer to Paclitaxel and 5-fluorouracil. *Cancer Manag. Res.* 11:4905–4915. doi:10.2147/CMAR.S196372

Xu, Z., Li, X., Feng, S., Liu, J., Zhou, L., Yuan, M., et al. (2016). Characteristics and Bioactivities of Different Molecular Weight Polysaccharides from *Camellia* Seed Cake. *Int. J. Biol. Macromol.* 91:1025–1032. doi:10.1016/j.ijbiomac.2016.06.067

Young, M. D., Wakefield, M. J., Smyth, G. K., and Oshlack, A. (2010). Gene Ontology Analysis for RNA-Seq: Accounting for Selection Bias. *Genome Biol.* 11:R14. doi:10.1186/gb-2010-11-2-r14

Yu, W., Ren, Z., Zhang, X., Xing, S., Tao, S., Liu, C., et al. (2018a). Structural Characterization of Polysaccharides from *Dendrobium Officinale* and Their Effects on Apoptosis of HeLa Cell Line. *Molecules*. 23:2484. doi:10.3390/molecules23102484

Yu, X., Zhou, C., Yang, H., Huang, X., Ma, H., Qin, X., et al. (2015). Effect of Ultrasonic Treatment on the Degradation and Inhibition Cancer Cell Lines of Polysaccharides from *Porphyra yezoensis*. *Carbohydr. Polym.* 117:650–656. doi:10.1016/j.carbpol.2014.09.086

Yu, Y., Shen, M., Song, Q., and Xie, J. (2018b). Biological Activities and Pharmaceutical Applications of Polysaccharide from Natural Resources: A Review. *Carbohydr. Polym.* 183:91–101. doi:10.1016/j.carbpol.2017.12.009

Zhang, X., Luo, Y., Wei, G., Li, Y., Huang, Y., Huang, J., et al. (2019). Physicochemical and Antioxidant Properties of the Degradations of Polysaccharides from *Dendrobium Officinale* and Their Suitable Molecular Weight Range on Inducing HeLa Cell Apoptosis. *Evid. Based Complement. Alternat. Med.* 2019, 1–11. doi:10.1155/2019/4127360

Zhang, X., Qi, C., Guo, Y., Zhou, W., and Zhang, Y. (2016). Toll-like Receptor 4-related Immunostimulatory Polysaccharides: Primary Structure, Activity Relationships, and Possible Interaction Models. *Carbohydr. Polym.* 149: 186–206. doi:10.1016/j.carbpol.2016.04.097

Zhang, X., Ruan, Z., You, X., Wang, J., Chen, J., Peng, C., et al. (2017). *De Novo* assembly and Comparative Transcriptome Analysis of the Foot from Chinese green Mussel (*Perna Viridis*) in Response to Cadmium Stimulation. *Plos One.* 12:e0176677. doi:10.1371/journal.pone.0176677

Zhang, X., Duan, S., Tao, S., Huang, J., Liu, C., Xing, S., et al. (2020). Polysaccharides from *Dendrobium Officinale* Inhibit Proliferation of Osteosarcoma Cells and Enhance Cisplatin-Induced Apoptosis. *J. Funct. Foods.* 73:104143. doi:10.1016/j.jff.2020.104143

Zhang, Y., Li, S., Wang, X., Zhang, L., and Cheung, P. C. K. (2011). Advances in Lentinan: Isolation, Structure, Chain Conformation and Bioactivities. *Food Hydrocolloids*. 25:196–206. doi:10.1016/j.foodhyd.2010.02.001

Zhou, L., Liu, Z., Wang, Z., Yu, S., Long, T., Zhou, X., et al. (2017). *Astragalus* Polysaccharides Exerts Immunomodulatory Effects via TLR4-Mediated MyD88-dependent Signaling Pathway *In Vitro* and *In Vivo*. *Sci. Rep.* 7: 44822. doi:10.1038/srep44822

Conflict of Interest: The authors declare that the research was conducted in the absence of any commercial or financial relationships that could be construed as a potential conflict of interest.

Publisher's Note: All claims expressed in this article are solely those of the authors and do not necessarily represent those of their affiliated organizations, or those of the publisher, the editors, and the reviewers. Any product that may be evaluated in this article, or claim that may be made by its manufacturer, is not guaranteed or endorsed by the publisher.

GLOSSARY

APS *Astragalus membranaceus* polysaccharides

CRC Colorectal cancer

DEGs Differentially expressed genes

D. officinale *Dendrobium officinale* Kimura & Migo

DOPW-1 *Dendrobium officinale* Kimura & Migo polysaccharide

FPKM Fragments per kilobase of transcript per million mapped

GO Gene Ontology

KOG Clusters of protein homology

KEGG Kyoto Encyclopedia of Genes and Genomes

LNT *Lentinus edodes* polysaccharides

MTC maximum tolerance concentration

Mw molecular weight

RNA-seq RNA sequencing

frontiers in Pharmacology

ORIGINAL RESEARCH
published: 09 December 2021
doi: 10.3389/fphar.2021.784187

Burdock Fructooligosaccharide Attenuates High Glucose-Induced Apoptosis and Oxidative Stress Injury in Renal Tubular Epithelial Cells

Mengru Ding[1†], *Zhiyan Tang*[1†], *Wei Liu*[1], *Taili Shao*[1,2,3], *Pingchuan Yuan*[1,2,3], *Kaoshan Chen*[1,2,3], *Yuyan Zhou*[1,2,3], *Jun Han*[1,2,3]*, *Jing Zhang*[4]* and *Guodong Wang*[1,2,3]*

[1]*Drug Research and Development Center, School of Pharmacy, Wannan Medical College, Wuhu, China,* [2]*Anhui Provincial Engineering Laboratory for Screening and Re-evaluation of Active Compounds of Herbal Medicines, Anhui Provincial Engineering Research Center for Polysaccharide Drugs, Wuhu, China,* [3]*Anhui Province Key Laboratory of Active Biological Macromolecules, Wuhu, China,* [4]*Department of Nephrology, The First Affiliated Hospital, Yijishan Hospital of Wannan Medical College, Wuhu, China*

OPEN ACCESS

Edited by:
Jing Zhao,
University of Macau, China

Reviewed by:
Haci Ahmet Deveci,
University of Gaziantep, Turkey
Acharaporn Duangjai,
University of Phayao, Thailand

***Correspondence:**
Jun Han
hanjun@wnmc.edu.cn
Jing Zhang
jingzhang721@163.com
Guodong Wang
wangguodong@wnmc.edu.cn

[†]*These authors have contributed equally to this work*

Specialty section:
This article was submitted to Ethnopharmacology, a section of the journal Frontiers in Pharmacology

Received: *27 September 2021*
Accepted: *26 November 2021*
Published: *09 December 2021*

Citation:
Ding M, Tang Z, Liu W, Shao T, Yuan P, Chen K, Zhou Y, Han J, Zhang J and Wang G (2021) Burdock Fructooligosaccharide Attenuates High Glucose-Induced Apoptosis and Oxidative Stress Injury in Renal Tubular Epithelial Cells. Front. Pharmacol. 12:784187. doi: 10.3389/fphar.2021.784187

Hyperglycemia-induced apoptosis and oxidative stress injury are thought to play important roles in the pathogenesis of diabetic nephropathy (DN). Attenuating high glucose (HG)-induced renal tubular epithelial cell injury has become a potential approach to ameliorate DN. In recent years, burdock fructooligosaccharide (BFO), a water-soluble inulin-type fructooligosaccharide extracted from burdock root, has been shown to have a wide range of pharmacological activities, including antiviral, anti-inflammatory, and hypolipidemic activities. However, the role and mechanism of BFO in rat renal tubular epithelial cells (NRK-52E cells) have rarely been investigated. The present study investigated the protective effect of BFO on HG-induced damage in NRK-52E cells. BFO could protect NRK-52E cells against the reduced cell viability and significantly increased apoptosis rate induced by HG. These anti-oxidative stress effects of BFO were related to the significant inhibition of the production of reactive oxygen species, stabilization of mitochondrial membrane potential, and increased antioxidant (superoxide dismutase and catalase) activities. Furthermore, BFO increased the expression of Nrf2, HO-1, and Bcl-2 and decreased the expression of Bax. In conclusion, these findings suggest that BFO protects NRK-52E cells against HG-induced damage by inhibiting apoptosis and oxidative stress through the Nrf2/HO-1 signaling pathway.

Keywords: burdock fructooligosaccharide, NRK-52E cells, high glucose, apoptosis, oxidative stress

INTRODUCTION

Diabetic nephropathy (DN) is the most common chronic kidney disease and a common cause of end-stage renal disease (Johansen et al., 2021). In the past 20 years, the morbidity and mortality of DN have increased significantly in the global population (Bell et al., 2015; Heerspink et al., 2019). The histological features of DN mainly include mesangial expansion, glomerular basement membrane thickening, and podocyte loss (Lin and Susztak, 2016). Currently, the main treatment for DN is to control blood glucose level and blood pressure to delay the development of the disease; however, the effect is not satisfactory (Hsiao et al., 2019). Furthermore, studies that attempted to clarify specific mechanisms leading to the progression of DN remain inconclusive. Although the specific mechanism of DN has not

been identified, hyperglycemia is thought to be a potential trigger of renal tubular cell damage (Wang et al., 2017; Zhang YH. et al., 2020; Das et al., 2020).

The occurrence and development of DN are related to oxidative stress and apoptosis caused by hyperglycemia (Chen et al., 2019; Calle and Hotter, 2020). High glucose (HG) can reduce the ability of the cell's antioxidant enzyme system, increase cell apoptosis rate, and promote reactive oxygen species (ROS) overproduction in renal tubular epithelial cells (He et al., 2015; Lee et al., 2019), thereby causing cell oxidative stress damage. Therefore, regulation of oxidative stress and cell apoptosis is an important approach to attenuate HG-induced injury in renal cells. Nuclear factor erythroid 2–related factor 2 (Nrf2) is a transcriptional regulator and an important cell defense factor (Qaisiya et al., 2014). The Nrf2 signaling pathway plays a critical role in apoptosis and oxidative stress (Nezu et al., 2017) and is also the main antioxidant signaling pathway (Nezu et al., 2017). Nrf2 is considered to be a potential therapeutic target for DN (Tong et al., 2019). Activated Nrf2 can reduce oxidative stress damage, thereby resisting DN *in vivo* and *in vitro* (Zhang et al., 2014; Shin et al., 2019).

Burdock (*Arctium lappa L.*) is a common herb and health supplement in Asia (Gao Q. et al., 2018). Burdock fructooligosaccharide (BFO), a reserve carbohydrate, is a water-soluble inulin-type fructooligosaccharide extracted from burdock root, which consists of a linear chain of α-2,1-linked fructofuranose residues with a single β-1,2-linked glucopyranose (Hao et al., 2005; Wang Y. et al., 2019). Studies have shown that BFO has a wide range of pharmacological activities. BFO has antioxidant properties and the ability to scavenge free radicals (Jiang et al., 2019), it can significantly regulate lipid metabolism in diabetic rats (Li et al., 2019) and exert antithrombotic effects via regulating the ERK/NF-κB pathway (Qiu et al., 2020), and it has anti-inflammatory effects *in vivo* and *in vitro* (Zhang et al., 2019; Zhang X. et al., 2020), as well as anti-cancer effects (Xu et al., 2019). BFO can also lower fasting blood glucose (FBG) levels and improve glucose tolerance (Gao Y. et al., 2018; Annunziata et al., 2019; Yuan et al., 2021). However, no research has addressed the role of BFO in ameliorating NRK-52E cell apoptosis and oxidative stress injury induced by HG. Therefore, this study aimed to investigate the effects of BFO on NRK-52E cell injury induced by HG.

MATERIALS AND METHODS

Materials and Reagents

Rat renal tubular epithelial cells (NRK-52E cells) were purchased from the National Laboratory Cell Resource Sharing Platform (Beijing, China). Burdock roots were obtained from Yishunkang (Jiangsu, China). The kits for superoxide dismutase (SOD) and catalase (CAT) were acquired from Jiancheng Bioengineering Institute (Nanjing, Jiangsu, China). BCA protein assay kit, ROS assay kit and mitochondrial membrane potential detection kit were acquired from Beyotime Institute of Biotechnology (Haimen, Jiangsu, China). Antibodies specific for Nrf2, HO-1, Bcl-2, Bax, and β-actin were obtained from ABclonal (Wuhan, Hubei, China).

Burdock Fructooligosaccharide Preparation and Fractionation

BFO was isolated and fractionated following our previously reported method (Hao et al., 2005; Yuan et al., 2021). Briefly, burdock roots were submerged in hot water and 95% ethanol for alcohol precipitation. The precipitate was dissolved in distilled water and deproteinized using the Sevag method (Sevag, 1938). The aqueous phase was collected and decolorized using D101 macroporous resin (Solarbio, Beijing, China), followed by loading onto a DEAE-cellulose-52 chromatographic column (Solarbio). The collected fractions were filtered using a 0.22-μm filter membrane, inserted in a 1 kDa regenerated cellulose dialysis bag (Solarbio), and dialyzed at 4°C for 72 h. Then, BFO was further purified by gel filtration chromatography on a Sephadex G75 column (Solarbio) and eluted with distilled water at a flow rate of 0.5 ml/min. The homogeneous fractions from the eluted single peak were gathered, concentrated, and lyophilized to powder (BFO). The homogeneity and molecular weight of BFO were determined by high performance gel permeation chromatography (HPGPC) on a Shimadzu Lc-l0Avp instrument (Shimadzu, Japan) equipped with an Ultrahydrogel™ liner column. Elution was monitored using a Shimadzu RID-10A refractive index detector. A series of standard dextran solutions was run under the same conditions and a standard curve linear over a wide range (1–10 kDa) was obtained by correlation analysis between the dextran standard molar mass and retention time (Liu et al., 2014). The total sugar content of BFO was measured as D-fructose equivalents using the phenol-sulfuric acid method (Dubois et al., 1956). The presence of starch-type polysaccharides was detected using the triiodination reaction (Liu et al., 2018). The Bradford method was adapted to determine the total protein content using bovine serum albumin (BSA) as the standard (Bradford, 1976).

Cell Culture and Drug Dissolution

NRK-52E cells were maintained in Dulbecco's modified Eagle's medium (DMEM) (Gibco, CA, United States) supplemented with 10% fetal bovine serum and 1% penicillin/streptomycin in a humidified atmosphere of 5% CO_2 at 37°C. The cells were digested and passaged every 1–2 days and seeded into 6- or 96-well plates for experiments. BFO was dissolved in phosphate-buffered saline to prepare the stock solution.

Cell Viability Assay

NRK-52E cells were cultured in normal glucose (NG, 5.5 mM glucose), HG (30 mM glucose), and HG + different BFO concentrations (62.5, 125, and 250 μg/ml) for 48 h using 96-well plates. Then, CCK-8 kit reagent was added to wells and then the plates were incubated at 37°C for 1–2 h. A microplate reader (Biotek, Winooski, VT, United States) was used to measure the absorbance at 450 nm.

Cell Apoptosis

NRK-52E cells were subjected to the various culture conditions described above. Thereafter, 5 μL of propidium iodide and 10 μL of Annexin V-fluorescein isothiocyanate (FITC) were added to

TABLE 1 | Primers used for quantitative real-time PCR.

Gene	Forward (5'-3')	Reverse (5'-3')
Nrf2	AATTGCCACCGCCAGGACT	TCAAACACTTCTCGACTTACCCC
HO-1	CAGCATGTCCCAGGATTTGTC	CCTGACCCTTCTGAAAGTTCCTC
Bax	ATGGGCTGGACACTGGACTT	TTCCAGATGGTGAGTGAGGCA
Bcl-2	TTGTGGCCTTCTTTGAGTTCG	GCATCCCAGCCTCCGTTAT
GAPDH	CTGGAGAAACCTGCCAAGTATG	GGTGGAAGAATGGGAGTTGCT

each sample for 15 min at room temperature (RT) in the dark, followed by the addition of 500 μL binding buffer and filtration through a 300 μm mesh cell filter. Finally, flow cytometry was performed immediately.

Detection of Intracellular Reactive Oxygen Species Levels

NRK-52E cells were cultured with different substances, as described previously. Samples were then incubated with DCFH-DA for 30 min at 37°C. The percentage of fluorescently positive cells was measured by flow cytometry at 488 nm excitation wavelength and 525 nm emission wavelength.

Measurement of Mitochondrial Membrane Potential

NRK-52E cells were cultured with different substances, as described previously. Thereafter, JC-1 dyeing working solution was added to the samples, mixed well, and incubated at 37°C for 20 min. At the end of the treatment, JC-1 fluorescence was measured by flow cytometry at 490 nm excitation wavelength and 530 nm emission wavelength.

Antioxidant System Assay

NRK-52E cells were exposed to different substances, as described previously. The levels of SOD and CAT were determined using relevant detection kits according to the manufacturer's instructions. At the end of the reaction, a microplate reader was used to measure the absorbance of the samples.

Western Blotting

NRK-52E cells were incubated with different substances, as described previously. The protein concentration was determined using a BCA protein assay kit, and the denatured protein was separated on SDS-PAGE gel. Protein was transferred to a nitrocellulose membrane under constant current (300 mA) conditions, and then the membrane was blocked with 5% skim milk at RT for 2 h. The membranes were incubated with Nrf2 (1: 2000), HO-1 (1:500), Bax (1:1000), and Bcl-2 (1:1000) antibodies at 4°C overnight. Next, the membranes were washed with TBST (3 × 10 min) and then incubated with the secondary antibodies (1: 10,000) for 1 h. ECL detection reagent and a chemiluminescence imaging system were used to examine the membranes. The results were analyzed using the ImageJ software.

RNA Extraction and Quantitative Real-Time PCR

Total RNA was isolated from NRK-52E cells using TRIzol reagent (Beyotime), and cDNA was synthesized from total RNA using Prime Script RT kit (Thermo Fisher Scientific, Waltham, MA, United States) according to the manufacturer's instructions. GAPDH was used as an internal standard. The primer pairs used for real-time PCR are shown in **Table 1**. The cycle threshold (Ct) value was determined, and the level of the housekeeping gene GAPDH was used for normalization. The relative mRNA level of each target gene was calculated with the $2^{-\triangle\triangle}$Ct method.

Statistical Analysis

Statistical analysis was conducted with SPSS 22.0. Data are shown as the mean ± standard deviation. Differences among groups were compared by one-way analysis of variance, followed by Dunnett's post hoc test. $p < 0.05$ was considered statistically significant.

RESULTS

Isolation and Purification of Burdock Fructooligosaccharide

The elution curve of gel filtration chromatography on a Sephadex G75 column presented BFO as a single component (**Figure 1A**). The total sugar content of BFO was determined to be 99.7%. After concentration and lyophilization, BFO presented as a white powder and tested negative for the triiodide reaction, indicating the absence of starch-type polysaccharides. The Bradford test result was negative with no absorption at 280 or 260 nm, suggesting the absence of proteins and nucleic acids in BFO. The homogeneity and molecular weight of BFO were determined by high-performance gel permeation chromatography (HPGPC). The retention time and purity of BFO were 12.366 min and 99.753%, respectively. BFO presented a single and symmetrically sharp peak (**Figure 1B**), indicating a homogenous fraction with a molecular weight of 3,194 Da.

Burdock Fructooligosaccharide Increased the Cell Viability of NRK-52E Cells Under High Glucose Condition

The CCK-8 assay was conducted to investigate the effect of BFO on the viability of NRK-52E cells under HG condition. The cell

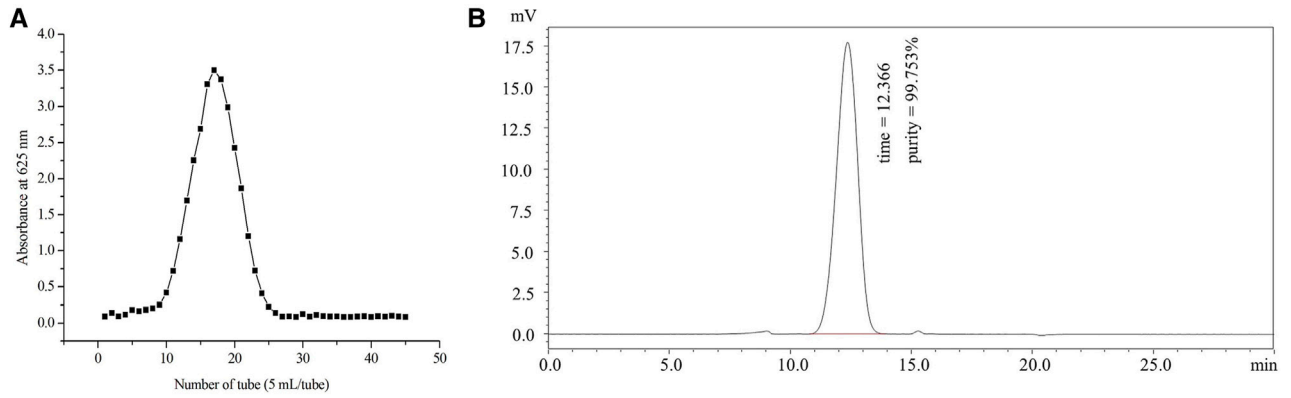

FIGURE 1 | Preparation and fractionation of BFO. **(A)** Elution curve of gel filtration chromatography on a Sephadex G75 column. **(B)** Molecular weight and homogeneity of BFO determined by HPGPC.

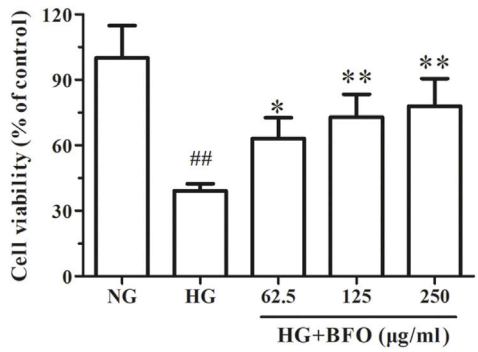

FIGURE 2 | Effect of BFO on the viability of NRK-52E cells. The cell viability was determined by a Cell Counting Kit-8 (CCK-8) test of NRK-52E cells cultured with high glucose (HG) and different concentrations of BFO. All data are expressed as the mean ± SD. $^{\#\#}p < 0.01$ vs. normal glucose (NG), $^{*}p < 0.05$ vs. HG, $^{**}p < 0.01$ vs. HG.

viability of the HG group was significantly reduced compared to that of the NG group. Conversely, when NRK-52E cells were incubated with HG + different BFO concentrations (62.5, 125, and 250 μg/ml), the cell viability increased (63.16, 72.97, and 77.98% of the control value, respectively) (**Figure 2**).

Burdock Fructooligosaccharide Reduced the Apoptosis Rate of NRK-52E Cells Under High Glucose Condition

To study the effect of BFO on the apoptosis rate of NRK-52E cells under HG condition, the cell apoptosis rate was measured by flow cytometry. The apoptosis rate of the cells cultured with NG, HG, and HG + different BFO concentrations (62.5, 125, and 250 μg/ml) were 7.183 ± 1.230; 30.210 ± 1.741; and 20.719 ± 1.280, 16.510 ± 1.697, and 10.84 ± 0.172%, respectively. The apoptosis rate of the HG group was significantly higher than that of the NG group. Conversely, compare with HG, the intervention with HG + different BFO concentrations significantly reduced the cell apoptosis rate (**Figure 3**).

Burdock Fructooligosaccharide Reduced the ROS Level of NRK-52E Cells Under High Glucose Condition

The DCFH-DA method was used to measure ROS level in NRK-52E cells exposed to HG and HG + different BFO concentrations. The results indicated that the ROS level of the HG group was higher than that of the NG group. Compare with HG, the intervention with HG + different BFO concentrations significantly reduced the level of ROS in a dose-dependent manner (**Figure 4**).

Burdock Fructooligosaccharide Decreased the Mitochondrial Membrane Potential of NRK-52E Cells Under High Glucose Condition

To elucidate the effect of BFO on the mitochondrial membrane potential in NRK-52E cells under HG condition, the mitochondrial membrane potential was determined by flow cytometry. The results demonstrated that in the HG group, the mitochondrial membrane potential was significantly decreased (**Figure 5**). The mitochondrial membrane potential of cells treated with HG + 62.5 μg/ml BFO did not increase significantly, and BFO at 125 and 250 μg/ml effectively inhibited the decrease in cell mitochondrial membrane potential induced by HG.

Burdock Fructooligosaccharide Increased the Levels of Superoxide Dismutase and Catalase in NRK-52E Cells Under High Glucose Condition

To elucidate whether BFO could protect NRK-52E cells against HG-induced oxidative stress damage, the activities of SOD and CAT were detected. The activities of SOD and CAT in the HG group were significantly lower than those in the NG group; both 125 μg/ml and 250 μg/ml BFO effectively inhibited the HG-induced reduction in SOD and CAT levels (**Figures 6A,B**).

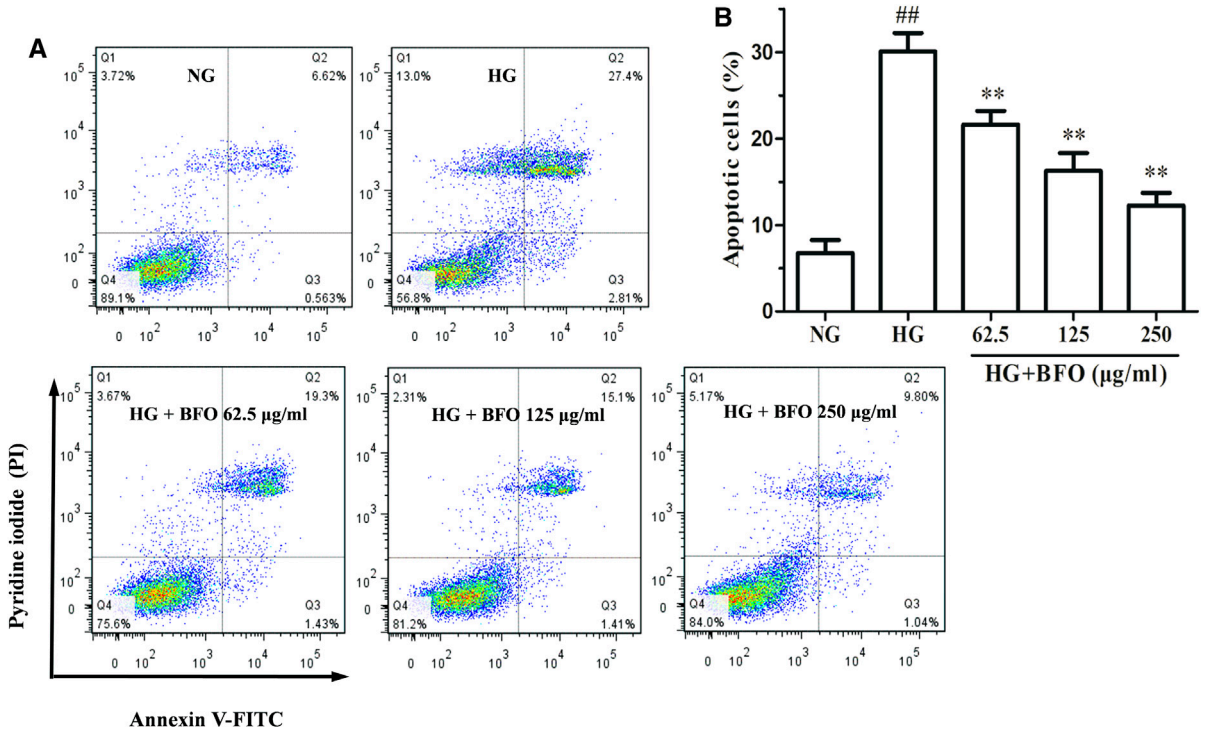

FIGURE 3 | Effect of BFO on apoptosis in NRK-52E cells. Apoptosis of NRK-52E cells cultured with high glucose (HG) and different concentrations of BFO was measured by Annexin V-FITC/PI staining. **(A)** Representative images of apoptotic NRK-52E cells determined *via* flow cytometry. **(B)** Quantification of apoptotic NRK-52E cells. All data are expressed as the mean ± SD. $^{\#\#}p < 0.01$ vs. normal glucose (NG), $^{**}p < 0.01$ vs. HG.

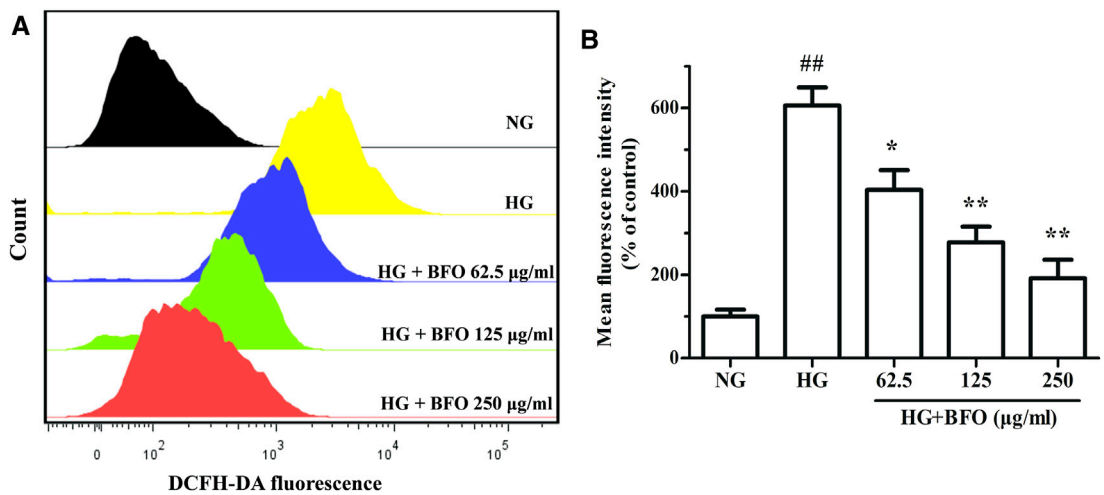

FIGURE 4 | Effect of BFO on the level of reactive oxygen species (ROS) in NRK-52E cells. **(A)** Representative images of ROS generation measured by flow cytometry using the DCFH-DA probe. **(B)** Histogram representing the quantitative analysis of ROS accumulation in NRK-52E cells. All data are expressed as the mean ± SD. $^{\#\#}p < 0.01$ vs. normal glucose (NG), $^{*}p < 0.05$ vs. HG, $^{**}p < 0.01$ vs. HG.

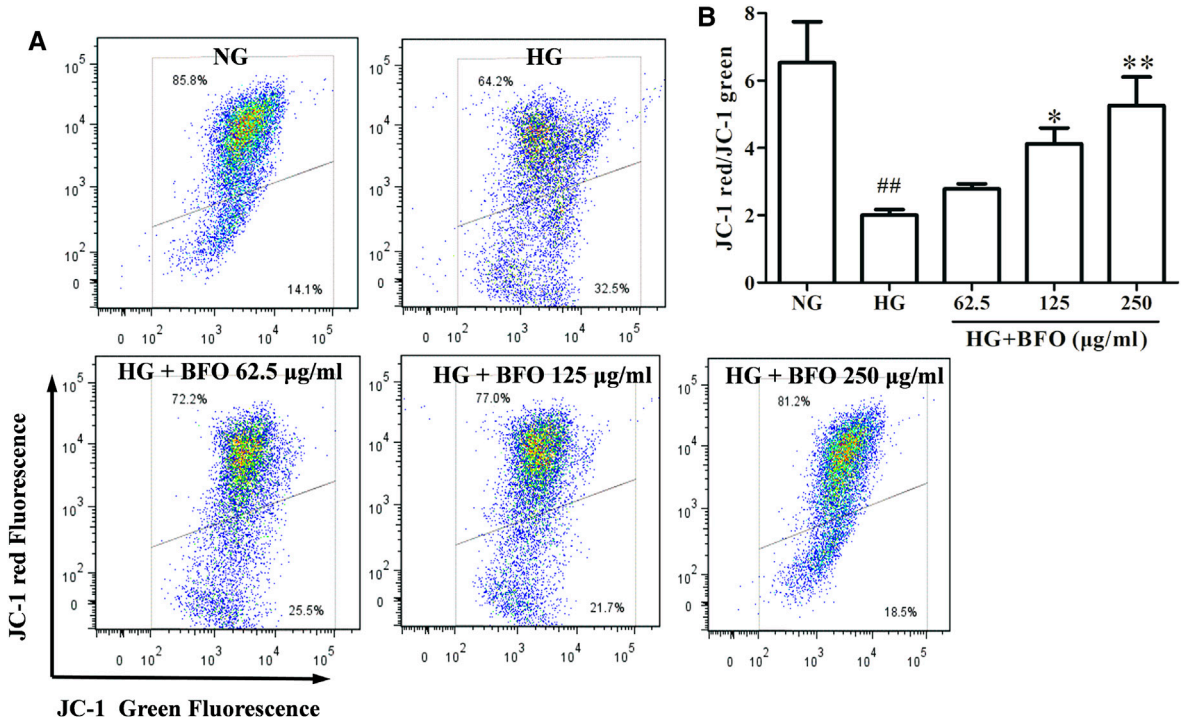

FIGURE 5 | Effect of BFO on mitochondrial membrane potential in NRK-52E cells. **(A)** Representative images of mitochondrial membrane potential determined by flow cytometry using the JC-1 probe. **(B)** Histogram representing the quantitative analysis of mitochondrial membrane potential in NRK-52E cells. All data are expressed as the mean ± SD. $^{\#\#}p < 0.01$ vs. normal glucose (NG), $^{*}p < 0.05$ vs. HG, $^{**}p < 0.01$ vs. HG.

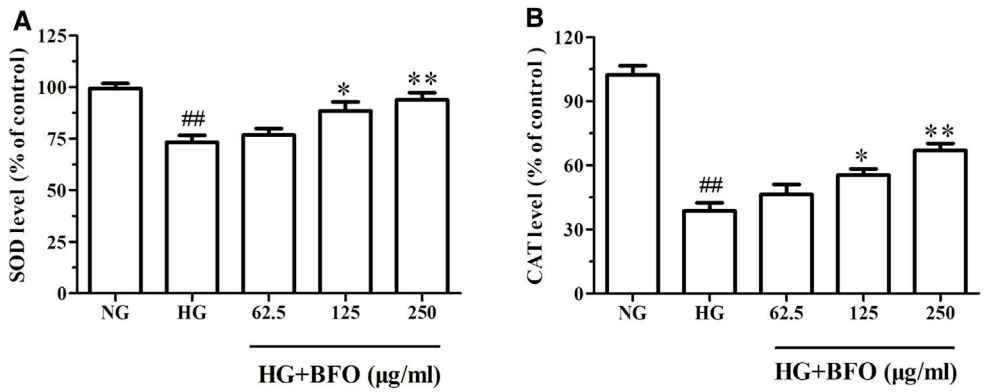

FIGURE 6 | Effect of BFO on SOD **(A)** and CAT **(B)** levels in NRK-52E cells. All data are expressed as the mean ± SD. $^{\#\#}p < 0.01$ vs. normal glucose (NG), $^{*}p < 0.05$ vs. HG, $^{**}p < 0.01$ vs. HG.

Burdock Fructooligosaccharide Affected Nrf2, HO-1, Bax, and Bcl-2 Protein and mRNA Expression in NRK-52E Cells Under High Glucose Condition

To observe the molecular mechanisms underlying the protective effects of BFO on NRK-52E cells, the protein and mRNA expression of Nrf2, HO-1, Bax, and Bcl-2 in NRK-52E cells induced by HG was determined by western blotting and real-time PCR, respectively. The protein levels of Bax in the HG group were significantly increased compared to those in the NG group, and the protein levels of Nrf2, HO-1, and Bcl-2 in the HG group were significantly decreased. In addition, the protein levels of Bax in the HG + BFO group were significantly decreased in a dose-dependent manner, and the protein levels of Nrf2, HO-1, and Bcl-2 in the HG + BFO group were significantly increased (**Figures**

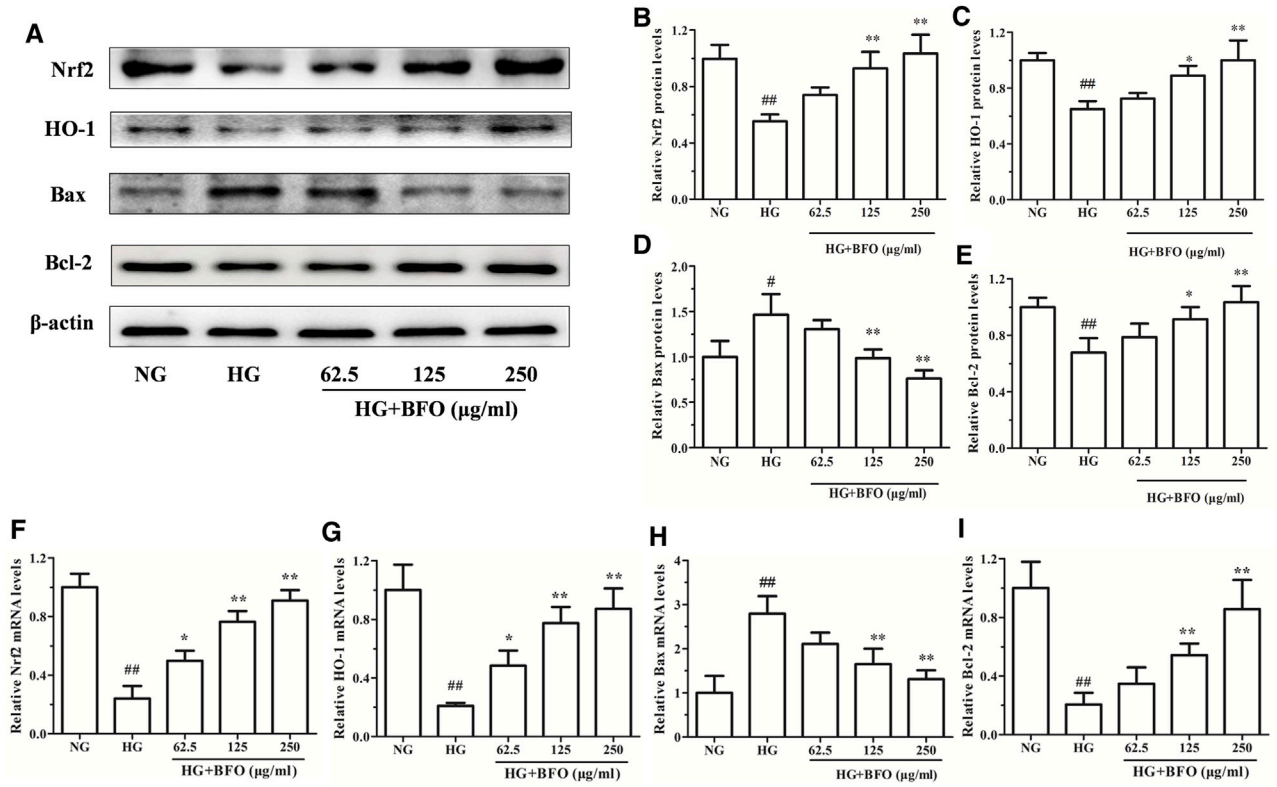

FIGURE 7 | Effect of BFO on the protein and mRNA expression in NRK-52E cells. **(A)** Representative bands of Nrf2, HO-1, Bax, and Bcl-2 obtained by western blotting. Relative protein levels (band density) of Nrf2 **(B)**, HO-1 **(C)**, Bax **(D)**, and Bcl-2 **(E)** were calculated by Image J. Relative mRNA levels of Nrf2 **(F)**, HO-1 **(G)**, Bax **(H)**, and Bcl-2 **(I)** in NRK-52E cells were determined by real-time PCR. All data are expressed as the mean ± SD. $^{\#}p < 0.05$ vs. normal glucose (NG), $^{\#\#}p < 0.01$ vs. NG, $^{*}p < 0.05$ vs. HG, $^{**}p < 0.01$ vs. HG.

7A–E). Furthermore, the mRNA expression of Nrf2, HO-1, Bax, and Bcl-2 in these groups was in accordance with the protein expression (**Figures 7F–I**).

DISCUSSION

In this study, we aimed to study the protective effect of BFO on NRK-52E cell apoptosis and oxidative stress induced by HG. Although the exact mechanism of HG-induced renal tubular epithelial cell injury has not yet been fully clarified, researches have shown that oxidative stress and apoptosis play important roles in the development and pathogenesis of DN (Tiong et al., 2019; Lee et al., 2020). NRK-52E cells cultured with HG are widely used as a DN model (Hou et al., 2014; Slyne et al., 2015). In addition, renal tubular epithelial cell injury is the main factor leading to DN. Some studies have shown that some plant polysaccharides can improve the oxidative stress damage caused by diabetes and its complications (Liao et al., 2019; Yang et al., 2020). BFO is a plant polysaccharide extracted from burdock that has been reported to exert antidiabetic effects (Yuan et al., 2021). Thus, we examined the effect of BFO on NRK-52E cell injury induced by HG and demonstrated that BFO has a protective effect on oxidative stress damage and apoptosis induced by HG *in vitro*. The protective effects of BFO were related to the inhibition of ROS, increase in mitochondrial membrane potential as well as CAT and SOD levels, and regulation of Bcl-2 and Bax protein expression. Furthermore, we also found that these protective effects depended on the regulation of the Nrf2/HO-1 signaling pathway.

Renal tubular epithelial cells undergo oxidative stress and apoptosis under HG, hypoxia, and other environments, leading to tubular interstitial fibrosis and even kidney failure in severe cases (Yao et al., 2017). Studies have found that under HG conditions, renal tubular epithelial cell viability is reduced, and apoptosis rate is increased (Lv et al., 2019). The DN model was constructed by culturing NRK-52E cells in DMEM medium containing 30 mM glucose. CCK-8 and Annexin V-FITC/PI double staining assays were used to measure the cell viability and cell apoptosis rate. Our results provided evidence that BFO significantly increased cell viability and decreased the apoptosis rate at 62.5–250 μg/ml concentrations at 48 h in an HG environment.

It has been reported that HG-induced oxidative stress in renal tubular epithelial cells plays a critical role in the pathogenesis of DN (Xie et al., 2019). Mitochondria are the main source of oxygen and ROS (Sinha et al., 2013). When mitochondria are challenged

by hyperglycemia, the mitochondrial membrane potential is affected, resulting in decreased mitochondrial membrane potential and increased ROS levels (Chen et al., 2018). Overproduction of ROS is known to be a major cause of oxidative stress and cell apoptosis (Volpe et al., 2018). Furthermore, ROS have been reported to play a key role in NRK-52E cell oxidative damage induced by HG (Tsikas, 2017). SOD and CAT are essential antioxidant enzymes in humans and animals that protect against oxidative stress (Altintas et al., 2010; Kehrer and Klotz, 2015). When the antioxidant defense system is destroyed, ROS production increases, thereby leading to ROS accumulation (Jha et al., 2016). Additionally, HG could result in oxidative injury, which eventually leads to the overproduction of ROS impairing cellular antioxidant systems (CAT and SOD) (Tong et al., 2018). Our current findings demonstrated that HG significantly decreased the mitochondrial membrane potential and resulted in ROS overproduction. In addition, the levels of SOD and CAT were decreased under HG conditions in NRK-52E cells. However, this change was partially reversed by BFO treatment in NRK-52E cells. These results proved that BFO might play a role in NRK-52E cell oxidative stress damage induced by HG.

Apoptosis is a type of programmed cell death that mainly occurs through the death receptor pathway and mitochondrial pathway (Xie et al., 2020). The Bax/Bcl-2 gene plays a key role in the process of apoptosis, and the pathway associated with it is the key pathway of cell apoptosis (Peña-Blanco and García-Sáez, 2018). Hyperglycemia can activate the apoptotic pathway and regulate the expression of apoptotic proteins, which play an important role in HG-induced renal tubular epithelial apoptosis (Wang Z. et al., 2019). Nrf2 is a transcriptional regulator, and under normal conditions, it binds to Keap1 in the cytoplasm. After external stimulation, Nrf2 dissociates from Keap1 and enters an activated state. Nrf2 enters the nucleus from the cytoplasm, regulates its downstream-related factors, and exerts an antioxidant effect (Eve et al., 2016; Figueroa and Wright, 2016). HO-1 is a downstream protein of Nrf2, which promotes the degradation of hemoglobin, effectively reducing inflammation and oxidative stress damage, thereby protecting cells (Humphries et al., 2016; Feng et al., 2019). Several researches have confirmed that the expression of Nrf2 and HO-1 proteins in renal tubular epithelial cells is downregulated by HG and that protein expression increases after administration of BFO (Zhou et al., 2019; Lu et al., 2020). To investigate the molecular mechanism underlying the effect of BFO in ameliorating NRK-52E cell oxidative stress and apoptosis *in vitro*, the protein expression of Bax, Bcl-2, Nrf2, and HO-1 in NRK-52E cells was detected. Bax expression increased after HG stimulation, and Bcl-2, Nrf2, and HO-1 expression decreased. BFO treatment reversed the effect of HG on the expression of Bax, Bcl-2, Nrf2, and HO-1, and prevented HG-induced oxidative stress and apoptosis in NRK-52E cells. Therefore, we speculate that BFO can prevent oxidative stress and apoptosis in renal tubular epithelial cells under HG conditions and that Nrf2-HO-1 plays an important role in NRK-52E cell damage induced by HG.

In conclusion, our experiments demonstrated that BFO increased cell viability and attenuated cell apoptosis and oxidative damage induced by HG in NRK-52E cells, and that the effect might be mediated through the Nrf2/HO-1 signaling pathway. Taken together, our results indicate that BFO may be an effective treatment for DN in clinical practice. However, the results of *in vitro* studies do not guarantee that BFO plays a similar role *in vivo*. In addition, the HG-induced diabetic nephropathy model is considerably different from naturally occurring diabetic nephropathy. Before clinical application, further in-depth research is needed to evaluate the anti-diabetic nephropathy effects of BFO.

DATA AVAILABILITY STATEMENT

The raw data supporting the conclusion of this article will be made available by the authors, without undue reservation.

AUTHOR CONTRIBUTIONS

JH, JZ, and GW conceived and designed the experiments. MD, ZT, and WL performed the experiments. YZ and TS analyzed the data. PY and KC provided some materials. MD, ZT, and GW wrote and edited the manuscript. All authors read and approved the manuscript.

FUNDING

This work was supported by Anhui Provincial Natural Science Foundation (1908085MH248), the Project of Anhui Provincial Engineering Research Center for Polysaccharide Drugs (WKGC202001), the Fund of Wannan Medical College (WK 2019F15), and the Natural Science Foundation of Education Department of Anhui Province (KJ2018ZD025, KJ2019ZD32, and KJ2020A0601).

REFERENCES

Altintas, L., Essiz, D., Eraslan, G., Ince, S., and Arslanbas, E. (2010). Prophylactic Effect of N-Acetylcysteine against Sodium Fluoride-Induced Blood Oxidative Stress in Mice. *Food Chem. Toxicol.* 48, 2838–2841. doi:10.1016/j.fct.2010.07.015

Annunziata, G., Barrea, L., Ciampaglia, R., Cicala, C., Arnone, A., Savastano, S., et al. (2019). Arctium Lappa Contributes to the Management of Type 2 Diabetes Mellitus by Regulating Glucose Homeostasis and Improving Oxidative Stress: A Critical Review of *In Vitro* and *In Vivo* Animal-Based Studies. *Phytother Res.* 33, 2213–2220. doi:10.1002/ptr.6416

Bell, S., Fletcher, E. H., Brady, I., Looker, H. C., Levin, D., Joss, N., et al. (2015). End-stage Renal Disease and Survival in People with Diabetes: a National Database Linkage Study. *QJM* 108, 127–134. doi:10.1093/qjmed/hcu170

Bradford, M. M. (1976). A Rapid and Sensitive Method for the Quantitation of Microgram Quantities of Protein Utilizing the Principle of Protein-Dye Binding. *Anal. Biochem.* 72, 248–254. doi:10.1006/abio.1976.9999

Calle, P., and Hotter, G. (2020). Macrophage Phenotype and Fibrosis in Diabetic Nephropathy. *Int. J. Mol. Sci.* 21, 2806. doi:10.3390/ijms21082806

Chen, M. F., Liou, S. S., Hong, T. Y., Kao, S. T., and Liu, I. M. (2018). Gigantol Has Protective Effects against High Glucose-Evoked Nephrotoxicity in Mouse Glomerulus Mesangial Cells by Suppressing ROS/MAPK/NF-κB Signaling Pathways. *Molecules* 24, 80. doi:10.3390/molecules24010080

Chen, M. F., Liou, S. S., Kao, S. T., and Liu, I. M. (2019). Erianin Protects against High Glucose-Induced Oxidative Injury in Renal Tubular Epithelial Cells. *Food Chem. Toxicol.* 126, 97–105. doi:10.1016/j.fct.2019.02.021

Das, N. A., Carpenter, A. J., Belenchia, A., Aroor, A. R., Noda, M., Siebenlist, U., et al. (2020). Empagliflozin Reduces High Glucose-Induced Oxidative Stress and miR-21-dependent TRAF3IP2 Induction and RECK Suppression, and Inhibits Human Renal Proximal Tubular Epithelial Cell Migration and Epithelial-To-Mesenchymal Transition. *Cell Signal* 68, 109506. doi:10.1016/j.cellsig.2019.109506

Dubois, M., Gilles, K. A., Hamilton, J. K., Rebers, P. A., and Smith, F. (1956). Colorimetric Method for Determination of Sugars and Related Substances. *Anal. Chem.* 28, 350–356. doi:10.1021/ac60111a017

Eve, D. J., Steele, M. R., Sanberg, P. R., and Borlongan, C. V. (2016). Hyperbaric Oxygen Therapy as a Potential Treatment for post-traumatic Stress Disorder Associated with Traumatic Brain Injury. *Neuropsychiatr. Dis. Treat.* 12, 2689–2705. doi:10.2147/NDT.S110126

Feng, Y., Cui, R., Li, Z., Zhang, X., Jia, Y., Zhang, X., et al. (2019). Methane Alleviates Acetaminophen-Induced Liver Injury by Inhibiting Inflammation, Oxidative Stress, Endoplasmic Reticulum Stress, and Apoptosis through the Nrf2/HO-1/NQO1 Signaling Pathway. *Oxid Med. Cell Longev* 2019, 7067619. doi:10.1155/2019/7067619

Figueroa, X. A., and Wright, J. K. (2016). Hyperbaric Oxygen: B-Level Evidence in Mild Traumatic Brain Injury Clinical Trials. *Neurology* 87, 1400–1406. doi:10.1212/WNL.0000000000003146

Gao, Q., Yang, M., and Zuo, Z. (2018a). Overview of the Anti-inflammatory Effects, Pharmacokinetic Properties and Clinical Efficacies of Arctigenin and Arctiin from Arctium Lappa L. *Acta Pharmacol. Sin* 39, 787–801. doi:10.1038/aps.2018.32

Gao, Y., Gu, C., Wang, K., Wang, H., Ruan, K., Xu, Z., et al. (2018b). The Effects of Hypoglycemia and Weight Loss of Total Lignans from Fructus Arctii in KKAy Mice and its Mechanisms of the Activity. *Phytother Res.* 32, 631–642. doi:10.1002/ptr.6003

Hao, L. H., Chen, L., Zhong, N., Chen, K. S., and Li, G. Y. (2005). Separation, Purification and Structure of Burdock Oligosaccharide. *Chem. J. Chin. Universities* 26, 1242–1247.

He, T., Guan, X., Wang, S., Xiao, T., Yang, K., Xu, X., et al. (2015). Resveratrol Prevents High Glucose-Induced Epithelial-Mesenchymal Transition in Renal Tubular Epithelial Cells by Inhibiting NADPH oxidase/ROS/ERK Pathway. *Mol. Cell Endocrinol* 402, 13–20. doi:10.1016/j.mce.2014.12.010

Heerspink, H. J. L., Parving, H. H., Andress, D. L., Bakris, G., Correa-Rotter, R., Hou, F. F., et al. (2019). Atrasentan and Renal Events in Patients with Type 2 Diabetes and Chronic Kidney Disease (SONAR): a Double-Blind, Randomised, Placebo-Controlled Trial. *Lancet* 393 (10184), 1937–1947. doi:10.1016/S0140-6736(19)30772-X

Hou, S., Zheng, F., Li, Y., Gao, L., and Zhang, J. (2014). The Protective Effect of Glycyrrhizic Acid on Renal Tubular Epithelial Cell Injury Induced by High Glucose. *Int. J. Mol. Sci.* 15, 15026–15043. doi:10.3390/ijms150915026

Hsiao, C. C., Huang, W. H., Cheng, K. H., and Lee, C. T. (2019). Low-Energy Extracorporeal Shock Wave Therapy Ameliorates Kidney Function in Diabetic Nephropathy. *Oxid Med. Cell Longev* 2019, 8259645. doi:10.1155/2019/8259645

Humphries, B., Wang, Z., and Yang, C. (2016). The Role of microRNAs in Metal Carcinogen-Induced Cell Malignant Transformation and Tumorigenesis. *Food Chem. Toxicol.* 98, 58–65. doi:10.1016/j.fct.2016.02.012

Jha, J. C., Banal, C., Chow, B. S., Cooper, M. E., and Jandeleit-Dahm, K. (2016). Diabetes and Kidney Disease: Role of Oxidative Stress. *Antioxid. Redox Signal.* 25, 657–684. doi:10.1089/ars.2016.6664

Jiang, Y. Y., Yu, J., Li, Y. B., Wang, L., Hu, L., Zhang, L., et al. (2019). Extraction and Antioxidant Activities of Polysaccharides from Roots of Arctium Lappa L. *Int. J. Biol. Macromol* 123, 531–538. doi:10.1016/j.ijbiomac.2018.11.087

Johansen, K. L., Chertow, G. M., Foley, R. N., Gilbertson, D. T., Herzog, C. A., Ishani, A., et al. (2021). US Renal Data System 2020 Annual Data Report: Epidemiology of Kidney Disease in the United States. *Am. J. Kidney Dis.* 77, A7–A8. doi:10.1053/j.ajkd.2021.01.002

Kehrer, J. P., and Klotz, L. O. (2015). Free Radicals and Related Reactive Species as Mediators of Tissue Injury and Disease: Implications for Health. *Crit. Rev. Toxicol.* 45, 765–798. doi:10.3109/10408444.2015.1074159

Lee, M., Zhao, H., Liu, X., Liu, D., Chen, J., Li, Z., et al. (2020). Protective Effect of Hydroxysafflor Yellow A on Nephropathy by Attenuating Oxidative Stress and Inhibiting Apoptosis in Induced Type 2 Diabetes in Rat. *Oxid Med. Cell Longev* 2020, 7805393. doi:10.1155/2020/7805393

Lee, W. C., Chau, Y. Y., Ng, H. Y., Chen, C. H., Wang, P. W., Liou, C. W., et al. (2019). Empagliflozin Protects HK-2 Cells from High Glucose-Mediated Injuries via a Mitochondrial Mechanism. *Cells* 8, 1085. doi:10.3390/cells8091085

Li, X., Zhao, Z., Kuang, P., Shi, X., Wang, Z., and Guo, L. (2019). Regulation of Lipid Metabolism in Diabetic Rats by Arctium Lappa L. Polysaccharide through the PKC/NF-κB Pathway. *Int. J. Biol. Macromol* 136, 115–122. doi:10.1016/j.ijbiomac.2019.06.057

Liao, Z., Zhang, J., Liu, B., Yan, T., Xu, F., Xiao, F., et al. (2019). Polysaccharide from Okra (Abelmoschus Esculentus (L.) Moench) Improves Antioxidant Capacity via PI3K/AKT Pathways and Nrf2 Translocation in a Type 2 Diabetes Model. *Molecules* 24, 1906. doi:10.3390/molecules24101906

Lin, J. S., and Susztak, K. (2016). Podocytes: the Weakest Link in Diabetic Kidney Disease? *Curr. Diab Rep.* 16, 45. doi:10.1007/s11892-016-0735-5

Liu, Q., Ge, X., Chen, L., Cheng, D., Yun, Z., Xu, W., et al. (2018). Purification and Analysis of the Composition and Antioxidant Activity of Polysaccharides from Helicteres Angustifolia L. *Int. J. Biol. Macromol* 107, 2262–2268. doi:10.1016/j.ijbiomac.2017.10.095

Liu, W., Wang, J., Zhang, Z., Xu, J., Xie, Z., Slavin, M., et al. (2014). *In Vitro* and *In Vivo* Antioxidant Activity of a Fructan from the Roots of Arctium Lappa L. *Int. J. Biol. Macromol* 65, 446–453. doi:10.1016/j.ijbiomac.2014.01.062

Lu, C., Fan, G., and Wang, D. (2020). Akebia Saponin D Ameliorated Kidney Injury and Exerted Anti-inflammatory and Anti-apoptotic Effects in Diabetic Nephropathy by Activation of NRF2/HO-1 and Inhibition of NF-KB Pathway. *Int. Immunopharmacol* 84, 106467. doi:10.1016/j.intimp.2020.106467

Lv, L., Li, D., Tian, F., Li, X., Jing Zhang, Z., and Yu, X. (2019). Silence of lncRNA GAS5 Alleviates High Glucose Toxicity to Human Renal Tubular Epithelial HK-2 Cells through Regulation of miR-27a. *Artif. Cells Nanomed Biotechnol* 47, 2205–2212. doi:10.1080/21691401.2019.1616552

Nezu, M., Souma, T., Yu, L., Suzuki, T., Saigusa, D., Ito, S., et al. (2017). Transcription Factor Nrf2 Hyperactivation in Early-phase Renal Ischemia-Reperfusion Injury Prevents Tubular Damage Progression. *Kidney Int.* 91, 387–401. doi:10.1016/j.kint.2016.08.023

Peña-Blanco, A., and García-Sáez, A. J. (2018). Bax, Bak and beyond - Mitochondrial Performance in Apoptosis. *FEBS J.* 285, 416–431. doi:10.1111/febs.14186

Qaisiya, M., Coda Zabetta, C. D., Bellarosa, C., and Tiribelli, C. (2014). Bilirubin Mediated Oxidative Stress Involves Antioxidant Response Activation via Nrf2 Pathway. *Cell Signal* 26, 512–520. doi:10.1016/j.cellsig.2013.11.029

Qiu, T., Zhou, H., Li, S., Tian, N., Li, Z., Wang, R., et al. (2020). Effects of Saccharides from Arctium Lappa L. Root on FeCl3-Induced Arterial Thrombosis via the ERK/NF-κB Signaling Pathway. *Oxid Med. Cell Longev* 2020, 7691352. doi:10.1155/2020/7691352

Sevag, M. G. (1938). The Presence of a Type-And Species-specific Conjugated Polysaccharide in Type I Pneumococcus. *Science* 87, 304–305. doi:10.1126/science.87.2257.304

Shin, J. H., Kim, K. M., Jeong, J. U., Shin, J. M., Kang, J. H., Bang, K., et al. (2019). Nrf2-Heme Oxygenase-1 Attenuates High-Glucose-Induced Epithelial-To-Mesenchymal Transition of Renal Tubule Cells by Inhibiting ROS-Mediated PI3K/Akt/GSK-3β Signaling. *J. Diabetes Res.* 2019, 2510105. doi:10.1155/2019/2510105

Sinha, K., Das, J., Pal, P. B., and Sil, P. C. (2013). Oxidative Stress: the Mitochondria-dependent and Mitochondria-independent Pathways of Apoptosis. *Arch. Toxicol.* 87, 1157–1180. doi:10.1007/s00204-013-1034-4

Slyne, J., Slattery, C., Mcmorrow, T., and Ryan, M. P. (2015). New Developments Concerning the Proximal Tubule in Diabetic Nephropathy: *In Vitro* Models and Mechanisms. *Nephrol. Dial. Transpl.* 30 (Suppl. 4), iv60–7. doi:10.1093/ndt/gfv264

Tiong, Y. L., Ng, K. Y., Koh, R. Y., Ponnudurai, G., and Chye, S. M. (2019). Melatonin Prevents Oxidative Stress-Induced Mitochondrial Dysfunction and Apoptosis in High Glucose-Treated Schwann Cells via Upregulation of Bcl2, NF-Kb, mTOR, Wnt Signalling Pathways. *Antioxidants (Basel)* 8, 198. doi:10.3390/antiox8070198

Tong, Y., Chuan, J., Bai, L., Shi, J., Zhong, L., Duan, X., et al. (2018). The Protective Effect of Shikonin on Renal Tubular Epithelial Cell Injury Induced by High Glucose. *Biomed. Pharmacother.* 98, 701–708. doi:10.1016/j.biopha.2017.12.112

Tong, Y., Liu, S., Gong, R., Zhong, L., Duan, X., and Zhu, Y. (2019). Ethyl Vanillin Protects against Kidney Injury in Diabetic Nephropathy by Inhibiting Oxidative Stress and Apoptosis. *Oxid Med. Cell Longev* 2019, 2129350. doi:10.1155/2019/2129350

Tsikas, D. (2017). Assessment of Lipid Peroxidation by Measuring Malondialdehyde (MDA) and Relatives in Biological Samples: Analytical and Biological Challenges. *Anal. Biochem.* 524, 13–30. doi:10.1016/j.ab.2016.10.021

Volpe, C. M. O., Villar-Delfino, P. H., Dos Anjos, P. M. F., and Nogueira-Machado, J. A. (2018). Cellular Death, Reactive Oxygen Species (ROS) and Diabetic Complications. *Cell Death Dis* 9, 119. doi:10.1038/s41419-017-0135-z

Wang, X., Meng, L., Zhao, L., Wang, Z., Liu, H., Liu, G., et al. (2017). Resveratrol Ameliorates Hyperglycemia-Induced Renal Tubular Oxidative Stress Damage via Modulating the SIRT1/FOXO3a Pathway. *Diabetes Res. Clin. Pract.* 126, 172–181. doi:10.1016/j.diabres.2016.12.005

Wang, Y., Zhang, N., Kan, J., Zhang, X., Wu, X., Sun, R., et al. (2019a). Structural Characterization of Water-Soluble Polysaccharide from Arctium Lappa and its Effects on Colitis Mice. *Carbohydr. Polym.* 213, 89–99. doi:10.1016/j.carbpol.2019.02.090

Wang, Z., Li, Y., Wang, Y., Zhao, K., Chi, Y., and Wang, B. (2019b). Pyrroloquinoline Quinine Protects HK-2 cells against High Glucose-Induced Oxidative Stress and Apoptosis through Sirt3 and PI3K/Akt/FoxO3a Signaling Pathway. *Biochem. Biophys. Res. Commun.* 508, 398–404. doi:10.1016/j.bbrc.2018.11.140

Xie, C., Wu, W., Tang, A., Luo, N., and Tan, Y. (2019). lncRNA GAS5/miR-452-5p Reduces Oxidative Stress and Pyroptosis of High-Glucose-Stimulated Renal Tubular Cells. *Diabetes Metab. Syndr. Obes.* 12, 2609–2617. doi:10.2147/DMSO.S228654

Xie, Q., Liu, Y., and Li, X. (2020). The Interaction Mechanism between Autophagy and Apoptosis in colon Cancer. *Transl Oncol.* 13, 100871. doi:10.1016/j.tranon.2020.100871

Xu, L., Lu, Y., Cong, Y., Zhang, P., Han, J., Song, G., et al. (2019). Polysaccharide Produced by Bacillus Subtilis Using Burdock Oligofructose as Carbon Source. *Carbohydr. Polym.* 206, 811–819. doi:10.1016/j.carbpol.2018.11.062

Yang, J., Chen, H., Nie, Q., Huang, X., and Nie, S. (2020). Dendrobium Officinale Polysaccharide Ameliorates the Liver Metabolism Disorders of Type II Diabetic Rats. *Int. J. Biol. Macromol* 164, 1939–1948. doi:10.1016/j.ijbiomac.2020.08.007

Yao, M., Gao, F., Wang, X., Shi, Y., Liu, S., and Duan, H. (2017). Nox4 Is Involved in High Glucose-Induced Apoptosis in Renal Tubular Epithelial Cells via Notch Pathway. *Mol. Med. Rep.* 15, 4319–4325. doi:10.3892/mmr.2017.6516

Yuan, P.-C., Shao, T.-L., Han, J., Liu, C.-Y., Wang, G.-D., He, S.-G., et al. (2021). Burdock Fructooligosaccharide as an α-glucosidase Inhibitor and its Antidiabetic Effect on High-Fat Diet and Streptozotocin-Induced Diabetic Mice. *J. Funct. Foods* 86, 104703. doi:10.1016/j.jff.2021.104703

Zhang, N., Wang, Y., Kan, J., Wu, X., Zhang, X., Tang, S., et al. (2019). *In Vivo* and *In Vitro* Anti-inflammatory Effects of Water-Soluble Polysaccharide from Arctium Lappa. *Int. J. Biol. Macromol* 135, 717–724. doi:10.1016/j.ijbiomac.2019.05.171

Zhang, X., Zhang, N., Kan, J., Sun, R., Tang, S., Wang, Z., et al. (2020a). Anti-inflammatory Activity of Alkali-Soluble Polysaccharides from Arctium Lappa L. And its Effect on Gut Microbiota of Mice with Inflammation. *Int. J. Biol. Macromol* 154, 773–787. doi:10.1016/j.ijbiomac.2020.03.111

Zhang, X., Zhao, Y., Chu, Q., Wang, Z. Y., Li, H., and Chi, Z. H. (2014). Zinc Modulates High Glucose-Induced Apoptosis by Suppressing Oxidative Stress in Renal Tubular Epithelial Cells. *Biol. Trace Elem. Res.* 158, 259–267. doi:10.1007/s12011-014-9922-x

Zhang, Y. H., Zhang, Y. Q., Guo, C. C., Wang, L. K., Cui, Y. J., Dong, J. J., et al. (2020b). Prostaglandin E1 Attenuates High Glucose-Induced Apoptosis in Proximal Renal Tubular Cells by Inhibiting the JNK/Bim Pathway. *Acta Pharmacol. Sin* 41, 561–571. doi:10.1038/s41401-019-0314-9

Zhou, J., Wang, T., Wang, H., Jiang, Y., and Peng, S. (2019). Obacunone Attenuates High Glucose-Induced Oxidative Damage in NRK-52E Cells by Inhibiting the Activity of GSK-3β. *Biochem. Biophys. Res. Commun.* 513, 226–233. doi:10.1016/j.bbrc.2019.03.201

Conflict of Interest: The authors declare that the research was conducted in the absence of any commercial or financial relationships that could be construed as a potential conflict of interest.

Publisher's Note: All claims expressed in this article are solely those of the authors and do not necessarily represent those of their affiliated organizations, or those of the publisher, the editors and the reviewers. Any product that may be evaluated in this article, or claim that may be made by its manufacturer, is not guaranteed or endorsed by the publisher.

frontiers in Pharmacology

ORIGINAL RESEARCH
published: 28 January 2022
doi: 10.3389/fphar.2021.806844

P. granatum Peel Polysaccharides Ameliorate Imiquimod-Induced Psoriasis-Like Dermatitis in Mice *via* Suppression of NF-κB and STAT3 Pathways

Haiming Chen[1,2,3,4†], *Cheng Wang*[5,6†], *Bin Tang*[1], *Jingjie Yu*[1,4], *Yue Lu*[1], *Junhong Zhang*[1], *Yuhong Yan*[1,4], *Hao Deng*[1,4], *Ling Han*[1,2], *Shaoping Li*[5,6*] *and Chuanjian Lu*[1,2,3,4*]

[1]State Key Laboratory of Dampness Syndrome of Chinese Medicine, The Second Affiliated Hospital of Guangzhou University of Chinese Medicine, Guangzhou, China, [2]Guangdong Provincial Key Laboratory of Clinical Research on Traditional Chinese Medicine Syndrome, Guangzhou, China, [3]Guangdong Clinical Research Center for Dermatosis in Chinese Medicine, Guangzhou, China, [4]Guangdong-Hong Kong-Macau Joint Lab on Chinese Medicine and Immune Disease Research, Guangzhou University of Chinese Medicine, Guangzhou, China, [5]State Key Laboratory of Quality Research in Chinese Medicine, Institute of Chinese Medical Sciences, University of Macau, Macao SAR, China, [6]Joint Laboratory of Chinese Herbal Glycoengineering and Testing Technology, University of Macau, Macao SAR, China

OPEN ACCESS

Edited by:
Angelo Sala,
University of Milan, Italy

Reviewed by:
Quan Xia,
First Affiliated Hospital of Anhui Medical University, China
Nagaraj M. Kulkarni,
Sravathi AI Technology Pvt Ltd., India

***Correspondence:**
Shaoping Li
spli@um.edu.mo
Chuanjian Lu
lcj@gzucm.edu.cn

[†]These authors have contributed equally to this work

Specialty section:
This article was submitted to Inflammation Pharmacology, a section of the journal Frontiers in Pharmacology

Received: 01 November 2021
Accepted: 10 December 2021
Published: 28 January 2022

Citation:
Chen H, Wang C, Tang B, Yu J, Lu Y, Zhang J, Yan Y, Deng H, Han L, Li S and Lu C (2022) P. granatum *Peel Polysaccharides Ameliorate Imiquimod-Induced Psoriasis-Like Dermatitis in Mice* via *Suppression of NF-κB and STAT3 Pathways. Front. Pharmacol. 12:806844. doi: 10.3389/fphar.2021.806844*

Psoriasis is a chronic and refractory inflammatory and autoimmune-mediated cutaneous disease affecting approximately 2%–3% of the global population. Most of the current therapies could relieve symptoms rapidly, while the side effects cannot be negligible. Hence, it is urgent to explore much safer and more effective treatments. In the current work, we evaluated the potential beneficial effect of *Punica granatum* peel polysaccharides (PPPs) in an imiquimod-elicited psoriasis-like mouse model and unraveled their mechanism of action. Firstly, PPPs were isolated from *P. granatum* peels, and then the molecular weight was determined and monosaccharide analysis was performed. The results revealed that PPPs significantly ameliorated psoriasis-like skin lesions and reduced the Psoriasis Area and Severity Index (PASI) scores and transepidermal water loss (TEWL). PPPs also attenuated the expressions of CD3 and Ki67 in psoriasis-like mouse skin and suppressed the serum or skin levels of pro-inflammatory cytokines, such as tumor necrosis factor alpha (TNF-α), interleukin 6 (IL-6), IL-1β, IL-8, IL-17, and IL-23. Moreover, PPPs were able to upregulate the mRNA and protein expressions of aquaporin-3 (AQP3) and filaggrin (FLG) in the skin of mice. In addition, PPPs inhibited the NF-κB and STAT3 signaling pathways. Overall, these results indicated that PPPs ameliorated the symptoms of psoriasis through inhibition of the inflammatory cytokines by suppressing the NF-κB and STAT3 signaling pathways and improved skin barrier protection *via* enhancing AQP3 and FLG. These observations potentially contribute to providing theoretical and experimental evidence for the clinical application of PPPs for psoriasis.

Keywords: *P. granatum* peel polysaccharides, anti-inflammation, skin barrier, imiquimod-induced psoriasis, NF-κB, STAT3

Abbreviations: AQP3, aquaporin-3; FLG, filaggrin; IMQ, imiquimod; NF-κB, nuclear factor-κB; PASI, Psoriasis Area and Severity Index; PPPs, *P. granatum* peel polysaccharides; TEWL, transepidermal water loss.

INTRODUCTION

Psoriasis is a refractory cutaneous ailment that is closely related to immune-mediated inflammation. The pathological manifestations of psoriasis include immune cell infiltration and abnormal keratinocyte proliferation in the epidermis (Greb et al., 2016). Approximately 2%–3% of the global population suffers from psoriasis (Zhou et al., 2020). The prevalence of psoriasis in adults is higher than that in children. Poor quality of life has been observed in most patients with psoriasis (Michalek et al., 2017). The primary treatment options for psoriasis are immunosuppression and biological agents, although these therapies can only relive symptoms for a short time. Relapse may occur when the treatment is ceased. Long-term use of these therapies is likely to cause side effects, including infection and liver toxicity (Chen et al., 2018; Mahil and Smith, 2019). Therefore, research and development of innovative effective and safe anti-psoriatic drugs is still an urgent need. Recently, the application of Chinese herbal medicines in psoriasis treatment has been widely reported (Di et al., 2021; Lu et al., 2021b; Lv et al., 2021; Yao et al., 2021).

Pomegranate peel is the dried peel of *Punica granatum* L., a plant in the pomegranate family. In traditional Chinese medicine, the functions of pomegranate peel include hemostasis, sedation, and antibacterial. Modern pharmacological studies have found that pomegranate peel polysaccharide has a significant immunomodulatory effect and good antioxidant activity in immunosuppressed mice induced by cyclophosphamide (Wu et al., 2019). In addition, it showed a significant preventive effect in a liver injury model induced by CCl_4 (Zhai et al., 2018b). An *in vitro* experiment has also shown that many parts of *P. granatum* peel polysaccharides (PPPs) have strong reducing activities and good scavenging activities to 2,2-diphenyl-1-picrylhydrazy (DPPH) free radicals, hydroxyl groups, and superoxide anions (Zhai et al., 2018a).

However, the protective effect of pomegranate peel polysaccharides on the skin lesions of an imiquimod (IMQ)-elicited psoriasis-like animal model has not been reported previously. In the present work, we explored the protective effects of PPPs in a psoriatic mice model and probed their potential biological mechanism.

MATERIALS AND METHODS

Chemical and Reagents

Compound dexamethasone acetate cream (DXA) was obtained from China Resources Sanjiu Medical and Pharmaceutical Co., Ltd. (Shenzhen, China). Imiquimod cream was purchased from Sichuan Mingxin Pharmaceutical Co., Ltd. (Sichuan, China). *P. granatum* peels were obtained from fruit purchased from Kangmei Pharmaceutical Co., Ltd. (Guangdong, China). The enhanced chemiluminescence (ECL) reagent was obtained from Millipore (Billerica, MA, USA). D-Fucose (Fuc), D-xylose (Xyl), D-galacturonic acid (GalA), D-galactose (Gal), D-glucose (Glc), D-mannose (Man), L-rhamnose (Rha), D-arabinose (Ara), D-glucuronic acid (GlcA), and D-fructose (Fru) were obtained from Sigma (St. Louis, MO, USA). Deionized water was prepared using a Millipore MilliQ Plus system (Millipore, Bedford, MA, USA). All the other reagents were of analytical grade.

Animals

BALB/c mice (20 ± 2 g) were from the Center of Laboratory Animals of Southern Medical University (Guangzhou, China) and were offered free access to food and water within a specific pathogen-free (SPF) environment. Ethics approval of all animal experiments was obtained from the Animal Experimental Ethics Committee of Guangdong Provincial Hospital of Chinese Medicine (no. 2019012).

Isolation of Polysaccharides

P. granatum peels were crushed into powder and the liposoluble ingredients removed with petroleum ether (1:5, *w*/*v*). Then, the skimmed materials were extracted with water (1:12, *w*/*v*) twice and the aqueous extracts collected, filtered, and evaporated. Subsequently, the obtained mixtures were precipitated by the addition of ethanol to 50% concentration for 24 h at 4°C. Precipitation was gathered by centrifuging at 5,000 rpm for 30 min. Lastly, the sediment was dialyzed (3,500 Da molecular weight cutoff, MWCO) and finally lyophilized to obtain crude PPPs.

HPSEC–MALLS/RID Analysis

Based on a previously reported method (Cheong et al., 2015; Deng et al., 2018), the content and the molecular weight of PPPs were measured using high-performance size exclusion chromatography with multi-angle laser light scattering/refractive index detector (HPSEC–MALLS/RID), which was composed of an Agilent 1200 series LC-DAD system (Agilent Technologies, Palo Alto, CA, USA), a RID (Optilab T-rEX; Wyatt Technology Co., Santa Barbara, CA, USA), and a multi-angle laser light scattering detector (DAWN HELEOS; Wyatt Technology Co.) equipped with a He–Ne laser (λ = 658 nm), based on d*n*/d*c* (0.15 ml/g). An appropriate amount of PPPs was dissolved in the mobile phase (0.9% NaCl water solution) to prepare the concentration of 2.0 mg/ml. The solution was filtered through a 0.45-μm membrane prior to analysis and 100 μl sample solution was injected. The separation was carried out on two columns in series, TSK-GEL G5000PWXL (300 mm × 7.8 mm, i.d.) and TSK-GEL G3000PWXL (300 mm × 7.8 mm, i.d.), with a flow rate of 0.5 ml min^{-1} at 35°C. Data collection and analysis were carried out using Astra software (version 6.0.2, Wyatt Technology Corp.).

Monosaccharide Analysis

Sample Preparation

The sample of polysaccharides in *P. granatum* peel (2.0 mg) was subjected to hydrolysis with 1.0 ml trifluoroacetic acid (TFA, 2.0 M) at 105°C for 6 h. Then, the reaction mixtures were washed with methanol and dried with a nitrogen evaporator 3 times to remove the TFA residue. Subsequently, 1.0 ml pure water was added for reconstitution and diluted 10 times, and then filtered using a 0.45-μm filter before analysis.

HPAEC–PAD Analysis

According to the method reported in a previous study (Alyassin et al., 2020), compositional monosaccharide analysis of PPPs was carried out with a Dionex ICS-3000 Ion Chromatography System (Dionex Corporation, Sunnyvale, CA, USA) containing an AS50 autosampler, an ICS-3000 dual pump, and an ICS-3000 DC. Chromeleon® (6.8) software was utilized to analyze the data. The samples and mix standard solutions were separated by a CarboPac PA200 (3 mm × 250 mm) with a CarboPac PA20 guard (3 mm × 30 mm) column at 25°C, and the flow rate was set at 0.5 ml/min. The injection volume was set at 5 μl and subjected to elution by a gradient prepared with deionized water (eluent A), 10 mM sodium hydroxide (eluent B), and 0.5 M sodium acetate (eluent C). Eluent B was constant (12%) and eluent A varied from 88% at 30 min to 43% at 22 min. This proportion was maintained constant until 25 min, when the initial conditions were recovered. An external standard method with a mixture consisting of 10 monosaccharide reference substances (Glc, Rha, Xyl, Ara, Fuc, GalA, GlcA, Gal, Fru, and Man) in 20 μg/ml was utilized to investigate the compositional monosaccharides of PPPs. All analyses were performed in duplicate.

Administration of Test Articles

BALB/c mice were randomly allocated into 5 groups ($n = 6$): control, vehicle, DXA (1 mg kg^{-1} day^{-1}), low-dose PPP group (0.25 g/ml, PPPs-L), and high-dose PPP group (0.5 g/ml, PPPs-H). The control group consisted of normal mice devoid of treatment. Mice in the PPP and DXA groups were topically treated with PPPs and DXA, respectively, and distilled water was topically administered to the control and vehicle groups. Topical use of IMQ cream was applied to mice in the vehicle and treatment groups in order to induce psoriasis for 7 consecutive days.

Imiquimod-Induced Psoriasis-Like Mouse Model

On the basis of our previous study (Chen et al., 2020), BALB/c mice were subjected to topical treatment with 5% IMQ cream (62.5 mg), which was applied on a shaved area (3 cm × 2.5 cm) on the back for 7 consecutive days. The PASI, measured on the 7th day, is an assessment tool combining (Lu et al., 2021a) skin erythema, scaling, and thickness, which was employed to evaluate the severity grade of psoriasis-like lesions. Transepidermal water loss (TEWL) was measured on the back skin of the psoriasis-like mouse model with VAPOSCANAS-VT100 (Tokyo, Japan).

Histological Evaluation and Immunohistochemistry

The mouse skin samples were removed and subjected to 24-h fixation in 4% paraformaldehyde and embedded in paraffin. Then, the skin samples in paraffin were cut into sections (5 μm) and hematoxylin and eosin (H&E) staining was applied for histological evaluation. For immunohistochemical staining, the slides were subjected to incubation overnight at 4°C with specific primary antibodies against Ki67 (1:1,000; Servicebio, Wuhan, China) and CD3 (1:1,000; Abcam, Waltham, MA, USA). Subsequently, the sections were incubated with biotinylated secondary antibodies (1:1,000; Abcam) for 1 h at 25°C, followed by diaminobenzidine staining and hematoxylin counter staining.

TABLE 1 | Primer sequences of target genes

Target gene		Primer sequence (5′→3′)
TNF-α	Forward	ACTGATGAGAGGGAGGCCAT
	Reverse	CCGTGGGTTGGACAGATGAA
IL-6	Forward	TTCTTGGGACTGATGCTGGT
	Reverse	CCTCCGACTTGTGAAGTGGT
IL-1β	Forward	TGCCACCTTTTGACAGTGATG
	Reverse	AAGGTCCACGGGAAAGACAC
AQP3	Forward	GCTTTTGGCTTCGCTGTCAC
	Reverse	TAGATGGGCAGCTTGATCCAG
FLG	Forward	ATGTCCGCTCTCCTGGAAAG
	Reverse	TGGATTCTTCAAGACTGCCTGTA
β-actin	Forward	GTGACGTTGACATCCGTAAAGA
	Reverse	GCCGGACTCATCGTACTCC

Measurements of TNF-α, IL-6, IL-1β, AQP3, and FLG mRNA Expression *via* RT-PCR

Furthermore, the mRNA levels of tumor necrosis factor alpha (TNF-α), interleukin 6 (IL-6), IL-1β, aquaporin-3 (AQP3), and filaggrin (FLG) in the skin samples were assessed *via* RT-PCR. Total mRNA was extracted from the skin samples *via* the TRIzol reagent, and mRNA was reversely transcribed to cDNA. The primer sequences are tabulated in **Table 1**. The relative mRNA expression of inflammatory cytokines *versus* β-actin was evaluated using an ABI 7500 Fast Real-Time PCR System (Thermo Fisher Scientific, Waltham, MA, USA).

Measurements of TNF-α, IL-6, IL-17, IL-23, and IL-8 Levels with ELISA

Meanwhile, the levels of TNF-α, IL-6, IL-17, IL-23, and IL-8 were assessed in the mouse serum with commercially available ELISA kits (Meimian, Jiangsu, China). The absorbance was read at 450 nm using a microplate spectrophotometer (Multiskan GO; Thermo Fisher Scientific).

Western Blotting Analysis

In addition, the protein expressions of p-NF-κB, NF-κB, p-STAT3, STAT3, AQP3, and FLG were evaluated *via* Western blotting. Firstly, RIPA lysis buffer was used to extract total protein from mouse skin samples, and a BCA assay kit (Thermo Fisher Scientific) was employed to measure the protein concentrations. An equal amount of protein from each sample was loaded to SDS-PAGE and transferred to PVDF membranes. The membranes were then blocked with 5% (*w*/*v*) skimmed milk in TBS-T containing 0.1% Tween-20 at room temperature for 2 h and subsequently incubated with specific primary antibody against p-NF-κB (p65) [1:1,000; Cell Signaling Technology

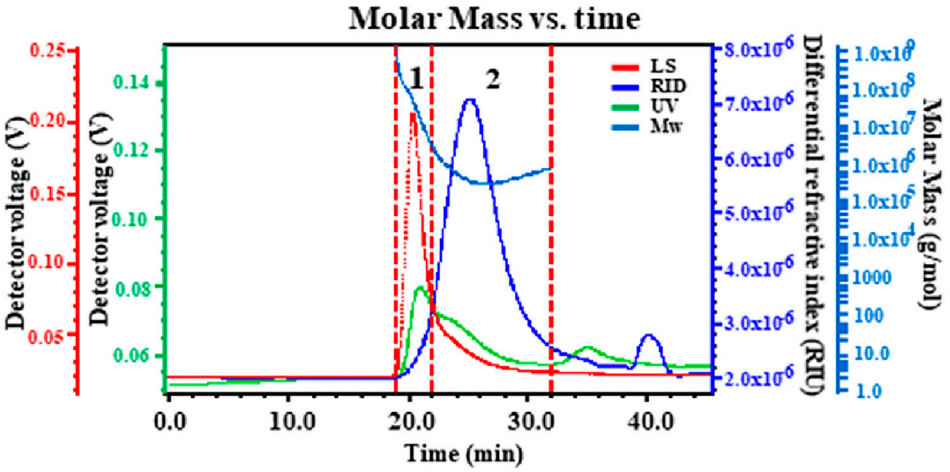

FIGURE 1 | Typical high-performance size exclusion chromatography (HPSEC) of *Punica granatum* peel polysaccharides (PPPs).

(CST), Danvers, MA, USA], NF-κB (p65) (1:1,000; CST), p-STAT3 (1:1,000; CST), STAT3 (1:1,000; CST), AQP3 (1:1,000; Cohesion Biosciences, London, UK), FLG (1:1,000; Cohesion Biosciences), and β-actin (1:1,000; CST) at 4°C overnight. Subsequently, the membranes were washed with TBS-T and blotted with the corresponding secondary antibody (1:1,000; CST) for 1 h. Finally, the immunoreactive band was monitored using an enhanced chemiluminescence (ECL) method. ImageJ software (NIH, Bethesda, MD, USA) was adopted to quantitate the band intensity, and β-actin was used as the loading control.

Statistical Analysis

Data were analyzed with one-way analysis of variance (ANOVA) followed by Dunnett's test and expressed as the mean ± standard deviation (SD). Statistically significant differences were identified when $p < 0.05$. Statistical analysis was performed using GraphPad Prism 5.0 (GraphPad Software, La Jolla, CA, USA).

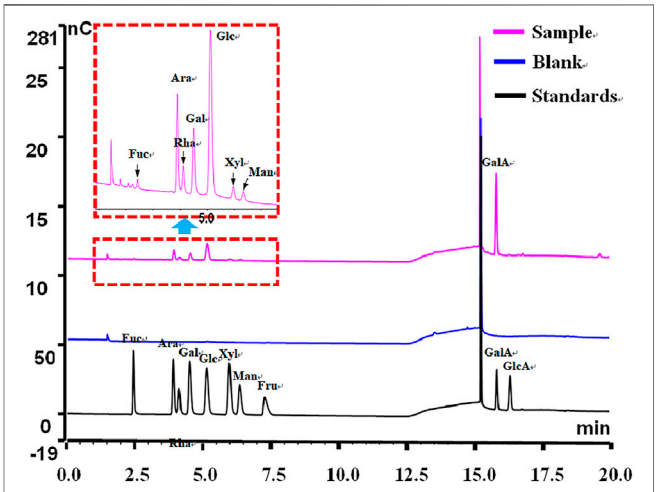

FIGURE 2 | Typical high-performance anion exchange chromatography (HPAEC) of *Punica granatum* peel polysaccharides (PPPs).

RESULTS

Molecular Parameter Analysis of Polysaccharides in *P. granatum* Peel

The biological activities of polysaccharides from a natural resource are likely influenced by their molecular weight. The performance of HPSEC–MALLS/RID on the determination of the molecular weights and the molecular weight distribution of polysaccharides was excellent. Therefore, the molecular weights (M_w), radius of gyrations (R_g), polydispersity (M_w/M_n), and molecular weight distributions of PPPs were investigated using HPSEC–MALLS/RID. The chromatograms were found to be divided into two peaks (**Figure 1**). UV detection (green lines) indicated that PPPs contained proteins. The M_w of peaks 1 and 2 of PPPs were 2.272×10^7 and 4.110×10^5, respectively. The M_w/M_n values were 2.391 and 1.479 and the R_g values were 33.9 and 35.9, respectively.

Monosaccharide Composition of Polysaccharides in *P. granatum* Peel

High-performance anion exchange chromatography/pulse amperometric detection (HPAEC–PAD) analysis has been commonly used for the identification and quantitative determination of monosaccharides due to the advantages of speed, high specificity, and high sensitivity, as well as sample derivatization generally not being required (Templeton et al., 2012; Wang et al., 2014). The monosaccharide composition of PPPs was determined with HPAEC-PAD. By comparing to standard chromatograms, the monosaccharide peaks were confirmed. The results showed that the monosaccharide composition of PPPs consisted of Fuc, Ara, Rha, Gal, Glc, Xyl, Man, and GalA (**Figure 2**), and their molar ratio was 1.00:13.38:7.21:7.58:22.39:1.62:1.86:131.63, respectively. The main neutral monosaccharides were Ara, Rha, and Glc, as well as minor Fuc.

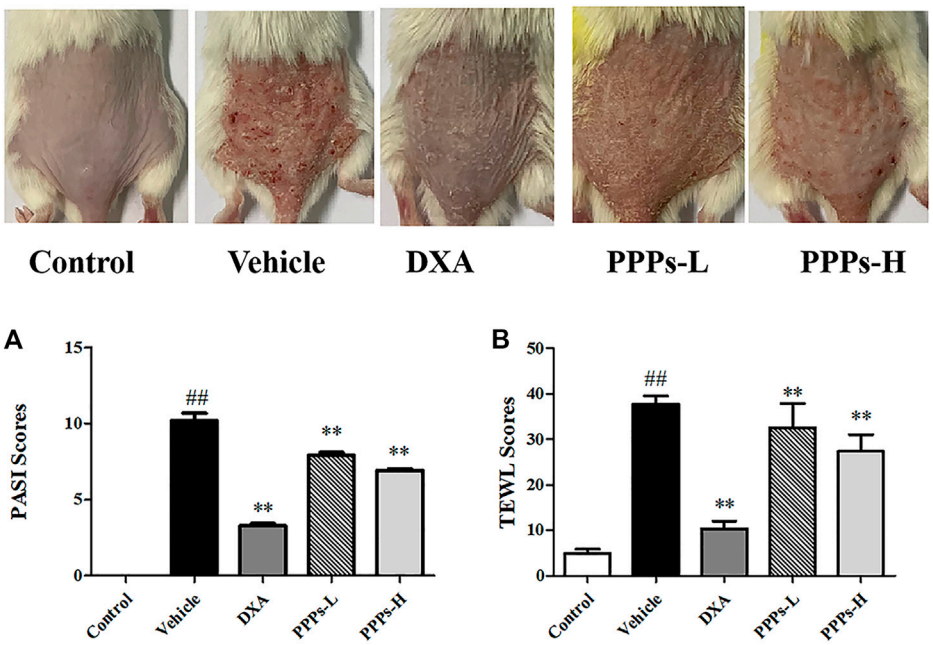

FIGURE 3 | *Punica granatum* peel polysaccharides (PPPs) ameliorated imiquimod (IMQ)-induced psoriasis in BALB/c mice. Representative photographs of the dorsal skin in the IMQ-elicited psoriasis mouse model post-IMQ treatment without or with PPPs. **(A)** Psoriasis Area and Severity Index (PASI) scores of the skin lesions in mice with IMQ-elicited psoriasis post-treatment. **(B)** Transepidermal water loss (TEWL) of the skin lesions in IMQ-induced psoriasis-like mice. Data are presented as the mean ± SD (n = 6). $^{\#}p < 0.05$, $^{\#\#}p < 0.01$ *vs*. the control group; $^{*}p < 0.05$, $^{**}p < 0.01$ *vs*. the vehicle group. *PPPs-L*, low-dose PPPs; *PPPs-H*, high-dose PPPs.

The content of GalA was high (17.69%) in the monosaccharide composition of PPPs. The results of the monosaccharide composition analysis were congruent with a preceding report (Shakhmatov et al., 2019).

P. granatum Peel Polysaccharides Attenuate Imiquimod-Elicited Psoriasis-Like Skin Lesion in Mice

In this study, the beneficial effects of PPPs were evaluated using an IMQ-elicited psoriasis mouse model. Marked epidermal scaling, erythema, and inflammatory infiltrates were observed on the dorsal skin after topical use of IMQ in comparison to the control group (**Figure 3**). The overall skin lesions of mice and the average PASI scores were notably decreased post-treatment with PPPs or DXA in comparison to the vehicle group (**Figure 3A**). TEWL is a known indicator that can serve to assess the function of the skin barrier (Agren et al., 2010). In our study, the TEWL was dramatically increased after exposure to IMQ (**Figure 3B**). However, PPPs could reverse the TEWL compared with the vehicle group, which indicated that PPPs were able to repair the skin barrier in the IMQ-elicited psoriasis mouse model.

Histological Analysis

H&E staining was carried out for histological examination of the lesion skins post-treatment with PPPs. As depicted in **Figures 4A,D**, the tissue slide of mouse skin in the control group showed a normal smooth epidermis devoid of any inflammation or lesion. However, noteworthy pathological variations characteristic of accentuated acanthosis, hyperkeratosis of the epidermis, and abnormal inflammatory infiltrates were shown in the mouse skin of the vehicle group. In contrast, the administration of PPPs led to a much smoother epidermis with attenuated parakeratosis and ameliorated epidermal thickening in comparison to the vehicle counterpart.

Effect of *P. granatum* Peel Polysaccharides on the Expressions of Ki67 and CD3 by Immunohistochemistry

The translational expressions of Ki67 and CD3 were detected in mouse skin since hyperproliferation and inflammation infiltration are crucial to psoriasis (Li et al., 2020). It was observed from the results (**Figures 4B, C**) that the expressions of Ki67 and CD3 in vehicle mice were markedly higher than those in the control counterpart. However, the expression levels of Ki67 and CD3 were noticeably suppressed by treatment with PPPs.

P. granatum Peel Polysaccharides Reduce Pro-Inflammatory Cytokines in the Skin and Serum of Imiquimod-Treated Psoriatic Mice

Multiple inflammatory cytokines could be generated by macrophages and dendritic cells in psoriasis (Shao et al., 2016). Therefore, we analyzed the expressions of pro-inflammatory cytokines (TNF-α, IL-6, IL-1β, IL-8, IL-17, and IL-23) in the skin tissue using RT-PCR and in serum

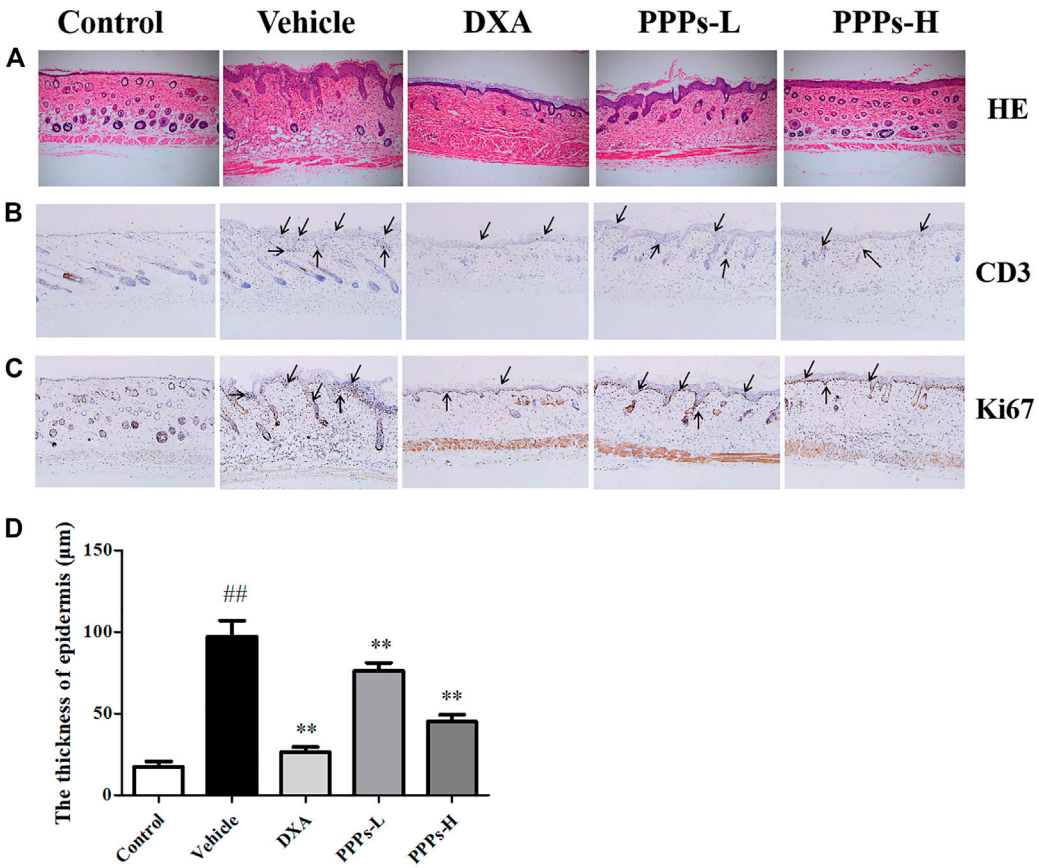

FIGURE 4 | Histological analysis and immunohistochemistry assay. Different treatments were administrated to mice. H&E staining **(A)** of the dorsal skin lesion in different groups. Immunohistochemical photographs of CD3 **(B)** and Ki67 **(C)** staining (magnification, ×100) of the dorsal skin in control or psoriatic mice post-treatment. The black arrows indicate the CD3 and Ki67 positive location. ##$p < 0.01$ compared with the control group; **$p < 0.01$ compared with the vehicle group. *PPPs-L*, low-dose PPPs; *PPPs-H*, high-dose PPPs.

using ELISA. As shown in **Figures 5**, **6**, the expressions of these inflammatory cytokines in vehicle mice were markedly improved compared to those in control mice, whereas there were remarkable reductions in the expressions of these inflammatory cytokine in the group treated with PPPs. These results indicated that PPPs could effectively reduce psoriasis-related inflammatory factors.

P. granatum Peel Polysaccharides Suppress the Expressions of Aquaporin-3 and Filaggrin in Imiquimod-Treated Psoriatic Mice

Decreased levels of AQP3 and FLG are commonly seen in skin barrier disruption, which appears to be a key player in epidermal biology in psoriasis (Proksch et al., 2008; Varma et al., 2019). Hence, we determined the expressions of AQP3 and FLG *via* RT-PCR. As shown in **Figures 5D, E**, the mRNA expressions of AQP3 and FLG were greatly decreased in the vehicle group. However, these two parameters were obviously increased by treatment with PPPs. These results indicated that PPPs could repair the skin barrier induced by topical intervention of IMQ.

P. granatum Peel Polysaccharides Suppress the NF-κB and STAT3 Signaling Pathways in Skin With Psoriasis-Like Lesions

Since the expressions of the pro-inflammatory cytokines (AQP3 and FLG) were suppressed by PPPs in IMQ-induced psoriasis, the underlying mechanism of their anti-psoriatic effects was further explored. Previous evidence has shown that both the NF-κB and STAT3 signaling pathways were overexpressed and activated in skin tissues with psoriasis (Wang et al., 2019). Therefore, Western blotting assay was carried out to explore the potential effect of PPPs on the protein expressions of p-NF-κB, NF-κB, p-STAT3, STAT3, AQP3, and FLG. As shown in **Figure 7**, the expressions of p-NF-κB and p-STAT3 were upregulated in the skin of psoriatic mice, in contrast to those in the control group. Treatment with PPPs effectively declined the phosphorylation of NF-κB and STAT3. On the other hand, PPPs also enhanced the

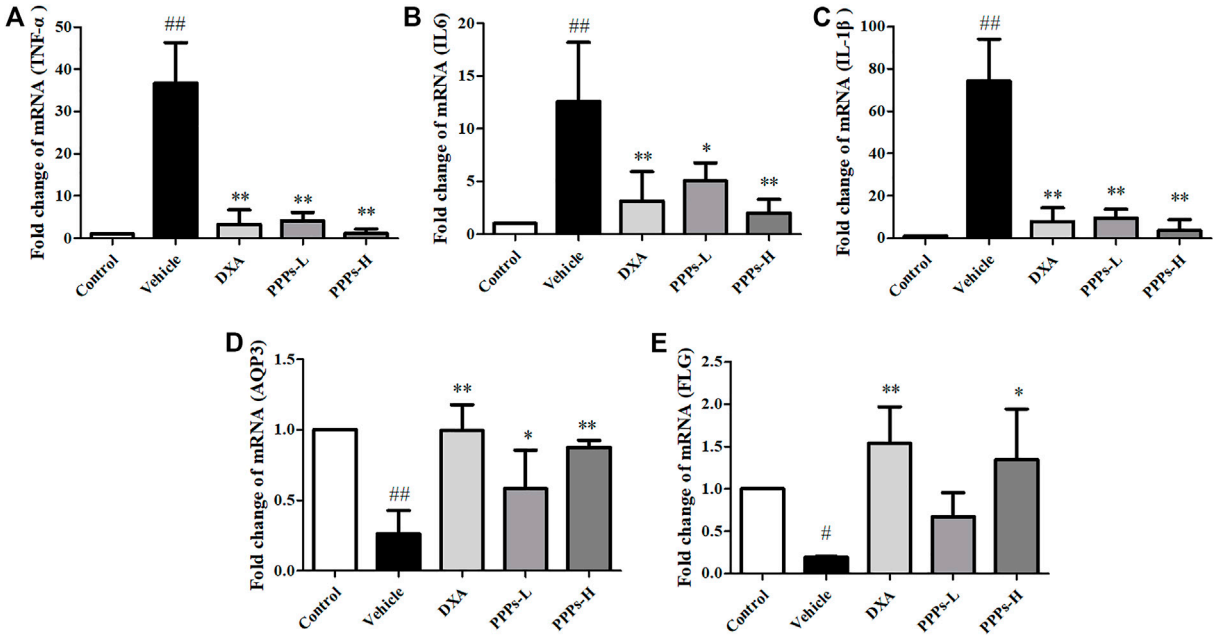

FIGURE 5 | Effect of *Punica granatum* peel polysaccharides (PPPs) on the mRNA expressions of inflammatory cytokines, aquaporin-3 (AQP3), and filaggrin (FLG) in imiquimod (IMQ)-elicited psoriasis. Mice were treated with dexamethasone (DXA) and PPPs and topically administered with IMQ. The mRNA expressions of TNF-α **(A)**, IL-6 **(B)**, IL-1β **(C)**, AQP3 **(D)**, and FLG **(E)** in the skin were measured by RT-PCR. Data are shown as the mean ± SD (n = 3). $^{\#}p < 0.05$, $^{\#\#}p < 0.01$ compared with the control group; $^{*}p < 0.05$, $^{**}p < 0.01$ compared with the vehicle group. *PPPs-L*, low-dose PPPs; *PPPs -H*, high-dose PPPs.

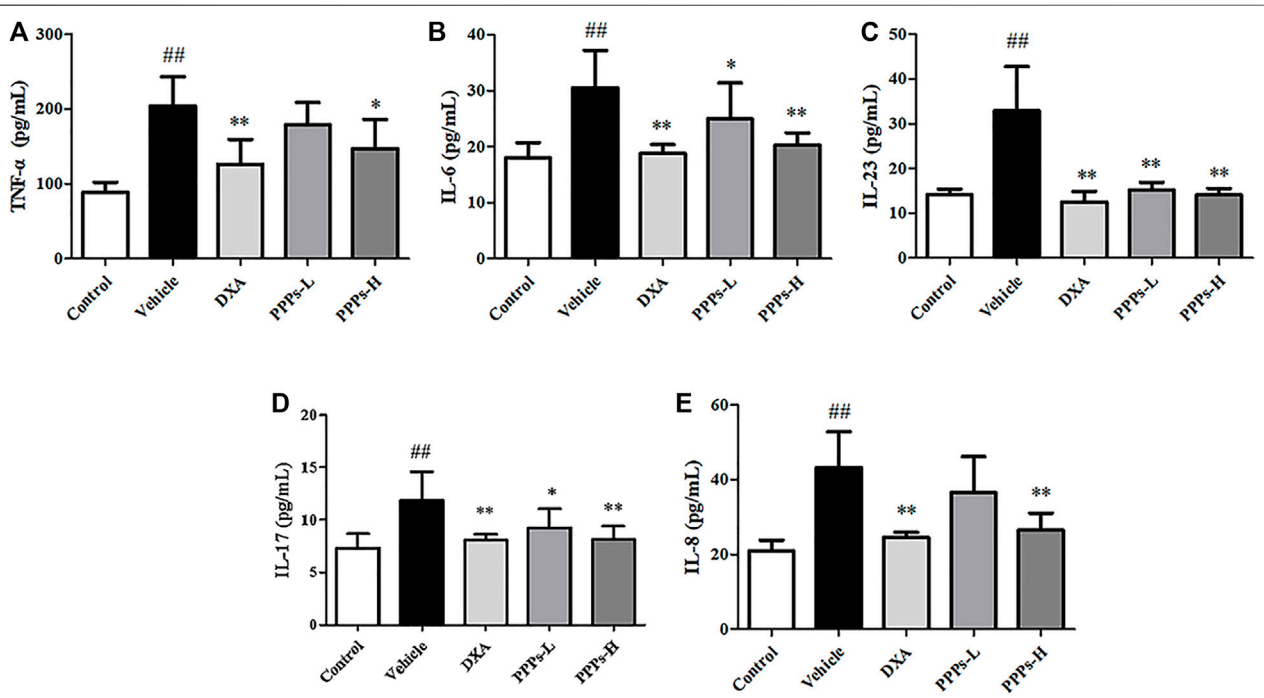

FIGURE 6 | *Punica granatum* peel polysaccharides (PPPs) decreased the levels of inflammatory mediators in mice with imiquimod (IMQ)-elicited psoriasis. The levels of the inflammatory mediators TNF-α **(A)**, IL-6 **(B)**, IL-23 **(C)**, IL-17 **(D)**, and IL-8 **(E)** were measured by ELISA in the serum of IMQ-induced psoriasis-like mice. Data are shown as the mean ± SD (n = 6). $^{\#}p < 0.05$, $^{\#\#}p < 0.01$ compared with the control group; $^{*}p < 0.05$, $^{**}p < 0.01$ compared with the vehicle group. *PPPs-L*, low-dose PPPs; *PPPs-H*, high-dose PPPs.

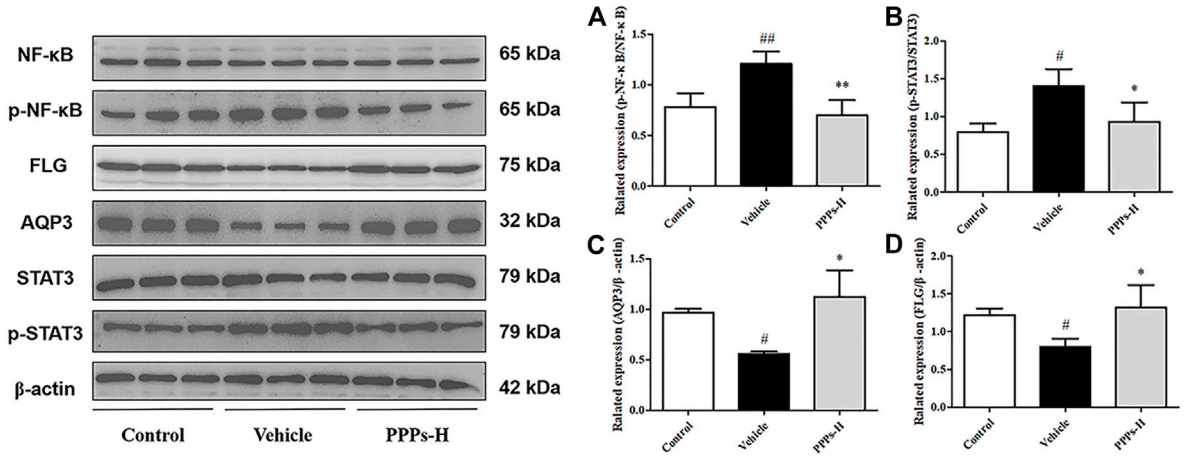

FIGURE 7 | *Punica granatum* peel polysaccharides (PPPs) suppressed aquaporin-3 (AQP3), filaggrin (FLG), and the NF-κB and STAT3 signaling pathways in skin with psoriatic lesions. Effect of PPPs on the translational expressions of p-NF-κB, NF-κB, p-STAT3, STAT3, AQP3, and FLG in the skin samples of mice with imiquimod (IMQ)-elicited psoriasis as determined by Western blotting post-treatment with PPPs. Densitometry analyses of the immunoblotting are shown as p-NF-κB/NF-κB **(A)**, p-STAT3/STAT3 **(B)**, AQP3/β-actin **(C)**, and p-STAT3/β-actin **(D)**. Data are shown as the mean ± SD (n = 3). $^{\#}p < 0.05$, $^{\#\#}p < 0.01$ *vs*. the control group; $^{*}p < 0.05$, $^{**}p < 0.01$ *vs*. the vehicle group. *PPPs-L*, low-dose PPPs; *PPPs-H*, high-dose PPPs.

expressions of AQP3 and FLG. Based on these results, it was indicated that the beneficial effects of PPPs on mice with IMQ-elicited psoriasis were related to their anti-inflammatory effect and skin barrier protection.

DISCUSSION

Psoriasis is a chronic and relapsing inflammatory and autoimmune-mediated cutaneous ailment that is highly related to excessive inflammatory cytokine production and destruction of the skin barrier function. Therefore, regulating the skin barrier and reducing skin inflammation represent effective treatment strategies for psoriasis. The treatment for psoriasis has achieved clinical improvement. However, the side effects and economic burden due to the long-term application of synthetic or biological agents still pose a frustrating challenge (Whartenby et al., 2008; Boehncke and Schön, 2015; Sikma et al., 2015). Therefore, more effective and safer agents for psoriasis have been in great demand in the drug discovery field over the decades (Greb et al., 2016; Li et al., 2016).

IMQ, which serves as a ligand for TLR7 and TLR8 and as an effective immune activator, can be topically used to induce psoriasis-like skin lesions in a mouse model. It is the most widely used inducer of psoriasis skin inflammation due to its easy modeling and the same phenotypic and histological characteristics as observed in human psoriasis (van der Fits et al., 2009; Di et al., 2021; Zhou et al., 2021).

In this research, the skin barrier protective effects and anti-inflammatory activity of PPPs were investigated. The results showed that PPPs effectively suppressed the PASI scores and TEWL and inhibited the expressions of CD3 and Ki67 in mice with IMQ-elicited psoriasis compared with those in the vehicle group. Moreover, PPPs were observed to remarkably inhibit the levels of psoriasis-related pro-inflammatory mediators in the serum, namely, IL-17, IL-6, TNF-α, IL-8, and IL-23. PPPs altered the mRNA expressions of the inflammatory cytokines (TNF-α, IL-6, and IL-1β) and improved the expressions of AQP3 and FLG in psoriasis-like mouse skin. In addition, PPPs significantly suppressed the NF-κB and STAT3 pathways and accentuated the expressions of AQP3 and FLG when compared to mice with IMQ-elicited psoriasis without treatment.

The H&E staining results indicated that PPPs efficiently ameliorated the IMQ-elicited epidermal thickening, hyperkeratosis, and dermal inflammatory cell infiltration. Ki67 is deemed as a proliferating marker that is indispensable in cell proliferation, and CD3 is considered as an inflammatory marker that can evaluate the effect on inflammatory cell recruitment in the skin (Herman and Herman, 2016; Song et al., 2021). In our study, immunohistochemistry was carried out to probe the expressions of Ki67 and CD3 in skin tissues. The protein expressions of CD3 and Ki67 were depressed in the skin lesions of PPP-treated mice in comparison to those of the vehicle counterpart, which suggested that PPPs could alleviate IMQ-elicited inflammation and proliferation of keratinocytes.

The skin, which is the outer tissue and the largest organ of the human body, not only has the important function of forming an outside barrier that provides chemical, physical, and biological protection against the external environment but also serves as an effective barrier between the inside and outside barriers to prevent excessive water loss (Proksch et al., 2008; Kasemsarn et al., 2016). Many chronic skin disorders, such as psoriasis, are associated with impaired skin barrier function (Segre, 2006;

Proksch, 2018). There is a strong connection between FLG and inflammatory dermatosis like psoriasis due to the key role of FLG in skin barrier function (McAleer and Irvine, 2013; Yosipovitch et al., 2019).

Accumulating pieces of evidence have shown that the water channel AQP3, which plays an important role in various skin diseases, is the most abundant aquaporin in the outer epithelial layer of the skin (Patel et al., 2017). Several reports have shown that the levels of FLG and AQP3 were decreased in psoriatic lesions (Voss et al., 2011; Lee et al., 2012; Seleit et al., 2015). Our results revealed that the levels of FLG and AQP3 in psoriatic-like skin were markedly decreased compared to those in the control skin. In contrast, the FLG and AQP3 contents increased simultaneously after PPP treatment compared to those in the vehicle group. These results indicated that PPPs displayed potentially beneficial effect on the skin barrier in IMQ-elicited psoriasis-like mice.

The increased production of pro-inflammatory mediators and chemokines such as IL-1, IL-6, IL-23, IL-17, and TNF-α plays a crucial role in the pathogenesis of psoriasis (Croxford et al., 2014; Grine et al., 2015; Harden et al., 2015; Kim and Krueger, 2015). Previous reports have already revealed that topical administration of IMQ cream on the back of mice stimulated the generation of pro-inflammatory cytokines and chemokines (Di et al., 2021; Song et al., 2021). It has been found that the phosphorylation of STAT3 was activated in psoriatic lesions. The IL-23/Th17 pathway was critical for inflammation in the pathogenesis of psoriasis, which has been demonstrated to have a close relationship with STAT3 activation (Andrés et al., 2013). The NF-κB pathway performed a crucial role in the development of psoriasis, which activated molecular patterns and promoted histological hallmarks (Andrés et al., 2013). Growing evidence has shown that both STAT3 and NF-κB were activated and overexpressed in both psoriasis patients and psoriasis-like mice (Sano et al., 2005; Andres-Ejarque et al., 2021; Yang et al., 2021). In this work, PPPs were found to inhibit the phosphorylation of STAT3 and NF-κB and to downregulate the expressions of pro-inflammatory mediators both in serum and skin lesions of psoriatic mice.

CONCLUSION

Overall, this study indicated that PPPs ameliorated the IMQ-elicited inflammation in psoriatic mice *via* restoring the impaired skin barrier function by elevating the expressions of FLG and AQP3 and suppressing the pro-inflammatory cytokines by modulating the STAT3 and NF-κB pathways. PPPs might have the potential to be further developed into a promising therapeutic option for the treatment of psoriasis.

DATA AVAILABILITY STATEMENT

The original contributions presented in the study are included in the article/**Supplementary Material**, further inquiries can be directed to the corresponding authors.

ETHICS STATEMENT

The animal study was reviewed and approved by The Animal Experimental Ethics Committee of Guangdong Provincial Hospital of Chinese Medicine.

AUTHOR CONTRIBUTIONS

CL and SL conceived and designed the experiments. HC, CW, BT, YL, JZ, and LH performed the experiments. HC, JY, YY, HD, and LH analyzed and interpreted the data. CL and SL revised and interpreted the data analysis. HC and JZ wrote the article. All authors have read and approved the manuscript.

FUNDING

This research was partially supported by grants from the Natural Science Foundation of Guangdong Province (nos. 2020A1515010607, 2019A1515111094, 2020B1111100006, and 2018A030310530), the Science and Technology Planning Project of Guangdong Province (nos. 2017B030314166 and 2017A050506041), the Science and Technology Planning Project of Guangzhou (no. 201807010051), Technology Research Projects of Guangdong Provincial Hospital of Chinese Medicine (nos. YN2019QJ08, YN2018HK01, YN2018RBA02, and YN2019QL11), the Chinese Medicinal Scientific Research Project of Guangdong Province(Nos. 20211176 and 20211185) and Technology Research Projects of State Key Laboratory of Dampness Syndrome of Chinese Medicine (nos. SZ2021ZZ34 and SZ2021ZZ29).

SUPPLEMENTARY MATERIAL

The Supplementary Material for this article can be found online at: https://www.frontiersin.org/articles/10.3389/fphar.2021.806844/full#supplementary-material

REFERENCES

Agren, J., Zelenin, S., Svensson, L. B., Nejsum, L. N., Nielsen, S., Aperia, A., et al. (2010). Antenatal Corticosteroids and Postnatal Fluid Restriction Produce Differential Effects on AQP3 Expression, Water Handling, and Barrier Function in Perinatal Rat Epidermis. *Dermatol. Res. Pract.* 2010, 789729. doi:10.1155/2010/789729

Alyassin, M., Campbell, G. M., Masey O'neill, H., and Bedford, M. R. (2020). Simultaneous Determination of Cereal Monosaccharides, Xylo- and Arabinoxylo-Oligosaccharides and Uronic Acids Using HPAEC-PAD. *Food Chem.* 315, 126221. doi:10.1016/j.foodchem.2020.126221

Andrés, R. M., Montesinos, M. C., Navalón, P., Payá, M., and Terencio, M. C. (2013). NF-κB and STAT3 Inhibition as a Therapeutic Strategy in Psoriasis: *In Vitro* and *In Vivo* Effects of BTH. *J. Invest. Dermatol.* 133, 2362–2371. doi:10.1038/jid.2013.182

Andres-Ejarque, R., Ale, H. B., Grys, K., Tosi, I., Solanky, S., Ainali, C., et al. (2021). Enhanced NF-Kb Signaling in Type-2 Dendritic Cells at Baseline Predicts Non-response to Adalimumab in Psoriasis. *Nat. Commun.* 12, 4741. doi:10.1038/s41467-021-25066-9

Boehncke, W.-H., and Schön, M. P. (2015). Psoriasis. *The LancetLancet* 386, 983–994. doi:10.1016/s0140-6736(14)61909-7

Chen, H., Liu, H., Tang, B., Chen, Y., Han, L., Yu, J., et al. (2020). The Protective Effects of 18β-Glycyrrhetinic Acid on Imiquimod-Induced Psoriasis in Mice via Suppression of mTOR/STAT3 Signaling. *J. Immunol. Res.* 2020, 1980456. doi:10.1155/2020/1980456

Chen, Y., Zhang, Q., Liu, H., Lu, C., Liang, C. L., Qiu, F., et al. (2018). Esculetin Ameliorates Psoriasis-like Skin Disease in Mice by Inducing CD4+Foxp3+ Regulatory T Cells. *Front. Immunol.* 9, 2092. doi:10.3389/fimmu.2018.02092

Cheong, K. L., Wu, D. T., Zhao, J., and Li, S. P. (2015). A Rapid and Accurate Method for the Quantitative Estimation of Natural Polysaccharides and Their Fractions Using High Performance Size Exclusion Chromatography Coupled with Multi-Angle Laser Light Scattering and Refractive index Detector. *J. Chromatogr. A.* 1400, 98–106. doi:10.1016/j.chroma.2015.04.054

Croxford, A. L., Karbach, S., Kurschus, F. C., Wörtge, S., Nikolaev, A., Yogev, N., et al. (2014). IL-6 Regulates Neutrophil Microabscess Formation in IL-17A-driven Psoriasiform Lesions. *J. Invest. Dermatol.* 134, 728–735. doi:10.1038/jid.2013.404

Deng, Y., Han, B. X., Hu, D. J., Zhao, J., and Li, S. P. (2018). Qualitation and Quantification of Water Soluble Non-starch Polysaccharides from Pseudostellaria Heterophylla in China Using Saccharide Mapping and Multiple Chromatographic Methods. *Carbohydr. Polym.* 199, 619–627. doi:10.1016/j.carbpol.2018.06.063

Di, T., Zhai, C., Zhao, J., Wang, Y., Chen, Z., and Li, P. (2021). Taxifolin Inhibits Keratinocyte Proliferation and Ameliorates Imiquimod-Induced Psoriasis-like Mouse Model via Regulating Cytoplasmic Phospholipase A2 and PPAR-γ Pathway. *Int. Immunopharmacol* 99, 107900. doi:10.1016/j.intimp.2021.107900

Greb, J. E., Goldminz, A. M., Elder, J. T., Lebwohl, M. G., Gladman, D. D., Wu, J. J., et al. (2016). Psoriasis. *Nat. Rev. Dis. Primers* 2, 16082. doi:10.1038/nrdp.2016.82

Grine, L., Dejager, L., Libert, C., and Vandenbroucke, R. E. (2015). An Inflammatory triangle in Psoriasis: TNF, Type I IFNs and IL-17An Inflammatory triangle in Psoriasis: TNF, Type I IFNs and IL-17. *Cytokine Growth Factor. Reviewscytokine Growth Factor. Rev.* 26, 25–33. doi:10.1016/j.cytogfr.2014.10.009

Harden, J. L., Krueger, J. G., and Bowcock, A. M. (2015). The Immunogenetics of Psoriasis: A Comprehensive Review. *J. Autoimmun.* 64, 66–73. doi:10.1016/j.jaut.2015.07.008

Herman, A., and Herman, A. P. (2016). Topically Used Herbal Products for the Treatment of Psoriasis - Mechanism of Action, Drug Delivery, Clinical Studies. *Planta Med.* 82, 1447–1455. doi:10.1055/s-0042-115177

Kasemsarn, P., Bosco, J., and Nixon, R. L. (2016). The Role of the Skin Barrier in Occupational Skin Diseases. *Curr. Probl. Dermatol.* 49, 135–143. doi:10.1159/000441589

Kim, J., and Krueger, J. G. (2015). The Immunopathogenesis of Psoriasis. *Dermatol. Clin.* 33, 13–23. doi:10.1016/j.det.2014.09.002

Lee, Y., Je, Y. J., Lee, S. S., Li, Z. J., Choi, D. K., Kwon, Y. B., et al. (2012). Changes in Transepidermal Water Loss and Skin Hydration According to Expression of Aquaporin-3 in Psoriasis. *Ann. Dermatol.* 24, 168–174. doi:10.5021/ad.2012.24.2.168

Li, G. B., Ma, S., Yang, L. L., Ji, S., Fang, Z., Zhang, G., et al. (2016). Drug Discovery against Psoriasis: Identification of a New Potent FMS-like Tyrosine Kinase 3 (FLT3) Inhibitor, 1-(4-((1h-Pyrazolo[3,4-D]pyrimidin-4-Yl)oxy)-3-Fluorophenyl)-3-(5-(tert-Butyl)isoxazol-3-Yl)urea, that Showed Potent Activity in a Psoriatic Animal Model. *J. Med. Chem.* 59, 8293–8305. doi:10.1021/acs.jmedchem.6b00604

Li, L., Zhang, H. Y., Zhong, X. Q., Lu, Y., Wei, J., Li, L., et al. (2020). PSORI-CM02 Formula Alleviates Imiquimod-Induced Psoriasis via Affecting Macrophage Infiltration and Polarization. *Life Sci.* 243, 117231. doi:10.1016/j.lfs.2019.117231

Lu, Y., Yang, Y., Zhang, J., Zhang, H., Ma, C., Tang, X., et al. (2021a). Anti-Angiogenic Efficacy of PSORI-CM02 and the Associated Mechanism in Psoriasis *In Vitro* and *In Vivo*. *Front. Immunol.* 12. doi:10.3389/fimmu.2021.649591

Lu, Y., Yang, Y., Zhang, J., Zhang, H., Ma, C., Tang, X., et al. (2021b). Anti-Angiogenic Efficacy of PSORI-CM02 and the Associated Mechanism in Psoriasis *In Vitro* and *In Vivo*. *Front. Immunol.* 12, 649591. doi:10.3389/fimmu.2021.649591

Lv, H., Liu, X., Chen, W., Xiao, S., Ji, Y., Han, X., et al. (2021). Yangxue Jiedu Fang Ameliorates Psoriasis by Regulating Vascular Regression via Survivin/PI3K/Akt Pathway. *J. Immunol. Res.* 2021, 4678087. doi:10.1155/2021/4678087

Mahil, S. K., and Smith, C. H. (2019). Psoriasis Biologics: a new era of Choice. *Lancet* 394, 807–808. doi:10.1016/s0140-6736(19)31772-6

Mcaleer, M. A., and Irvine, A. D. (2013). The Multifunctional Role of Filaggrin in Allergic Skin Disease. *J. Allergy Clin. Immunol.* 131, 280–291. doi:10.1016/j.jaci.2012.12.668

Michalek, I. M., Loring, B., and John, S. M. (2017). A Systematic Review of Worldwide Epidemiology of Psoriasis. *J. Eur. Acad. Dermatol. Venereol.* 31, 205–212. doi:10.1111/jdv.13854

Patel, R., Kevin Heard, L., Chen, X., and Bollag, W. B. (2017). Aquaporins in the Skin. *Adv. Exp. Med. Biol.* 969, 173–191. doi:10.1007/978-94-024-1057-0_11

Proksch, E., Brandner, J. M., and Jensen, J. M. (2008). The Skin: an Indispensable Barrier. *Exp. Dermatol.* 17, 1063–1072. doi:10.1111/j.1600-0625.2008.00786.x

Proksch, E. (2018). pH in Nature, Humans and Skin. *J. Dermatol.* 45, 1044–1052. doi:10.1111/1346-8138.14489

Sano, S., Chan, K. S., Carbajal, S., Clifford, J., Peavey, M., Kiguchi, K., et al. (2005). Stat3 Links Activated Keratinocytes and Immunocytes Required for Development of Psoriasis in a Novel Transgenic Mouse Model. *Nat. Med.* 11, 43–49. doi:10.1038/nm1162

Segre, J. A. (2006). Epidermal Barrier Formation and Recovery in Skin Disorders. *J. Clin. Invest.* 116, 1150–1158. doi:10.1172/jci28521

Seleit, I., Bakry, O. A., Al Sharaky, D., and Ragheb, E. (2015). Evaluation of Aquaporin-3 Role in Nonmelanoma Skin Cancer: An Immunohistochemical Study. *Ultrastruct. Pathol.* 39, 306–317. doi:10.3109/01913123.2015.1022241

Shakhmatov, E. G., Makarova, E. N., and Belyy, V. A. (2019). Structural Studies of Biologically Active Pectin-Containing Polysaccharides of Pomegranate Punica Granatum. *Int. J. Biol. Macromol* 122, 29–36. doi:10.1016/j.ijbiomac.2018.10.146

Shao, F., Tan, T., Tan, Y., Sun, Y., Wu, X., and Xu, Q. (2016). Andrographolide Alleviates Imiquimod-Induced Psoriasis in Mice via Inducing Autophagic Proteolysis of MyD88. *Biochem. Pharmacol.* 115, 94–103. doi:10.1016/j.bcp.2016.06.001

Sikma, M. A., Van Maarseveen, E. M., Van De Graaf, E. A., Kirkels, J. H., Verhaar, M. C., Donker, D. W., et al. (2015). Pharmacokinetics and Toxicity of Tacrolimus Early after Heart and Lung Transplantation. *Am. J. Transpl.* 15, 2301–2313. doi:10.1111/ajt.13309

Song, C., Yang, C., Meng, S., Li, M., Wang, X., Zhu, Y., et al. (2021). Deciphering the Mechanism of Fang-Ji-Di-Huang-Decoction in Ameliorating Psoriasis-like Skin Inflammation via the Inhibition of IL-23/Th17 Cell axis. *J. Ethnopharmacol* 281, 114571. doi:10.1016/j.jep.2021.114571

Templeton, D. W., Quinn, M., Van Wychen, S., Hyman, D., and Laurens, L. M. (2012). Separation and Quantification of Microalgal Carbohydrates. *J. Chromatogr. A.* 1270, 225–234. doi:10.1016/j.chroma.2012.10.034

Van Der Fits, L., Mourits, S., Voerman, J. S., Kant, M., Boon, L., Laman, J. D., et al. (2009). Imiquimod-induced Psoriasis-like Skin Inflammation in Mice Is Mediated via the IL-23/IL-17 axis. *J. Immunol.* 182, 5836–5845. doi:10.4049/jimmunol.0802999

Varma, S. R., Sivaprakasam, T. O., Arumugam, I., Dilip, N., Raghuraman, M., Pavan, K. B., et al. (2019). *In Vitro* anti-inflammatory and Skin Protective Properties of Virgin Coconut Oil. *J. Tradit Complement. Med.* 9, 5–14. doi:10.1016/j.jtcme.2017.06.012

Voss, K. E., Bollag, R. J., Fussell, N., By, C., Sheehan, D. J., and Bollag, W. B. (2011). Abnormal Aquaporin-3 Protein Expression in Hyperproliferative Skin Disorders. *Arch. Dermatol. Res.* 303, 591–600. doi:10.1007/s00403-011-1136-x

Wang, A., Wei, J., Lu, C., Chen, H., Zhong, X., Lu, Y., et al. (2019). Genistein Suppresses Psoriasis-Related Inflammation through a STAT3-NF-κb-dependent Mechanism in Keratinocytes. *Int. Immunopharmacol* 69, 270–278. doi:10.1016/j.intimp.2019.01.054

Wang, X., Xu, Y., Lian, Z., Yong, Q., and Yu, S. (2014). A One-step Method for the Simultaneous Determination of Five Wood Monosaccharides and the

Corresponding Aldonic Acids in Fermentation Broth Using High-Performance Anion-Exchange Chromatography Coupled with a Pulsed Amperometric Detector. *J. Wood Chem. Tech.* 34, 67–76. doi:10.1080/02773813.2013.838268

Whartenby, K. A., Small, D., and Calabresi, P. A. (2008). FLT3 Inhibitors for the Treatment of Autoimmune Disease. *Expert Opin. Investig. Drugs* 17, 1685–1692. doi:10.1517/13543784.17.11.1685

Wu, Y., Zhu, C. P., Zhang, Y., Li, Y., and Sun, J. R. (2019). Immunomodulatory and Antioxidant Effects of Pomegranate Peel Polysaccharides on Immunosuppressed Mice. *Int. J. Biol. Macromol* 137, 504–511. doi:10.1016/j.ijbiomac.2019.06.139

Yang, Z., Chen, Z., Wang, C., Huang, P., Luo, M., and Zhou, R. (2021). STAT3/SH3PXD2A-AS1/miR-125b/STAT3 Positive Feedback Loop Affects Psoriasis Pathogenesis via Regulating Human Keratinocyte Proliferation. *Cytokine* 144, 155535. doi:10.1016/j.cyto.2021.155535

Yao, D. N., Lu, C. J., Wen, Z. H., Yan, Y. H., Lu, L. M., Wu, H. M., et al. (2021). Comparison of PSORI-CM01 Granules and Yinxieling Tablets for Patients with Chronic Plaque Psoriasis: a Pilot Study for a Randomized, Double-Blinded, Double-Dummy, Multicentre Trial. *Ann. Palliat. Med.* 10, 2036–2047. doi:10.21037/apm-20-2575

Yosipovitch, G., Misery, L., Proksch, E., Metz, M., Ständer, S., and Schmelz, M. (2019). Skin Barrier Damage and Itch: Review of Mechanisms, Topical Management and Future Directions. *Acta Derm Venereol.* 99, 1201–1209. doi:10.2340/00015555-3296

Zhai, X., Zhu, C., Li, Y., Zhang, Y., Duan, Z., and Yang, X. (2018a). Optimization for Pectinase-Assisted Extraction of Polysaccharides from Pomegranate Peel with Chemical Composition and Antioxidant Activity. *Int. J. Biol. Macromol* 109, 244–253. doi:10.1016/j.ijbiomac.2017.12.064

Zhai, X., Zhu, C., Zhang, Y., Sun, J., Alim, A., and Yang, X. (2018b). Chemical Characteristics, Antioxidant Capacities and Hepatoprotection of Polysaccharides from Pomegranate Peel. *Carbohydr. Polym.* 202, 461–469. doi:10.1016/j.carbpol.2018.09.013

Zhou, T., Zhang, S., Zhou, Y., Lai, S., Chen, Y., Geng, Y., et al. (2021). Curcumin Alleviates Imiquimod-Induced Psoriasis in Progranulin-Knockout Mice. *Eur. J. Pharmacol.* 909, 174431. doi:10.1016/j.ejphar.2021.174431

Zhou, W., Hu, M., Zang, X., Liu, Q., Du, J., Hu, J., et al. (2020). Luteolin Attenuates Imiquimod-Induced Psoriasis-like Skin Lesions in BALB/c Mice via Suppression of Inflammation Response. *Biomed. Pharmacother.* 131, 110696. doi:10.1016/j.biopha.2020.110696

Conflict of Interest: The authors declare that the research was conducted in the absence of any commercial or financial relationships that could be construed as a potential conflict of interest.

Publisher's Note: All claims expressed in this article are solely those of the authors and do not necessarily represent those of their affiliated organizations, or those of the publisher, the editors, and the reviewers. Any product that may be evaluated in this article, or claim that may be made by its manufacturer, is not guaranteed or endorsed by the publisher.

frontiers in Pharmacology

ORIGINAL RESEARCH
published: 14 February 2022
doi: 10.3389/fphar.2022.786141

Restorative Effects of Inulin From *Codonopsis pilosula* on Intestinal Mucosal Immunity, Anti-Inflammatory Activity and Gut Microbiota of Immunosuppressed Mice

Yuan-Feng Zou[1†], Cen-Yu Li[1†], Yu-Ping Fu[1], Xin Feng[1], Xi Peng[1], Bin Feng[2], Li-Xia Li[1], Ren-Yong Jia[3], Chao Huang[3], Xu Song[1], Cheng Lv[1], Gang Ye[1], Ling Zhao[1], Yang-Ping Li[4], Xing-Hong Zhao[1], Li-Zi Yin[1] and Zhong-Qiong Yin[1,3*]*

[1]Natural Medicine Research Center, College of Veterinary Medicine, Sichuan Agricultural University, Chengdu, China, [2]Animal Nutrition Institute, Sichuan Agricultural University, Chengdu, China, [3]Key Laboratory of Animal Disease and Human Health of Sichuan Province, College of Veterinary Medicine, Sichuan Agricultural University, Chengdu, China, [4]Institute of Ecological Agriculture, Sichuan Agricultural University, Chengdu, China

OPEN ACCESS

Edited by:
Jing Zhao,
University of Macau, China

Reviewed by:
Bingxian Xie,
University of Pittsburgh, United States
Rui Tan,
Southwest Jiaotong University, China
Quan Xia,
First Affiliated Hospital of Anhui Medical University, China

***Correspondence:**
Yuan-Feng Zou
yuanfengzou@sicau.edu.cn
Zhong-Qiong Yin
yinzhongq@163.com

†These authors have contributed equally to this work and share first authorship

Specialty section:
This article was submitted to Ethnopharmacology, a section of the journal Frontiers in Pharmacology

Received: 29 September 2021
Accepted: 05 January 2022
Published: 14 February 2022

Citation:
Zou Y-F, Li C-Y, Fu Y-P, Feng X, Peng X, Feng B, Li L-X, Jia R-Y, Huang C, Song X, Lv C, Ye G, Zhao L, Li Y-P, Zhao X-H, Yin L-Z and Yin Z-Q (2022) Restorative Effects of Inulin From Codonopsis pilosula on Intestinal Mucosal Immunity, Anti-Inflammatory Activity and Gut Microbiota of Immunosuppressed Mice. Front. Pharmacol. 13:786141. doi: 10.3389/fphar.2022.786141

An inulin (CPPF), isolated from a traditional Chinese herbal medicine *Codonopsis pilosula*, was characterized and demonstrated with potential prebiotic activity *in vitro* before. Based on its non-digested feature, the intestinal mucosa and microbiota modulatory effects *in vivo* on immunosuppressed mice were investigated after oral administration of 200, 100 and 50 mg/kg of CPPF for 7 days. It was demonstrated that the secretions of sIgA and mucin 2 (Muc2) in ileum were improved by CPPF, and the anti-inflammatory activities in different intestine parts were revealed. The intestine before colon could be the target active position of CPPF. As a potential prebiotic substance, a gut microbiota restorative effect was also presented by mainly modulating the relative abundance of *Eubacteriales*, including *Oscillibacter*, *unidentified Ruminococcus* and Lachnospiraceae after high-throughput pyrosequencing of V4 region of 16S rRNA analysis. All these results indicated that this main bioactive ingredient inulin from *C. pilosula* was a medicinal prebiotic with enhancing mucosal immune, anti-inflammatory and microbiota modulatory activities.

Keywords: inulin-type fructan, *Codonopsis pilosula*, immune-enhancement, antiinflammatory, gut microbiota

INTRODUCTION

The inulin, consisting of fructose units linked by β-(2→1) bonds and a terminal glucose by α-(1→2) bond, remains relatively intact after transition through the digestive system (Shoaib et al., 2016). It was demonstrated with effects of improving immune and promoting the proliferation of beneficial bacteria, which are related with their degree of polymerization and plants species (Moreno-Vilet et al., 2014; García Gamboa et al., 2018). All these benefits are related to body health through positively balancing gut microbiota via increasing the abundance of beneficial bacteria and reducing potential pathogens. The pathogens colonization were inhibited by the antagonism from organic acids or inhibitory peptides (García Gamboa et al., 2018). Inulin is also identified with anti-obesity, anti-diabetes, anti-inflammatory, anti-hypertension, anti-oxidative and anti-cancer activities, as well

as exerts abilities to control inflammatory bowel disease, promote colonic absorption of minerals and stimulate the immune system (Karimi et al., 2015; Vogt et al., 2015; Ahmed and Rashid, 2017; Shang HM et al., 2018; Mazraeh et al., 2019). These activities support inulin a widely use as function foods on reducing cardiovascular disease, lowering blood urea and uric-acid levels (Karimi et al., 2015).

The roots of *Condonopsis pilosula* (Radix Codonopsis) has been used in Traditional Chinese Medicine (TCM) for hundreds of years. Three species of its plant sources are recorded in the Pharmacopoeia of the People's Republic of China, including *Codonopsis pilosula* (Franch.) Nannf., *C. pilosula* Nannf. var. *modesta* (Nannf.) L. T. Shen and *C. tangshen* Oliv. (Chinese Pharmacopoeia Committee, 2020), for the treatment of nourishing the spleen and stomach and tonifying *Qi* of stomach. Modern pharmacological studies have uncovered Radix Codonopsis with effects like immunomodulation, anti-ulcer, lowering blood pressure, as well as intestinal flora modulation. It has also been widely used as nutritional supplement in China on homology as both medicine and food (Gao et al., 2018). The polysaccharide fraction is considered as a potential bioactive natural product possessing modulatory effect on immunity and intestinal microbiota (Fu et al., 2018a; Peng et al., 2018; Deng et al., 2019; Zou et al., 2019). Similar functions of polysaccharides from *C. pilosula* Nannf. var. *modesta* (Nannf.) L. T. Shen (CPP), have been reported in our previous studies, like decreasing the levels of interferon-γ (IFN-γ), interleukin-2 (IL-2), IL-10, elevating serum ileum IgG, intestinal secretory immunoglobulin A (sIgA), and the amount of *Lactobacillus* and acetic acid content in cecum on cyclophosphamide (CY)-induced immunosuppressed mice (Fu et al., 2018a). And inulin, a reserve carbohydrate of Radix *Codonopsis,* has also been identified with high proportion (62%, w/w) as the neutral composition of CPP, with degree of polymerization (DP) of 2–17, and exerted underlying prebiotic activity *in vitro* (Fu et al., 2018b). Therefore, we deduced that the inulin as the main bioactive component of CPP, acts on intestinal mucosal improvement and microbiota regulation. The active target organ is possibly the intestine due to its non-digested property and the conclusions in our experimental work mentioned above. Moreover, the fermentable properties of inulin are related to their chemical structure, especially Mw (Gibson and Delzenne, 2008). There is a possibility that certain short inulin could have been digested completely when it arrives specific intestinal positions, which is seldom proofed by study of inulin from natural herbs. It is consequently of interest to figure out its efficacy on anti-inflammation in different intestinal segments, which could be helpful for the clinical application of inulin on various intestinal inflammatory disease.

Therefore, in this study, the intestinal modulatory effects of inulin from *C. pilosula* was evaluated from aspects of intestinal mucosal immunity, anti-inflammatory and gut microbiota modulatory functions on immunosuppressed mice. Among them, a comparison of anti-inflammatory with different intestinal segments was investigated in order to find the target intestine location.

MATERIALS AND METHODS

Materials and Chemicals

The roots of *C. pilosula* Nannf. var. *modesta* L. T. Shen were collected in October 2017 from Jiuzhaigou County (Tibetan Qiang Autonomous Prefecture of Ngawa, China), and identified by Yuan-Feng Zou, College of Veterinary Medicine, Sichuan Agricultural University. The roots were dried and pulverized to a fine powder, and the fructan was obtained by DEAE-sepharose gel chromatograph, and identified as inulin-type fructan (the fructan form *C. pilosula*, CPPF) (Fu et al., 2018b).

The cyclophosphamide (CY, C8650) was obtained from Solarbio technology Co., Ltd., (Beijing, China). The ELISA kits, including mouse IL-1β, tumor necrosis factor-α (TNF-α), sIgA and mucin 2 (Muc2), were purchased from Enzyme-linked Biotechnology Co., Ltd., (Shanghai, China). The acetic acid (71251), propionic acid (94425) and butyric acid (19215) standards were purchased from Sigma-Aldrich (St. Louis, MO, United States). The primeScript RT reagent kit (with gDNA Eraser, RR047A), the TB Green Premix Ex Taq II (Tli RNaseH Plus, RR821A) and Trizol RNA isolation reagent were obtained from TAKARA, Japan. All other chemicals, such as chloroform, isopropanol, etc., were of analytical grade, obtained from the Chengdu Kelong chemical factory (Chengdu, China).

Animal Care and Experimental Design

Sixty male specific-pathogen-free C57BL/6 mice (6–8 weeks old) were purchased from Beijing Vital River Laboratory Animal Technology Co., Ltd (Beijing China). They were maintained in a specific pathogen-free environment, where the temperature was 25 ± 2°C, with humidity of 60%. All mice were acclimatized for 7 days with an automatically-controlled 12 h light/dark cycle and free access to sterile food and distilled water.

Although CY is an alkylating drug used on cancer and autoimmune disease, it has been used as an immunosuppression-inducing agent due to its major side effect (Wang Z et al., 2019). In this study, a stable and classical CY-induced immunosuppression model was used to evaluate the recovery effect of CPPF on both intestinal immunity and microbiota modulation, according to several previous studies (Tang et al., 2018; Zhu et al., 2018; Wang Z et al., 2019). The mice were divided into five groups, 12 mice each. The immunosuppressed mice (4 groups) were given 60 mg/kg (0.1 ml/10 g body weight) CY for 3 days *via* intraperitoneal injection, once a day (Fu et al., 2018a). The normal mice were injected with 0.1 ml/10 g body weight saline as Control group. After 3 days of CY/saline treatment, the mice were administrated orally with freshly prepared CPPF (dissolved in saline) at dosage of 200, 100, 50 mg/kg (dosages were set in line with that of CPP in our previous study (Fu et al., 2018a) or saline (0.1 ml/10 g body weight) for 7 days in succession, as CY + CPPF-H, CY + CPPF-M, CY + CPPF-L and Control/CY groups, respectively. After 24 h of the last administration, all mice were euthanized with carbon dioxide followed by cervical dislocation, and the different

segments of intestinal tissues, and the content of cecum were separated immediately and stored at −80°C.

Determination of the Intestinal Cytokines, sIgA and Muc 2

IL-1β and TNF-α secretions in intestine tissues (including jejunum, ileum, and colon), and sIgA, Muc2 in ileum, were determined using ELISA kits. The intestinal tissues were ground in liquid nitrogen and homogenized in saline (50 mg/ml). The supernatants after centrifugation at 2,862 g for 20 min, 4°C, were collected and determined according to the manufacturer's instructions.

Quantitative Real-Time PCR

RNA extraction from jejunum, ileum and colon tissues (without content) and the quantitative real-time PCR (qRT-PCR) were performed as previously reported (Huang et al., 2014). Briefly, total RNA was extracted using Trizol reagent, and the quality and nucleic acid concentration were measured using spectrophotometer (NanoDrop 2000; Thermo Scientific, Shanghai, China). Reverse transcription was processed according to the manufacturer's instructions (two-step). Quantitative real-time PCR was performed using the Bio-Rad CFX-96 system and TB Green Premix Ex Taq II kit. Gene expressions were normalized related to β-Actin, with primer sequences for SYBR Green probes of NGB obtained from Primer Bank: β-actin (No. 6671509a1), IL-1β (No.118130747c1) and TNF-α (No.133892368c2).

Bacteriological Analysis and the Determination of Short-Chain Fatty Acids

The intestinal digesta of cecum were isolated after last gavage, and divided into two parts stored at −20°C (for SCFAs determination) and −80°C (for the bacteriological analysis). The samples stored at −80°C were transported to Beijing Novogene Science and Technology Co., Ltd. under dry-ice cooling environment. The DNA was extracted using CTAB/SDS method, and diluted to 1 ng/μL using sterile water. The V4 region of 16S rRNA was amplified through PCR using specific primer (515F: CCTAYGGGRBGCASCAG; 806R: GGACTACNNGGGTATCTAAT) with the barcode, then purified with GeneJETTM Gel Extraction Kit (Thermo Scientific). Sequencing libraries were generated using Ion Plus Fragment Library Kit 48 rxns (Thermo Scientific) following manufacturer's recommendations. The library quality was assessed on the Qubit@ 2.0 Fluorometer (Thermo Scientific). The library was sequenced on an Ion S5^{TM} XL platform and 400 bp/600 bp single-end reads were generated. Sequences analysis were performed by Uparse software (Uparse v7.0.1001), and the analysis of diversity were calculated with QIIME (Version1.7.0) and displayed with R software (Version 2.15.3). The concentrations of SCFAs, including acetic acid, propionic acid and butyric acid, were detected on gas chromatography (GC) after several procedures for pretreatment based on the method of previous study (Fu et al., 2018a). They were quantitated according to the standard curve with crotonic acid as internal standard.

Statistical Analysis

The SPSS 22.0 software was used to carry out a One-way ANOVA test, followed by LSD post-hoc test. All the experimental data were expressed as Mean ± SD ($\bar{x}$ ± SD) in table and Mean ± SEM ($\bar{x}$ ± SEM) in figures. The p-value of 0.05 or less was considered with statistically significance.

RESULTS

The sIgA and Muc2 Secretion Were Promoted by CPPF

As the basic and essential immune antibody secreted in intestinal mucosa, sIgA could be promoted by polysaccharides from plenty of traditional medicines (Huang X et al., 2017; Sheng et al., 2017). It was demonstrated that CPPF, in both CPPF-H and CPPF-M groups, significantly promoted the secretion of sIgA in ileum ($p > 0.05$), even though it was not inhibited by CY, as shown in **Figure 1A**. Mucin, one of the chemical components in intestinal immune system, acts as the main line of defense to protect the epithelial cells from plenty of microbiota in the gut lumen (Kim and Ho, 2010). It was also revealed that the Muc2 secretion in ileum was not influenced by CY, but was facilitated markedly by CPPF in a dosage-dependent manner, as shown in **Figure 1B**. These results suggested that CPPF could play a promotive effect on intestinal mucosal immune system.

The Anti-Inflammatory Effect of CPPF in Intestine

CY has been demonstrated with an induction of inflammatory reaction, as well as damages on intestinal mucosa and microbiota balance (Shang et al., 2016; Lee and Kang, 2017). While, the biological functions of inulin have been reported through anti-inflammation and modulation on gut microbiota as prebiotics (Li et al., 2019). However, the degradation status of inulin in intestinal tract is unknown so far, and whether its biological activities would be affected is also unclear. We investigated a polysaccharide from *Ligusticum chuanxiong*, the LCP-II-I, that it only displayed antioxidant activity well before colon *in vivo* (Huang C et al., 2017). Thus, the anti-inflammatory effect of CPPF on different intestinal segments were assessed, including jejunum, ileum and colon, in both mRNA and protein expression aspects.

The gene expressions of IL-1β and TNF-α were significantly increased both in jejunum and ileum after CY injection ($p < 0.05$) compared with the Control group (**Figures 2A,B,D,E**), except colon ($p > 0.05$) (**Figures 2C,F**). However, CPPF at high and medium dosage inhibited these inflammatory reactions induced by CY ($p < 0.05$), especially at high dosage group ($p < 0.01$). But, these suppression didn't appear in colon, as shown in **Figure 2**. Given a poor expression and lower recovery effect by CPPF in colon, the protein secretion of IL-1β and TNF-α were not determined in further studies. Being consistent with their

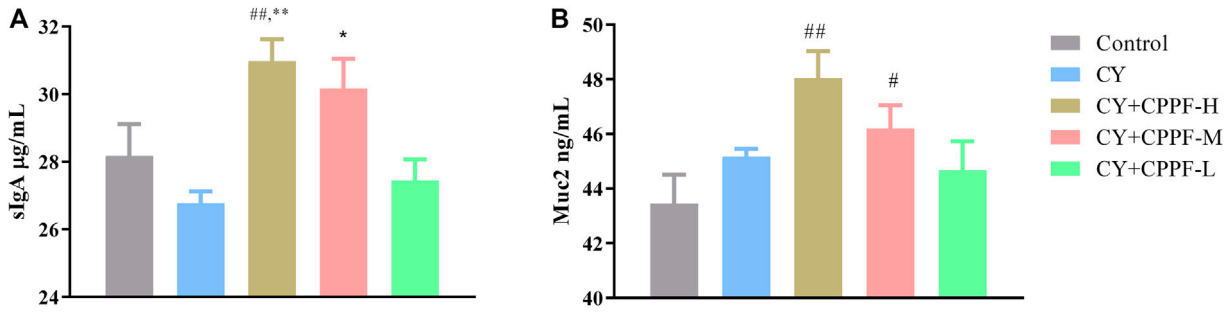

FIGURE 1 | The effect of CPPF on sIgA (**A**) and Muc2 (**B**) secretion in ileum tissue; * indicated significant difference compared with CY group, $p < 0.05$; ** indicated significant difference compared with CY group, $p < 0.01$; # indicated significant difference compared with Control group, $p < 0.05$; ## indicated significant difference compared with Control group, $p < 0.01$; $n = 12$.

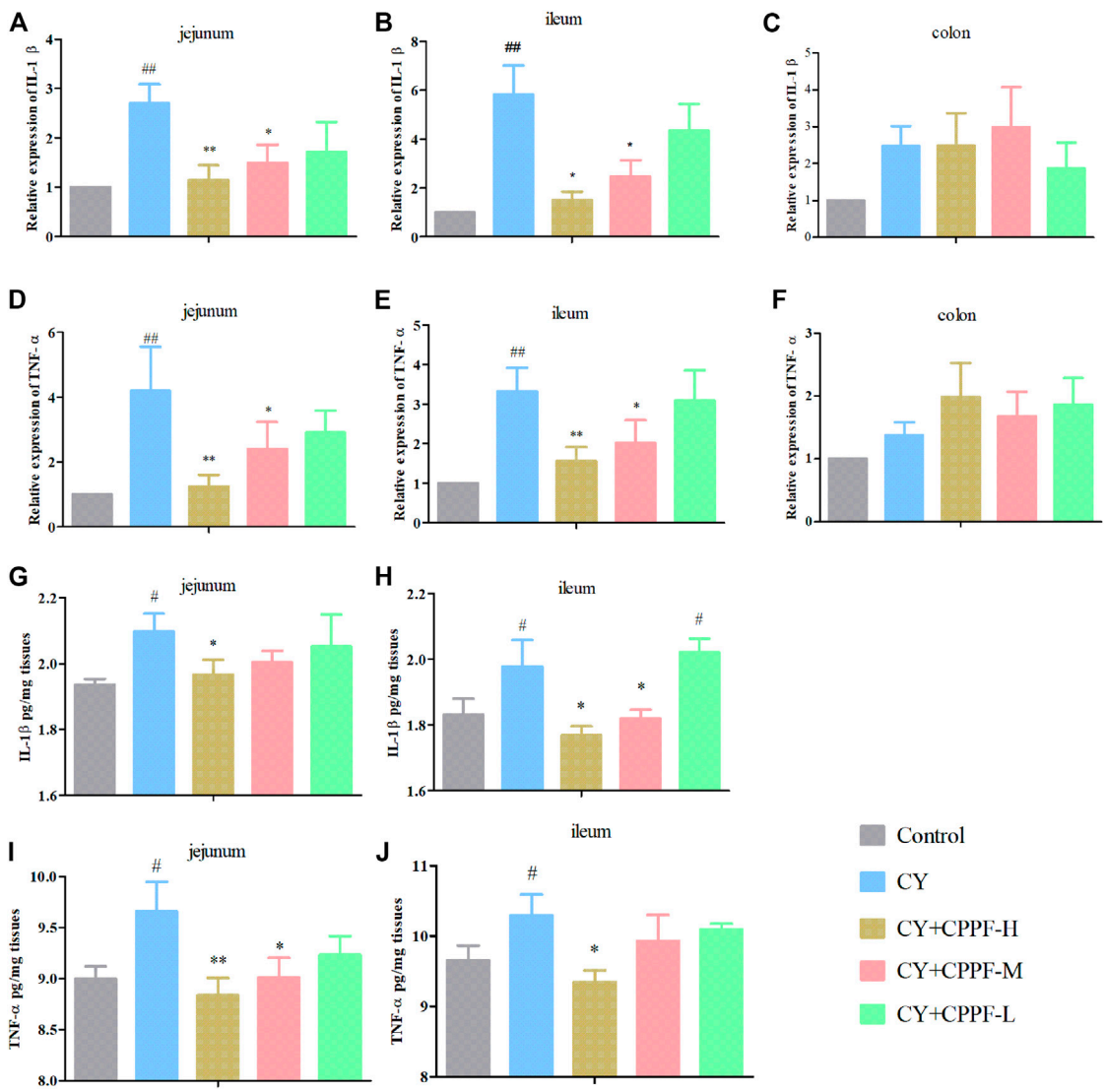

FIGURE 2 | The effect of CPPF on IL-1β (**A–C,G,H**) and TNF-α (**D–F,I,J**) mRNA and protein expression in different parts of intestine tissue; * indicated significant difference compared with CY group, $p < 0.05$; ** indicated significant difference compared with CY group, $p < 0.01$; ## indicated significant difference compared with Control group, $p < 0.01$; # indicated significant difference compared with Control group, $p < 0.05$, $n = 12$.

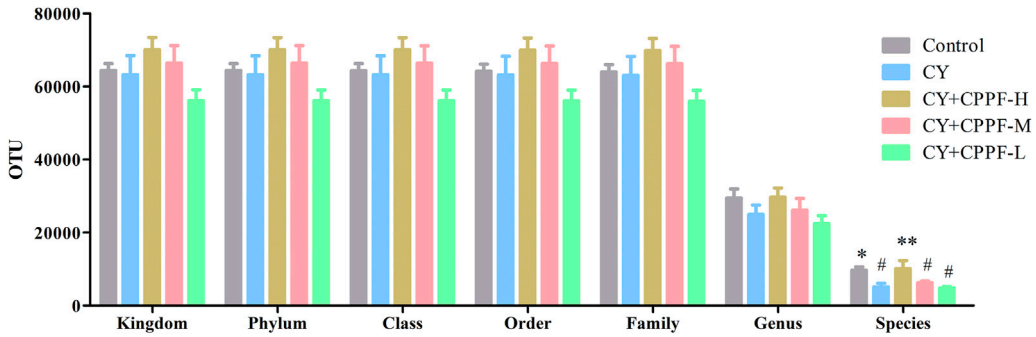

FIGURE 3 | The Operational Taxonomic Units (OTUs) at Kingdom, phylum, class, order, family, genus and species levels of cecal content. * indicated significant difference compared with CY group, $p < 0.05$; ** indicated significant difference compared with CY group, $p < 0.01$; # indicated significant difference compared with Control group, $p < 0.05$; $n = 7$.

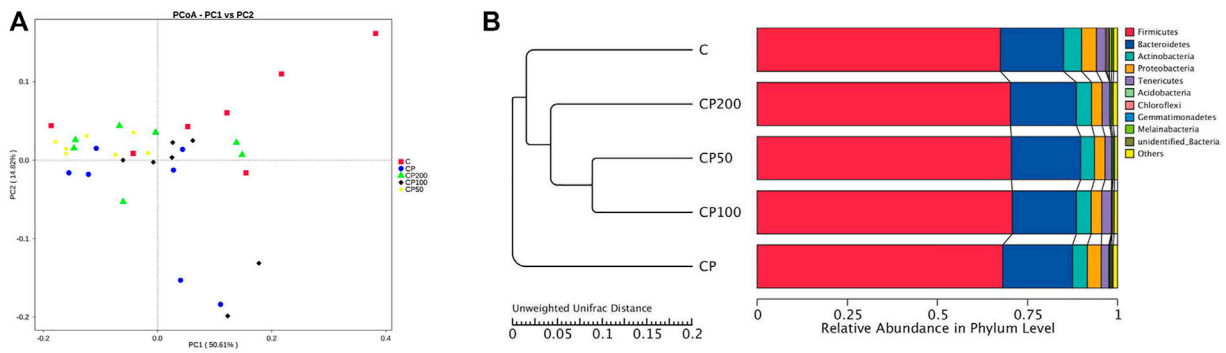

FIGURE 4 | PCoA **(A)** and UPGMA **(B)** analysis; C was the Control group, CP was the CY group, CP200 was the CY + CPPF-H group, CP100 was the CY + CPPF-M group, and CP50 was the CY + CPPF-L group; $n = 7$.

mRNA expression, the protein secretions of IL-1β and TNF-α in jejunum and ileum were enhanced remarkably after CY treatment, and were restored by CPPF (**Figures 2G–J**), especially that in CPPF-H group. Hence, it was revealed that the CPPF exerted an anti-inflammatory effect on immunosuppressed mice, and only worked before colon.

The CPPF Modulated the Gut Microbiota Composition

The Operational Taxonomic Units, α-Diversity and β-Diversity Analysis

In order to study the bacterial composition of immunosuppressed mice, the OTUs (97% consistency) were clustered on the effective tags of all samples, and species annotation was further performed on the representative sequences of OTUs, as shown in **Figure 3**. It was classified and counted after removing low-quality sequences, and indicated that CPPF showed a trend of increasing OTUs at different levels compared with CY group ($p > 0.05$). Among them, OTUs value was reduced by around 50% in CY group at species level compared with that in Control group ($p < 0.05$), and was recovered after 200 mg/kg CPPF administration ($p < 0.05$). The other two CPPF groups also showed a recovery trend in a certain extent ($p > 0.05$).

All the differences and similarities of bacterial communities between groups were revealed by the weighed UniFrac distances at the phylum level, and displayed by PCoA analysis (**Figure 4A**). Based on the reduced observed species, ACE and PD whole tree index in α-diversity (**Table 1**), CY was suggested with an obvious regulation relatively to control group ($p < 0.05$), and a recovery trend by CPPF was also observed ($p > 0.05$). The Unweighted Pair-Group Method with Arithmetic Mean (UPGMA) was used to study the similarities and cluster analysis, which was showed as a systematic clustering tree (**Figure 4B**). It was exhibited that the bacteria belonging to *Firmicutes* were promoted after CPPF supplement. While, the bacteria belonging to *Bacteroidetes* were regulated in any group ($p>0.05$). The relative abundance of other phylum, like *Acidobacteria*, *Chloroflexi*, *Gemmatimonadetes*, *Melainabacteria* in CY treated groups, differed with those in control group, which also demonstrated a microbial dysbiosis affected by CY.

The Modulation of Gut Microbiota Composition by CPPF

The relative abundance of top 10 bacteria was calculated based on the species annotation and classification, and expressed as histograms and heatmap both at phylum and genus levels in

TABLE 1 | The statistical results of α-diversity indices.

	Control	CY	CY + CPPF-H	CY + CPPF-M	CY + CPPF-L
observed_species	498.43 ± 52.43	458.86 ± 49.54[a]	464.86 ± 19.66	462.57 ± 16.70	463.71 ± 29.10
ACE	536.20 ± 51.91	494.55 ± 50.42[a]	503.95 ± 24.95	500.60 ± 24.49	496.49 ± 33.57
PD_whole_tree	36.25 ± 4.17	31.54 ± 3.91[a]	32.42 ± 3.40	33.41 ± 4.48	31.02 ± 4.00[a]

$p < 0.05$; *it was indicated that there was dramatically decrease of alpha diversity in CY, group compared with control group.*
[a]*Indicated significant difference compared with Control group.*

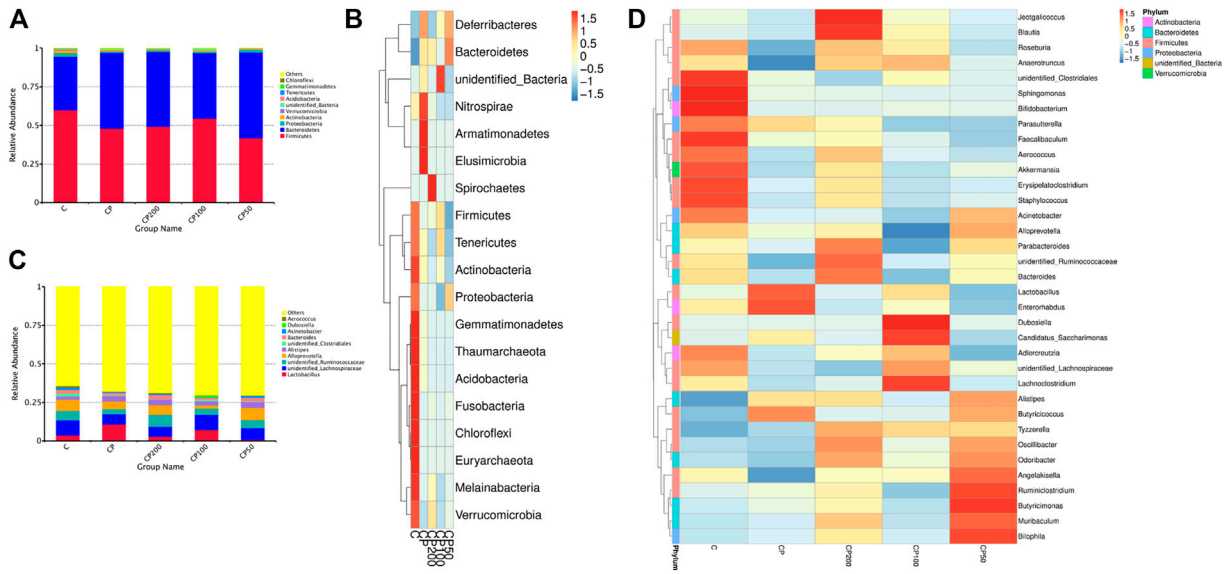

FIGURE 5 | The histograms and heatmaps of bacterial composition change at phylum **(A,B)** and genus level **(C,D)**; C was the Control group, CP was the CY group, CP200 was the CY + CPPF-H group, CP100 was the CY + CPPF-M group, and CP50 was the CY + CPPF-L group; $n = 7$.

Figure 5. The main bacteria compositions of immunosuppressed mice were changed, showing a remarkable lower relative abundance of *Firmicutes* (like *Erysipelatoclostridium, Lachnoclostridium, Unidentified* Ruminococcaceae, and Ruminococcaceae, **Supplementary Figures S1, S2**), *Melainabacteria*, and *Actinobacteria* ($p > 0.05$), and a higher abundance of *Bacteroidetes* (like family Muribaculaceae, **Supplementary Figure S2**) and *Deferribacteres* ($p < 0.05$, **Figure 6A**). While the bacteria of *Firmicutes* phyla, such as genus *Unidentified* Ruminococcaceae, *Oscillibacter* (**Supplementary Figures S3, S4**), *Lachnoclostridium, Anaerotruncus,* and *Angelakisella* (**Supplementary Figures S4, S5**) were enhanced dramatically in mice treated with CPPF ($p < 0.05$), and those of *Bacteroidetes* were notably reduced, such as genus *Alloprevotella* (**Supplementary Figure S5**, $p < 0.05$).

The difference of microbial community structure was analyzed by the analysis of similarities (Anosim), MRPP and AMOVA (data not shown), the species with significant change on abundance at different levels among those five groups were found by MetaStat method, as presented in **Figure 6**. It was demonstrated that CY has led to a gut microbiota imbalance, primarily altered the bacterial abundance of *Deferribacteres* (**Figure 6A**), Muribaculaceae (**Figure 6B**), *Papillibacter* (**Figure 6C**), *Lactobacillus reuteri* (**Figure 6D**), *Mucispirillum schaedleri* (**Figure 6E**), and *Clostridium* sp ASF356 (**Figure 6F**). However, after supplementation of CPPF, the abundance of bacteria of *Deferribacteres*, *Papillibacter* and *Clostridium* sp ASF356, were recovered prominently within just 7 days of treatment, compared with CY or Control group ($p < 0.05$), which indicated a promising modulatory effect of CPPF on gut bacterial community.

Moreover, in order to discover and interpret the high-dimensional biomarkers, the LEfSe (LDA Effect Size) was used to find the statistical differences among groups. The significantly different species were picked out after analysis with LDA score (above 4) and cladogram (data not shown). Muribaculaceae and Undentified Ruminococcaceae were the two that have been specifically modulated among such huge population, and accordingly, a prebiotic and restorative effect against CY by CPPF were performed (**Figure 7**). Briefly, the bacteria of order *Eubacteriales* were mainly regulated by CPPF, including genus *Oscillibacter, Ruminococcus, Papillibacter* in family Oscillospiraceae, and Lachnospiraceae.

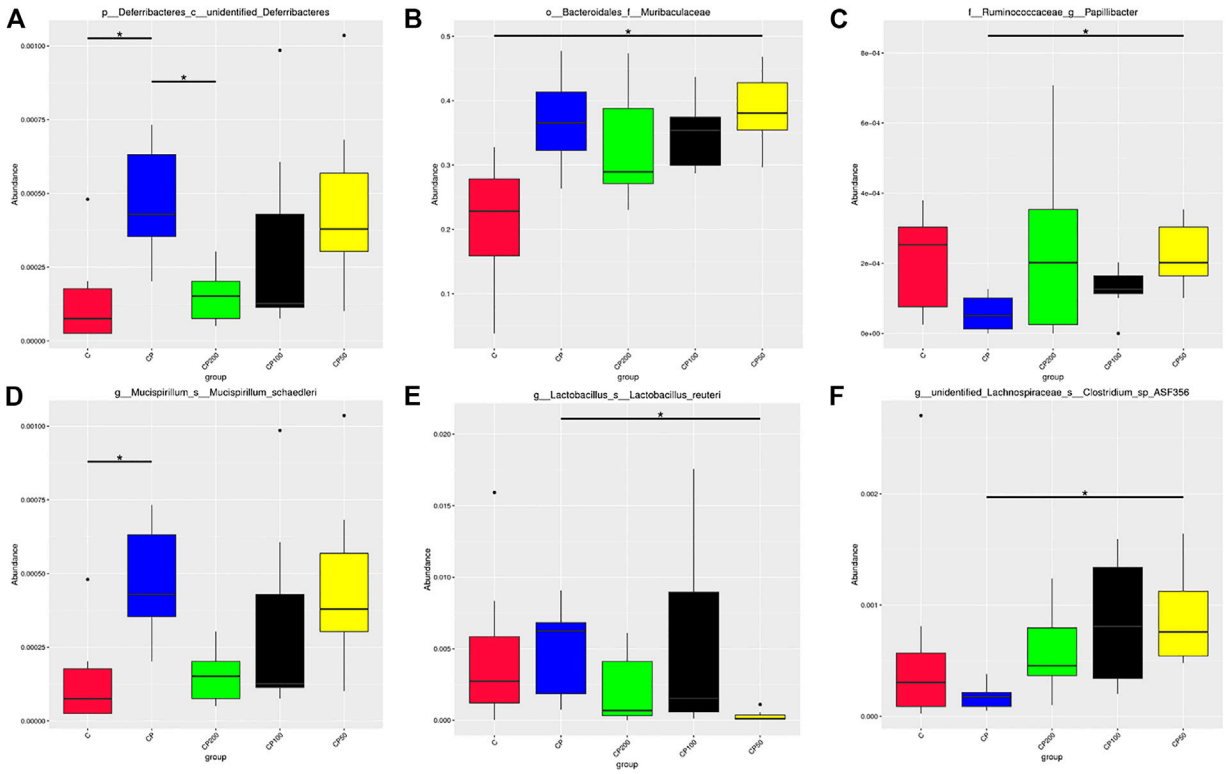

FIGURE 6 | Species with significant differences at the level of class **(A)**, family **(B)**, genus **(C)**, and species **(D–F)**; * indicated that the difference between groups was significant $p < 0.05$; C was the Control group, CP was the CY group, CP200 was the CY + CPPF-H group, CP100 was the CY + CPPF-M group, and CP50 was the CY + CPPF-L group; $n = 7$.

The Determination of SCFAs

It has been revealed that inulin can be metabolized into SCFAs by microbial fermentation. The reduced gut lumen pH by SCFAs could inhibit the proliferation of pathogenic bacteria and stimulate intestinal peristalsis. These acids could be further utilized by intestinal epithelial cells for protecting the integrity of barrier function (Meijer et al., 2010). In this study, SCFAs concentrations in the cecal content, the position rich in bacterial community, were detected. The levels of acetic (**Figure 8A**) and propionic acids (**Figure 8B**) were decreased significantly by CY ($p < 0.05$), and the high dosage of CPPF could reverse this reduction, even without statistical difference. The butyric acid showed scarce change among different groups, but that in CPPF groups displayed an underlying increase ($p > 0.05$), as shown in **Figure 8C**.

DISCUSSION

As a common medicinal material, *C. pilosula* and its polysaccharide component have presented versatile pharmacological activities. Particularly, the polysaccharide from *C. pilosula* have been evidenced possessing both prebiotic and immunomodulatory activities *in vitro* or *in vivo*, by a range of previous studies (Peng et al., 2018; Deng et al., 2019) and experimental results in our group, including crude polysaccharide CPP (Fu et al., 2018a), inulin-type fructan CPPF (Fu et al., 2018b) and pectic polysaccharides (Zou et al., 2019). Considering its macromolecular and non-digestible properties in upper gastrointestinal tract, such natural polysaccharides can reach to intestine without degradation because of the limited hydrolysis enzymes in human (Wilson and Whelan, 2017; García Gamboa et al., 2018). Considering the modulation effects of *Codonopsis*-derived polysaccharides (Zhou et al., 2015; Li et al., 2018; Zou et al., 2019) or inulin (Vogt et al., 2015; Akram et al., 2019) on intestinal mucosal immune, the intestinal mucosa and/or gut microbiota were considered as a potential way that CPPF probably act.

Studies have demonstrated that CY destroys intestinal mucosal system by reducing barrier function, injuring intestinal villi and crypts, inhibiting secretion of sIgA and damaging Peyer's patch (Miao et al., 2015; Zhao et al., 2016; Wang Z et al., 2019). In gastrointestinal mucosal barrier, goblet cells continually produce mucins to replenish and maintain the mucus barrier, where some chemical composition like sIgA is higher concentrated (Ouwerkerk et al., 2013; Cornick et al., 2015). The Muc2 and sIgA secretion were facilitated by CPPF, in accordance with other inulin reported before (Ito et al., 2008; Nagata et al., 2018). It could be directly resulted from activation of mucosal receptors cooperated with downstream signal pathways, or gut-associated lymphoid tissues (GALTs). Secretion cells, such as goblet cell, Paneth cells and enteroendocrine cells could also be

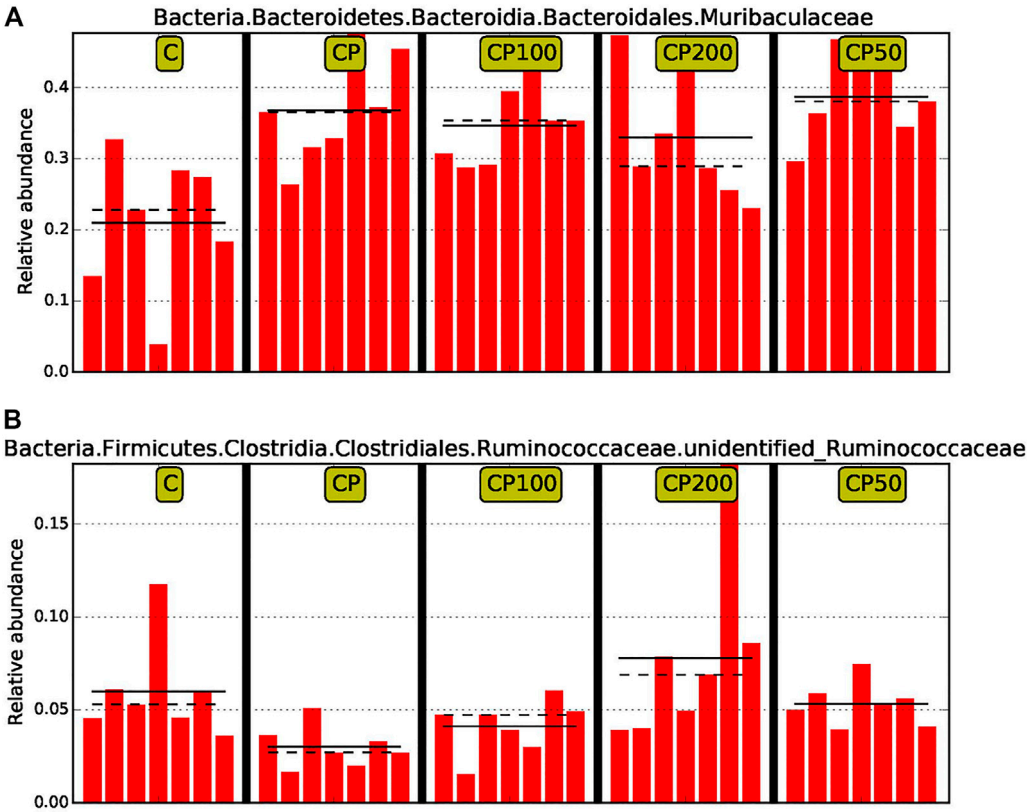

FIGURE 7 | The comparison of relative abundance of biomarkers with statistical differences between groups based on the LefSe results. The highest abundance of each biomarker in the sample was set as 1, while the rest samples were expressed by the value of relative abundance to the highest abundance sample. The solid line and dotted line represented the mean and median of the relative abundance of each sample respectively; C was the Control group, CP was the CY group, CP200 was the CY + CPPF-H group, CP100 was the CY + CPPF-M group, Q18 and CP50 was the CY + CPPF-L group; n = 7.

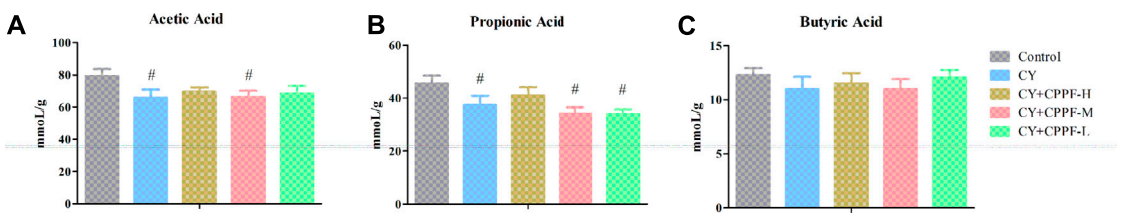

FIGURE 8 | The effect of CPPF on the levels of SCFAs including **(A)** acetic acid, **(B)** propionic acid and **(C)** butyric acid in ileum tissue; C was the Control group, CP was the CY group, CP200 was the CY + CPPF-H group, CP100 was the CY + CPPF-M group, and CP50 was the CY + CPPF-L group; N = 7.

involved (Kim and Ho, 2010; Vogt et al., 2015). It also possibly came from the intestinal bacteria change in an indirect way (Kim and Ho, 2010), that the abundance of certain mucus-degrading bacteria could be reduced (Schroeder et al., 2018; van den Abbeele et al., 2018). Thus, detailed composition changes in gut microbiota were analyzed.

Tissues with high proliferation rate, like intestinal epithelia cells, are vulnerable to CY because of its ability of killing dividing cells. Those damaged cells and produced reactive oxygen species (ROS) will induce apoptosis and up-regulate inflammatory cytokines (Taminiau et al., 1980; Moore, 1984; Sonis, 2004). There are numerous studies indicated that the treatment of CY could promote inflammatory cytokine secretion like IL-1β, TNF-α of porcine epithelial cells (Lee and Kang, 2017) or in small intestine (Shi et al., 2017; Wang X et al., 2019). Moreover, commercial inulin from Mexican blue agave (*Agave tequilana* Weber var. azul) or Chicory have been used as nutritional supplements with an anti-inflammatory effect in intestine (Rivera-Huerta et al., 2017; Akram et al., 2019; Zhao et al., 2019). However, it was very likely the first time showing the active target location of inulin from natural medicinal plants. Some studies indeed found an anti-inflammatory effect in

intestinal mucosa of polysaccharide from *C. pilosula* (Zhou et al., 2015; Chen, 2016; Li et al., 2018). But no comprehensive investigation was declared that which intestinal part it can work on. Combing with previous studies of LCP-II-I (Huang C et al., 2017), we now have sufficient experimental evidence proving that these polymers could be active only before colon *in vivo*, since they could already been degraded or fermented in colon. In addition, the main factor of fermentation rate of inulin could be the DP variation (Gibson and Delzenne, 2008). Zhao et al. (2019) revealed that 28 days of short chain fructooligosaccahrides (scFOS) with maximum DP of 6, could down-regulate IL-1β expression in jejunal mucosa, but not active in ileum. Comparatively, the DP of CPPF in our study was higher (about 2–17) (Fu et al., 2018b), and could be degraded much slowly and even far in intestine tract. That was probably the main reason that CPPF displayed well on anti-inflammatory effect in both jejunum and ileum.

Polysaccharides from marine animals, fruits, vegetables and natural medical plants, have been found with high fermentable and modulatory effect by gut microbiota (Bosscher et al., 2006; Xu et al., 2013; Shoaib et al., 2016; Shang Q et al., 2018). Although immunosuppressed mice were treated with CPPF for only 7 days, there was still bacterial community change observed in our research. Some similar studies (Chen et al., 2017; Moens and De Vuyst, 2017; Zhu et al., 2017; Hoving et al., 2018; Baxter et al., 2019; Li et al., 2019) also manifested that the abundance of *Clostridium*, *Deferribacteres*, Ruminococcaceae, Lachnospiraceae or *Oscillospira* were regulated by several weeks of inulin treatment. As one of probiotics, *Ruminococccceae* has been well reported with a responsible relation to polysaccharides degradation, like fucoidans and inulin (Shang et al., 2016; Moens and De Vuyst, 2017). In this study, a remarkable increase of *unidentified* Ruminococcaceae was demonstrated by CPPF, which proved it with a prebiotic activity. CPPF also displayed an ameliorated effect by decreasing the amount of *Mucispirillum schaedleri*, which is parasitic in intestinal mucous layer, and can easily translocate in intestinal mucosa and activate NF-kB or PPAR-delta receptors to trigger inflammatory response (Loy et al., 2017). The *Oscillospira* recovered by CPPF is one of the butyrate-producing bacteria, and are usually considered as protector against several pathogens by acidifying intestinal environment. This recovery has also been achieved by polysaccharides from purple sweet potato on immunosuppressed mice (Tang et al., 2018). Moreover, it was found that the *Blautia* in the family of Lachnospiraceae was promoted after CPPF administration as shown in **Figure 5D**. It has been proved that the relative abundance of *Lachnospiraceae* has significant correlation with host physiological dysfunctions, such as obesity, diabetes, cancer, and various inflammatory diseases, and could be an underlying probiotic (Liu et al., 2021).

Furthermore, the relative abundance of *Lactobacillus* was displayed an opposite trend with our previous results, that it was reduced relatively in mice treated with inulin, which was also showed in study of Hoving et al. (2018). After reviewing the overall microflora data, we inferred that it might be due to the different *Lactobacillus* species that we used in previous and current study. And the overwhelming reduction by CY on the abundance of other bacteria could lead to a relatively increase of *Lactobacillus*. A comparatively lower abundance in CPPF groups may therefore be observed. The dose could be another factor leading to a lower prebiotic effect. No significant change on the relative abundance of Bifidobacteriaceae and Lactobacillus was observed after even above 1.25 g/kg of inulin/FOS administration (Zhu et al., 2017).

As one of the non-digested polymers, inulin can reach to intestine intactly, and serve as energy source for beneficial bacteria that generate metabolites like SCFAs. The increase of butyric acid, the main one utilized by colonocytes, was related to a higher abundance of genera Ruminococcaceae (Biddle et al., 2013; Fernández et al., 2016), which produces butyrate as most abundant family in the order *Clostridiales*. Additionally, Ruminococcaceae was indicated with positive correlation with butyrate/SCFA ratio *in vivo* (Biddle et al., 2013). And the *Oscillibacter*, *Ruminococcus* and *Papillibacter,* belonging to family Ruminococcaceae, were all promoted by CPPF in our study. This alteration on bacterial composition could be the main reason of the certain high butyric acid in CPPF group compared with CY group, similar with previous studies (Moens and De Vuyst, 2017; Baxter et al., 2019). The acetic acid is produced by most enteric bacteria. Its dramatically drop in cecal content could because of the lower bacterial OTUs induced by CY. While the less restoration in CPPF groups could be due to the lower abundance of acetic acid-producing bacteria, like *Lactobacillus* (Fernández et al., 2016) (**Figure 5**). The relative abundance of genera *Bacteroides*, who converts sugars to beneficial metabolites, like propionic acids (Biddle et al., 2013; Fernández et al., 2016), were higher in CPPF-H group than CY group, and was coincident with results of SCFAs levels. Propionic acid could be produced mainly by ketone fermentation (e.g., fructose, arabinose and tagatose) *in vitro* (Hu et al., 2013). The abundant fructose in CPPF could be one of the reasons of its higher concentration. Comparatively, the acetic and butyric acids are produced mainly by aldehydes fermentation (e.g., glucose, galactose, mannose and xylose) (Hu et al., 2013). These changes on acetic and butyric acids are likely coming from bacteria modulated by CPPF in current research, rather than its degradation metabolites, as CPPF is consisted of a lower amount of glucose relatively to fructose. However, such advantageous SCFAs were not promoted by CPPF. The possible reason is that the mice were not intervened enough to show a significantly change on gut flora and carbohydrate fermentation. And the relative abundance of those SCFAs-producing bacteria could be influenced by complicated micro-environment, which is also a challenge of studies on microbiota and polysaccharide degradation.

CONCLUSION

After identification of the structural and prebiotic features, the inulin-type fructan from *Codonopsis pilosula* (CPPF) was further studied on its modulatory effect on intestinal mucosa and gut microbiota. It was demonstrated that the intestinal mucosal immune of CY-induced immunosuppressed mice was restored by CPPF through promotion of Muc2 and sIgA secretions. A new

view that the intestinal anti-inflammatory effects of CPPF only worked before colon was also provided. The modulatory effect on gut microbiota was also investigated, that CPPF increased the relative abundance of *Oscillibacter*, *unidentified Ruminococcus*, Lachnospiraceae and decreased that of *Deferribacteres*. It was suggested that CPPF could be considered as the main bioactive component of *C. pilosula* polysaccharide, being used as a potential prebiotic with improving intestinal mucosal immune, anti-inflammatory and microbiota modulation activities.

DATA AVAILABILITY STATEMENT

The original contributions presented in the study are included in the article/**Supplementary Material**, further inquiries can be directed to the corresponding authors.

ETHICS STATEMENT

The animal study was reviewed and approved by Ethics Committee of Sichuan Agricultural University (No. 20180514) which was issued according to the regulation of Administration of Affairs Concerning Experimental Animals of China.

AUTHOR CONTRIBUTIONS

Y-FZ and Z-QY designed and funded this study, and revised the manuscript; C-YL wrote and revised the main draft of this manuscript; Y-PF prepared the inulin sample, finished the serum and intestine samples, and analyzed the microbiota composition; XP and XF helped with the animal management, sample orally administration; BF helped the formal improvement and revision of the manuscript, as well as the SCFAs determination. L-XL and Y-PL helped with plant material resources; R-YJ, CH, and CL organized all animal experiments, ethic training and daily management; XS, GY, LZ, L-ZY and X-HZ improved the visualization and methodology, and helped with instrument training and data analysis.

FUNDING

This research was funded by the International Cooperation Projects of Science and Technology Department of Sichuan Province (2017HH0093), General Financial Grant from the China Postdoctoral Science Foundation (2016M602704), and Sichuan Veterinary Medicine and Drug Innovation Group of China Agricultural Research System (SCCXTD-2020-18).

ACKNOWLEDGMENTS

We acknowledge the support by the Key Laboratory of Animal disease and Human Health of Sichuan Province.

SUPPLEMENTARY MATERIAL

The Supplementary Material for this article can be found online at: https://www.frontiersin.org/articles/10.3389/fphar.2022.786141/full#supplementary-material

REFERENCES

Ahmed, W., and Rashid, S. (2017). Functional and Therapeutic Potential of Inulin: A Comprehensive Review. *Crit. Rev. Food Sci. Nutr.* 59 (1), 1–13. doi:10.1080/10408398.2017.1355775

Akram, W., Garud, N., and Joshi, R. (2019). Role of Inulin as Prebiotics on Inflammatory Bowel Disease. *Drug Discov. Ther.* 13 (1), 1–8. doi:10.5582/ddt.2019.01000

Baxter, N. T., Schmidt, A. W., Venkataraman, A., Kim, K. S., Waldron, C., and Schmidt, T. M. (2019). Dynamics of Human Gut Microbiota and Short-Chain Fatty Acids in Response to Dietary Interventions with Three Fermentable Fibers. *MBio* 10 (2), e02566–02518. doi:10.1128/mBio.02566-18

Biddle, A., Stewart, L., Blanchard, J., and Leschine, S. (2013). Untangling the Genetic Basis of Fibrolytic Specialization by Lachnospiraceae and Ruminococcaceae in Diverse Gut Communities. *Diversity* 5 (3), 627–640. doi:10.3390/d5030627

Bosscher, D., Van Loo, J., and Franck, A. (2006). Inulin and Oligofructose as Prebiotics in the Prevention of Intestinal Infections and Diseases. *Nutr. Res. Rev.* 19 (2), 216–226. doi:10.1017/S0954422407249686

Chen, K., Chen, H., Faas, M. M., de Haan, B. J., Li, J., Xiao, P., et al. (2017). Specific Inulin-type Fructan Fibers Protect against Autoimmune Diabetes by Modulating Gut Immunity, Barrier Function, and Microbiota Homeostasis. *Mol. Nutr. Food Res.* 61 (8). doi:10.1002/mnfr.201601006

Chen, X. J. (2016). *Sijunzi Decoction and Codonopsis Pilosula Polysaccharide Alleviate DSS-Induced Mice Colitis by Modulating Gut Microbiota*. Master's Thesis. University of Lanzhou.

Chinese Pharmacopoeia Committee (2020). *2020 Edition of Chinese Pharmacopoeia*. Beijing: Chemical Industry Press, 281–282.

Cornick, S., Tawiah, A., and Chadee, K. (2015). Roles and Regulation of the Mucus Barrier in the Gut. *Tissue Barriers* 3 (1-2), e982426. doi:10.4161/21688370.2014.982426

Deng, X., Fu, Y., Luo, S., Luo, X., Wang, Q., Hu, M., et al. (2019). Polysaccharide from Radix Codonopsis Has Beneficial Effects on the Maintenance of T-Cell Balance in Mice. *Biomed. Pharmacother.* 112, 108682. doi:10.1016/j.biopha.2019.108682

Fernández, J., Redondo-Blanco, S., Gutiérrez-del-Río, I., Miguélez, E. M., Villar, C. J., and Lombó, F. (2016). Colon Microbiota Fermentation of Dietary Prebiotics towards Short-Chain Fatty Acids and Their Roles as Anti-inflammatory and Antitumour Agents: A Review. *J. Funct. Foods* 25, 511–522. doi:10.1016/j.jff.2016.06.032

Fu, Y. P., Feng, B., Zhu, Z. K., Feng, X., Chen, S. F., Li, L. X., et al. (2018a). The Polysaccharides from Codonopsis Pilosula Modulates the Immunity and Intestinal Microbiota of Cyclophosphamide-Treated Immunosuppressed Mice. *Molecules* 23 (7), 1801. doi:10.3390/molecules23071801

Fu, Y. P., Li, L. X., Zhang, B. Z., Paulsen, B. S., Yin, Z. Q., Huang, C., et al. (2018b). Characterization and Prebiotic Activity *In Vitro* of Inulin-type Fructan from Codonopsis Pilosula Roots. *Carbohydr. Polym.* 193, 212–220. doi:10.1016/j.carbpol.2018.03.065

Gao, S. M., Liu, J. S., Wang, M., Cao, T. T., Qi, Y. D., Zhang, B. G., et al. (2018). Traditional Uses, Phytochemistry, Pharmacology and Toxicology of *Codonopsis*: A Review. *J. Ethnopharmacol.* 219 (12), 50–70. doi:10.1016/j.jep.2018.02.039

García Gamboa, R., Ortiz Basurto, R. I., Calderón Santoyo, M., Bravo Madrigal, J., Ruiz Álvarez, B. E., and González Avila, M. (2018). *In Vitro* evaluation of Prebiotic Activity, Pathogen Inhibition and Enzymatic Metabolism of Intestinal

Bacteria in the Presence of Fructans Extracted from Agave: A Comparison Based on Polymerization Degree. *LWT* 92, 380–387. doi:10.1016/j.lwt.2018.02.051

Gibson, G. R., and Delzenne, N. (2008). Inulin and Oligofructose. *Nutr. Today* 43 (2), 54–59. doi:10.1097/01.NT.0000303311.36663.39

Hoving, L. R., Katiraei, S., Pronk, A., Heijink, M., Vonk, K. K. D., Amghar-El Bouazzaoui, F., et al. (2018). The Prebiotic Inulin Modulates Gut Microbiota but Does Not Ameliorate Atherosclerosis in Hypercholesterolemic APOE*3-Leiden.CETP Mice. *Sci. Rep.* 8 (1), 16515. doi:10.1038/s41598-018-34970-y

Hu, J.-L., Nie, S.-P., Li, C., and Xie, M.-Y. (2013). *In Vitro* fermentation of Polysaccharide from the Seeds of Plantago Asiatica L. By Human Fecal Microbiota. *Food Hydrocolloids* 33 (2), 384–392. doi:10.1016/j.foodhyd.2013.04.006

Huang C, C., Cao, X., Chen, X., Fu, Y., Zhu, Y., Chen, Z., et al. (2017). A Pectic Polysaccharide from Ligusticum Chuanxiong Promotes Intestine Antioxidant Defense in Aged Mice. *Carbohydr. Polym.* 174, 915–922. doi:10.1016/j.carbpol.2017.06.122

Huang, C., Chen, M., Pang, D., Bi, D., Zou, Y., Xia, X., et al. (2014). Developmental and Activity-dependent Expression of LanCL1 Confers Antioxidant Activity Required for Neuronal Survival. *Dev. Cel* 30 (4), 479–487. doi:10.1016/j.devcel.2014.06.011

Huang X, X., Nie, S., and Xie, M. (2017). Interaction between Gut Immunity and Polysaccharides. *Crit. Rev. Food Sci. Nutr.* 57 (14), 2943–2955. doi:10.1080/10408398.2015.1079165

Ito, H., Wada, T., Ohguchi, M., Sugiyama, K., Kiriyama, S., and Morita, T. (2008). The Degree of Polymerization of Inulin-like Fructans Affects Cecal Mucin and Immunoglobulin A in Rats. *J. Food Sci.* 73 (3), H36–H41. doi:10.1111/j.1750-3841.2008.00686.x

Karimi, R., Azizi, M. H., Ghasemlou, M., and Vaziri, M. (2015). Application of Inulin in Cheese as Prebiotic, Fat Replacer and Texturizer: a Review. *Carbohydr. Polym.* 119, 85–100. doi:10.1016/j.carbpol.2014.11.029

Kim, Y. S., and Ho, S. B. (2010). Intestinal Goblet Cells and Mucins in Health and Disease: Recent Insights and Progress. *Curr. Gastroenterol. Rep.* 12 (5), 319–330. doi:10.1007/s11894-010-0131-2

Lee, S. I., and Kang, K. S. (2017). Function of Capric Acid in Cyclophosphamide-Induced Intestinal Inflammation, Oxidative Stress, and Barrier Function in Pigs. *Sci. Rep.* 7 (1), 16530. doi:10.1038/s41598-017-16561-5

Li, C., Yin, L., Zhu, D., He, Y., Li, M., Ding, X., et al. (2018). Effect of *Codonopsis Pilosula* Polysaccharide on Small Intestinal Mucosa Immunity of Piglets. *Jiangsu J. Agric. Sci.* 34 (2), 337–255. doi:10.3969/j.issn.1000-4440.2018.02.018

Li, K., Zhang, L., Xue, J., Yang, X., Dong, X., Sha, L., et al. (2019). Dietary Inulin Alleviates Diverse Stages of Type 2 Diabetes Mellitus via Anti-inflammation and Modulating Gut Microbiota in Db/db Mice. *Food Funct.* 10 (4), 1915–1927. doi:10.1039/c8fo02265h

Liu, X., Mao, B., Gu, J., Wu, J., Cui, S., Wang, G., et al. (2021). Blautia-a New Functional Genus with Potential Probiotic Properties? *Gut Microbes* 13 (1), 1–21. doi:10.1080/19490976.2021.1875796

Loy, A., Pfann, C., Steinberger, M., Hanson, B., Herp, S., Brugiroux, S., et al. (2017). Lifestyle and Horizontal Gene Transfer-Mediated Evolution of Mucispirillum Schaedleri, a Core Member of the Murine Gut Microbiota. *mSystems* 2 (1), e00171. doi:10.1128/mSystems.00171-16

Mazraeh, R., Azizi-Soleiman, F., Jazayeri, S. M. H. M., and Noori, S. M. A. (2019). Effect of Inulin-type Fructans in Patients Undergoing Cancer Treatments: A Systematic Review. *Pak J. Med. Sci.* 35 (2), 575–580. doi:10.12669/pjms.35.2.701

Meijer, K., de Vos, P., and Priebe, M. G. (2010). Butyrate and Other Short-Chain Fatty Acids as Modulators of Immunity: what Relevance for Health? *Curr. Opin. Clin. Nutr. Metab. Care* 13 (6), 715–721. doi:10.1097/MCO.0b013e32833eebe5

Miao, M., Cheng, B., Guo, L., and Shi, J. (2015). Effects of Fuzheng Paidu Tablet on Peripheral Blood T Lymphocytes, Intestinal Mucosa T Lymphocytes, and Immune Organs in Cyclophosphamide-Induced Immunosuppressed Mice. *Hum. Vaccin. Immunother.* 11 (11), 2659–2663. doi:10.1080/21645515.2015.1082694

Moens, F., and De Vuyst, L. (2017). Inulin-type Fructan Degradation Capacity of Clostridium Cluster IV and XIVa Butyrate-Producing colon Bacteria and Their Associated Metabolic Outcomes. *Benef. Microbes* 8 (3), 473–490. doi:10.3920/bm2016.0142

Moore, J. V. (1984). Death of Intestinal Crypts and of Their Constituent Cells after Treatment by Chemotherapeutic Drugs. *Br. J. Cancer* 49, 25–32. doi:10.1038/bjc.1984.5

Moreno-Vilet, L., Garcia-Hernandez, M. H., Delgado-Portales, R. E., Corral-Fernandez, N. E., Cortez-Espinosa, N., Ruiz-Cabrera, M. A., et al. (2014). *In Vitro* assessment of Agave Fructans (Agave Salmiana) as Prebiotics and Immune System Activators. *Int. J. Biol. Macromol.* 63, 181–187. doi:10.1016/j.ijbiomac.2013.10.039

Nagata, R., Echizen, M., Yamaguchi, Y., Han, K. H., Shimada, K., Ohba, K., et al. (2018). Effect of a Combination of Inulin and Polyphenol-Containing Adzuki Bean Extract on Intestinal Fermentation *In Vitro* and *In Vivo*. *Biosci. Biotechnol. Biochem.* 82 (3), 489–496. doi:10.1080/09168451.2018.1429886

Ouwerkerk, J. P., de Vos, W. M., and Belzer, C. (2013). Glycobiome: Bacteria and Mucus at the Epithelial Interface. *Best Pract. Res. Clin. Gastroenterol.* 27 (1), 25–38. doi:10.1016/j.bpg.2013.03.001

Peng, X., Lan, Y., and Kun, F. (2018). Extraction of Polysaccharides from Codonopsis Pilosula *In Vivo*,*In Vitro* Immunization of Polysaccharide. *Harbin Med. J.* 38 (4), 301–303.

Rivera-Huerta, M., Lizárraga-Grimes, V. L., Castro-Torres, I. G., Tinoco-Méndez, M., Macías-Rosales, L., Sánchez-Bartéz, F., et al. (2017). Functional Effects of Prebiotic Fructans in Colon Cancer and Calcium Metabolism in Animal Models. *Biomed. Res. Int.* 2017, 9758982. doi:10.1155/2017/9758982

Schroeder, B. O., Birchenough, G. M. H., Ståhlman, M., Arike, L., Johansson, M. E. V., Hansson, G. C., et al. (2018). Bifidobacteria or Fiber Protects against Diet-Induced Microbiota-Mediated Colonic Mucus Deterioration. *Cell Host Microbe* 23 (1), 27. doi:10.1016/j.chom.2017.11.004

Shang, Q., Shan, X., Cai, C., Hao, J., Li, G., and Yu, G. (2016). Dietary Fucoidan Modulates the Gut Microbiota in Mice by Increasing the Abundance of Lactobacillus and Ruminococcaceae. *Food Funct.* 7 (7), 3224–3232. doi:10.1039/c6fo00309e

Shang HM, H. M., Zhou, H. Z., Yang, J. Y., Li, R., Song, H., and Wu, H. X. (2018). *In Vitro* and *In Vivo* Antioxidant Activities of Inulin. *PLoS One* 13 (2), e0192273. doi:10.1371/journal.pone.0192273

Shang Q, Q., Jiang, H., Cai, C., Hao, J., Li, G., and Yu, G. (2018). Gut Microbiota Fermentation of marine Polysaccharides and its Effects on Intestinal Ecology: An Overview. *Carbohydr. Polym.* 179, 173–185. doi:10.1016/j.carbpol.2017.09.059

Sheng, X., Yan, J., Meng, Y., Kang, Y., Han, Z., Tai, G., et al. (2017). Immunomodulatory Effects of *Hericium erinaceus* Derived Polysaccharides Are Mediated by Intestinal Immunology. *Food Funct.* 8 (3), 1020–1027. doi:10.1039/c7fo00071e

Shi, H., Chang, Y., Gao, Y., Wang, X., Chen, X., Wang, Y., et al. (2017). Dietary Fucoidan of Acaudina Molpadioides Alters Gut Microbiota and Mitigates Intestinal Mucosal Injury Induced by Cyclophosphamide. *Food Funct.* 8 (9), 3383–3393. doi:10.1039/c7fo00932a

Shoaib, M., Shehzad, A., Omar, M., Rakha, A., Raza, H., Sharif, H. R., et al. (2016). Inulin: Properties, Health Benefits and Food Applications. *Carbohydr. Polym.* 147, 444–454. doi:10.1016/j.carbpol.2016.04.020

Sonis, S. T. (2004). The Pathobiology of Mucositis. *Nat. Rev. Cancer* 4, 277–284. doi:10.1038/nrc1318

Taminiau, J. A., Gall, D. G., and Hamilton, J. R. (1980). Response of the Rat Small-Intestine Epithelium to Methotrexate. *Gut* 21 (6), 486–492. doi:10.1136/gut.21.6.486

Tang, C., Sun, J., Zhou, B., Jin, C., Liu, J., Kan, J., et al. (2018). Effects of Polysaccharides from Purple Sweet Potatoes on Immune Response and Gut Microbiota Composition in normal and Cyclophosphamide Treated Mice. *Food Funct.* 9 (2), 937–950. doi:10.1039/c7fo01302g

van den Abbeele, P., Taminiau, B., Pinheiro, I., Duysburgh, C., Jacobs, H., Pijls, L., et al. (2018). Arabinoxylo-oligosaccharides and Inulin Impact Inter-individual Variation on Microbial Metabolism and Composition, Which Immunomodulates Human Cells. *J. Agric. Food Chem.* 66 (5), 1121–1130. doi:10.1021/acs.jafc.7b04611

Vogt, L., Meyer, D., Pullens, G., Faas, M., Smelt, M., Venema, K., et al. (2015). Immunological Properties of Inulin-type Fructans. *Crit. Rev. Food Sci. Nutr.* 55 (3), 414–436. doi:10.1080/10408398.2012.656772

Wang X, X., Yuan, Z., Zhu, L., Yi, X., Ou, Z., Li, R., et al. (2019). Protective Effects of Betulinic Acid on Intestinal Mucosal Injury Induced by Cyclophosphamide in Mice. *Pharmacol. Rep.* 71 (5), 929–939. doi:10.1016/j.pharep.2019.05.004

Wang Z, Z., Li, Y., Wang, C., Xia, H., Liang, Y., and Li, Z. (2019). Oral Administration of Urtica Macrorrhiza Hand.-Mazz. Polysaccharides to Protect against Cyclophosphamide-Induced Intestinal Immunosuppression. *Exp. Ther. Med.* 18 (3), 2178–2186. doi:10.3892/etm.2019.7792

Wilson, B., and Whelan, K. (2017). Prebiotic Inulin-type Fructans and Galacto-Oligosaccharides: Definition, Specificity, Function, and Application in Gastrointestinal Disorders. *J. Gastroenterol. Hepatol.* 32 (S1), 64–68. doi:10.1111/jgh.13700

Xu, X., Xu, P., Ma, C., Tang, J., and Zhang, X. (2013). Gut Microbiota, Host Health, and Polysaccharides. *Biotechnol. Adv.* 31 (2), 318–337. doi:10.1016/j.biotechadv.2012.12.009

Zhao, R., Li, G., Kong, X. J., Huang, X. Y., Li, W., Zeng, Y. Y., et al. (2016). The Improvement Effects of Edible Bird's Nest on Proliferation and Activation of B Lymphocyte and its Antagonistic Effects on Immunosuppression Induced by Cyclophosphamide. *Drug Des. Devel. Ther.* 10, 371–381. doi:10.2147/DDDT.S88193

Zhao, W., Yuan, M., Li, P., Yan, H., Zhang, H., and Liu, J. (2019). Short-chain Fructo-Oligosaccharides Enhances Intestinal Barrier Function by Attenuating Mucosa Inflammation and Altering Colonic Microbiota Composition of Weaning Piglets. *Ital. J. Anim. Sci.* 18 (1), 976–986. doi:10.1080/1828051x.2019.1612286

Zhou, W., Xiang, L., Lu, H., Chen, Z., Gong, Q., Luo, R., et al. (2015). Radix Codonopsi Polysaccharide against 5-Fluorouracil-Induced Gastrointestinal Mucositis in Mice Model. *Liaoning J. Tradit. Chin. Med.* 43 (7), 1495–1498. doi:10.13192/j.issn.1000-1719.2016.07.051

Zhu, L., Qin, S., Zhai, S., Gao, Y., and Li, L. (2017). Inulin with Different Degrees of Polymerization Modulates Composition of Intestinal Microbiota in Mice. *FEMS Microbiol. Lett.* 364 (10), fnx075. doi:10.1093/femsle/fnx075

Zhu, G., Luo, J., Du, H., Jiang, Y., Tu, Y., Yao, Y., et al. (2018). Ovotransferrin Enhances Intestinal Immune Response in Cyclophosphamide-Induced Immunosuppressed Mice. *Int. J. Biol. Macromol.* 120 (Pt), 1–9. doi:10.1016/j.ijbiomac.2018.08.058

Zou, Y. F., Zhang, Y. Y., Fu, Y. P., Inngjerdingen, K. T., Paulsen, B. S., Feng, B., et al. (2019). A Polysaccharide Isolated from Codonopsis Pilosula with Immunomodulation Effects Both *In Vitro* and *In Vivo*. *Molecules* 24 (20), 3632. doi:10.3390/molecules24203632

Conflict of Interest: The authors declare that the research was conducted in the absence of any commercial or financial relationships that could be construed as a potential conflict of interest.

Publisher's Note: All claims expressed in this article are solely those of the authors and do not necessarily represent those of their affiliated organizations, or those of the publisher, the editors, and the reviewers. Any product that may be evaluated in this article, or claim that may be made by its manufacturer, is not guaranteed or endorsed by the publisher.

frontiers in Pharmacology

PERSPECTIVE
published: 18 March 2022
doi: 10.3389/fphar.2022.790136

Polysaccharides, Next Potential Agent for the Treatment of Epilepsy?

Xuemin Xie[1†], Youliang Wu[1†], Haitao Xie[1†], Haiyan Wang[1], Xiaojing Zhang[1], Jiabin Yu[1], Shaofang Zhu[1], Jing Zhao[2], Lisen Sui[1]* and Shaoping Li[2]**

[1]Department of Epilepsy Center, The Second Affiliated Hospital of Guangzhou University of Chinese Medicine (Guangdong Provincial Hospital of Chinese Medicine), Guangzhou, China, [2]Joint Laboratory of Chinese Herbal Glycoengineering and Testing Technology, State Key Laboratory of Quality Research in Chinese Medicine, Institute of Chinese Medical Sciences, University of Macau, Macao, China

Epilepsy is a chronic neurological disorder. Current pharmacological therapies for epilepsy have limited efficacy that result in refractory epilepsy (RE). Owing to the limitations of conventional therapies, it is needed to develop new anti-epileptic drugs. The beneficial effects of polysaccharides from Chinese medicines, such as *Lycium barbarum* polysaccharides (COP) and *Ganoderma lucidum* polysaccharides (GLP), for treatment of epilepsy include regulation of inflammatory factors, neurotransmitters, ion channels, and antioxidant reactions. Especially, polysaccharides could be digested by intestinal microbial flora, referred as "intestinal brain organ" or "adult's second brain", may be the target for treatment of epilepsy. Actually, polysaccharides can effectively improve the type and quantity of intestinal flora such as bifidobacteria and lactic acid bacteria and achieve the purpose of treating epilepsy. Therefore, polysaccharides are hypothesized and discussed as potential agent for treatment of epilepsy.

Keywords: polysaccharides, epilepsy, traditional Chinese medicines, gut microbiome, treatment

OPEN ACCESS

Edited by:
Shuai Ji,
Xuzhou Medical University, China

Reviewed by:
Alberto Lazarowski,
University of Buenos Aires, Argentina
Gopal Khatik,
National Institute of Pharmaceutical Education and Research, India

****Correspondence:***
Jing Zhao
jingzhao@um.edu.mo
Lisen Sui
13711580891@163.com
Shaoping Li
spli@um.edu.mo
lishaoping@hotmail.com

[†]These authors have contributed equally to this work

Specialty section:
This article was submitted to Ethnopharmacology, a section of the journal Frontiers in Pharmacology

Received: *06 October 2021*
Accepted: *20 January 2022*
Published: *18 March 2022*

Citation:
Xie X, Wu Y, Xie H, Wang H, Zhang X, Yu J, Zhu S, Zhao J, Sui L and Li S (2022) Polysaccharides, Next Potential Agent for the Treatment of Epilepsy? Front. Pharmacol. 13:790136. doi: 10.3389/fphar.2022.790136

1 INTRODUCTION

Epilepsy is a chronic neurological disease that affects more than 50 million people worldwide and accounts for 0.6% of the global economic disease burden (WHO, 2016). Although WHO estimates that the seizures can be controlled by appropriate medications in 70% of epilepsy patients, only less than half of them have access to antiepileptic drugs in developing countries. In addition, there is still an estimated of 15 million patients have refractory epilepsy (RE) due to the pool response to existing anti-epileptic drugs (Lum et al., 2020). Therefore, RE has become a hot research topic of neurological treatment. In the past few decades, more than 20 kinds of anti-epileptic drugs have been developed while the incidence of RE has not been significantly reduced. The commonly used clinical antiepileptic drugs include sodium valproate (VPA), carbamazepine, phenobarbital, phenytoin sodium, ethylamine, oxcarbazepine, lamotrigine, topiramate, levetiracetam, lacoamide and so on. Each drug has its own unique physiological activity. For example, VPA is a broad-spectrum antiepileptic agent that can be used as either monotherapy or adjunctive therapy for generalized epilepsy. Common adverse reactions of VPA include gastrointestinal reaction, liver injury, tremor, increased sleep, and long-term application may include weight gain, hair loss, menstrual disorders, polycystic ovary syndrome, etc. Compared with carbamazepine, oxcarbazepine is characterized by weak liver enzyme induction, high bioavailability, better efficacy and safety. oxcarbazepine is mainly used for partial epilepsy in children. Common adverse reactions of oxcarbazepine include nausea, dizziness and diplopia. It is important to note that these drugs require long-term or even lifelong use, which makes patients more prone to hematopoietic damage, Stevens-Johnson syndrome, severe liver

dysfunction, and aggravated cognitive impairment. Considering the limitation of anti-epileptics, it is need to develop new drugs with lower side effects and higher efficacy (Mehla et al., 2010). In last years, more and more studies have shown that chemicals in traditional Chinese medicines (TCMs), such as triglycerides and saponins, could be used as therapeutic agents for epilepsy by regulating inflammatory factors, neurotransmitters, ion channels and antioxidant responses (Zhang et al., 2019), which has unique advantages such as low side effects and reduced complications (Yuan et al., 2019). Polysaccharides might also be a potential agent for treatment of epilepsy. The therapeutic efficacy may be mainly derived from their prebiotic effect on gut microbiota.

2 GUT MICROBIOTA AND EPILEPSY

Gut microbiota, which is called "intestinal brain organ" and "adult's second brain", is related to metabolic diseases, autoimmune diseases, and nervous system diseases (Pellegrini et al., 2018). Recent studies indicate that gut dysfunction/dysbiosis is presumably involved in the pathogenesis of and susceptibility to epilepsy. In addition, the reconstruction of the intestinal microbiome through, for example, faecal microbiota transplantation, probiotic intervention, and a ketogenic diet, has exhibited beneficial effects on drug-resistant epilepsy (Yue et al., 2021). Indeed, a few recent studies have highlighted differences in fecal microbiota profiles from selected epileptic individuals as compared to healthy controls (Lum et al., 2020). In addition, a 22-year-old Crohn's disease patient with a 17-year history of seizures underwent a fecal microbiota transplant to treat Crohn's disease (He et al., 2017). During the 20-month follow-up, the patient had no seizures despite discontinuation of the antiepileptic treatment with sodium valproate. Another study showed that probiotic treatment reduced the frequency of seizures by more than 50% in 28.9% of patients with drug-resistant to epilepsy (Gómez-Eguílaz et al., 2018). It was found that intestinal dysbiosis is associated with chronic stress-induced epilepsy in rats and members of the intestinal microbiota influence the anti-seizure effect of the ketogenic diet in mice. Recent studies in human cohorts suggest a dysbiosis in children with epilepsy. It may be possible that dysbiosis is more relevant in certain subtypes of epilepsy though larger studies with age-matched controls are needed to confirm (Dahlin and Prast-Nielsen, 2019). Braakman and Ingen described 6 cases of drug-resistant epilepsy, of which 5 had no seizures and 1 had a reduction in seizure frequency by more than 90% during antibiotic treatment. This effect disappeared within 2 weeks of stopping treatment, presumably due to the recovery of certain gut microbes (Braakman and Van Ingen, 2018) though other potential mechanisms might not be excluded (Sander and Perucca, 2003). Peng et al. (2018) found that the abundance of rare intestinal flora in patients with drug-resistant epilepsy increased abnormally, and the number of beneficial bacteria such as bifidobacteria and lactobacilli decreased. Olson et al. (2018) found that the ketogenic diet changes intestinal flora, which is a necessary part of the ketogenic diet, to exert its anti-epileptic effect. This information is linked to that a decreased amount of long-chain (such as arachidic, and oleic acid) and medium-chain fatty acids (sebacic acid and isocaproic acid) as well as bile acid was observed in patients with inflammatory bowel disease (Weng et al., 2019). Indeed, sebacic acid (SA) is a component of ketogenic diet and administered in pure form to inhibit the P-glycoprotein function and expression in an experimental model of refractory epilepsy (Enrique et al., 2021). Those above studies have indicated that regulating gut microbiota can achieve therapeutic effect of epilepsy. There are multiple interactions between gut microbiota and central nervous system (CNS). Gut microbiota affects the development and homeostasis of CNS through immune, circulatory and neural pathways, while CNS induces gut microbiota through stress and endocrine responses (Dinan and Cryan, 2017; Tremlett et al., 2017). The term "brain gut axis" is used to describe these two-way interactions (Bauer et al., 2016). Bagheri et al. found that there was a significant imbalance of intestinal flora in experimentally induced epileptic rats, and there was a certain proportion between the dominant flora in intestinal flora and seizures (Bagheri et al., 2019). The concentration of the inhibitory neurotransmitter gamma-aminobutyric acid (GABA) increased and the severity of epileptic seizures was significantly reduced in rats treated with probiotic supplements. This may be related to the fact that selective probiotics modulate the expression of specific GABA receptor subunits in brain regions (Liang et al., 2017). Studies have found that intestinal microflora α-diversity significantly increased in patients with refractory epilepsy, and the lower level of *bifidobacteria* and *lactobacillus*, the more frequent the seizures. Recently, some scholars have observed that intestinal flora can regulate the function of CNS in multiple ways and can affected epileptic seizures. In addition, intestinal microflora disorder may be caused by regulating immune and inflammatory responses, changing nutrient metabolism, activating and improving microglia and astrocyte functions, changing vagal nerve activity, and reducing neuroactive substances in limbic system such as hippocampus [such as brain-derived neurotrophin (neurotrophic factor)] increased the risk and susceptibility of epilepsy (Vuong et al., 2017). Therefore, it is believed that the intestinal flora may be a target for RE treatment (De Caro et al., 2019; He et al., 2021). The gut-brain bidirectional axis and the underlying mechanism of KD-based therapy targeting gut microbiome in *in vivo* animal models and clinical studies in neurological diseases have been reviewed (Rawat et al., 2020). Briefly, the intestinal microbiota can affect the balance of excitement/inhibition through neurotransmitters (mainly GABA, glutamate and 5-HT) or their precursors (such as tryptophan) (O'Mahony et al., 2015; Mittal et al., 2017), thereby affecting the occurrence and maintenance of epileptic seizures and the occurrence of epilepsy. Immune system-mediated pro-inflammatory effects (for example, the release of cytokines and chemokines) also increase the level of LPS due to the passage of the intestinal barrier. Increased permeability (Belkaid and Hand, 2014; Blander et al., 2017) and production of short-chain fatty acids (especially butyric acid, propionic acid and acetic acid) has an anti-inflammatory effect (Stilling et al., 2016; van de Wouw et al., 2018). In addition, neural (such as vagus nerve afferent, enteric

TABLE 1 | Components from TCMs and their effects and cell culture or animal models.

TCMs component	Model	Mechanisms	References
GLP	NF-KB in hippocampal nerve cells of epileptic rats	Reduce the influx of calcium ions in nerve cells,so as to indirectly inhibit the activity of nerve cells	Zhang J et al. (2018)
	excitatory amino acid transporter in brain of epileptic rat	Glutamate transporter GLAS↑GLT1↑EAAC1↑	Zhu K et al. (2015)
ASP	lipopolysaccharide-evoked inflammatory injury in neuronal cell line HT22	interdicted NF-jB and JAK2/STAT3 pathways via enhancing miR-10a	Zhou Y et al. (2019)
LBP	epileptic rats induced by lithium chloride-pilocarpine	Number of BrdU positive granular cells ↑ Map-2 positive neuron perimeter ↑	Feng et al. (2017)
	hippocampal neural stem cell	Differentiation rate of NeuN positive neurons↑	
	epileptic rats induced by lithium chloride-pilocarpine hippocampus	The escape latency↓ The percentage of plateau quadrant path and plateau quadrant residence time↑	Chen et al. (2020)
COP	epileptic rats induced by lithium chloride-pilocarpine	SOD↓MDA↑mitochondrial ROS↑ The mitochondrial membrane potential↓cytochrome C and activation of cleaved-caspase-3↓ MAPK phosphorylation↑ Morphological abnormalities with neurons in CA1 area of hippocampal were alleviated	Sun X et al. (2018)
GUP	Epileptic rat model was established by pentylenetetrazol kindling	SOD↑MDA↓IL-18↓TNF-α↓	Xiao J et al. (2021)
DOP	Effects of Dendrobium Officinale Polysaccharides on Brain Inflammation of Epileptic Rats	IL-1β↓TNF-α↓ MAPK↓ P-mcp-1↑	Zhang L et al. (2019)
DOP	Effects of Dendrobium Officinale Polysaccharides on Brain Inflammation of Epileptic Rats	IL-1β↓TNF-α↓ MAPK↓ P-mcp-1↑	Zhang L et al. (2019)
GBPw	Middle cerebral artery occlusion rats	MDA↓ TNF-α↓ and IL-1β↓ SOD↑ MPO ↑ IL-10↑	Yang Y et al. (2013)
DOPS	Animalmodels of learning andmemory disabilitie	ctivateNrf2/HO-1 pathway to reduce oxidative stress and neuro-inflammation	Liang J et al. (2019)
LJPB2	Focal ischemia/reperfusion (I/R) injuried rat brain	SOD↑ GSH-Px↑	Su D et al. (2017)
GPP1	PC12 cells	Prevent Aβ(25–35)-induced oxidative stress, excessive [Ca2+]i influx, loss of mitochondrial membrane potential (ψm) and elevation of Bax/Bcl-2 protein expression and cleaved caspase-3, or by some combination of these effects	Jia D et al. (2015)
APS	APP/PS1 mice	activates Nrf2 pathway to regulate oxidative stress, improve apoptotic level and cognitive ability and reduce the accumulation of Ab	Qin X et al. (2020)

GLP, Ganoderma lucidum *polysaccharides; ASP,* Angelica sinensis *polysaccharides; LBP,* Lycium barbarum *polysaccharides; COP,* Cornus officinalis *fruit polysaccharides; GUP,* Glycyrrhiza uralensis *polysaccharides; DOP,* Dendrobium officinale *polysaccharide; GBPw, an araban type polysaccharide was purified from the leaves of* Ginkgo biloba*; DOPS,* Dendrobium officinale *polysaccharides; LJPB2, a polysaccharide from Lonicera japonica flowers; GPP1, a purified polysaccharide from* Gynostemma pentaphyllum*; APS,* Astragalus *polysaccharide.*

nervous system) and neuroendocrine (such as hypothalamus-pituitary-adrenal axis) networks (Sudo et al., 2004; Cheung et al., 2019), as well as the endocannabinoid system (Rousseaux et al., 2007) and brain-derived neurotrophic factor level, may be affected by gut microbiota, and therefore further effect on the seizure mechanism. Many highly modifiable gut microbiota–brain axis pathways may be related to epilepsy.

3 EFFECTS OF POLYSACCHARIDES ON EPILEPSY THROUGH GUT MICROBIOTA

Polysaccharides are biological macromolecules formed by the polymerization of more than 10 monosaccharides through glycosidic bonds. They are widely found in animals, plants and microorganisms. Indeed, TCMs are usually administered as decoction which contains larger proportion of polysaccharides. In recent years, with the development of "glycobiology", studies have found that polysaccharides not only participate in various physiological activities, but also have a wide range of biological effects (Chen et al., 2016). Since lack of polysaccharides hydrolase, most polysaccharides cannot be directly digested and absorbed by human body. Intestinal flora play a mediating role in the process of interaction between polysaccharides and human body. Most of the beneficial health effects of polysaccharides have been associated with its reversal impacts on gut microbiota dysbiosis (Wang et al., 2021b). Mental illnesses, such as depression, Parkinson's disease, Alzheimer's disease and autism have been linked to gut microbiota. Actually, *Flammulina velutipes* polysaccharides contributed to significant improvements in mice learning and memory behavior through its gut microbiota regulation (Ma et al., 2021). Polysaccharides may also mainly contribute to their treatment of epilepsy through gut microbiota. The potential effects of polysaccharides from edible mushroom *Grifola frondosa* (GFP) on gut microbiota dysbiosis were investigated (Li et al., 2019). Metagenomic analysis revealed that GFP supplementation (400 mg/kg/day) resulted in

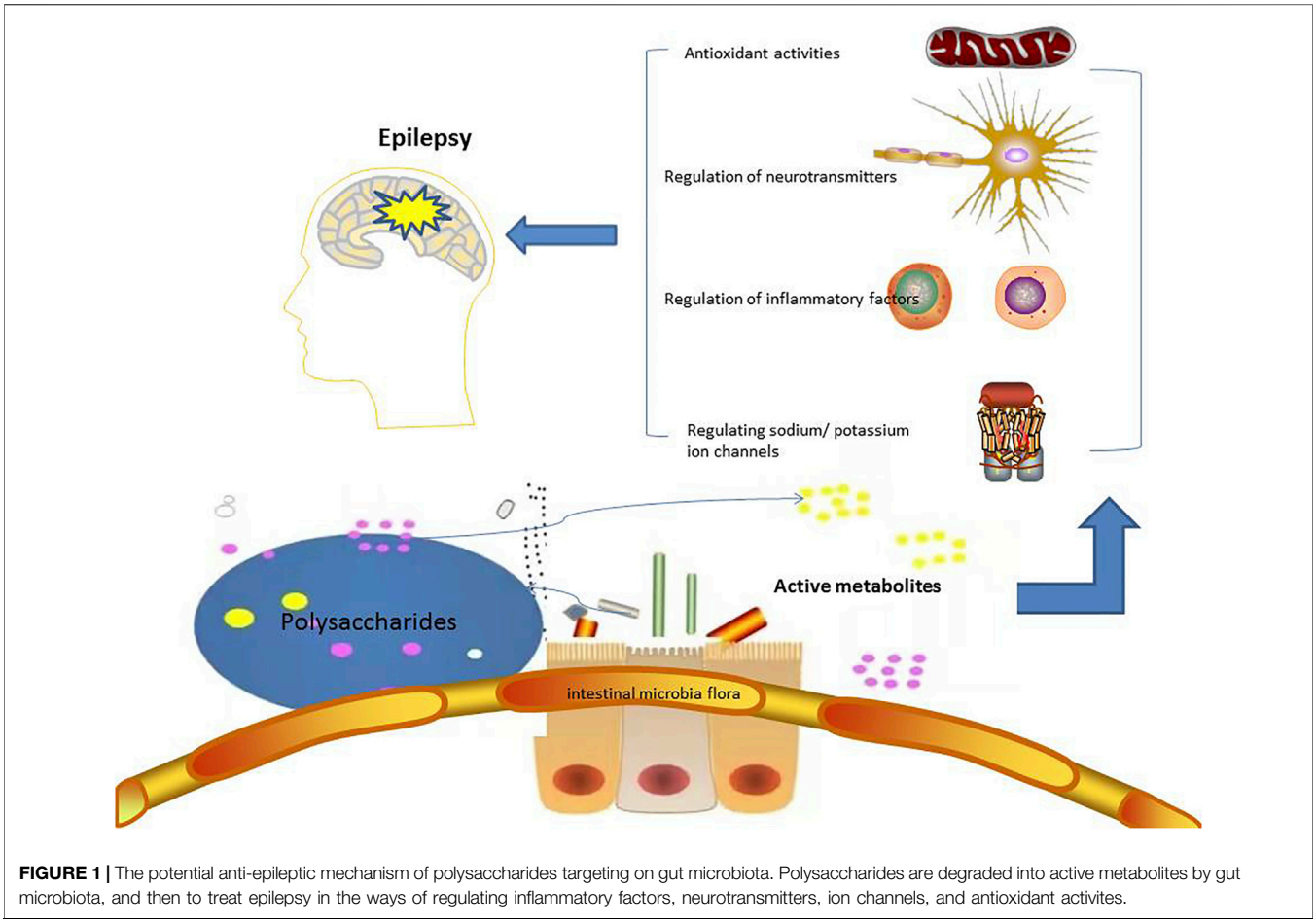

FIGURE 1 | The potential anti-epileptic mechanism of polysaccharides targeting on gut microbiota. Polysaccharides are degraded into active metabolites by gut microbiota, and then to treat epilepsy in the ways of regulating inflammatory factors, neurotransmitters, ion channels, and antioxidant activites.

significant structure changes on gut microbiota in high-fat diet (HFD)-fed rats, in particular modulating the relative abundance of functionally relevant microbial phylotypes compared with the HFD group. SP2-1, one homogeneous polysaccharide isolated from *Scutellaria baicalensis* Georgi can repair the intestinal barrier through up-regulated expressions of ZO-1, Occludin and Claudin-5. Furthermore, as compared with model group, the abundance of Firmicutes, Bifidobacterium, *Lactobacillus*, and Roseburia were significantly increased and the levels of *Bacteroides*, Proteobacteria and *Staphylococcus* were significantly inhibited with SP2-1 treatment. The modulatory effects of jujube (*Ziziphus jujuba* Mill.) polysaccharides (ZJP) on intestinal microbiota were investigated and the gut flora structure was then analyzed using high-throughput sequencing. After ZJP treatment, there was a significant decrease in Firmicutes/ Bacteroidetes, which suggested that ZJP showed prebiotic-like activities by positively modulating intestinal microbiota (Ji et al., 2020). *Lycium barbarum* polysaccharides (LBPS) treatment also could modulate the composition of the gut microbiota, increasing the relative abundances of Bacteroidaceae, Lactobacillaceae, Prevotellaceae and Verrucomicrobiaceae, which were positively associated with immune traits. The present results indicated that LBPS might regulate the immune response depending on the modulation of the gut microbiota, suggesting that LBPS could be developed as special ingredients for immunoregulation in association with the modulation of the gut microbiota (Ding et al., 2019).

A few studies provided evidence that intestinal inflammation was also a contributing factor to epileptic events for susceptible patients and a possible reason for the reduced efficacy of antiepileptic drugs, which made intestinal inflammation a promising antiepileptic drug target (Yue et al., 2021). Many Chinese herbal polysaccharides have immune regulation functions such as protecting the body's immune organs, activating immune cells, activating the complement system, and releasing cytokines (Hong et al., 2019; Zeng et al., 2019; Xi et al., 2020; Wang et al., 2021a), these are beneficial to the treatment of epilepsy. In the early stage of epilepsy, excessive reactive oxygen species (ROS) free radical is produced in the body, causing inflammation. Polysaccharides are beneficial for the treatment of epilepsy through antiinflammation, regulating excitatory neurotransmitters and receptors, sodium/potassium ion channels and antioxidant activities (Yuan et al., 2019). *Dendrobium officinale* polysaccharides have anti-inflammatory, antioxidative and immunity-enhancement effects, which attribute to the treatment of epilepsy due to their strong anti-inflammatory and antioxidative effects (Zhang et al., 2019). *Cornus officinalis* fruit polysaccharides reduce the activation of

ROS and Mitogen-activated protein kinaseMAPK cascade pathways in hippocampus after epilepsy, the change of mitochondrial membrane potential, the leakage of cytochrome C, and the activation of cleaved caspase-3, thereby reducing neuronal apoptosis and having neuroprotective effects on epilepsy (Sun et al., 2018). *Glycyrrhiza uralensis* polysaccharides (GUP) may inhibit the oxidative stress and inflammation in epileptic rats ignited by pentylenetetrazol by down-regulating the expression of hippocampal P2X7 receptor and NF-κB protein, and reduce neuropathological damage (Xiao et al., 2021). Additionally, after the intervention of LBPS in epilepsy model rats, the number of BrdU-positive cells in the granular layer of the hippocampus dentate gyrus, the expression of MAP-2 and NeuN-positive neurons were improved to a certain extent, and it has a good neuroprotective effect (Feng et al., 2017). LBPS also can improve the learning and memory ability of epileptic rats, and its mechanism may be related to the protection of hippocampal neurons by enhancing the anti-oxidative stress effect (Chen et al., 2020). GLP may increase the expression of GLAST, GLT-1 and EAAC1 to reduce neuronal excitability and reduce or inhibit epileptic seizures (Zhu et al., 2015). It may reduce the influx of calcium ions in nerve cells, thereby indirectly inhibiting the activation of NF-κB induced by pentylenetetrazol, reducing the excitability of nerve cells, and achieving anti-epileptic effects (Zhang et al., 2010). **Table 1** summarized some TCMs polysaccharides and their effects on cell culture or animal model, and the mechanism.

The relationship among polysaccharides, intestinal flora and human health have been well reviewed and summarized (Liu et al., 2019; Song et al., 2021; Liang et al., 2021; Ma et al., 2021; Yin et al., 2020; Su et al., 2021). Polysaccharides could improve intestinal microecology by repairing intestinal barrier function, regulating the composition of intestinal flora, and regulating intestinal cytokine levels. Under normal circumstances, polysaccharides from TCMs can increase the number of beneficial bacteria such as *Bacteroides*, Firmicutes, and lactic acid bacteria, and reduce the number of harmful bacteria such as *Enterococcus* and *Fusobacterium*. It has also been detected that Chinese medicine polysaccharides can affect TNF-α, sIgA, and NF-κB and other disease-related changes in biochemical indicators (Zhou et al., 2019). The effects of gut microbiota on epilepsy and potential anti-epileptic mechanism of polysaccharides were shown in **Figure 1**.

4 CONCLUSION

Current studies support the hypothesis that polysaccharides could be beneficial to the treatment of epilepsy. The evidence includes: 1) polysaccharides have the abilities to regulate inflammatory factors, neurotransmitters, ion channels, enhance immune function, promote the growth of intestinal flora and antioxidant responses. 2) polysaccharide can improve the gastrointestinal health function of the body, regulate the composition of intestinal flora, reshape the intestinal flora ecology and finally to produce anti-epileptic effects. Studies have shown that microbiota intervention could control seizures in animal models. However, in patients with epilepsy, polysaccharides as the next treatment of epilepsy drugs need to be comprehensively investigated with or without combination of anti-epilepsy drugs.

DATA AVAILABILITY STATEMENT

The original contributions presented in the study are included in the article/Supplementary Material, further inquiries can be directed to the corresponding authors.

AUTHOR CONTRIBUTIONS

SL, JZ, and LS designed the topic and reviewed the manuscript. HW, XZ, JY, and SZ collected the references and did the statistical analysis. XX, YW, and HX wrote the manuscript. All authors contributed to the article and approved the submitted version.

FUNDING

The research was partially funded by grants from the Science and Technology Development Fund, Macau SAR (File no. 034/2017/A1 and 0017/2019/AKP), the Key-Area Research and Development Program of Guangdong Province (File no. 2020B1111110006) and the University of Macau (File no. MYRG2018-00083-ICMS/MYRG2019-00128-ICMS/CPG2022-00014-ICMS).

REFERENCES

Bagheri, S., Heydari, A., Alinaghipour, A., and Salami, M. (2019). Effect of Probiotic Supplementation on Seizure Activity and Cognitive Performance in PTZ-Induced Chemical Kindling. *Epilepsy Behav.* 95, 43–50. doi:10.1016/j.yebeh.2019.03.038

Bauer, K. C., Huus, K. E., and Finlay, B. B. (2016). Microbes and the Mind: Emerging Hallmarks of the Gut Microbiota-Brain axis. *Cell. Microbiol.* 18, 632–644. doi:10.1111/cmi.12585

Belkaid, Y., and Hand, T. W. (2014). Role of the Microbiota in Immunity and Inflammation. *Cell* 157, 121–141. doi:10.1016/j.cell.2014.03.011

Blander, J. M., Longman, R. S., Iliev, I. D., Sonnenberg, G. F., and Artis, D. (2017). Regulation of Inflammation by Microbiota Interactions with the Host. *Nat. Immunol.* 18, 851–860. doi:10.1038/ni.3780

Braakman, H. M. H., and van Ingen, J. (2018). Can Epilepsy Be Treated by Antibiotics. *J. Neurol.* 265, 1934–1936. doi:10.1007/s00415-018-8943-3

Chen, B., Song, X., Song, Y., and Li, Y. (2020). Effects Of Lycium barbarum Polysaccharides On Learning And Memory Ability And Antioxidant Stress In Epileptic Rats. *Chin. J. Tradit. Med. Sci. Technol.* 27, 204–207.

Chen, Y., Yao, F., Ming, K., Wang, D., Hu, Y., and Liu, J. (2016). Polysaccharides from Traditional Chinese Medicines: Extraction, Purification, Modification, and Biological Activity. *Molecules* 21, 1705. doi:10.3390/molecules21121705

Cheung, S. G., Goldenthal, A. R., Uhlemann, A. C., Mann, J. J., Miller, J. M., and Sublette, M. E. (2019). Systematic Review of Gut Microbiota and Major Depression. *Front. Psychiatry* 10, 34. doi:10.3389/fpsyt.2019.00034

Dahlin, M., and Prast-Nielsen, S. (2019). The Gut Microbiome and Epilepsy. *EBioMedicine* 44, 741–746. doi:10.1016/j.ebiom.2019.05.024

De Caro, C., Iannone, L. F., Citraro, R., Striano, P., De Sarro, G., Constanti, A., et al. (2019). Can We 'seize' the Gut Microbiota to Treat Epilepsy. *Neurosci. Biobehav. Rev.* 107, 750–764. doi:10.1016/j.neubiorev.2019.10.002

Dinan, T. G., and Cryan, J. F. (2017). Gut Instincts: Microbiota as a Key Regulator of Brain Development, Ageing and Neurodegeneration. *J. Physiol.* 595, 489–503. doi:10.1113/JP273106

Ding, Y., Yan, Y., Peng, Y., Chen, D., Mi, J., Lu, L., et al. (2019). *In Vitro* digestion under Simulated Saliva, Gastric and Small Intestinal Conditions and Fermentation by Human Gut Microbiota of Polysaccharides from the Fruits of *Lycium Barbarum*. *Int. J. Biol. Macromol.* 125, 751–760. doi:10.1016/j.ijbiomac.2018.12.081

Enrique, A. V., Di Ianni, M. E., Goicoechea, S., Lazarowski, A., Valle-Dorado, M. G., Costa, J. J. L., et al. (2021). New Anticonvulsant Candidates Prevent P-Glycoprotein (P-Gp) Overexpression in a Pharmacoresistant Seizure Model in Mice. *Epilepsy Behav.* 121, 106451. doi:10.1016/j.yebeh.2019.106451

Feng, Y., Liu, J., Tang, H. D., Huang, X. H., Chen, H. Y., and Su, L. (2017). Nervous Protection And Mechanism Of Lycium Barbarum Polysaccharides On Epileptic Rats. *Chin. J. Gerontol.* 37, 6036–6038.

Gómez-Eguílaz, M., Ramón-Trapero, J. L., Pérez-Martínez, L., and Blanco, J. R. (2018). The Beneficial Effect of Probiotics as a Supplementary Treatment in Drug-Resistant Epilepsy: a Pilot Study. *Benef. Microbes* 9, 875–881. doi:10.3920/BM2018.0018

He, L. Y., Hu, M. B., Li, R. L., Zhao, R., Fan, L. H., He, L., et al. (2021). Natural Medicines for the Treatment of Epilepsy: Bioactive Components, Pharmacology and Mechanism. *Front. Pharmacol.* 12, 604040. doi:10.3389/fphar.2021.604040

He, Z., Cui, B. T., Zhang, T., Li, P., Long, C. Y., Ji, G. Z., et al. (2017). Fecal Microbiota Transplantation Cured Epilepsy in a Case with Crohn's Disease: The First Report. *World J. Gastroenterol.* 23, 3565–3568. doi:10.3748/wjg.v23.i19.3565

Hong, C. Y., Zhang, H. D., Liu, X. Y., and Xu, Y. (2019). Attenuation of Hyperoxic Acute Lung Injury by *Lycium Barbarum* Polysaccharide via Inhibiting NLRP3 Inflammasome. *Arch. Pharm. Res.* 42, 902–908. doi:10.1007/s12272-019-01175-4

Ji, X., Hou, C., Gao, Y., Xue, Y., Yan, Y., and Guo, X. (2020). Metagenomic Analysis of Gut Microbiota Modulatory Effects of Jujube (*Ziziphus Jujuba* Mill.) Polysaccharides in a Colorectal Cancer Mouse Model. *Food Funct.* 11, 163–173. doi:10.1039/c9fo02171j

Jia, D., Rao, C., Xue, S., and Lei, J. (2015). Purification, Characterization and Neuroprotective Effects of a Polysaccharide from *Gynostemma Pentaphyllum*. *Carbohydr. Polym.* 122, 93–100. doi:10.1016/j.carbpol.2014.12.032

Li, L., Guo, W. L., Zhang, W., Xu, J. X., Qian, M., Bai, W. D., et al. (2019). *Grifola Frondosa* Polysaccharides Ameliorate Lipid Metabolic Disorders and Gut Microbiota Dysbiosis in High-Fat Diet Fed Rats. *Food Funct.* 10, 2560–2572. doi:10.1039/c9fo00075e

Liang, J., Wu, Y., Yuan, H., Yang, Y., Xiong, Q., Liang, C., et al. (2019). *Dendrobium Officinale* Polysaccharides Attenuate Learning and Memory Disabilities via Anti-oxidant and Anti-inflammatory Actions. *Int. J. Biol. Macromol.* 126, 414–426. doi:10.1016/j.ijbiomac.2018.12.230

Liang, J., Zhang, M., Wang, X., Ren, Y., Yue, T., Wang, Z., et al. (2021). Edible Fungal Polysaccharides, the Gut Microbiota, and Host Health. *Carbohydr. Polym.* 273, 118558. doi:10.1016/j.carbpol.2021.118558

Liang, L., Zhou, H., Zhang, S., Yuan, J., and Wu, H. (2017). Effects of Gut Microbiota Disturbance Induced in Early Life on the Expression of Extrasynaptic GABA-A Receptor α5 and δ Subunits in the hippocampus of Adult Rats. *Brain Res. Bull.* 135, 113–119. doi:10.1016/j.brainresbull.2017.09.014

Liu, L., Li, M., Yu, M., Shen, M., Wang, Q., Yu, Y., et al. (2019). Natural Polysaccharides Exhibit Anti-tumor Activity by Targeting Gut Microbiota. *Int. J. Biol. Macromol.* 121, 743–751. doi:10.1016/j.ijbiomac.2018.10.083

Lum, G. R., Olson, C. A., and Hsiao, E. Y. (2020). Emerging Roles for the Intestinal Microbiome in Epilepsy. *Neurobiol. Dis.* 135, 104576. doi:10.1016/j.nbd.2019.104576

Ma, G., Du, H., Hu, Q., Yang, W., Pei, F., and Xiao, H. (2021). Health Benefits of Edible Mushroom Polysaccharides and Associated Gut Microbiota Regulation. *Crit. Rev. Food Sci. Nutr.*, 1–18. doi:10.1080/10408398.2021.1903385

Mehla, J., Reeta, K. H., Gupta, P., and Gupta, Y. K. (2010). Protective Effect of Curcumin against Seizures and Cognitive Impairment in a Pentylenetetrazole-Kindled Epileptic Rat Model. *Life Sci.* 87, 596–603. doi:10.1016/j.lfs.2010.09.006

Mittal, R., Debs, L. H., Patel, A. P., Nguyen, D., Patel, K., O'Connor, G., et al. (2017). Neurotransmitters: The Critical Modulators Regulating Gut-Brain Axis. *J. Cel. Physiol.* 232, 2359–2372. doi:10.1002/jcp.25518

O'Mahony, S. M., Clarke, G., Borre, Y. E., Dinan, T. G., and Cryan, J. F. (2015). Serotonin, Tryptophan Metabolism and the Brain-Gut-Microbiome axis. *Behav. Brain Res.* 277, 32–48. doi:10.1016/j.bbr.2014.07.027

Olson, C. A., Vuong, H. E., Yano, J. M., Liang, Q. Y., Nusbaum, D. J., and Hsiao, E. Y. (2018). The Gut Microbiota Mediates the Anti-seizure Effects of the Ketogenic Diet. *Cell* 173, 1728–e13. doi:10.1016/j.cell.2018.04.027

Pellegrini, C., Antonioli, L., Colucci, R., Blandizzi, C., and Fornai, M. (2018). Interplay Among Gut Microbiota, Intestinal Mucosal Barrier and Enteric Neuro-Immune System: a Common Path to Neurodegenerative Diseases. *Acta Neuropathol.* 136, 345–361. doi:10.1007/s00401-018-1856-5

Peng, A., Qiu, X., Lai, W., Li, W., Zhang, L., Zhu, X., et al. (2018). Altered Composition of the Gut Microbiome in Patients with Drug-Resistant Epilepsy. *Epilepsy Res.* 147, 102–107. doi:10.1016/j.eplepsyres.2018.09.013

Qin, X., Hua, J., Lin, S. J., Zheng, H. T., Wang, J. J., Li, W., et al. (2020). Astragalus Polysaccharide Alleviates Cognitive Impairment and β-amyloid Accumulation in APP/PS1 Mice via Nrf2 Pathway. *Biochem. Biophys. Res. Commun.* 531, 431–437. doi:10.1016/j.bbrc.2020.07.122

Rawat, K., Singh, N., Kumari, P., and Saha, L. (2020). A Review on Preventive Role of Ketogenic Diet (KD) in CNS Disorders from the Gut Microbiota Perspective. *Rev. Neurosci.* 32, 143–157. doi:10.1515/revneuro-2020-0078

Rousseaux, C., Thuru, X., Gelot, A., Barnich, N., Neut, C., Dubuquoy, L., et al. (2007). Lactobacillus Acidophilus Modulates Intestinal Pain and Induces Opioid and Cannabinoid Receptors. *Nat. Med.* 13, 35–37. doi:10.1038/nm1521

Sander, J. W., and Perucca, E. (2003). Epilepsy and Comorbidity: Infections and Antimicrobials Usage in Relation to Epilepsy Management. *Acta Neurol. Scand. Suppl.* 180, 16–22. doi:10.1034/j.1600-0404.108.s180.3.x

Song, Q., Wang, Y., Huang, L., Shen, M., Yu, Y., Yu, Q., et al. (2021). Review of the Relationships Among Polysaccharides, Gut Microbiota, and Human Health. *Food Res. Int.* 140, 109858. doi:10.1016/j.foodres.2020.109858

Stilling, R. M., van de Wouw, M., Clarke, G., Stanton, C., Dinan, T. G., and Cryan, J. F. (2016). The Neuropharmacology of Butyrate: The Bread and Butter of the Microbiota-Gut-Brain axis. *Neurochem. Int.* 99, 110–132. doi:10.1016/j.neuint.2016.06.011

Su, D., Li, S., Zhang, W., Wang, J., Wang, J., and Lv, M. (2017). Structural Elucidation of a Polysaccharide from *Lonicera japonica* Flowers, and its Neuroprotective Effect on Cerebral Ischemia-Reperfusion Injury in Rat. *Int. J. Biol. Macromolecules* 99, 350–357. doi:10.1016/j.ijbiomac.2017.02.096

Su, Y., Li, J., Wu, L., and Kuang, H. (2021). Polysaccharides from TCM Herbs Exhibit Potent Anti-obesity Effect by Mediating the Community Structure of Gut Microbiota. *Pharmazie* 76, 473–479. doi:10.1691/ph.2021.1463

Sudo, N., Chida, Y., Aiba, Y., Sonoda, J., Oyama, N., Yu, X. N., et al. (2004). Postnatal Microbial Colonization Programs the Hypothalamic-Pituitary-Adrenal System for Stress Response in Mice. *J. Physiol.* 558, 263–275. doi:10.1113/jphysiol.2004.063388

Sun, X., Kong, L., and Zhou, L. (2018). Protective Effect of Fructus Corni Polysaccharide on Hippocampal Tissues and its Relevant Mechanism in Epileptic Rats Induced by Lithium Chloride-Pilocarpine. *Exp. Ther. Med.* 16, 445–451. doi:10.3892/etm.2018.6142

Tremlett, H., Bauer, K. C., Appel-Cresswell, S., Finlay, B. B., and Waubant, E. (2017). The Gut Microbiome in Human Neurological Disease: A Review. *Ann. Neurol.* 81, 369–382. doi:10.1002/ana.24901

van de Wouw, M., Boehme, M., Lyte, J. M., Wiley, N., Strain, C., O'Sullivan, O., et al. (2018). Short-chain Fatty Acids: Microbial Metabolites that Alleviate Stress-Induced Brain-Gut axis Alterations. *J. Physiol.* 596, 4923–4944. doi:10.1113/JP276431

Vuong, H. E., Yano, J. M., Fung, T. C., and Hsiao, E. Y. (2017). The Microbiome and Host Behavior. *Annu. Rev. Neurosci.* 40, 21–49. doi:10.1146/annurev-neuro-072116-031347

Wang, Y., Sun, M., Jin, H., Yang, J., Kang, S., Liu, Y., et al. (2021b). Effects of *Lycium Barbarum* Polysaccharides on Immunity and the Gut Microbiota in Cyclophosphamide-Induced Immunosuppressed Mice. *Front. Microbiol.* 12, 701566. doi:10.3389/fmicb.2021.701566

Wang, Y., Zhang, X., Wang, Y., Zhao, W., Li, H., Zhang, L., et al. (2021a). Application of Immune Checkpoint Targets in the Anti-tumor Novel Drugs and Traditional Chinese Medicine Development. *Acta Pharm. Sin. B* 11, 2957–2972. doi:10.1016/j.apsb.2021.03.004

Weng, Y. J., Gan, H. Y., Li, X., Huang, Y., Li, Z. C., Deng, H. M., et al. (2019). Correlation of Diet, Microbiota and Metabolite Networks in Inflammatory Bowel Disease. *J. Dig. Dis.* 20, 447–459. doi:10.1111/1751-2980.12795

Xi, S., Li, Y., Yue, L., Gong, Y., Qian, L., Liang, T., et al. (2020). Role of Traditional Chinese Medicine in the Management of Viral Pneumonia. *Front. Pharmacol.* 11, 582322. doi:10.3389/fphar.2020.582322

Xiao, Z., Deng, Q., Zhou, W., and Zhang, Y. (2021). Immune Activities of Polysaccharides Isolated from *Lycium Barbarum* L. What Do We Know So Far. *Pharmacol. Ther.* 229, 107921. doi:10.1016/j.pharmthera.2021.107921

Yang, Y., Liu, P., Chen, L., Liu, Z., Zhang, H., Wang, J., et al. (2013). Therapeutic Effect of Ginkgo Biloba Polysaccharide in Rats with Focal Cerebral Ischemia/reperfusion (I/R) Injury. *Carbohydr. Polym.* 98, 1383–1388. doi:10.1016/j.carbpol.2013.07.045

Yin, C., Noratto, G. D., Fan, X., Chen, Z., Yao, F., Shi, D., et al. (2020). The Impact of Mushroom Polysaccharides on Gut Microbiota and its Beneficial Effects to Host: A Review. *Carbohydr. Polym.* 250, 116942. doi:10.1016/j.carbpol.2020.116942

Yuan, X., Li, Z., Wang, X. T., Li, X. Y., Hua, H., Li, X. C., et al. (2019). *China J. Chin. Materia Med.* 44, 9–18. doi:10.19540/j.cnki.cjcmm.20181012.006

Yue, Q., Cai, M., Xiao, B., Zhan, Q., and Zeng, C. (2021). The Microbiota-Gut-Brain axis and Epilepsy. *Cell. Mol. Neurobiol.*. doi:10.1007/s10571-021-01130-210.1007/s10571-021-01130-2

Zeng, P., Li, J., Chen, Y., and Zhang, L. (2019). The Structures and Biological Functions of Polysaccharides from Traditional Chinese Herbs. *Prog. Mol. Biol. Transl. Sci.* 163, 423–444. doi:10.1016/bs.pmbts.2019.03.003

Zhang, L., Peng, H., Xu, J., Xu, Y., Yin, Y., He, B., et al. (2019). Effects of *Dendrobium Officinale* Polysaccharides on Brain Inflammation of Epileptic Rats. *Int. J. Polym. Sci.* 2019, 1–6. doi:10.1155/2019/9058161

Zhang, T., Yang, Y., Liang, Y., Jiao, X., and Zhao, C. (2018). Beneficial Effect of Intestinal Fermentation of Natural Polysaccharides. *Nutrients* 10, 1055. doi:10.3390/nu10081055

Zhang, X. Y., Guo, Z. Y., Chen, Y., Wang, D., and Chen, Y. (2010). Recent advance in Antiepileptic Chinese Medicine Monomer. *J. Liaoning Univ. Tradit. Chin. Med.* 22, 129–132. doi:10.1016/S1875-5364(20)60031-0

Zhou, Y., Guo, X., Chen, W., and Liu, J. (2019). *Angelica* Polysaccharide Mitigates Lipopolysaccharide-Evoked Inflammatory Injury by Regulating microRNA-10a in Neuronal Cell Line HT22. *Artif. Cell Nanomed. Biotechnol.* 47, 3194–3201. doi:10.1080/21691401.2019.1614595

Zhu, K. L., Xie, L. L., and Liu, H. (2015). *Ganoderma Lucidum* Polysaccharide on Excitatory Amino Acid Transporter in Brain of Epileptic Rat. *J. Changchun Univ. Chin. Med.* 1104–1106. doi:10.13463/j.cnki.cczyy.2015.06.002

Conflict of Interest: The authors declare that the research was conducted in the absence of any commercial or financial relationships that could be construed as a potential conflict of interest.

Publisher's Note: All claims expressed in this article are solely those of the authors and do not necessarily represent those of their affiliated organizations, or those of the publisher, the editors and the reviewers. Any product that may be evaluated in this article, or claim that may be made by its manufacturer, is not guaranteed or endorsed by the publisher.

Advantages of publishing in Frontiers

OPEN ACCESS
Articles are free to read for greatest visibility and readership

FAST PUBLICATION
Around 90 days from submission to decision

HIGH QUALITY PEER-REVIEW
Rigorous, collaborative, and constructive peer-review

TRANSPARENT PEER-REVIEW
Editors and reviewers acknowledged by name on published articles

Frontiers
Avenue du Tribunal-Fédéral 34
1005 Lausanne | Switzerland

Visit us: www.frontiersin.org
Contact us: frontiersin.org/about/contact

REPRODUCIBILITY OF RESEARCH
Support open data and methods to enhance research reproducibility

DIGITAL PUBLISHING
Articles designed for optimal readership across devices

FOLLOW US
@frontiersin

IMPACT METRICS
Advanced article metrics track visibility across digital media

EXTENSIVE PROMOTION
Marketing and promotion of impactful research

LOOP RESEARCH NETWORK
Our network increases your article's readership